Development of hyaluronic acid-based materials

Laurianne Legay

PSL
UNIVERSITÉ PARIS

THÈSE DE DOCTORAT
DE L'UNIVERSITÉ PSL

Préparée à Mines Paris-PSL

Development of hyaluronic acid-based materials

Développement de matériaux à base d'acide hyaluronique

Soutenue par
Laurianne LEGAY
Le 26 mars 2024

Ecole doctorale n° 364
Sciences Fondamentales et appliquées

Spécialité
Mécanique numérique et matériaux

Composition du jury :

Bernard CATHALA Directeur de recherche INRAE Nantes	*Président du jury*
Irina SMIRNOVA Professor Technische Universität Hamburg	*Rapporteur*
Jacques DESBRIÈRES Professeur émérite Université de Pau et des Pays de l'Adour	*Rapporteur*
Sijtze BUWALDA Chargé de recherche CEMEF – Mines Paris	*Co-directeur de thèse*
Tatiana BUDTOVA Directeur de recherche CEMEF – Mines Paris	*Directrice de thèse*

MINES PARIS | PSL

Remerciements

Tout d'abord, je remercie infiniment mes encadrants de thèse, Sijtze Buwalda et Tatiana Budtova, pour les 3 ans de thèse passés au CEMEF à Sophia-Antipolis : pour votre bienveillance, votre patience, votre écoute et votre gentillesse. Plus important encore, pour avoir encouragé ma curiosité scientifique, avoir cru en moi et m'avoir fait confiance. Merci de m'avoir envoyée dans un autre laboratoire à l'autre bout du monde, à Vancouver au Canada pendant 1 mois, pour faire des expériences avec l'acide hyaluronique et les fibres de nanochitin. Aussi, c'était la première fois que j'encadrais un stagiaire, Pierre Antonczak (Mai-Juin 2023). J'ai aussi apprécié d'avoir amélioré mon anglais à votre contact. Merci de m'avoir comprise et guidée, pour au final, me permettre de m'épanouir autant scientifiquement qu'humainement. Grâce à vous, je suis passée de la doctorante timide à une jeune chercheuse, prête à relever de nouveaux défis en R&D.

Je remercie les membres de mon jury pour avoir accepté d'évaluer mon travail de thèse : Pr. Irina Smirnova et Pr. Jacques Desbrières d'avoir été mes rapporteurs, ainsi que Dr. Bernard Cathala d'avoir été mon examinateur et président du jury. Merci pour votre bienveillance, votre considération, et pour les discussions enrichissantes sur les aérogels, sur le séchage supercritique, la physico-chimie des biopolymères, la rhéologie que nous avons pu avoir après la présentation de mon travail de thèse.

Je remercie le post-doctorant Dr. Daniel Aguilera-Bulla pour m'avoir accompagné au début de ma thèse (mars 2021), notamment pour mon initiation sur les aérogels d'acide hyaluronique et les différentes techniques de caractérisations.

Je remercie Marion Négrier et Coraline Chartier pour leur accueil dans l'équipe BIO, équipe qui s'est ensuite agrandie avec l'arrivée de nouveaux doctorants (Sujie Yu, Loris Gelas, Veronika Khodyrieva, Eleni Effraimopoulou, Hiba Bouras). Il y a toujours eu une ambiance de travail sympa dans le bureau, et dans les laboratoires de chimie.

Loris, tu as été un super collègue de bureau avec qui je pouvais parler de tout, aussi bien de nos expériences/résultats/problèmes sur les aérogels, que de nos week-ends ! Une fois nos expériences terminées, on pouvait facilement rigoler de tout. Ton aide de pro pour les expériences de libération avec ma capsule de méthylène bleu m'a vraiment été utile.

J'aimerai remercier également Oriane Senninger pour sa gentillesse, sa bienveillance et pour tous ses conseils donnés au début et après la rédaction de ma thèse.

Ce doctorat n'aurait jamais pu être aussi bien vécu sans les autres collègues doctorants. Le début de la thèse a été marqué par le confinement dans les Alpes Maritimes. Une fois celui-ci terminé, la vie a repris avec repas, restos dans le vieil Antibes, pique-niques, plage... Marion Roth, Laurianne Viora, Nitish Chandrappa et Nathan Sylvestre, merci pour avoir partagé avec vous les nombreuses activités sportives le week-end : randonnées dans l'arrière-pays de Nice, dans l'Estérel et le long de la Côte d'Azur près de la mer, bivouac dans la Vallée des Merveilles, camping en Italie aux 5 terres, via-Ferrata à Puget-Théniers… En 2ème et 3ème année de thèse, le groupe s'est agrandi, et c'était toujours très chouette : le ski à Isola et Auron, le bivouac au lac d'Allos, le ski de fond au Boréon, la mémorable rando raquette au refuge de la Madone, le camping au Cap Taillat, le weekend des Oscars CEMEF dans le Var, le week-end ski à Praloup, l'escalade en salle à Nice, la rando raquette à la Colmiane. Merci également pour les agréables discussions à midi près de la « salle convi » avec Cynthia Hayek, Lucas Ravix, Charles Brissot, Nelly Pons, Alan Taboré… Enfin, merci Lukas Stippel, Eleni Effraimopoulou et Owen Palmer du laboratoire PERSEE pour les moments passés à parler en anglais et en allemand. J'ai adoré parler une autre langue que le français et découvrir quelles étaient les particularités de vos pays respectifs.

Le séjour d'un mois dans le laboratoire du BioProducts Institute de l'Université de Colombie Britannique à Vancouver au Canada était autant riche professionnellement que personnellement. Je n'oublierai pas les midis à manger et discuter avec Oliver Musl pas loin du Tim Hortons à deux pas du laboratoire, les sorties faites le weekend dans Vancouver avec des membres du labo (Angela Arnosa Prieto, Kenza Belmir, Elisa Ferreira, Eupidio Scopel) et les activités organisées par le laboratoire.

Pour finir, j'aimerai remercier mes proches qui m'ont accompagné et soutenu durant cette thèse : mes parents, mon frère Mathis, ma sœur Maude, et mes grands-parents.

Je garderai de très bons souvenirs, autant professionnellement qu'humainement,

de ces 3 années de thèse au CEMEF et sur la côte d'Azur,

remplies de rencontres, de soleil, de partages, de discussions !

Merci à tous !

General Table of Contents

Abbreviations and symbols

- **Materials**

DTT	1,4-dithioerythritol
EDC	1-ethyl-3-(3-dimethylaminopropyl)carbodiimide hydrochloride
FITC-dextran	Fluorescein isothiocyanate-dextran
HA	Hyaluronic acid
KH_2PO_4	Monopotassium phosphate
MB	Methylene blue
Na_2HPO_4	Disodium phosphate
nCh	Chitin nanofibers
NHS	N-hydroxysuccinimide
PBS	Phosphate buffered saline
$scCO_2$	Supercritical CO_2

- **Methods and techniques**

AFM	Atomic force microscopy
BET method	Brunauer, Emmett and Teller method for determination of specific surface area
BJH method	Barrett, Joyner and Halenda method for determination of pore size distribution
FT method	Freezing-thawing method
FTIR spectroscopy	Fourier transform infrared spectrocopy
NIPS method	Non-solvent induced phase separation method
SEM	Scanning electron microscopy
UV-Vis spectroscopy	Ultraviolet-visible spectroscopy

- **Quantities**

wt%	Weight percent
G’	Storage modulus
G’’	Loss modulus
η	Steady state viscosity
$[\eta]$	Intrinsic viscosity
V_i (%)	Volume of the initial HA solution
V_{org} (%)	Volume of the organogel
V_f (%)	Volume of the dry material (including aerogel)
ρ_{bulk}	Bulk or apparent density
$\rho_{skeletal}$	Skeletal density
V_{pores}	Specific pore volume
S_{BET}	Specific surface area determined using the BET method
DDA	Degree of deacetylation
ε_N	Nominal strain
σ_N	Nominal stress
E	Young’s modulus
$\varepsilon_{model\ drug}$	Molar extinction coefficient of a model drug

General introduction

The development of bio-based materials for biomedical applications attracts increasing attention, due to the recent demands for a sustainable society. A biomaterial is usually a natural or synthetic material, used in the medical area, that is intended to interact with living tissues.[1] So far, several materials such as metals, ceramics and polymers have been used to meet the needs of various biomedical areas. Bio-based polymers, which can be obtained from renewable natural resources (plants or animals), are particularly attractive for biomedical applications as they possess several interesting properties such as biodegradability, and they are often biocompatible and non-toxic.[2] Moreover, they can undergo several chemical modifications that can be useful for tissue regeneration.

Various biomedical applications require porous materials, such as scaffolds for wound dressings. Porosity represents the fraction of pores volume to the total material volume.[3] Pores are classified into two types:

- Open pores, which are interconnected and connect to the outside of the material
- Closed pores, which are isolated from the outside of the material

Porous materials can be of different morphology and based on different matters. Porous metals, ceramics and glasses are used in many domains such as chemistry, mechanical engineering, biotechnology and electronics. For most industrial applications, open pores are required. For example, filters or carriers for catalysts and bioreactors need to have a high fraction of open pores to be efficient. Materials with closed porosity are mainly used for acoustic and thermal insulation or low-density structural components. The properties of a porous material depend on the pore volume and geometry, the pore size and the pore distribution, which shows the importance to control porosity. According to IUPAC definition, porous materials are classified based on pore size[4]:

- Microporous (pore diameter < 2 nm)
- Mesoporous (2 nm < pore diameter < 50 nm)
- Macroporous (50 nm < pore diameter)

Aerogels constitute a special family of porous materials. Aerogels were first synthesized by Kistler in 1931 from silica gels, prepared by a sol-gel method, and dried using supercritical conditions to remove the solvent.[5] According to the IUPAC Goldbook, an aerogel is described as “a gel comprised of a microporous solid in which the dispersed phase is a gas”.[6] This description is rather restrictive as it focuses on materials with pore size below 2 nm, thus excluding even classical silica aerogels which are mesoporous. According to the agreement

between aerogel scientists, aerogels are materials with low density (< 0.2 g/cm^3), high specific surface areas (at least 100 m^2/g) and high and open porosity (> 90%).[7,8] These nanostructured materials generally contain meso- (2 nm < d < 50 nm) and small macropores (few hundreds of nanometers). In the last twenty years, a novel generation of aerogels, based on biomass, was developed.[9] Till now, the majority of bio-aerogels have been prepared from polysaccharides, with few works on protein-based aerogels. Polysaccharides are often biocompatible, biodegradable and possess anti-inflammatory and antibacterial effects, making them potentially attractive for preparing materials for biomedical applications. The interest in bio-aerogels is also due to the desire to use sustainable resources instead of fossil-based ones to reduce the environmental impact of the polymer industry and to realize a bio-based and sustainable society. The preparation of bio-aerogels includes several steps, starting with the dissolution of a polysaccharide in a solvent (often water), followed by gelation or not (depending on the polysaccharide and experimental conditions) and solvent exchange, necessary perform supercritical drying (often, with CO_2). Several polysaccharides have been used to prepare bio-aerogels such as cellulose[10], starch[11], pectin[12], alginate[13] and chitosan[14]. Bio-aerogels have many applications such as in gas sorption, filtration, catalysts, energy and thermal insulation.

Recently, hyaluronic acid (HA), a natural polysaccharide, has proven to be a promising bio-based material for biomedical applications, in particular as wound dressings.[15] HA is a major component of skin extracellular matrix (ECM), which plays crucial roles during wound healing. Due to its intrinsic properties such as biocompatibility, biodegradability and high hydrophilicity, this polymer has been used to produce different materials, namely hydrogels, cryogels, sponges and films, with various stiffness and bioactivity.

Currently, some HA-based hydrogels promoting wound healing such as Hyalofill or Hylase Wound Gel are available commercially, but they have poor mechanical properties and bacteria can develop easily. No cryogels exist commercially, probably due to high energy consumption during their manufacturing. Native HA gels usually have poor mechanical properties and a fast degradation rate. In order to prolong the degradation rate and improve the mechanical properties, different strategies such as chemical modification and crosslinking through its hydroxyl and carboxyl groups, and mixing with other polymers to form a composite, have been used.[16,17] Very few papers report on HA aerogels, with no examples for wound dressings applications.

The objective of the thesis is thus to explore the development of HA-based aerogels for potential biomedical applications, including wound dressings. This work was financed by the

French National Research Agency (JCJC project '3D-AER-HYAL'), which is warmly acknowledged. This project was realized in the frame of a thesis at the Center of Materials Forming (CEMEF) of Mines Paris, PSL University, in Sophia-Antipolis.

This manuscript is divided into five chapters:

Chapter 1 presents the state of the art on aerogels, and on HA and its applications. Aerogels are obtained from a gel in which the liquid phase has been replaced by air, without destroying the solid network, usually under supercritical conditions. Silica, synthetic polymer aerogels and bio-aerogels with their properties and applications are reviewed. The physicochemical and biological properties of HA are presented, as well as chemical modifications and crosslinking methods, followed by an overview of biomedical applications of HA, thereby focusing on wound dressings. An overview of the wound healing process and HA-based porous materials, already used as dressings, are described. This part is mainly focused on HA hydrogels and cryogels because very few articles exist regarding aerogels made from HA.

Chapter 2 describes the materials used and protocols developed to prepare three novel HA-based materials for potential biomedical applications:

- Physically crosslinked aerogels are prepared via freezing-thawing of HA solutions, solvent exchange, and drying with supercritical CO_2 ($scCO_2$).
- Chemically crosslinked HA aerogels are developed using covalent crosslinking for the formation of HA hydrogels, followed by solvent exchange and supercritical drying.
- Mixing of nanochitin (nCh) fibers suspension with HA solution leads to the formation of HA-nCh based capsules, due to strong polyelectrolyte complexation.

The methods to characterize these new materials are also detailed.

Chapter 3 focuses on physically crosslinked HA aerogels. First, the molecular weight of HA is determined and the rheological properties of HA solutions are studied. Then, the preparation of HA aerogels is described. The influence of processing conditions (HA concentration, the solution pH, the number of freeze-thaw cycles and the type of non-solvent) on the morphology and properties of physically crosslinked HA aerogels is investigated. The mechanical properties of the aerogels upon compression are analyzed. The absorption of aerogels in an aqueous medium and their behavior upon exposure to air are examined.

Chapter 4 concerns the development of HA aerogels using chemical crosslinking for the formation of the HA network. Here, the reaction between the carboxylic acid groups of HA with

the amino groups of cystamine is employed. The latter acts as reduction-responsive crosslinker, which forms potentially cleavable links between HA chains. The influence of the HA concentration and the molar ratio between the COOH groups of HA and NH_2 groups of cystamine on the structure and several properties of HA aerogels is investigated. The behavior of chemically crosslinked HA aerogels in an aqueous environment, under either standard or reductive conditions, and upon exposure to air is also presented.

Chapter 5 focuses on the development of HA-nCh fiber capsules. Initially, we were willing to reinforce HA aerogels with nCh fibers, but it turned out that upon mixing HA solutions and nCh suspensions, strong polyelectrolyte complexation occurred leading to the formation of a HA/nCh "membrane". The electrostatic interactions occurring between HA and nCh are confirmed by FTIR spectroscopy. The membrane robustness is tested in several aqueous media such as acids or bases. It is demonstrated that capsules are formed when a droplet of one system (e.g. HA solution) is placed in another one (e.g. nCh suspension), and vice versa. The composition of HA-nCh capsules is determined using FTIR spectroscopy. The morphology of the capsule membrane is examined by SEM. Finally, these capsules are explored for drug delivery applications.

The last part concludes on the work presented in this manuscript and gives the perspectives.

The work on HA-nCh capsules was performed in the frame of the project entitled "Nanochitin and hyaluronic acid bio-aerogels for biomedical applications", financed by the France-Canada Research Fund, which we kindly acknowledge. We thank all persons from the Bioproducts Institute of the University of British Columbia in Vancouver (Canada), who were involved in this project. We also thank Pierre ILBIZIAN and Julien JAXEL (PERSEE, Mines Paris, France) for supercritical drying, Christophe PRADILLE (MatXper, Mines Paris, France) for his help in mechanical testing and Suzanne JACOMET (CEMEF, Mines Paris, France) for her help in SEM imaging.

Introduction générale

Le développement de matériaux biosourcés pour des applications biomédicales attire de plus en plus l'attention, en raison des exigences récentes d'une société durable. Un biomatériau est généralement un matériau naturel ou synthétique, utilisé dans le domaine médical, destiné à interagir avec les tissus vivants.[1] Jusqu'à présent, plusieurs matériaux tels que les métaux, les céramiques et les polymères ont été utilisés pour répondre aux besoins de divers domaines biomédicaux. Les polymères biosourcés, obtenus à partir de ressources naturelles renouvelables (végétales ou animales), sont particulièrement attractifs pour les applications biomédicales car ils possèdent plusieurs propriétés intéressantes pour les applications biomédicales telles que la biodégradabilité, et ils sont souvent biocompatibles et non toxiques.[2] De plus, ils peuvent subir plusieurs modifications chimiques qui peuvent être utiles à la régénération des tissus.

De nombreuses applications biomédicales nécessitent des matériaux poreux, comme un scaffold pour des applications de pansements. La porosité représente la fraction du volume des pores par rapport au volume total du matériau.[3] Les pores sont classés en deux types :

- Pores ouverts, qui sont interconnectés et sont connectés à l'extérieur du matériau
- Pores fermés, isolés de l'extérieur du matériau

Les matériaux poreux peuvent être de morphologie différente et sont basés sur des matières différentes. Les métaux poreux, les céramiques poreuses et les verres poreux sont utilisés dans de nombreux domaines tels que la chimie, la construction mécanique, la biotechnologie ou l'électronique. Pour la plupart des applications industrielles, des pores ouverts sont nécessaires. Par exemple, pour être efficaces, les filtres ou supports pour catalyseurs et bioréacteurs doivent avoir une fraction élevée de pores ouverts. Les matériaux à porosité fermée sont principalement utilisés pour l'isolation acoustique et thermique ou pour des éléments structurels de faible densité. Les propriétés d'un matériau poreux dépendent du volume et de la géométrie des pores, de la taille des pores et de la répartition des pores, ce qui montre l'importance de contrôler la porosité. Selon la définition de l'IUPAC, les matériaux poreux sont classés en fonction de la taille des pores[4]:

- Micropores (pore diameter < 2 nm)
- Mesopores (2 nm < pore diameter < 50 nm)
- Macropores (50 nm < pore diameter)

Les aérogels constituent une famille singulière de matériaux poreux. Les aérogels ont été synthétisés pour la première fois par Kistler en 1931 à partir de gels de silice, préparés par une méthode sol-gel et séchés dans des conditions supercritiques afin d'éliminer le solvant.[5] Selon le

Goldbook de l'IUPAC, un aérogel est décrit comme « un gel composé d'un solide microporeux dans lequel la phase dispersée est un gaz ».[6] Cette description est plutôt restrictive car elle se concentre sur des matériaux dont la taille des pores est inférieure à 2 nm, excluant ainsi même les aérogels de silice classiques qui sont mésoporeux. Selon un accord entre les scientifiques des aérogels, les aérogels sont des matériaux à faible densité (< 0.2 g/cm^3), à surfaces spécifiques élevées (au moins 100 m^2/g) et à porosité élevée et ouverte (> 90 %).[7,8] Ces matériaux nanostructurés contiennent généralement des méso- (2 nm < d < 50 nm) et des petits macropores (quelques centaines de nanomètres). Au cours des vingt dernières années, une nouvelle génération d'aérogels, basée sur la biomasse, a été développée.[9] Jusqu'à présent, la majorité des bio-aérogels ont été préparés à partir de polysaccharides, avec peu de travaux sur les aérogels à base de protéines. Les polysaccharides sont souvent biocompatibles, biodégradables et possèdent des effets anti-inflammatoires et antibactériens, ce qui les rend potentiellement intéressants pour préparer des matériaux destinés à des applications biomédicales. L'intérêt pour les bio-aérogels est également dû au désir d'utiliser des ressources durables plutôt que fossiles pour réduire l'impact environnemental de l'industrie des polymères et réaliser une société biosourcée et durable. La préparation des bio-aérogels comprend plusieurs étapes, en commençant par la dissolution d'un polysaccharide dans un solvant (souvent de l'eau), suivie d'une gélification ou non (selon le polysaccharide et les conditions expérimentales) et d'un échange de solvant, nécessaire pour effectuer un séchage supercritique (souvent, avec du CO_2). Plusieurs polysaccharides ont été utilisés pour préparer des bio-aérogels tels que la cellulose[10], l'amidon[11], la pectine[12], l'alginate[13] et le chitosane[14]. Les bio-aérogels ont de nombreuses applications comme dans la sorption des gaz, la filtration, les catalyseurs, l'énergie et l'isolation thermique.

Récemment, l'acide hyaluronique (HA), un polysaccharide naturel, s'est révélé être un matériau biosourcé prometteur pour des applications biomédicales, notamment comme pansements.[15] L'acide hyaluronique est un composant majeur de la matrice extracellulaire cutanée, qui joue un rôle crucial lors de la cicatrisation des plaies. En raison de ses propriétés intrinsèques telles que la biocompatibilité, la biodégradabilité et la haute hydrophilie, ce polymère a été utilisé pour fabriquer différents matériaux, à savoir des hydrogels, des cryogels, des éponges et des films, avec diverses rigidités et de bioactivités.

Actuellement, certains hydrogels à base d'acide hyaluronique favorisant la cicatrisation des plaies comme Hyalofill ou Hylase Wound Gel sont disponibles dans le commerce, mais ils possèdent de mauvaises propriétés mécaniques et des bactéries se développent à partir de ces matériaux. Aucun cryogel n'existe commercialement, probablement en raison de la forte

consommation d'énergie lors de leur fabrication. Les gels d'acide hyaluronique purs ont généralement de mauvaises propriétés mécaniques et un taux de dégradation rapide. Afin de réduire la vitesse de dégradation et d'améliorer ses propriétés et sa vitesse mécaniques, différentes stratégies telles que la modification chimique et la réticulation via ses groupes hydroxyle et carboxyle, ainsi que le mélange avec d'autres polymères pour former un composite, ont été utilisées.[16,17] Très peu d'articles font état d'aérogels d'acide hyaluronique, avec des exemples pour les applications de pansements. À notre connaissance, aucun aérogel à base d'acide hyaluronique pour pansements n'est aujourd'hui disponible dans le commerce.

L'objectif de la thèse est donc d'explorer le développement d'aérogels à base d'acide hyaluronique pour de potentielles applications de pansements. Ces travaux ont été financés par l'Agence Nationale de la Recherche (projet JCJC « 3D-AER-HYAL »), qui sont chaleureusement salués. Ce projet a été réalisé dans le cadre d'une thèse au Centre de Mise en Forme des Matériaux (CEMEF) de Mines Paris, Université PSL, à Sophia-Antipolis.

Ce manuscrit est divisé en cinq chapitres :

Le chapitre 1 présente un état de l'art sur les aérogels, ainsi que sur l'acide hyaluronique et ses applications. Les aérogels sont obtenus à partir d'un gel dont la phase liquide a été remplacée par de l'air, sans détruire le réseau solide, généralement dans des conditions supercritiques. La silice, les aérogels de polymères synthétiques et les bio-aérogels avec leurs propriétés et applications sont également passés en revue. Les propriétés physicochimiques et biologiques de l'acide hyaluronique sont présentées, ainsi que les modifications chimiques et les méthodes de réticulation pouvant être effectuées, suivies d'un aperçu des applications biomédicales de l'acide hyaluronique, se concentrant ainsi sur les pansements. Un aperçu du processus de cicatrisation des plaies et des matériaux poreux à base d'acide hyaluronique, déjà utilisés comme pansements, est décrit. Cette partie est principalement axée sur les hydrogels et cryogels d'acide hyaluronique car très peu d'articles existent concernant les aérogels à base d'acide hyaluronique.

Le chapitre 2 décrit les matériaux utilisés et les protocoles développés pour préparer trois nouveaux matériaux à base d'acide hyaluronique pour de potentielles applications biomédicales :

- Les aérogels physiquement réticulés sont préparés par congélation-décongélation de solutions d'acide hyaluronique, échange de solvant et séchage au CO_2 supercritique ($scCO_2$).

- Les aérogels d’acide hyaluronique chimiquement réticulés sont développés par réticulation covalente pour la formation d'hydrogels, suivie d'un échange de solvant et d'un séchage supercritique.

- Le mélange de la suspension de fibres de nanochitine (nCh) avec une solution d’acide hyaluronique conduit à la formation de capsules à base de HA-nCh, en raison d'une forte complexation polyélectrolytique.

Les méthodes permettant de caractériser ces nouveaux matériaux sont également détaillées.

Le chapitre 3 se concentre sur les aérogels d’acide hyaluronique physiquement réticulés. Tout d’abord, le poids moléculaire de l’acide hyaluronique est déterminé et les propriétés rhéologiques des solutions d’HA sont étudiées. Ensuite, la préparation des aérogels HA est décrite. L'influence des conditions de traitement (concentration en HA, pH initial de la solution, nombre de cycles de gel-dégel et type de non-solvant) sur la morphologie et les propriétés des aérogels HA physiquement réticulés est étudiée. Les propriétés mécaniques des aérogels sous compression sont analysées. L'absorption des aérogels en milieu aqueux et leur comportement lors de l’exposition à l'air sont explorés.

Le chapitre 4 concerne le développement d'aérogels d’acide hyaluronique via l’utilisation de la réticulation chimique pour la formation du réseau polymérique. Ici, la réaction entre les groupes acide carboxylique de HA avec les groupes amino de la cystamine est utilisée. Ce dernier agit comme un agent de réticulation sensible à la réduction, formant des liens potentiellement clivables entre les chaînes d’acide hyaluronique. L'influence de la concentration en HA et du rapport molaire entre les groupes COOH de l’acide hyaluronique et les groupes NH_2 de la cystamine sur la structure et plusieurs propriétés des aérogels HA est étudiée. Le comportement des aérogels d’acide hyaluronique chimiquement réticulés en milieu aqueux, dans des conditions standards ou réductrices, et lors de l’exposition à l'air est également présenté.

Le chapitre 5 se concentre sur le développement de capsules de fibres HA-nCh. Initialement, nous voulions renforcer les aérogels HA avec des fibres nCh, mais il s'est avéré qu'en mélangeant des solutions HA et de suspensions nCh, une forte complexation polyélectrolytique s’est produit, conduisant à la formation d’une « membrane » HA/nCh. Les interactions électrostatiques se produisant entre HA et nCh sont confirmées par spectroscopie FTIR. La robustesse de la membrane est testée dans plusieurs milieux aqueux tels que des acides ou des bases. Il est démontré que des capsules se forment lorsqu'une gouttelette d'un système (par exemple, une solution d’acide hyaluronique) est placée dans un autre (par exemple, une

suspension de nCh), et vice versa. La composition des capsules HA-nCh est déterminée par spectroscopie FTIR. La morphologie de la membrane de la capsule est examinée par SEM. Enfin, ces capsules sont étudiées pour des applications d'administration de médicaments.

La dernière partie conclut les travaux présentés dans ce manuscrit et donne les perspectives.

Les travaux sur les capsules HA-nCh ont été réalisés dans le cadre du projet intitulé «Bio-aérogels de nanochitine et d'acide hyaluronique pour des applications biomédicales», financé par le Fonds France-Canada pour la Recherche. Nous les remercions. Nous remercions également toutes les personnes du Bioproducts Institute de l'Université de Colombie-Britannique à Vancouver (Canada), qui ont participé à ce projet. Nous remercions également Pierre ILBIZIAN et Julien JAXEL (PERSEE, Mines Paris, France) pour le séchage supercritique, Christophe PRADILLE (MatXper, Mines Paris, France) pour son aide aux essais mécaniques et Suzanne JACOMET (CEMEF, Mines Paris, France) pour son aide en imagerie SEM.

References

(1) Williams, D. F. On the Nature of Biomaterials. *Biomaterials* **2009**, *30* (30), 5897–5909. https://doi.org/10.1016/j.biomaterials.2009.07.027.

(2) Birajdar, M. S.; Joo, H.; Koh, W.-G.; Park, H. Natural Bio-Based Monomers for Biomedical Applications: A Review. *Biomaterials Research* **2021**, *25* (1), 8. https://doi.org/10.1186/s40824-021-00208-8.

(3) Ishizaki, K.; Komarneni, S.; Nanko, M. *Porous Materials: Process Technology and Applications*; Springer Science & Business Media, **2013**.

(4) Sing, K. S. W. Reporting Physisorption Data for Gas/Solid Systems with Special Reference to the Determination of Surface Area and Porosity (Recommendations 1984). *Pure and Applied Chemistry* **1985**, *57* (4), 603–619. https://doi.org/10.1351/pac198557040603.

(5) Kistler, S. S. Coherent Expanded Aerogels and Jellies. *Nature* **1931**, *127* (3211), 741–741. https://doi.org/10.1038/127741a0.

(6) *IUPAC Compendium of Chemical Terminology, 2nd Ed. (the "Gold Book").*; Compiled by McNaught, A.D. and Wilkinson, A. Blackwell Scientific Publications, Oxford (**1997**). XML on-line corrected version: http://goldbook.iupac.org (2006) created by Nic, M., Jirat, J. and Kosata, B.; updates Compiled by Jenkins, A., Ed.; 2014. https://doi.org/10.1351/goldbook.

(7) *Aerogels Handbook*; Aegerter, M. A., Leventis, N., Koebel, M. M., Eds.; Springer New York: New York, NY, **2011**. https://doi.org/10.1007/978-1-4419-7589-8.

(8) Aegerter, M. A.; Leventis, N.; Koebel, M.; III, S. A. S. *Springer Handbook of Aerogels*; Springer International Publishing, **2023**.

(9) Budtova, T.; Aguilera, D. A.; Beluns, S.; Berglund, L.; Chartier, C.; Espinosa, E.; Gaidukovs, S.; Klimek-Kopyra, A.; Kmita, A.; Lachowicz, D.; Liebner, F.; Platnieks, O.; Rodríguez, A.; Tinoco Navarro, L. K.; Zou, F.; Buwalda, S. J. Biorefinery Approach for Aerogels. *Polymers* **2020**, *12* (12), 2779. https://doi.org/10.3390/polym12122779.

(10) Budtova, T. Cellulose II Aerogels: A Review. *Cellulose* **2019**, *26* (1), 81–121. https://doi.org/10.1007/s10570-018-2189-1.

(11) Druel, L.; Bardl, R.; Vorwerg, W.; Budtova, T. Starch Aerogels: A Member of the Family of Thermal Superinsulating Materials. *Biomacromolecules* **2017**, *18* (12), 4232–4239. https://doi.org/10.1021/acs.biomac.7b01272.

(12) Groult, S.; Budtova, T. Tuning Structure and Properties of Pectin Aerogels. *European Polymer Journal* **2018**, *108*, 250–261. https://doi.org/10.1016/j.eurpolymj.2018.08.048.

(13) García-González, C. A.; Alnaief, M.; Smirnova, I. Polysaccharide-Based Aerogels—Promising Biodegradable Carriers for Drug Delivery Systems. *Carbohydrate Polymers* **2011**, *86* (4), 1425–1438. https://doi.org/10.1016/j.carbpol.2011.06.066.

(14) Chartier, C.; Buwalda, S.; Van Den Berghe, H.; Nottelet, B.; Budtova, T. Tuning the Properties of Porous Chitosan: Aerogels and Cryogels. *International Journal of Biological Macromolecules* **2022**, *202*, 215–223. https://doi.org/10.1016/j.ijbiomac.2022.01.042.

(15) Graça, M. F. P.; Miguel, S. P.; Cabral, C. S. D.; Correia, I. J. Hyaluronic Acid—Based Wound Dressings: A Review. *Carbohydrate Polymers* **2020**, *241*, 116364. https://doi.org/10.1016/j.carbpol.2020.116364.

(16) Collins, M. N.; Birkinshaw, C. Hyaluronic Acid Based Scaffolds for Tissue Engineering—A Review. *Carbohydrate Polymers* **2013**, *92* (2), 1262–1279. https://doi.org/10.1016/j.carbpol.2012.10.028.

(17) Khunmanee, S.; Jeong, Y.; Park, H. Crosslinking Method of Hyaluronic-Based Hydrogel for Biomedical Applications. *J Tissue Eng* **2017**, *8*, 204173141772646. https://doi.org/10.1177/2041731417726464.

Articles, communications and formations

This PhD work has led to one article published in an international journal. Several communications (oral presentations and posters) were given at national and international conferences.

- ## Articles

As co-author (by performing experiments asked for the revised version):

Aguilera-Bulla, D.; Legay, L.; Buwalda, S. J.; Budtova, T. Crosslinker-Free Hyaluronic Acid Aerogels. *Biomacromolecules* **2022**, *23* (7), 2838–2845. https://doi.org/10.1021/acs.biomac.2c00207.

As first author:

Legay, L.; Budtova, T.; Buwalda, S. Hyaluronic Acid Aerogels Made Via Freeze–Thaw-Induced Gelation. *Biomacromolecules* **2023**, *24* (10), 4502–4509. https://doi.org/10.1021/acs.biomac.2c01518.

- ## Oral presentations

Laurianne Legay, Sytze Buwalda, Tatiana Budtova

"Engineering of hyaluronic acid aerogels". American Chemical Society (ACS) Spring conference 2022, San Diego, United States of America, March 20-24th, 2022 – Oral presentation online.

Laurianne Legay, Milad Kamkar, Sytze Buwalda, Orlando J. Rojas, Tatiana Budtova

"Interfacial complexation of hyaluronic acid and nanochitin enabling fibrous capsules formation for drug delivery applications". American Chemical Society (ACS) Spring conference 2023, Indianapolis, United States of America, March 26-30th, 2023 – Oral presentation online.

Laurianne Legay, Milad Kamkar, Sytze Buwalda, Orlando J. Rojas, Tatiana Budtova

"Preparation of hyaluronic and nanochitin fibers capsules for drug delivery applications". 8th EPNOE International Polysaccharides conference, Graz, Austria, September 18th-22nd, 2023 – Oral presentation.

- ## Posters

Coraline Chartier, Laurianne Legay, Marion Négrier, Sytze Buwalda, Tatiana Budtova

"Bio-aerogels". Aerogel Industry-Academia Forum, Switzerland, July 13rd-15th, 2021 – Online meeting.

Laurianne Legay, Sytze Buwalda, Tatiana Budtova

"Hyaluronic acid aerogels prepared via freeze-thaw induced gelation". Colloque des doctorants de 2ème année – EDSFA, Nice, France, May 16th, 2022.

Laurianne Legay, Sytze Buwalda, Tatiana Budtova

"Preparation of hyaluronic acid-based aerogels". Advanced Functional Polymers for Medicine (AFPM) Conference, Nice, France, June 1st-3rd, 2022.

Laurianne Legay, Christophe Pradille, Sytze Buwalda, Tatiana Budtova

"Preparation of physically crosslinked hyaluronic acid-based aerogels". EPNOE Junior Scientist Meeting, Aveiro, Portugal, September 8-9th, 2022.

Laurianne Legay, Christophe Pradille, Sytze Buwalda, Tatiana Budtova

"Hyaluronic acid aerogels via freeze-thaw induced gelation". 6th International Seminar on Aerogels, Hamburg, Germany, September 28-30th, 2022.

- ## Formations

Besides the experimental work, scientific courses on polymers and polymer materials (45h) and personalized formations (74h), mandatory in the frame of the PhD, were followed. A SST (Sauveteur Secouriste du travail) formation was also followed during the PhD.

Chapter 1. State of the art

1. Introduction

[English]

Bio-based polymers, originating from renewable natural resources, are particularly attractive for biomedical applications, thanks to their biodegradability, biocompatibility and non-toxicity.[1] The properties of these polymers can be modified chemically to meet the medical requirements. Natural polymers commonly used medically include collagen, alginate and gelatin.

Recently, hyaluronic acid (HA), a natural polysaccharide, has proved to be a promising bio-based material for biomedical applications, in particular as wound dressings.[2] HA is a major component of skin extracellular matrix (ECM), which is involved in wound healing and tissue regeneration. Thanks to its biocompatibility, biodegradability and hydrophilicity, HA has been used to produce hydrogels, sponges and films, with desired stiffness and bioactivity.

Several HA-based porous materials as hydrogels and cryogels (freeze-dried hydrogels) have been developed as wounds dressings. Novel nanostructured materials, aerogels, attract interest for wound dressing applications, in view of their low density (< 0.2 g/cm^3), high porosity (> 90%) and high specific surface area (at least 100 m^2/g).[3] Due to their high surface area and porosity, aerogels can potentially absorb high amount of wound exudate, have a good adherence to the wound site with an easy removal, promote O_2/CO_2 exchange and act as drug carrier with high loading capacity.[4] The first aerogels were developed by Kistler in 1931 from silica gels, using supercritical conditions to replace the solvent by air.[5] In the last twenty years, a new generation of aerogels, based on biomass, was developed.[3] Several polysaccharides as pectin, cellulose, starch, alginate and chitosan have been used to prepare bio-aerogels. However, only very few HA aerogels have been reported[6,7], despite their high potential.

In this chapter, the first part is dedicated to the state of the art on aerogels (definition, history, preparation method via sol-gel approach, focusing on bio-based aerogels, their properties and their biomedical applications). The second part covers HA, the polymer of interest in the thesis. An overview of its source, structure, physico-chemical and biological properties and its chemical modifications is made. Specific attention is paid to the use of HA for biomedical applications, more specifically as wound dressing. The concept of wounds, the wound healing process and the ideal wound dressing are also described. Finally, the state of the art on HA-based porous materials, developed for wound dressing applications, is reviewed.

[Français]

Les polymères biosourcés, issus de ressources naturelles renouvelables, sont particulièrement attractifs pour des applications biomédicales, grâce à leur biodégradabilité, biocompatibilité et non-toxicité.[1] Les propriétés de ces polymères peuvent être modifiées chimiquement pour répondre aux exigences médicales. Les polymères naturels utilisés dans le domaine médical incluent, généralement, le collagène, l'alginate et la gelatine.

Récemment, l'acide hyaluronique, un polysaccharide naturel, s'est avéré être un matériau biosourcé prometteur pour les applications biomédicales, telles que les pansements.[2] L'acide hyaluronique est un composant majeur de la matrice extracellulaire de la peau, qui intervient lors du processus de guérison d'une blessure et de la régénération des tissus. Grâce à sa biocompatibilité, sa biodégradabilité et son hydrophilicité, l'acide hyaluronique a été utilisé pour fabriquer des hydrogels, des éponges et des films, avec une rigidité et une bioactivité bien définies.

Plusieurs matériaux poreux à base d'acide hyaluronique, tels que les hydrogels et les cryogels (hydrogels lyophilisés), ont été développés pour des applications de pansements. Récemment, de nouveaux matériaux nanostructurés, aérogels, ont suscité de l'intérêt pour ce type d'application, en raison de leur faible densité (< 0.2 g/cm^3), leur grande porosité (> 90%) et leur grande surface spécifique (au moins 100 m^2/g).[3] Leur grande surface spécifique et leur grande porosité leur permettent potentiellement d'absorber de grandes quantités d'exsudat d'une blessure, d'avoir une bonne adhérence à la blessure avec un retrait facile, de favoriser les échanges gazeux O_2/CO_2 et de fonctionner comme vecteur de médicaments avec une grande capacité de chargement.[4] Les premiers aérogels ont été développés par Kistler en 1931 à partir de gels de silice, en utilisant des conditions supercritiques pour remplacer le solvant par de l'air.[5] Au cours des vingt dernières années, une nouvelle génération d'aérogels, basée sur la biomasse, a été mise au point.[3] Plusieurs polysaccharides comme la pectine, la cellulose, l'amidon, l'alginate et le chitosan ont été utilisés pour préparer des bio-aérogels. Cependant, très peu d'aérogels à base d'acide hyaluronique ont été rapportés[6,7], malgré leur fort potentiel.

Dans ce chapitre, la première partie est consacrée à un état de l'art sur les aérogels (définition, histoire, méthode de préparation via l'approche sol-gel, focus sur les aérogels biosourcés, leur propriétés et leurs applications biomédicales). Une seconde partie concerne l'acide hyaluronique, le polymère d'intérêt dans cette thèse. Un aperçu de sa provenance, de sa structure, de ses propriétés physico-chimiques et biologiques, et de ses modifications chimiques est donné. Une attention particulière est accordée à l'utilisation de l'acide hyaluronique pour les

applications biomédicales, et plus spécifiquement pour les pansements. Le concept de blessure, le processus de guérison et le pansement idéal sont également décrits. Pour finir, un état de l'art sur les matériaux poreux à base d'acide hyaluronique, développés pour des applications de pansements, est effectué.

2. Aerogels

2.1. Definition

The word "aerogel" was introduced by Kistler in 1931 to describe gels in which the liquid is replaced by gas (air), without collapsing the gel network, using supercritical conditions.[3] Drying with supercritical fluid such as CO_2 ($scCO_2$) consists of exchanging the fluid in the gel pores by CO_2, which is heated above the critical pressure P_c and temperature T_c.

Aerogels are materials with low density (< 0.2 g/cm^3), high specific surface areas (at least 100 m^2/g) and high and open porosity (> 90%). These nanostructured materials generally contain meso- (2 nm < d < 50 nm) and small macropores (d > 50 nm). In the IUPAC Gold Book, an aerogel is described as "a gel comprised of a microporous solid in which the dispersed phase is a gas".[8] This description is rather restrictive as it focuses on materials with pore size below 2 nm, thus excluding even classical silica aerogels which are mesoporous. A European project COST "AERoGELS" (18125) is now negotiating with IUPAC to modify this definition. In 2022, IUPAC named aerogels among "Ten Emerging Technologies in Chemistry".[9]

2.2. History of aerogels

Aerogels were firstly made by Kistler in 1931 from silica gels, prepared by a sol-gel method, using supercritical fluid extraction.[10] One year after, Kistler developed aerogels based on inorganic oxides such as alumina, tungsten oxide, ferric oxide, stannic oxide, and on biobased polymers such as cellulose, gelatin, agar, egg albumin and rubber, but no data on the properties exist.[5] From 1941, silica aerogels were commercialized, under the name Santocel, by Monsanto.[11] The industrial application was thermal insulation. Unfortunately, in the late 1970's, the production was stopped, because of high-cost manufacturing. Next, new generations of aerogels based on oxides of metals (i.e. titanium, zirconium, aluminum) were developed. These new aerogels attracted increasing attention, particularly, thanks to the high specific surface area (up to 1000 m^2/g), transparency and low thermal conductivity of silica aerogels (0.015 W/(m.K)).[3] In the late 80's, organic aerogels were synthesized by Pekala et al.[13] These aerogels are stiffer than silica aerogels.[13,14] Aerogels based on synthetic polymers as polyurethane[15], polyimide[16] and polyamide[17] were also prepared. In the last twenty years, a new type of aerogel, based on biomass, has emerged: bio-aerogels.[3]

2.3. Preparation of aerogels

2.3.1. Silica aerogels

Silica aerogels are by far the most known and commercially available class of aerogels.[5] They are prepared using the sol-gel route, followed by supercritical drying; the latter can be avoided using silica gel pore walls functionalisation.[3,18–20] The silica sol is a colloidal suspension of silica alkoxide, dispersed in a solvent such as ethanol, methanol or acetone. The most used silica alkoxides are tetraethyl orthosilicate (TEOS) and tetramethyl orthosilicate (TMOS). In the presence of an aqueous acid or base catalyst, the colloidal suspension undergoes a sol-gel transition, forming a 3D network.

The gelation of silica is divided into two steps. The first one is the acid-catalyzed hydrolysis step and forms reactive silanol monomers, with one hydroxyl function bound to a silicon atom (Si-OH). This reaction is followed by an acid- or base-catalyzed polycondensation reaction of two silanol groups, which forms silicon-oxygen-silicon linkages (Si-O-Si). This results in a 3D network of silicon oxide filled with solvent, called silica gel.

Before drying, silica gels are often aged to reinforce the network formed during the sol-gel process. Aging favors syneresis. Thus, a finer 3D structure can be obtained. After washing steps with solvent, silica gels are supercritically dried to obtain aerogels or silica gels are silylated, followed by ambient pressure drying. The resulting silica aerogels are highly porous, with density around 0.1 g/cm^3 and specific surface area up to 1000 m^2/g or even higher. The properties of silica aerogels are influenced by several parameters such as the type and concentration of silica, the type of catalyst, and the temperature and time for hydrolysis, gelation and aging. One of the most famous applications of silica aerogels is thermal insulation, due to their extremely low thermal conductivity (around 0.013 W/m.K), significantly lower than that of ambient air (0.025 W/m.K).[8] They have also other potential applications in space (to collect dust particles, to protect space mirrors), in acoustic insulation, in catalysis and in storage.[8]

2.3.2. Synthetic organic polymer aerogels

The first synthetic organic aerogels, described by Pekala et al.[12] in 1989, were based on resorcinol–formaldehyde (RF) resin. RF aerogels are the best known synthetic organic aerogels. Other organic aerogels were then developed based on other types of resins such as melamine-formaldehyde, phenol-formaldehyde, phenol-furfural or on organic compounds such as polyimides, polyacrylamides, polyacrylonitriles, polyacrylates, polystyrene and polyurethanes.[3,19]

The principle of production of RF aerogels is quasi similar to the one of silica aerogels (cf. Section 2.3.1. Silica aerogels of this Chapter). RF gels are synthesized by the polycondensation of resorcinol with formaldehyde under alkaline or acidic conditions.[3] The synthesis involves two steps. First, resorcinol (trifunctional monomer) reacts with formaldehyde to form hydroxymethylated derivatives of resorcinol. Then, the hydroxymethyl groups condense with each other to form nanoclusters that crosslink to form a gel, through methylene (-CH_2-) or methylene ether (-CH_2OCH_2-) bridges. In case of basic catalysis, the reaction is carried out in aqueous alkaline solution with for example sodium carbonate as catalyst. Gelation occurs at high temperatures (80-100°C) for prolonged periods. In the case of acid catalysis, gelation is much faster: monomers are mixed with the acid catalyst either in aqueous or non-aqueous medium and gelation can take place at room temperature. The size of the clusters and their crosslinking are influenced by the pH of the solution, temperature, concentration and ratio of monomers and type of catalyst. Gels are aged in organic solvent, for defined time, to increase the crosslinking density. Solvent exchange and supercritical drying are then used to obtain RF aerogels.

RF aerogels are dark red in color and transparent. They have very low density (from 0.035 to 0.1 g/cm^3), high porosity (> 80%), high specific surface area (up to 900 m^2/g), and ultrafine pore size (< 50 nm). Lower thermal conductivity (W = 0.012 W/(m.K)) was found for RF aerogels, as compared to silica aerogels, which offers the opportunity for the development of better heat thermal insulators.[21] Higher compressive moduli (up to E = 800 Kpa) were found for organic aerogels with a density of 0.08-0.25 g/cm^3, as compared to silica aerogels (up to E = 380 Kpa for densities of 0.14-0.25 g/cm^3).[13] RF aerogels can be used as membrane for separation of gases or liquids.[3] Moreover, RF aerogels can be pyrolyzed to form carbon aerogels, which can be further used as materials for hydrogen storage, as anodes in batteries, as electrodes for supercapacitors or as non-reflective panels.

2.3.3. New generation of aerogels: bio-aerogels

At the beginning of the 21st century, a new generation of aerogels was developed: they are bio-based. The interest in bio-aerogels is in part due to the desire to use sustainable resources instead of fossil-based ones to reduce the environmental impact of the polymer industry and to realize a bio-based and sustainable society. In addition, bio-based polymers are often biocompatible as well as biodegradable and many exhibit anti-inflammatory and antibacterial effects. Bio-aerogels can be prepared from a solution of a natural polymer such as polysaccharides, proteins, lignin, or from a suspension of natural particles such as nanochitin and nanocellulose.[22] The fundamental difference between bio-aerogels and (in)organic aerogels

is that in the case of synthetic organic polymer or inorganic aerogels, the process starts with polymerization, while in the case of biopolymers, no polymerization, and often even no gelation or crosslinking, is needed. Here, we will only focus on aerogels based on polysaccharides solution, as it concerns the PhD topic.

The preparation of bio-aerogels starts with the dissolution of a polysaccharide in a solvent (often, water). Then, depending on the polysaccharide and experimental conditions (pH, ionic strength, polymer concentration), the solution either gels or not.[23] During gelation, network formation occurs via physical (i.e. hydrogen bonds) or chemical crosslinking. The network can also be created by coagulation (also known as non-solvent induced phase separation[6]), with direct addition of a non-solvent. To avoid pores collapse during drying, it is usually performed under supercritical conditions, and, thus, the fluid in the network must be replaced by a fluid miscible with CO_2, such as ethanol or acetone. Supercritical CO_2 is often used for drying, as supercritical conditions of other fluids such as water (P_c = 221 bar and T_c = 374°C) can degrade biopolymers.[24] After drying with $scCO_2$, bio-aerogels are obtained. Figure 1.1 illustrates the complete process.

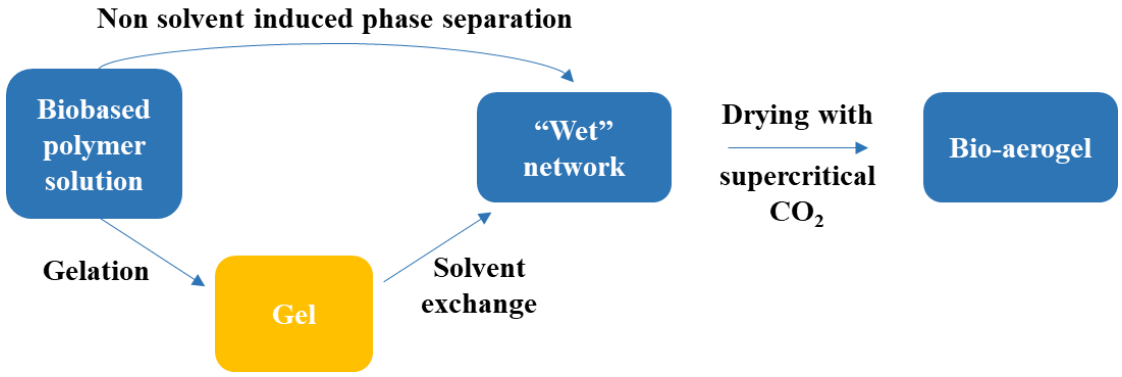

Figure 1.1. Preparation of bio-aerogels.

The properties of bio-aerogels can be tuned by varying the type of polysaccharide and the preparation conditions.

2.3.4. Drying methods to get porous networks

Different methods can be used to obtain porous networks from a polysaccharide solution or gel. We will describe below each method and try to find the one(s) that allows the formation of a nanostructured material without pores collapse.

Evaporative drying is the simplest way to remove liquid from a polymer solution or a gel. As liquid evaporates, liquid phase stretches to cover the network and goes into tension, forming a concave meniscus. The tension is balanced by compressive stresses on the network.[25] Thus, with evaporation, the meniscus curvature increases, inducing a stress applied to pore walls, called capillary pressure. The developed pressure is expressed with the Young-Laplace equation:

$$\Delta P = \frac{2\gamma\cos\theta}{R} \qquad (1)$$

where γ is the surface tension between liquid and gas ($N.m^{-1}$); θ is the contact angle between the two phases and r is the pore radius (m). An example of a concave meniscus formed when a pore is in contact with liquid is presented in Figure 1.2.

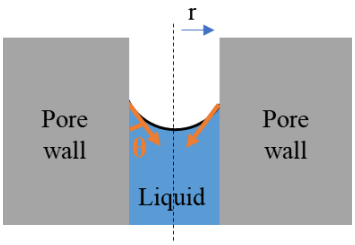

Figure 1.2. Illustration of a pore in contact with a liquid.

High surface tension and small pore radius induce higher pressure, often leading to complete pores collapse and dense materials, with practically no porosity; here, they will be called "*xerogels*". Only few exceptions are known where evaporative drying results in aerogel-like materials: this is the case for silylated silica gels[26], of cellulose when dissolved in 2M NaOH or starch hydrogels, coagulated in ethanol and dried from ethanol.[27,28]

One option to keep pores open during drying is to use freeze-drying. The liquid phase is frozen and then sublimated at reduced pressure.[3] This method bypasses the triple point of the liquid phase. Usually, freeze-drying is applied on hydrogels. The formation and growth of ice crystals may deform pore walls and the network structure. Freeze-dried materials (here they will be called "*cryogels*") possess large macropores (several μm in diameter) and high porosity (> 90%). Usually, the specific surface area of cryogels is low. The exception is when the growth of ice crystals is suppressed, which occurs in a mixture of water and tert-butanol.[29]

Drying under supercritical conditions suppresses the liquid/vapor boundary line, by placing the fluid above its supercritical point.[3] This type of drying avoids the formation of any liquid-vapor meniscus in the gel pores. CO_2 is often used as supercritical fluid, thanks to its mild conditions (P_c = 72.8 bar and T_c = 31°C). To perform drying with supercritical CO_2, water in gel pores must be replaced by a non-polar fluid miscible with CO_2. Solvent exchange with ethanol or acetone is usually performed. The progressive addition of a non-solvent to polysaccharide solution or gel results in phase separation.[30] The solubility of the polysaccharide decreases as the non-solvent proportion increases, leading to polymer coagulation and contraction. Solvent exchange is performed either in a gradual way, by slowly increasing the fraction of non-solvent, or in a direct way (i.e. direct addition of a large quantity of non-solvent), depending on the polysaccharide. During solvent exchange, polymer macromolecules do not totally collapse, even if they are not gelled. Above the polymer overlap concentration, a 3D network is formed. Thanks to a certain polymer chain rigidity, the coagulated polysaccharide forms a 3D network, corresponding to the aerogel precursor. By drying with $scCO_2$, solid porous nanostructured materials are formed. Aerogels, either obtained from a non-gelled or gelled solution, have interesting properties such as a low density (< 0.2 g/cm^3), high porosity (> 90%) and high specific surface area (> 100 m²/g).[23,31]

A phase diagram illustrates the three drying routes, as described above (Figure 1.3). In this thesis, only $scCO_2$ drying was used to get a solid porous nanostructured material with a low density, high porosity and high specific surface area, potentially suitable for biomedical applications such as wound dressings.

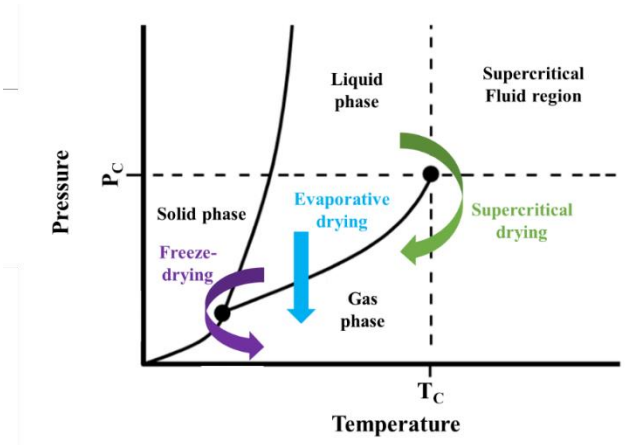

Figure 1.3. Phase diagram demonstrating various drying methods.

2.4. Examples of bio-aerogels

The most common polysaccharides used to make bio-aerogels are cellulose, starch, pectin, alginate and chitosan.[32] Examples of bio-aerogels with their properties and morphologies are discussed below. Hyaluronic acid (HA) emerges as a promising candidate, yet it will be more detailed in the following part, due to its central role in the thesis.

2.4.1. Cellulose aerogels

Cellulose, mainly found in plant cell walls (cotton, flax, hemp), is the most abundant natural polymer on earth.[33] It is composed of D-glucopyranose units linked by β-1,4 glycosidic bonds. Native cellulose is a highly crystalline polymer, organized into long and entangled fibrils. It is insoluble in water but soluble in NaOH-water, in organic solvents such as N,N-dimethylacetamide with lithium chloride (LiCl/DMAc) and N-methylmorpholine N-oxide (NMMO), or in ionic liquids such as 1-ethyl-3-methylimidazolium acetate (EMIAc). After pulp dissolution and coagulation or mercerization (treatment with NaOH), cellulose is transformed from cellulose I to cellulose II. After dissolving cellulose in NaOH/water at -6°C, physical gelation occurs at room temperature, due to irreversible chain aggregation.[34] Chemical gels can also be prepared by crosslinking cellulose with epichlorohydrin.[35] Then, depending on the preparation method used, the solvent in cellulose gels or solutions is washed out with ethanol or acetone, which are miscible with CO_2.[36] The time needed for cellulose solvent to diffuse out and non-solvent to diffuse in depends on cellulose concentration and sample shape.[36] Finally, the 3D structure containing the non-solvent is supercritically dried to get cellulose aerogels.

When non-solvent is added, cellulose solution or gel is shrinking. The total volume shrinkage of samples from cellulose solution or gel to aerogel is usually not higher than 50%.[37] Cellulose aerogels exist in the form of fibers[38], monoliths[37] and beads[39]. Different types of cellulose were used to produce aerogels. For instance, Pääko et al.[40] developed cellulose I based aerogels with a high porosity (98%) and a very low density (0.02 g/cm^3). Ultra lightweight cellulose aerogels (density of 0.008 g/cm^3) were prepared from bacterial cellulose.[41] Cellulose II aerogels typically present a bulk density ranging from 0.05 to 0.2 g/cm^3 and specific surface areas up to 400 m^2/g, depending on cellulose concentration and process route.[36] Some cellulose derivatives such as cellulose acetate[42] or cellulose ester[43] were also employed for the preparation of highly porous aerogels. Thanks to their biocompatibility and biodegradability, cellulose aerogels have a high potential in biomedical applications such as scaffolds for drug release.[44,45] Aerogels from cellulose I and II can be used as absorbents.[36]

Recently, nanocellulose aerogels attract interest due to their low density (0.001-0.2 g/cm^3), high specific surface areas (500-600 m^2/g) and small and open pores (< 50 nm).[46] They are prepared from a suspension of nanofibers or nanocrystals, followed by solvent exchange and supercritical drying.[22] The properties of nanocellulose aerogels can be tuned. For example, denser cellulose aerogels (i.e. increase from 0.08 to 0.15 g/cm^3) were obtained by increasing the initial concentration of cellulose nanowhiskers (crystals) by a factor 2.[47] Due to the use of different processes of fabrication, nanocellulose aerogels have different properties from cellulose II aerogels. For example, better insulating properties were obtained for nanocellulose aerogels (W = 0.018 w/m.K)[48], as compared to cellulose II aerogels (W > 0.03 w/m.K).[36] Cellulose II aerogels probably possess thick pores walls and many large macropores, limiting their use as thermal insulators.

2.4.2. Starch aerogels

Starch is commonly present in corn, potatoes and wheat. Starch is composed of amylose (linear α-1,4-D-glucose polymer) and amylopectin (branched α-1,4-D-glucose polymer). The proportion of these components varies as a function of the source. The gelation of starch is divided in 3 steps: hydration – gelatinization – retrogradation.[45] First, starch granules are dissolved in water under heating. Due to water absorption, starch granules swell. Then, gelatinization occurs, leading to irreversible physical changes and destruction of the granule structure. Finally, a retrogradation step occurs: the hydrogel structure is formed upon cooling and aging, followed by a reorganization and partial recrystallization. Gelatinization temperature and amylose content influence gel formation. For example, gelation is promoted with higher amylose content.

To prepare starch aerogels, solvent exchange and $scCO_2$ were applied to starch gels and non-gelled solutions.[49] The total volume shrinkage from hydrogel to aerogel state decreases as the amylose content increases. For example, lower volume shrinkage (40%) was observed for aerogels prepared with 80 wt% of amylose (vs 55% for aerogels prepared with no amylose).[50] Starch aerogels exist in the shape of monoliths[50], microspheres[51] and beads[52]. The properties of starch aerogels depend on the starch source. Lower density (0.1 g/cm^3) and higher specific surface areas (170-250 m^2/g) were observed for pea starch aerogels and higher density (0.3-0.6 g/cm^3) and lower specific surface areas (7-90 m^2/g) for waxy maize starch.[49] Druel et al. demonstrated that a longer retrogradation time increases thermal conductivity.[50] For example, for an aerogel density of 0.14 g/cm^3, the thermal conductivity increased from 0.023 to 0.027 W/m.K for a retrogradation time difference of 50 h. Starch aerogel morphology also depends on

the amylose content. Higher amylose content leads to a finer and more ramified network.[49] Thanks to these properties, starch aerogels could be used as thermal insulating materials.[50] Furthermore, starch aerogels can serve as potential matrix for the controlled release of various drugs.[51] For example, ketoprofen[53] and ibuprofen[54] releases were studied.

2.4.3. Pectin aerogels

Pectin is a linear polymer, mainly present in vegetables and fruits. This polysaccharide is made up of α-1,4 linked D-galacturonic acid units, with different degrees of methyl esterification of the carboxyl group, depending on the source. Pectin solution can gel or not. Physical gelation may occur in acidic conditions (pH < 3.5). At pH values close to the pKa of pectin, another gelation mechanism occurs if a polyvalent metal salt is added, involving the formation of intermolecular junction zones via ionic bonds, according to the egg-box model.[55] For example, strong pectin gels were prepared by calcium-induced gelation at pH 3 at 65°C by Groult et al.[23] Then, solvent exchange and $scCO_2$ drying led to the formation of pectin aerogels. The overall volume shrinkage after drying for pectin aerogels is around 50-80%. Pectin aerogels can be of any shape, from beads[56] to monoliths and microspheres[57]. The properties of pectin aerogels were tuned by the pectin concentration and the type of non-solvent (ethanol or acetone). For example, higher specific surface areas, around 630 m^2/g, and lower density, 0.065 g/cm^3, were observed for pectin aerogels prepared with acetone as non-solvent.[23] SEM pictures demonstrated that pectin aerogels present some mesopores and small macropores. More homogeneous 3D networks were formed using ionic gelation, because of more regular crosslink points. Pectin aerogels can also have very low thermal conductivity (0.016-0.020 W/(m.K)) and strong mechanical properties (4-18 MPa).[58] Thanks to these interesting properties, pectin aerogels can be used as thermal insulators. Moreover, pectin aerogels are promising for biomedical applications. They can be used as scaffolds for nicotinic acid[59], curcumine[60] or theophylline[61] delivery.

2.4.4. Alginate aerogels

Alginate is a marine anionic polysaccharide, with 1,4-linked β-D-mannuronic (M) and α-L-guluronic (G) acids.[62] There are two conventional ways to gel alginate. It is usually crosslinked ionically with Ca^{2+} (as for pectin). Another method consists of decreasing the pH of the solution below the pKa values of alginate (3.4 and 3.6 for M and G units) to induce hydrogen bonds between chains.[63] The properties of alginate gels are mainly influenced by the G/M ratio and sequence, and the divalent cation content.[64] Solvent exchange and the subsequent $scCO_2$ drying of alginate gels and non-gelled solutions led to the formation of alginate aerogels. The total

volume shrinkage during aerogel preparation is around 60-90%.[65] Different shapes of alginate aerogels are reported in literature: monoliths, beads and microspheres.[45]

Varying the M/G ratio changes the aerogels properties. For example, aerogels with a higher specific surface area of 507 m^2/g were obtained upon increasing the percentage of G units from 20 % to 76 % in 2 % (w/v) alginate solution.[66] Alginate aerogels contain few macropores and mesopores.[67] The mesopores volume of alginate aerogels depends on the composition of the alginate. For instance, with the guluronate fractions of alginate, respectively, 20, 45 and 74%, the mesopore volumes were 0.25, 0.76 and 2.15 cm^3/g. Thanks to these properties, alginate aerogels can be used for many applications. Valentin et al.[68] developed the first alginate aerogels for catalysis. Alginate aerogels can also be used for drug release, for example, ibuprofen.[54] Alginate-hyaluronic acid aerogels were also developed for pulmonary drug delivery applications.[69]

2.4.5. Chitosan aerogels

Chitin is the second most abundant polymer on earth. It consists of repeating units of N-acetyl-D-glucosamine, linked by β-1,4 glycosidic bonds.[70] This polymer is found in crustacean shells (crabs, shrimps or lobsters) and also in fungi cell walls. The extraction of chitin from crustacean shells involves three steps: demineralization, deproteinization and decolorization. Chitin is biocompatible, non-toxic, biodegradable and antibacterial.

Chitosan can be obtained by deacetylation of chitin under alkaline treatment, at 80°C, under a nitrogen stream.[71] Deacetylation randomly removes acetyl groups of chitin and replaces them with amino groups (NH_2). The number of replaced acetyl groups is represented by the degree of deacetylation (DDA). DDA depends on NaOH concentration, the reaction temperature and time.[72] DDA is employed to differentiate chitin and chitosan: above 50%, the polymer is considered chitosan. Like chitin, chitosan contains β-1,4-linked D-glucosamine and N-acetyl-D-glucosamine repeating units. It is soluble in acids. In acidic medium, chitosan becomes a cationic polymer. Physical chitosan hydrogels were obtained by precipitation of acidic chitosan solutions in alkaline solutions such as diluted NaOH.[67] Washings with water were needed to remove NaOH from chitosan gels. The gelling properties of chitosan depend on the DDA and the source of chitin. Chitosan can also be crosslinked using formaldehyde[73] or sodium tripolyphosphate.[74] Gels undergo solvent exchange and $scCO_2$ drying to get chitosan aerogels. The overall volume shrinkage from hydrogel to aerogel state was around 40%.[75] Chitosan aerogels can be shaped in different forms as beads[76], microspheres[77] or monoliths[78].

The properties of chitosan aerogels were tuned by varying the concentration of chitosan and the NaOH coagulation bath.[75] An increase in NaOH concentration in the coagulation bath and in chitosan concentration slightly increased the aerogel density (values between 0.07-0.26 g/cm^3) and slightly increased specific surface area (200-270 m^2/g). A higher specific surface area, almost 500 m^2/g, was obtained for chitosan aerogels prepared using formaldehyde as crosslinker.[79] Chitosan aerogels showed a mesoporous structure.[78] Thanks to these properties, aerogels have a wide range of applications. Takeshita et al. demonstrated the super-insulating properties of crosslinked chitosan aerogels (W = 0.022 W/(m.K)).[73] A strong antibacterial effect of chitosan aerogels was demonstrated by Batista et al.[80] The release kinetics of dexamethasone from chitosan aerogels was also reported.[81] Chitosan aerogels may also promote wound healing, due to stimulation of collagen deposition.[80,82]

2.4.6. Hyaluronic acid aerogels

Only three articles report on the use of hyaluronic acid (HA) for the preparation of aerogels. Two describe alginate-HA aerogels microspheres as potential carriers for pulmonary drug delivery.[69,83] Microspheres were prepared from HA and alginate using an emulsion-gelation process, ionic crosslinking of alginate with calcium ions, and drying with $scCO_2$. HA-alginate aerogels had a low density (0.035−0.063 g/cm^3), a high porosity, and a microsphere diameter of 5 μm, which gave them good *in vitro* aerodynamic properties.

Recently, our group reported on crosslinker-free neat HA aerogels, prepared using non-solvent-induced phase separation, solvent exchange, and drying with $scCO_2$.[6] Various preparation conditions (pH of HA solution, polymer concentration, type of non-solvent) were tested, and only a few resulted in aerogels, i.e., materials with low density and high surface area. Even if several obtained materials were porous, aerogels resulted only from HA solutions of low pH, either 1.5 or 2.5. These aerogels had a high specific surface area (up to 510 m^2/g) and low density (as low as 0.057 g/cm^3).

3. Hyaluronic acid

3.1. Sources

Hyaluronic acid (also known as hyaluronate[84]) is a natural polysaccharide, occurring in the extracellular matrix (ECM) of human connective tissues that plays an important role in several biological processes such as wound healing and tissue regeneration.[85] HA was discovered by Meyer and Palmer, in 1934, in the vitreous humor of bovine eyes.[86] Human synovial joint fluids, cartilage and umbilical cord also contain HA, in high concentrations.[87]

HA is present in all connective tissues of vertebrates.[87] For example, rooster comb and shark skin have been used as sources of isolation of high molecular weight HA.[87] The extraction of HA was performed by precipitation in organic solvents such as ethanol or chloroform.[88] The fermentation of bacteria as Streptococcus zooepidemicus also produces HA, in higher quantities than what could be achieved with the extraction method.[88] Thus, various sources are available to produce HA with different molecular weights.

3.2. Hyaluronic acid structure

HA is a high molecular weight polymer, composed of a repeating disaccharide unit of β-1,3 D-glucuronic acid and β-1,4 N-acetyl-D-glucosamine, linked by glycosidic bonds (Figure 1.4).[88] HA belongs to the group of linear anionic polysaccharides, called glycosaminoglycans, found in the ECM.[85]

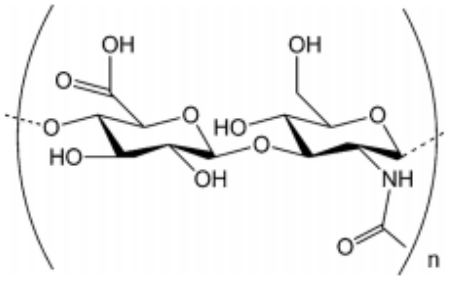

Figure 1.4. Chemical structure of HA.

HA can have up to 25 000 disaccharide unit repeats in length, with a molecular weight ranging from 5 to 20 000 kDa.[87] HA classification, according to its molecular weight, is presented in Table 1.1.[88]

Table 1.1. Classification of HA.

Oligosaccharide HA (o-HA)	< 10 kDa

Low molecular weight HA (LMW-HA)	10 – 250 kDa
Medium molecular weight HA (MMW-HA)	250 – 1000 kDa
High molecular weight (HMW-HA)	> 1000 kDa
Very high molecular weight HA (vHMW-HA)	> 6000 kDa

For example, HA is mainly present as vHMW-HA in articular synovial joints and the vitreous body, whereas blood, saliva, and urine contain LMW-HA. Tissues like cartilage and skin contain HMW-HA.

3.3. Hyaluronic acid properties

3.3.1. Physico-chemical properties

HA is soluble in water and insoluble in organic solvents such as ethanol, isopropanol alcohol (IPA) and acetone.[89] In solution, HA forms a highly hydrated polymeric network, stabilized by hydrogen bonds, depending on pH and if the concentration is sufficiently high.[90] At physiological conditions, HA has a stiffened random coil conformation.[90] The pK value of HA was found around 2.9, while it is 3.23 for the D-glucuronic unit.

Different affinities between HA and non-solvents are observed.[6] The use of a less polar non-solvent as acetone led to higher shrinkage of a HA network, as compared to ethanol. The reason is the higher affinity of HA toward ethanol compared to acetone, as determined from the Hansen solubility parameters (δ) of HA, ethanol, and acetone: 35.8, 26.5, and 19.9 $MPa^{1/2}$, respectively.

HA shows different conformations, depending on the non-solvent used. For example, smaller spherical HA nanoparticles (120 ± 12.14 nm) with lower polydispersity (0.27) were synthesized by precipitation, when acetone was used at 21°C in a glass reactor.[89] The use of IPA as non-solvent led to the formation of coils with larger sizes (421.98 ± 15.34 nm) and higher polydispersity (0.54).

Changes in pH or ionic strength (Na^+, K^+ or Ca^{2+}) in solution vary the HA degree of ionization, which, in turn, influences the interactions between HA chains, their shape and the rheological properties of HA solutions.[88] The influence of pH on HA solutions viscosity is shown in Figure 1.5.

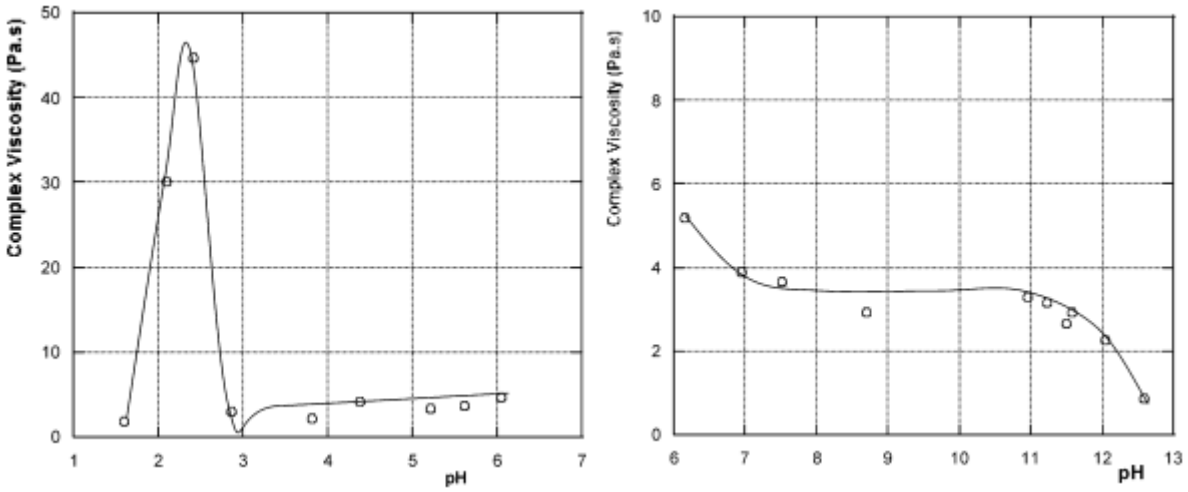

Figure 1.5. Complex viscosity of HA solutions as function of pH under acid (left) and basic (right) conditions. Reprinted with permission from[91]. Copyright (2005) American Chemical Society.

In acid conditions, for pH values at 1.6 and in the range of 2.86 up to 6.05, the viscosity of HA solutions remains unchanged.[91] A slight change in ionic concentration may result in a decrease of the net charge. At pH 2.5, the viscosity of HA solutions increases sharply. A gel-like structure is formed, because of cooperative interchain interactions. This corresponds to a critical balance of charges in the polymer. At this pH, the HA carboxylic groups are practically not dissociated (i.e. in -COOH form), which favors H-bonds formation. The protonation of the acetamido group (-NH-) giving a positive net charge able to complex with the negative charge of few -COOH may also explain this phenomenon. This effect can be interpreted in terms of an isoelectric point, located around pH 2.5.[91]

In basic conditions, with the addition of NaOH to the HA initial solution, viscosity decreases slightly up to pH 11.58, followed by a transition around pH 12.[91] This can be explained by a decrease of the molar mass of the HA backbone.

HA solutions exhibit a shear thinning behavior.[88] At high shear rates, HA chains align in the flow direction, resulting in a decrease in viscosity.

Elastic and viscous properties of HA solutions depend on HA molecular weight and concentration.[92] For example, by decreasing the HA solution concentration from 10 to 2 mg/L, for a constant HA molecular weight of 4.3 x 10^6 g/mol, the initial viscosity decreased from 400 000 to 30 mPas. The viscosity of 10 mg/mL HA solutions also decreased (from 400 000 to 400 mPas) with decreasing HA molecular weight (4.3 x 10^6 and 0.67 x 10^6 g/mol, respectively). Concerning the viscoelastic properties, at 0.01 Hz, a solution prepared with HA of 6 x 10^6 g/mol

behaves as an elastic body, while a solution prepared with HA of 0.75 x 10^6 g/mol remains viscous, even at high frequencies (10 Hz).

3.3.2. Biological properties

HA is synthesized by three synthases (HAS1, HAS2, HAS3) located at the plasma membrane and is extruded out of the cell into the ECM, where it interacts with constituents of the ECM to provide mechanical support.[93] HAS1 and HAS2 synthesize HMW-HA chains, while HAS3 produces shorter polymers (100–1000 kDa).

In the body, HA has a high turnover rate. For instance, the half-life of HA varies from less than a day in skin to 2–3 weeks in cartilage. HA can be degraded by enzymes, called hyaluronidases, such as Hyal1 or Hyal2.[93] Hyal2 is located at the cell surface and cleaves HMW HA into fragments of 20 kDa at pH 6–7, whereas Hyal1 is intracellular and cleaves, at low pH values (3.5-3.8), high or low MW HA into tetramers.

In addition to enzymatic degradation, HA can be fragmented by reactive oxygen species under stress conditions.[90] UV irradiation also reduces HA solution viscosity.[94] The HA molecular weight can be decreased by ultrasonication.[95] Hydrolytic degradation of HA in aqueous solution depends on pH and is attributed to chain scission.[57] HA is most stable at neutral pH and more sensitive to acidic conditions than to basic conditions. At high pH values, cleavage of HA is performed on the C_1 position of the N-acetylglucosamine unit, whereas acid hydrolysis occurs on the C_1, C_4 and carbonyl positions of the HA glucuronic acid. The degradation of HA increases with higher temperature and time of heating. Mondek et al.[96] demonstrated that a moderate HA molar mass decrease occurred at 60°C (3.7 % for a 1.6 MDa solution after 1 h), very similar to the decrease at 37°C, but very different from the molar mass reduction at 90°C (12% for a 1.6 MDa solution after 1h). Moreover, higher mass loss was recorded over time (for 1.67 MDa: 3% after 1 h vs 13.4% after 12 h). HA solutions are most stable at temperatures no higher than 25°C.[97] After 8 days, at room temperature, the HA molecular weight strongly decreased, because of the development of microorganisms.[98] Long term storage at 0 - 5°C improved the stability of HA solutions.

HA and its degraded fragments exhibit diverse biological functions that are manifested through interactions with different protein receptors including CD44 (cluster of differentiation 44) or RHAMM (receptor for hyaluronan mediated motility).[93] RHAMM is expressed on the cell surface and initiates several processes such as inflammation, angiogenesis and tissue repair.[99] CD44 is a transmembrane protein that regulates cell–cell and cell-matrix interactions, such as

cell proliferation and adhesion and lymphocyte activation. Both receptors simultaneously activate signaling pathways, regulating cell functions, tumor progression and metastasis, and especially wound healing.[93] During wound healing, HA initiates an inflammatory response, angiogenesis, and contributes to the recovery of the tissue from injury. Moreover, it facilitates cell detachment, migration, and proliferation. Its ability to promote tissue repair and wound healing depends on its molecular weight, tissue location and the specific cells with which it interacts. For example, low HA molecular weight fragments are inflammatory, immunostimulatory and pro-angiogenic, and they bind to HA receptors on cell surfaces.[93] Contrarily, HMW HA species are anti-angiogenic and immunosuppressive.

3.4. Strategies to reinforce HA materials

It is known that neat HA hydrogels have poor mechanical properties and may dissolve rapidly. Different strategies such as noncovalent crosslinking (H-bonding and hydrophobic interactions), covalent crosslinking of unfunctionalized or functionalized HA and mixing with other polymers, have been used to obtain a more stable material maintaining, at the same time, its biocompatibility and biodegradability.[90,100–103]

3.4.1. HA chemical modifications

The commonly used sites of chemical modifications are the carboxylic acid of the glucuronic acid unit and the hydroxyl group of the N-acetylglucosamine unit.[88] The hydroxyl group on HA can be modified using ether formation, ester formation, hemiacetal formation, and oxidation.[102] For example, HA hydroxyl groups can be functionalized with glycidyl methacrylate (GM), resulting in a GMHA conjugate with pendant methacrylate groups.[100] Many other chemical modifications such as esterification[104] or carbodiimide modification with hydrazides[100] can be performed on the HA carboxyl group.

3.4.2. Examples of covalent crosslinking

Before or after modifying HA, covalent crosslinking can occur. For example, the HA carboxyl group can be condensed with amino groups of adipic dihydrazide to form amide bonds. During crosslinking, 1-ethyl-3-(3-dimethylaminopropyl) carbodiimide hydrochloride (EDC) activates the HA carboxyl group in the presence of N-hydroxysuccinimide (NHS). Thiol groups can also be grafted onto HA carboxyl using hydrazides containing a disulfide bond.[105] The addition of thiolated HA derivatives to (meth)acrylate derivatives of polyethylene glycol forms crosslinked HA. Crosslinking using pyridyl disulfide derived HA and α,ω-thiolated PEG can also be carried out upon thiol-disulfide exchange reaction at pH 7.4.[106] Dimaleimide PEG acts as

crosslinker via Diels Alder reaction for furan-modified HA derivatives.[107] Enzymatic crosslinking can also be performed by adding hydrogen peroxide and horseradish peroxidase.[108] These reactions involve the carboxyl groups of HA, but crosslinking can also occur on the HA hydroxyl group. Kim et al.[109] employed the epoxide butanediol diglycidyl ether for the crosslinking of HA. Long HA chains can be crosslinked using divinylsulfone, using a simple and very fast process, which avoids organic solvents.[110] Tomihata et al.[111] used glutaraldehyde as crosslinker, under acidic conditions. Crosslinking of methacrylated HA can be performed upon exposure to UV light.[112]

3.4.3. Examples of mixing with other polymers

Instead of using chemical crosslinkers, some bio-based polymers have been used to reinforce the HA network, which may preserve the biocompatibility of the composites. In literature, the combination of HA and chitosan has recently raised interest for biomedical applications such as wound healing[113], vitreous substitute[114] or tissue engineering[115], thanks to the synergic effect in the properties of the final composite. The interesting properties of HA, (i.e. high-water absorption, promotion of cell proliferation and tissue regeneration) were combined with those of chitosan (i.e. good hemostatic and antibacterial properties). Interactions between the carboxylate group of HA and the amino groups on chitosan help to strengthen the resulting network. Hydrogels using modified chitosan or hyaluronic acid[113–115] were prepared through chemical crosslinking, or a third chemical was added with those two polymers.[116,117] Several chitosan-hyaluronic acid polyelectrolyte complexes were reported for biomedical applications, when neat HA and chitosan were mixed.[118–120] The carboxylate groups of HA interact with the free cationic NH_3^+ amino groups of chitosan through strong electrostatic interactions to form complexes. However, literature reports no hydrogel formation by simply mixing those two oppositely charged polymers.

Recently, due to their excellent mechanical properties and biocompatibility, an emerging class of materials from chitin attracts interest as reinforcing material: nanochitins (nanofibers and nanocrystals).[121] We will particularly focus on nanofibers as it will be used in the thesis to reinforce the HA network.

From deacetylated chitin, two types of nanochitin are produced: chitin nanofibers (nCh) and chitin nanocrystals (ChNC). Strong acid hydrolysis at high temperatures produces ChNC. This process selectively removes the disordered part of deacetylated chitin, leaving chitin crystallites intact.[122–124] The crystallites measure approximately 10-15 nm in width and 200-500 nm in

length. nCh fibers are obtained from mechanical treatment of deacetylated chitin under acidic conditions. The nanofibrillation process simultaneously keeps disordered (noncrystalline) and ordered (crystalline) regions of chitin and exposes amine groups of deacetylated chitin to positive charge.[125,126] The nCh fibers width ranges between few nm up to tens of nm and their length from submicrometers to micrometers. nCh fibers have not been yet commercialized, because the production process is still very long. nCh fibers differ from chitosan, due to the use of a mechanical treatment of deacetylated chitin under acidic conditions.

nCh fibers have unique properties such as a high aspect ratio and superior mechanical properties.[127] nCh fibers were prepared with aspect ratios larger than 60 and the Young's modulus of microfibers based on nCh fibers and alginate was around 4.5 GPa.[128] By increasing nCh fibers content, the Young's modulus of chitin macrofibers was increased to 12 GPa.[129] Films based on nCh fibers had a tensile strength of approximately 90 MPa.[130] nCh fibers are also biocompatible, biodegradable and non-toxic. They have very good antimicrobial properties, depending on the DDA and on pH.[131] Low pH and higher DDA improve the antibacterial properties. Concerning their morphology, the nCh fibers length was significantly decreased by increasing DDA.[131]

Thanks to these interesting properties, nCh fibers have already been used to prepare films[130], beads[132] and hydrogels[133,134]. Emerging applications of nCh fibers include the biomedical area, such as scaffolds for tissue engineering, antimicrobial materials, biosensors, and drug carriers.[135,136] Prolonged release and higher drug loading efficiency were obtained from nCh fibers-based drug systems in comparison with cellulose fibers, because of the smaller length of nCh fibers and the formation of a wider drug release channel (caused by electrostatic repulsions between amino groups of nCh fibers in acidic environments).[137] nCh fibers were also used to prepare hydrogels for wound dressing applications.[138,139] These hydrogels had high stability and good antibacterial properties. During wound healing, nCh fibers showed to initiate cell proliferation, stimulated macrophages and synthesis of HA at the wound site and influenced collagen deposition, thereby accelerating wound healing.

3.5. Biomedical applications of HA

3.5.1. Main applications

HA is biocompatible, biodegradable, non-immunogenic and bioactive.[140] Thanks to these properties as well as its physicochemical and biological properties, and due to the ease of chemical functionalization, HA is already used in several biomedical applications.[92] Clinically, it is used in ophthalmologic surgery to protect delicate eye tissues from mechanical damage by

surgical tools, to create space for surgical manipulation and as a substitute for the vitreous fluid loss during cataract surgery. HA is also used for supplementation of impaired synovial fluid in arthritic patients, in aesthetic medicine as dermal filler to fill facial wrinkles or as creams to rehydrate tissues and in soft tissue surgery for tissue augmentation, as scaffold for drug delivery and in tissue engineering. Finally, HA is employed as a diagnostic marker for many diseases including cancer, rheumatoid arthritis, and liver pathologies and as an early marker for impending rejection following organ transplantation.[110]

Currently, the use of HA for wound dressings is of interest, in view of its biocompatibility, biodegradability, non-immunogenicity and its biological functions. First, we will provide an overview of the characteristics of a wound, the wound healing process and the ideal wound dressing. In a second part, we will review HA-based materials that have been already developed as wound dressing.

3.5.2. Wounds and wound dressings

A wound is defined as a disruption of the skin resulting from physical, chemical or thermal damage.[141] According to the nature and the duration of healing, wounds are classified as acute or chronic. An acute wound occurs suddenly, due to an accident or a surgical injury. It usually heals within 8-12 weeks, depending on the size, the depth, and the extent of damage in the skin. Chronic wounds fail to heal in an orderly and timely manner. These wounds include leg ulcers, decubitus ulcers and burns.

Immediately after an injury, a cascade of physiological reactions is triggered to restore the integrity of the injured tissue.[142] Wound healing involves four overlapping phases: hemostasis, inflammation, proliferation and remodeling (Figure 1.6).

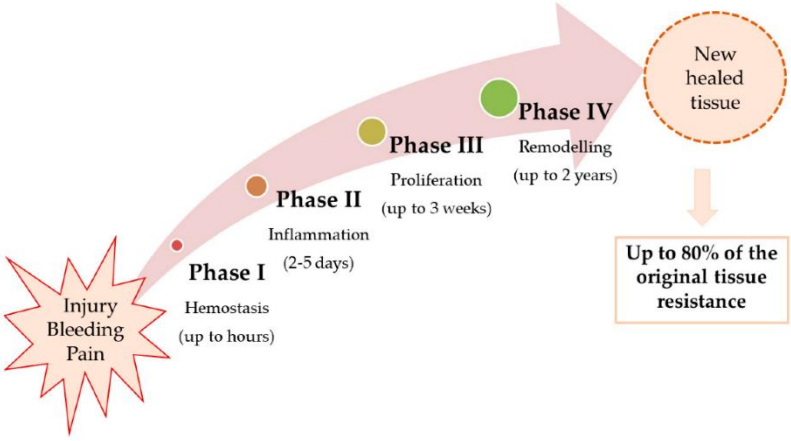

Figure 1.6. Different phases of wound healing. Reprinted with permission from[142].

After bleeding has stopped, the inflammatory phase starts immediately. This phase clears pathogens and foreign materials from the wound.[143] Vascular permeability increases with vasodilation, allowing inflammatory cells, the neutrophils and monocytes, to move to the wound site. Cytokines direct the monocyte conversion to macrophages, which further phagocytose and digest tissue debris and secrete growth factors that promote tissue proliferation and cell migration.

After about 2 days from the initial wound, the proliferative phase triggers granulation, contraction and epithelialization.[142] Meanwhile, epithelial cells proliferate and cover defects, collagen fibers reorganize, and the formation of new blood vessels (angiogenesis) occurs within the novel granulating tissue, creating a rich vascular network supplying this active area.

After about 3 weeks, the remodeling phase begins, where new collagen fibers are formed. The wound tissue matures, resulting in a scar. The remodeling phase can last up to 2 years.

Wound healing depends on the nature of the wound (its location, size, depth, and type) and is affected by several factors such as diabetes, blood pressure, obesity or medications.[143] Poor nutrition and age can prolong healing times. Healing is also influenced by external factors such temperature or moisture.

In 1962, Winter demonstrated that moist conditions promote wound healing.[144] Under these conditions, the wound does not dry and healing is more efficient. Wound dressings have been developed to protect wounds from infection and to promote healing by providing an optimal environment for wound closure.[141] More than 3000 wounds dressings are available to treat different types of wounds to treat all types of wounds from traumatic wounds to surgical wounds and chronic wounds (e.g. pressure sores or diabetic ulcers).[141] These dressings have various forms ranging from foams to hydrocolloids or hydrogels. The ideal wound dressing should offer a therapeutic solution and provide comfort to the patient. Thus, the dressing should[141]:

- Promote wound healing (assure a moist environment for the wound, maintain an appropriate tissue temperature, absorb wound exudate, stimulate tissue synthesis, protection against bacterial infection, promotion of O_2/CO_2 exchange and serve as drug carrier)
- Perfectly fit the wound morphology
- Have suitable mechanical properties (strong and flexible)
- Allow for proper and painless removal

- Be non-toxic and biocompatible

A wound dressing, including all the demands described above, does not exist yet. My project (3D-AER-HYAL project) aims to develop innovative HA-based materials with potential use as wound dressings.

3.5.3. HA for wound dressings

Thanks to its interesting properties, HA can be transformed into high value-added porous materials such as hydrogels, cryogels and, potentially, aerogels, for wound dressings. Several HA-based hydrogels promoting wound healing have been found in literature.[2] Hydrogels are 3D polymer networks containing large quantities of water. The highly hydrated porous network provides a moist environment promoting wound healing. However, hydrogels may have poor mechanical properties and bacteria can develop easily in hydrogels.

A collagen I/HA hydrogel promoting spontaneous healing was formed through coupling of phenol moieties of a collagen I-hydroxybenzoic acid derivative with a HA-tyramine derivative through the use of HRP.[145] It showed a porous surface suitable for gas, medium and nutrition exchange and important proliferation of human endothelial cells and fibroblasts.

A dopamine-functionalized HA hydrogel loaded with arginine was fabricated for wound healing application.[146] It showed a highly swelling 3D microporous structure with enhanced antioxidant properties.

An injectable chitosan/HA based hydrogel with metal organic framework (MOF)-loaded lipoic acid was developed for diabetic wound healing.[147] This promising hydrogel exhibited antibacterial activity and antioxidant performance, and promoted cell proliferation and migration. Improvement of granulation, tissue formation and collagen deposition was demonstrated with *in vivo* tests on diabetic rats.

Biocompatible carboxymethyl chitosan/HA hydrogels loaded with taurine were developed using Schiff base reaction to accelerate wound healing.[148] They had a short gelation time, promoted cell migration, inhibited inflammatory cells, and had self-healing performance. Anti-inflammatory activity and angiogenesis were provided by taurine. This hydrogel seems to be a promising dressing for chronic wounds, due to good results of *in vivo* tests performed on rats.

A 3D printed composite hydrogel based on collagen and hyaluronic acid loaded with silver nanoparticles was developed for chronic diabetic wound repair.[149] Crosslinking of

methacrylated recombinant human collagen with methacrylated HA occurred under UV irradiation. A 3D network with high porosity, good mechanical properties, good printability and biocompatibility was obtained. *In vivo* studies showed that the hydrogel enhanced tissue regeneration and collagen deposition.

Today, several HA-based wound dressings are commercially available such as Hyalofill, Hylase Wound Gel and Bionect.[2] Hylasponge and Laserskin are used to treat acute and chronic wounds, while Connettivina is recommended for the treatment of skin irritation.

Cryogels are freeze-dried hydrogels or solutions.[150] Freeze-drying is the sublimation of solvent crystals (ice in case of aqueous systems) from the pores of a precursor. Cryogels typically possess interconnected large macropores. It was demonstrated that HA is gelling upon freezing, thus HA can form "real" cryogels.[151] Literature reports that HA cryogels can be used for wound dressings thanks to their unique structure and their osmotic, chemical and mechanical stability. However, these materials do not yet exist commercially, due to the high energy consumption of the process.

For example, biocompatible and non-toxic poly(vinyl alcohol)/HA cryogels loaded with methotrexate were produced by freezing at −20 °C for 20 h to treat affected skin in psoriasis disease.[152] Cryogels had pH-responsive swelling and suitable drug release properties.

HA cryogels with genipin as non-cytotoxic crosslinking agent were produced as wound healing substrate by freezing at -20°C for 6 days.[153] Cryogels with a lamellar porous structure with a homogeneous pore size of ~100 µm showed a shear elasticity of ~2 kPa and a high swelling capacity in water, due to strong intermolecular bonds.

Gelatine/HA/cellulose nanocrystals cryogels were prepared for skin wound repair using EDC/NHS crosslinking and freeze-drying at -80°C.[154] These spongy cryogels, with a pore diameter of 80 – 120 µm, had a high swelling due to water-binding, which helped to provide necessary channels for transporting nutrition and waste and to promote cell viability and proliferation.

Shape recoverable and biocompatible cryogels based on HA and waterborne polyurethane promoted quick hemostasis and wound healing.[155] Cryogels were prepared at −20°C for 48 h. They absorbed a high amount of water and recovered rapidly to their original shape. The prominent hemostatic properties of the macroporous cryogels were found to promote angiogenesis and suppression of inflammation.

HA cryogels loaded with polydopamine for hemostasis and infectious wound repair were prepared using EDC/NHS crosslinking and cryogelation at -12°C for 48 h.[156] Macroporous cryogels had a high swelling ratio (> 4500%) and large macropores (50 to 140 µm), promoting wound healing. Cryogels had excellent mechanical strength and hemostatic, antioxidant and antibacterial properties.

Recently, novel nanostructured materials, bio-aerogels, attracted interest for wound dressing applications, due to their intrinsic properties such as low density (< 0.2 g/cm^3), high and open porosity (small macro- (d > 50 nm) and mesopores (2 nm < d < 50 nm)) and high specific surface area.[4] These unique properties potentially allow them to absorb a large amount of wound exudate, to promote gas exchange with the wound, to safely cover the wound without pain and to serve as matrix for the sustained release of therapeutic agents, thus helping wound healing.[5]

Bio-aerogels are prepared from natural and renewable polysaccharides via polymer dissolution, gelation and drying under supercritical CO_2, with no toxic compounds involved in the entire process. Furthermore, in the dry state, aerogels are more stable with respect to hydrogels, contamination during storage is avoided and their transport is facilitated, due to an extremely low density. Surprisingly, only a limited number of publications exist on HA-aerogels for biomedical applications (see Paragraph 2.4.6. Hyaluronic acid aerogels of this chapter), despite their tremendous potential. Only one article reports on neat HA aerogels, which offers the scientific challenge of further defining processing-structure-properties relationships.

4. Conclusions

This chapter provides an overview of literature related to aerogels, hyaluronic acid and its applications, as the goal of my work is to make hyaluronic acid aerogels.

First, the state of the art in polysaccharide-based aerogels was presented. Aerogels are obtained from a gel in which the liquid phase is replaced by gas, without collapsing the gel solid network, using supercritical conditions. Silica aerogels are the first generation of aerogels. Recently, novel nanostructured materials, bio-aerogels, based on polysaccharides have attracted attention, thanks to their biodegradability and non-toxicity; several of them showed biocompatibility. The properties and applications of the most common bio-aerogels were detailed.

Next, the main physico-chemical properties of hyaluronic acid were presented. HA is a natural polysaccharide present in the ECM of the skin; it plays crucial roles, especially during wound healing. For example, it initiates the inflammatory response, angiogenesis and contributes to the recovery of the injured tissue. Moreover, HA possesses special viscoelastic properties, which are tuned by HA concentration, molecular weight, the pH and the ionic strength of the solution. HA is characterized by its high hydrophilicity, biocompatibility and ability to be chemically modified through the hydroxyl and carboxyl groups. Thanks to all these properties, HA is already used in several biomedical applications, in particular, as wound dressings.

Wound healing is a dynamic and complex process, which restores the integrity of an injured tissue. Several wound dressings exist for different types of wounds to protect them from infection and promote healing. So far, several HA-based porous materials such as hydrogels and cryogels have been reported in literature as wound dressings. Novel nanostructured materials, aerogels, are promising materials for wound dressings. According to literature, only two articles reported on HA/alginate aerogels for biomedical applications, and only one article described the preparation of neat HA aerogels via non-solvent induced phase separation. To advance in the preparation of HA aerogels and to better understand processing-structure-properties relationships remain scientific challenges.

5. References

(1) Birajdar, M. S.; Joo, H.; Koh, W.-G.; Park, H. Natural Bio-Based Monomers for Biomedical Applications: A Review. *Biomaterials Research* **2021**, *25* (1), 8. https://doi.org/10.1186/s40824-021-00208-8.

(2) Graça, M. F. P.; Miguel, S. P.; Cabral, C. S. D.; Correia, I. J. Hyaluronic Acid—Based Wound Dressings: A Review. *Carbohydrate Polymers* **2020**, *241*, 116364. https://doi.org/10.1016/j.carbpol.2020.116364.

(3) *Aerogels Handbook*; Aegerter, M. A., Leventis, N., Koebel, M. M., Eds.; Springer New York: New York, NY, **2011**. https://doi.org/10.1007/978-1-4419-7589-8.

(4) Maleki, H.; Durães, L.; García-González, C. A.; Del Gaudio, P.; Portugal, A.; Mahmoudi, M. Synthesis and Biomedical Applications of Aerogels: Possibilities and Challenges. *Adv Colloid Interface Sci* **2016**, *236*, 1–27. https://doi.org/10.1016/j.cis.2016.05.011.

(5) Kistler, S. S. Coherent Expanded-Aerogels. *J. Phys. Chem.* **1932**, *36* (1), 52–64. https://doi.org/10.1021/j150331a003.

(6) Aguilera-Bulla, D.; Legay, L.; Buwalda, S. J.; Budtova, T. Crosslinker-Free Hyaluronic Acid Aerogels. *Biomacromolecules* **2022**, *23* (7), 2838–2845. https://doi.org/10.1021/acs.biomac.2c00207.

(7) Legay, L.; Budtova, T.; Buwalda, S. Hyaluronic Acid Aerogels Made Via Freeze–Thaw-Induced Gelation. *Biomacromolecules* **2023**, *24* (10), 4502–4509. https://doi.org/10.1021/acs.biomac.2c01518.

(8) *IUPAC Compendium of Chemical Terminology, 2nd Ed. (the "Gold Book").*; Compiled by McNaught, A.D. and Wilkinson, A. Blackwell Scientific Publications, Oxford (**1997**). XML on-line corrected version: http://goldbook.iupac.org (2006) created by Nic, M., Jirat, J. and Kosata, B.; updates Compiled by Jenkins, A., Ed.; 2014. https://doi.org/10.1351/goldbook.

(9) Gomollón-Bel, F. IUPAC Top Ten Emerging Technologies in Chemistry 2022: Discover the innovations that will transform energy, health, and materials science, to tackle the most urgent societal challenges and catalyse sustainable development. *Chemistry International* **2022**, *44* (4), 4–13. https://doi.org/10.1515/ci-2022-0402.

(10) Kistler, S. S. Coherent Expanded Aerogels and Jellies. *Nature* **1931**, *127* (3211), 741–741. https://doi.org/10.1038/127741a0.

(11) Kistler, S. S. Method of Making Aerogels. US2249767A, July 22, 1941. https://patents.google.com/patent/US2249767A/en (accessed 2023-12-14).

(12) Pekala, R. W. Organic Aerogels from the Polycondensation of Resorcinol with Formaldehyde. *J Mater Sci* **1989**, *24* (9), 3221–3227. https://doi.org/10.1007/BF01139044.

(13) Lemay, J. D.; Tillotson, T. M.; Hrubesh, L. W.; Pekala, R. W. Microstructural Dependence Of Aerogel Mechanical Properties. *MRS Online Proceedings Library* **1990**, *180* (1), 321. https://doi.org/10.1557/PROC-180-321.

(14) Pekala, R. W.; Alviso, C. T.; LeMay, J. D. Organic Aerogels: Microstructural Dependence of Mechanical Properties in Compression. *Journal of Non-Crystalline Solids* **1990**, *125* (1–2), 67–75. https://doi.org/10.1016/0022-3093(90)90324-F.

(15) Biesmans, G.; Randall, D.; Francais, E.; Perrut, M. Polyurethane-Based Organic Aerogels' Thermal Performance. *Journal of Non-Crystalline Solids* **1998**, *225*, 36–40. https://doi.org/10.1016/S0022-3093(98)00103-3.

(16) Meador, M. A. B.; Malow, E. J.; Silva, R.; Wright, S.; Quade, D.; Vivod, S. L.; Guo, H.; Guo, J.; Cakmak, M. Mechanically Strong, Flexible Polyimide Aerogels Cross-Linked with Aromatic Triamine. *ACS Appl Mater Interfaces* **2012**, *4* (2), 536–544. https://doi.org/10.1021/am2014635.

(17) Williams, J. C.; Meador, M. A. B.; McCorkle, L.; Mueller, C.; Wilmoth, N. Synthesis and Properties of Step-Growth Polyamide Aerogels Cross-Linked with Triacid Chlorides. *Chem. Mater.* **2014**, *26* (14), 4163–4171. https://doi.org/10.1021/cm5012313.

(18) Pajonk, G. M.; Elaloui, E.; Achard, P.; Chevalier, B.; Chevalier, J.-L.; Durant, M. Physical Properties of Silica Gels and Aerogels Prepared with New Polymeric Precursors. *Journal of Non-Crystalline Solids* **1995**, *186*, 1–8. https://doi.org/10.1016/0022-3093(95)00210-3.

(19) Pierre, A. C.; Pajonk, G. M. Chemistry of Aerogels and Their Applications. *Chem. Rev.* **2002**, *102* (11), 4243–4266. https://doi.org/10.1021/cr0101306.

(20) Schwertfeger, F.; Frank, D.; Schmidt, M. Hydrophobic Waterglass Based Aerogels without Solvent Exchange or Supercritical Drying. *Journal of Non-Crystalline Solids* **1998**, *225*, 24–29. https://doi.org/10.1016/S0022-3093(98)00102-1.

(21) Lu, X.; Arduini-Schuster, M. C.; Kuhn, J.; Nilsson, O.; Fricke, J.; Pekala, R. W. Thermal Conductivity of Monolithic Organic Aerogels. *Science* **1992**, *255* (5047), 971–972. https://doi.org/10.1126/science.255.5047.971.

(22) Budtova, T.; Lokki, T.; Malakooti, S.; Rege, A.; Lu, H.; Milow, B.; Vapaavuori, J.; Vivod, S. L. Acoustic Properties of Aerogels: Current Status and Prospects. *Advanced Engineering Materials* **2023**, *25* (6), 2201137. https://doi.org/10.1002/adem.202201137.

(23) Groult, S.; Budtova, T. Tuning Structure and Properties of Pectin Aerogels. *European Polymer Journal* **2018**, *108*, 250–261. https://doi.org/10.1016/j.eurpolymj.2018.08.048.

(24) Hitchen, S. M.; Dean, J. R. Properties of Supercritical Fluids. In *Applications of Supercritical Fluids in Industrial Analysis*; Dean, J. R., Ed.; Springer Netherlands: Dordrecht, **1993**; pp 1–11. https://doi.org/10.1007/978-94-011-2146-0_1.

(25) Brinker, C. J.; Scherer, G. W. *Sol-Gel Science: The Physics and Chemistry of Sol-Gel Processing*; Academic Press, **1990**.

(26) Schwertfeger, F.; Frank, D.; Schmidt, M. Hydrophobic Waterglass Based Aerogels without Solvent Exchange or Supercritical Drying. *Journal of Non Crystalline Solids* **1998**, *225*, 24–29. https://doi.org/10.1016/S0022-3093(98)00102-1.

(27) Druel, L.; Budtova, T. Aerogel-like (Low Density and High Surface Area) Cellulose Monoliths and Beads Obtained without Supercritical- or Freeze-Drying. *Cellulose* **2023**, *30*, 1–15. https://doi.org/10.1007/s10570-023-05349-8.

(28) Zou, F.; Budtova, T. Starch Alcogels, Aerogels, and Aerogel-like Xerogels: Adsorption and Release of Theophylline. *ACS Sustainable Chemistry & Engineering* **2023**, *11* (14), 5617–5625. https://doi.org/10.1021/acssuschemeng.2c07762.

(29) Borisova, A.; De Bruyn, M.; Budarin, V. L.; Shuttleworth, P. S.; Dodson, J. R.; Segatto, M. L.; Clark, J. H. A Sustainable Freeze-Drying Route to Porous Polysaccharides with

Tailored Hierarchical Meso- and Macroporosity. *Macromol Rapid Commun* **2015**, *36* (8), 774–779. https://doi.org/10.1002/marc.201400680.

(30) Wijmans, J. G.; Altena, F. W.; Smolders, C. A. Diffusion during the Immersion Precipitation Process. *Journal of Polymer Science: Polymer Physics Edition* **1984**, *22* (3), 519–524. https://doi.org/10.1002/pol.1984.180220313.

(31) Buchtová, N.; Budtova, T. Cellulose Aero-, Cryo- and Xerogels: Towards Understanding of Morphology Control. *Cellulose* **2016**, *23* (4), 2585–2595. https://doi.org/10.1007/s10570-016-0960-8.

(32) Aegerter, M. A.; Leventis, N.; Koebel, M.; III, S. A. S. *Springer Handbook of Aerogels*; Springer International Publishing, 2023.

(33) Heinze, T. Cellulose: Structure and Properties. In *Cellulose Chemistry and Properties: Fibers, Nanocelluloses and Advanced Materials*; Rojas, O. J., Ed.; Advances in Polymer Science; Springer International Publishing: Cham, **2016**; pp 1–52. https://doi.org/10.1007/12_2015_319.

(34) Roy, C.; Budtova, T.; Navard, P. Rheological Properties and Gelation of Aqueous Cellulose−NaOH Solutions. *Biomacromolecules* **2003**, *4* (2), 259–264. https://doi.org/10.1021/bm020100s.

(35) Ciolacu, D.; Rudaz, C.; Vasilescu, M.; Budtova, T. Physically and Chemically Cross-Linked Cellulose Cryogels: Structure, Properties and Application for Controlled Release. *Carbohydrate Polymers* **2016**, *151*, 392–400. https://doi.org/10.1016/j.carbpol.2016.05.084.

(36) Budtova, T. Cellulose II Aerogels: A Review. *Cellulose* **2019**, *26* (1), 81–121. https://doi.org/10.1007/s10570-018-2189-1.

(37) Gavillon, R.; Budtova, T. Aerocellulose: New Highly Porous Cellulose Prepared from Cellulose-NaOH Aqueous Solutions. *Biomacromolecules* **2008**, *9* (1), 269–277. https://doi.org/10.1021/bm700972k.

(38) Karadagli, I.; Schulz, B.; Schestakow, M.; Milow, B.; Gries, T.; Ratke, L. Production of Porous Cellulose Aerogel Fibers by an Extrusion Process. *Journal of Supercritical Fluids The* **2015**.

(39) Druel, L.; Niemeyer, P.; Milow, B.; Budtova, T. Rheology of Cellulose-[DBNH][CO2Et] Solutions and Shaping into Aerogel Beads. *Green Chem.* **2018**, *20* (17), 3993–4002. https://doi.org/10.1039/C8GC01189C.

(40) Pääkkö, M.; Vapaavuori, J.; Silvennoinen, R.; Kosonen, H.; Ankerfors, M.; Lindström, T.; Berglund, L. A.; Ikkala, O. Long and Entangled Native Cellulose I Nanofibers Allow Flexible Aerogels and Hierarchically Porous Templates for Functionalities. *Soft Matter* **2008**, *4* (12), 2492–2499. https://doi.org/10.1039/B810371B.

(41) Liebner, F.; Haimer, E.; Wendland, M.; Neouze, M.-A.; Schlufter, K.; Miethe, P.; Heinze, T.; Potthast, A.; Rosenau, T. Aerogels from Unaltered Bacterial Cellulose: Application of scCO2 Drying for the Preparation of Shaped, Ultra-Lightweight Cellulosic Aerogels. *Macromol Biosci* **2010**, *10* (4), 349–352. https://doi.org/10.1002/mabi.200900371.

(42) Fischer, F.; Rigacci, A.; Pirard, R.; Berthon-Fabry, S.; Achard, P. Cellulose-Based Aerogels. *Polymer* **2006**, *47* (22), 7636–7645. https://doi.org/10.1016/j.polymer.2006.09.004.

(43) Tripathi, A.; Parsons, G. N.; Rojas, O. J.; Khan, S. A. Featherlight, Mechanically Robust Cellulose Ester Aerogels for Environmental Remediation. *ACS Omega* **2017**, *2* (8), 4297–4305. https://doi.org/10.1021/acsomega.7b00571.

(44) Balakrishnan, P.; Chandradhara, D.; Poovathankandy, D.; Thomas, S. General Scenarios of Cellulose and Its Use in the Biomedical Field. *Materials Today Chemistry* **2019**, *13*, 59–78. https://doi.org/10.1016/j.mtchem.2019.04.012.

(45) García-González, C. A.; Alnaief, M.; Smirnova, I. Polysaccharide-Based Aerogels—Promising Biodegradable Carriers for Drug Delivery Systems. *Carbohydrate Polymers* **2011**, *86* (4), 1425–1438. https://doi.org/10.1016/j.carbpol.2011.06.066.

(46) Lavoine, N.; Bergström, L. Nanocellulose-Based Foams and Aerogels: Processing, Properties, and Applications. *J. Mater. Chem. A* **2017**, *5* (31), 16105–16117. https://doi.org/10.1039/C7TA02807E.

(47) Heath, L.; Thielemans, W. Cellulose Nanowhisker Aerogels. *Green Chem.* **2010**, *12* (8), 1448–1453. https://doi.org/10.1039/C0GC00035C.

(48) Kobayashi, Y.; Saito, T.; Isogai, A. Aerogels with 3D Ordered Nanofiber Skeletons of Liquid-Crystalline Nanocellulose Derivatives as Tough and Transparent Insulators. *Angewandte Chemie International Edition* **2014**, *53* (39), 10394–10397. https://doi.org/10.1002/anie.201405123.

(49) Zou, F.; Budtova, T. Tailoring the Morphology and Properties of Starch Aerogels and Cryogels via Starch Source and Process Parameter. *Carbohydrate Polymers* **2021**, *255*, 117344. https://doi.org/10.1016/j.carbpol.2020.117344.

(50) Druel, L.; Bardl, R.; Vorwerg, W.; Budtova, T. Starch Aerogels: A Member of the Family of Thermal Superinsulating Materials. *Biomacromolecules* **2017**, *18* (12), 4232–4239. https://doi.org/10.1021/acs.biomac.7b01272.

(51) García-González, C. A.; Uy, J. J.; Alnaief, M.; Smirnova, I. Preparation of Tailor-Made Starch-Based Aerogel Microspheres by the Emulsion-Gelation Method. *Carbohydrate Polymers* **2012**, *88* (4), 1378–1386. https://doi.org/10.1016/j.carbpol.2012.02.023.

(52) Kenar, J. A.; Eller, F. J.; Felker, F. C.; Jackson, M. A.; Fanta, G. F. Starch Aerogel Beads Obtained from Inclusion Complexes Prepared from High Amylose Starch and Sodium Palmitate. *Green Chem.* **2014**, *16* (4), 1921–1930. https://doi.org/10.1039/C3GC41895B.

(53) García-González, C. A.; Smirnova, I. Use of Supercritical Fluid Technology for the Production of Tailor-Made Aerogel Particles for Delivery Systems. *The Journal of Supercritical Fluids* **2013**, *79*, 152–158. https://doi.org/10.1016/j.supflu.2013.03.001.

(54) Mehling, T.; Smirnova, I.; Guenther, U.; Neubert, R. H. H. Polysaccharide-Based Aerogels as Drug Carriers. *Journal of Non-Crystalline Solids* **2009**, *355* (50), 2472–2479. https://doi.org/10.1016/j.jnoncrysol.2009.08.038.

(55) Grant, G. T.; Morris, E. R.; Rees, D. A.; Smith, P. J. C.; Thom, D. Biological Interactions between Polysaccharides and Divalent Cations: The Egg-Box Model. *FEBS Letters* **1973**, *32* (1), 195–198. https://doi.org/10.1016/0014-5793(73)80770-7.

(56) De Cicco, F.; Russo, P.; Reverchon, E.; García-González, C. A.; Aquino, R. P.; Del Gaudio, P. Prilling and Supercritical Drying: A Successful Duo to Produce Core-Shell Polysaccharide Aerogel Beads for Wound Healing. *Carbohydrate Polymers* **2016**, *147*, 482–489. https://doi.org/10.1016/j.carbpol.2016.04.031.

(57) García-González, C. A.; Carenza, E.; Zeng, M.; Smirnova, I.; Roig, A. Design of Biocompatible Magnetic Pectin Aerogel Monoliths and Microspheres. *RSC Adv.* **2012**, *2* (26), 9816–9823. https://doi.org/10.1039/C2RA21500D.

(58) Rudaz, C.; Courson, R.; Bonnet, L.; Calas-Etienne, S.; Sallée, H.; Budtova, T. Aeropectin: Fully Biomass-Based Mechanically Strong and Thermal Superinsulating Aerogel. *Biomacromolecules* **2014**, *15* (6), 2188–2195. https://doi.org/10.1021/bm500345u.

(59) Veronovski, A.; Tkalec, G.; Knez, Ž.; Novak, Z. Characterisation of Biodegradable Pectin Aerogels and Their Potential Use as Drug Carriers. *Carbohydr Polym* **2014**, *113*, 272–278. https://doi.org/10.1016/j.carbpol.2014.06.054.

(60) Pantić, M.; Horvat, G.; Knez, Ž.; Novak, Z. Preparation and Characterization of Chitosan-Coated Pectin Aerogels: Curcumin Case Study. *Molecules* **2020**, *25* (5), 1187. https://doi.org/10.3390/molecules25051187.

(61) Groult, S.; Buwalda, S.; Budtova, T. Tuning Bio-Aerogel Properties for Controlling Theophylline Delivery. Part 1: Pectin Aerogels. *Materials Science and Engineering: C* **2021**, *126*, 112148. https://doi.org/10.1016/j.msec.2021.112148.

(62) Smidsrød, O.; Draget, K. I. Alginate Gelation Technologies. In *Food Colloids*; Dickinson, E., Bergenståhl, B., Eds.; Woodhead Publishing Series in Food Science, Technology and Nutrition; Woodhead Publishing, **2004**; pp 279–293. https://doi.org/10.1533/9781845698263.5.279.

(63) Gurikov, P.; Smirnova, I. Non-Conventional Methods for Gelation of Alginate. *Gels* **2018**, *4* (1), 14. https://doi.org/10.3390/gels4010014.

(64) Ingar Draget, K.; Østgaard, K.; Smidsrød, O. Homogeneous Alginate Gels: A Technical Approach. *Carbohydrate Polymers* **1990**, *14* (2), 159–178. https://doi.org/10.1016/0144-8617(90)90028-Q.

(65) Subrahmanyam, R.; Gurikov, P.; Dieringer, P.; Sun, M.; Smirnova, I. On the Road to Biopolymer Aerogels—Dealing with the Solvent. *Gels* **2015**, *1* (2), 291–313. https://doi.org/10.3390/gels1020291.

(66) Valentin, R.; Molvinger, K.; Quignard, F.; Di Renzo, F. Methods to Analyse the Texture of Alginate Aerogel Microspheres. *Macromolecular Symposia* **2005**, *222* (1), 93–102. https://doi.org/10.1002/masy.200550410.

(67) Quignard, F.; Valentin, R.; Renzo, F. D. Aerogel Materials from Marine Polysaccharides. *New J. Chem.* **2008**, *32* (8), 1300–1310. https://doi.org/10.1039/B808218A.

(68) Valentin, R.; Molvinger, K.; Viton, C.; Domard, A.; Quignard, F. From Hydrocolloids to High Specific Surface Area Porous Supports for Catalysis. *Biomacromolecules* **2005**, *6* (5), 2785–2792. https://doi.org/10.1021/bm050264j.

(69) Athamneh, T.; Amin, A.; Benke, E.; Ambrus, R.; Leopold, C. S.; Gurikov, P.; Smirnova, I. Alginate and Hybrid Alginate-Hyaluronic Acid Aerogel Microspheres as Potential Carrier for Pulmonary Drug Delivery. *The Journal of Supercritical Fluids* **2019**, *150*, 49–55. https://doi.org/10.1016/j.supflu.2019.04.013.

(70) Rinaudo, M. Chitin and Chitosan: Properties and Applications. *Progress in Polymer Science* **2006**, *31* (7), 603–632. https://doi.org/10.1016/j.progpolymsci.2006.06.001.

(71) Kurita, K.; Tomita, K.; Tada, T.; Ishii, S.; Nishimura, S.-I.; Shimoda, K. Squid Chitin as a Potential Alternative Chitin Source: Deacetylation Behavior and Characteristic Properties.

Journal of Polymer Science Part A: Polymer Chemistry **1993**, *31* (2), 485–491. https://doi.org/10.1002/pola.1993.080310220.

(72) Yeul, V. S.; Rayalu, S. S. Unprecedented Chitin and Chitosan: A Chemical Overview. *J Polym Environ* **2013**, *21* (2), 606–614. https://doi.org/10.1007/s10924-012-0458-x.

(73) Takeshita, S.; Yoda, S. Chitosan Aerogels: Transparent, Flexible Thermal Insulators. *Chem. Mater.* **2015**, *27* (22), 7569–7572. https://doi.org/10.1021/acs.chemmater.5b03610.

(74) Obaidat, R. M.; Tashtoush, B. M.; Bayan, M. F.; Al Bustami, R. T.; Alnaief, M. Drying Using Supercritical Fluid Technology as a Potential Method for Preparation of Chitosan Aerogel Microparticles. *AAPS PharmSciTech* **2015**, *16* (6), 1235–1244. https://doi.org/10.1208/s12249-015-0312-2.

(75) Chartier, C.; Buwalda, S.; Van Den Berghe, H.; Nottelet, B.; Budtova, T. Tuning the Properties of Porous Chitosan: Aerogels and Cryogels. *International Journal of Biological Macromolecules* **2022**, *202*, 215–223. https://doi.org/10.1016/j.ijbiomac.2022.01.042.

(76) Gioia, C.; Ricci, A.; Bernardi, L.; Bourahla, K.; Tanchoux, N.; Robitzer, M.; Quignard, F. Chitosan Aerogel Beads as a Heterogeneous Organocatalyst for the Asymmetric Aldol Reaction in the Presence of Water: An Assessment of the Effect of Additives. *European Journal of Organic Chemistry* **2013**, *2013* (3), 588–594. https://doi.org/10.1002/ejoc.201201187.

(77) Kadib, A. E.; Molvinger, K.; Cacciaguerra, T.; Bousmina, M.; Brunel, D. Chitosan Templated Synthesis of Porous Metal Oxide Microspheres with Filamentary Nanostructures. *Microporous and Mesoporous Materials* **2011**, *142* (1), 301–307. https://doi.org/10.1016/j.micromeso.2010.12.012.

(78) Chang, X.; Chen, D.; Jiao, X. Chitosan-Based Aerogels with High Adsorption Performance. *J Phys Chem B* **2008**, *112* (26), 7721–7725. https://doi.org/10.1021/jp8011359.

(79) Takeshita, S.; Sadeghpour, A.; Malfait, W. J.; Konishi, A.; Otake, K.; Yoda, S. Formation of Nanofibrous Structure in Biopolymer Aerogel during Supercritical CO2 Processing: The Case of Chitosan Aerogel. *Biomacromolecules* **2019**, *20* (5), 2051–2057. https://doi.org/10.1021/acs.biomac.9b00246.

(80) Batista, M. P.; Gonçalves, V. S. S.; Gaspar, F. B.; Nogueira, I. D.; Matias, A. A.; Gurikov, P. Novel Alginate-Chitosan Aerogel Fibres for Potential Wound Healing Applications. *International Journal of Biological Macromolecules* **2020**, *156*, 773–782. https://doi.org/10.1016/j.ijbiomac.2020.04.089.

(81) Chartier, C.; Buwalda, S.; Ilochonwu, B. C.; Van Den Berghe, H.; Bethry, A.; Vermonden, T.; Viola, M.; Nottelet, B.; Budtova, T. Release Kinetics of Dexamethasone Phosphate from Porous Chitosan: Comparison of Aerogels and Cryogels. *Biomacromolecules* **2023**, *24* (10), 4494–4501. https://doi.org/10.1021/acs.biomac.2c01408.

(82) López-Iglesias, C.; Barros, J.; Ardao, I.; Monteiro, F. J.; Alvarez-Lorenzo, C.; Gómez-Amoza, J. L.; García-González, C. A. Vancomycin-Loaded Chitosan Aerogel Particles for Chronic Wound Applications. *Carbohydr Polym* **2019**, *204*, 223–231. https://doi.org/10.1016/j.carbpol.2018.10.012.

(83) Athamneh, T.; Amin, A.; Benke, E.; Ambrus, R.; Gurikov, P.; Smirnova, I.; Leopold, C. S. Pulmonary Drug Delivery with Aerogels: Engineering of Alginate and Alginate–Hyaluronic Acid Microspheres. *Pharmaceutical Development and Technology* **2021**, *26* (5), 509–521. https://doi.org/10.1080/10837450.2021.1888979.

(84) Laurent, T. C.; Fraser, J. R. E. Hyaluronan1. *The FASEB Journal* **1992**, *6* (7), 2397–2404. https://doi.org/10.1096/fasebj.6.7.1563592.

(85) Kogan, G.; Soltés, L.; Stern, R.; Gemeiner, P. Hyaluronic Acid: A Natural Biopolymer with a Broad Range of Biomedical and Industrial Applications. *Biotechnol Lett* **2007**, *29* (1), 17–25. https://doi.org/10.1007/s10529-006-9219-z.

(86) Meyer, K.; Palmer, J. W. THE POLYSACCHARIDE OF THE VITREOUS HUMOR. *Journal of Biological Chemistry* **1934**, *107* (3), 629–634. https://doi.org/10.1016/S0021-9258(18)75338-6.

(87) Longinotti, C. The Use of Hyaluronic Acid Based Dressings to Treat Burns: A Review. *Burn Trauma* **2014**, *2* (4), 162. https://doi.org/10.4103/2321-3868.142398.

(88) Tavianatou, A. G.; Caon, I.; Franchi, M.; Piperigkou, Z.; Galesso, D.; Karamanos, N. K. Hyaluronan: Molecular Size-Dependent Signaling and Biological Functions in Inflammation and Cancer. *The FEBS Journal* **2019**, *286* (15), 2883–2908. https://doi.org/10.1111/febs.14777.

(89) Bicudo, R. C. S.; Santana, M. H. A. Effects of Organic Solvents on Hyaluronic Acid Nanoparticles Obtained by Precipitation and Chemical Crosslinking. *j nanosci nanotechnol* **2012**, *12* (3), 2849–2857. https://doi.org/10.1166/jnn.2012.5814.

(90) Lapčík, L.; Lapčík, L.; De Smedt, S.; Demeester, J.; Chabreček, P. Hyaluronan: Preparation, Structure, Properties, and Applications. *Chem. Rev.* **1998**, *98* (8), 2663–2684. https://doi.org/10.1021/cr941199z.

(91) Gatej, I.; Popa, M.; Rinaudo, M. Role of the pH on Hyaluronan Behavior in Aqueous Solution. *Biomacromolecules* **2005**, *6* (1), 61–67. https://doi.org/10.1021/bm040050m.

(92) Balazs, E. A. Chapter 20 - Viscoelastic Properties of Hyaluronan and Its Therapeutic Use In *Chemistry and Biology of Hyaluronan*; Garg, H. G., Hales, C. A., Eds.; Elsevier Science Ltd: Oxford, **2004**; pp 415–455. https://doi.org/10.1016/B978-008044382-9/50051-0.

(93) Dicker, K. T.; Gurski, L. A.; Pradhan-Bhatt, S.; Witt, R. L.; Farach-Carson, M. C.; Jia, X. Hyaluronan: A Simple Polysaccharide with Diverse Biological Functions. *Acta Biomaterialia* **2014**, *10* (4), 1558–1570. https://doi.org/10.1016/j.actbio.2013.12.019.

(94) Balazs, E. A.; Laurent, T. C. Viscosity Function of Hyaluronic Acid as a Polyelectrolyte. *Journal of Polymer Science* **1951**, *6* (5), 665–667. https://doi.org/10.1002/pol.1951.120060517.

(95) Dřímalová, E.; Velebný, V.; Sasinková, V.; Hromádková, Z.; Ebringerová, A. Degradation of Hyaluronan by Ultrasonication in Comparison to Microwave and Conventional Heating. *Carbohydrate Polymers* **2005**, *61* (4), 420–426. https://doi.org/10.1016/j.carbpol.2005.05.035.

(96) Mondek, J.; Kalina, M.; Simulescu, V.; Pekař, M. Thermal Degradation of High Molar Mass Hyaluronan in Solution and in Powder; Comparison with BSA. *Polymer Degradation and Stability* **2015**, *120*, 107–113. https://doi.org/10.1016/j.polymdegradstab.2015.06.012.

(97) Lowry, K. M.; Beavers, E. M. Thermal Stability of Sodium Hyaluronate in Aqueous Solution. *Journal of Biomedical Materials Research* **1994**, *28* (10), 1239–1244. https://doi.org/10.1002/jbm.820281014.

(98) Simulescu, V.; Kalina, M.; Mondek, J.; Pekař, M. Long-Term Degradation Study of Hyaluronic Acid in Aqueous Solutions without Protection against Microorganisms.

Carbohydrate Polymers **2016**, *137*, 664–668. https://doi.org/10.1016/j.carbpol.2015.10.101.

(99) Cowman, M. K.; Turley, E. A. Functional Organization of Extracellular Hyaluronan, CD44, and RHAMM. *Proteoglycan Research* **2023**, *1* (2), e4. https://doi.org/10.1002/pgr2.4.

(100) Burdick, J. A.; Prestwich, G. D. Hyaluronic Acid Hydrogels for Biomedical Applications. *Adv. Mater.* **2011**, *23* (12), H41–H56. https://doi.org/10.1002/adma.201003963.

(101) Collins, M. N.; Birkinshaw, C. Hyaluronic Acid Based Scaffolds for Tissue Engineering—A Review. *Carbohydrate Polymers* **2013**, *92* (2), 1262–1279. https://doi.org/10.1016/j.carbpol.2012.10.028.

(102) Khunmanee, S.; Jeong, Y.; Park, H. Crosslinking Method of Hyaluronic-Based Hydrogel for Biomedical Applications. *J Tissue Eng* **2017**, *8*, 204173141772646. https://doi.org/10.1177/2041731417726464.

(103) Luo, Z.; Wang, yu; Xu, Y.; Wang, J.; Yu, Y. Modification and Crosslinking Strategies for Hyaluronic Acid-based Hydrogel Biomaterials. *Smart Medicine* **2023**. https://doi.org/10.1002/SMMD.20230029.

(104) Collins, M. N. Hyaluronic Acid Based Scaffolds for Tissue Engineering—A Review. *Carbohydrate Polymers* **2013**, 18.

(105) Zheng Shu, X.; Liu, Y.; Palumbo, F. S.; Luo, Y.; Prestwich, G. D. In Situ Crosslinkable Hyaluronan Hydrogels for Tissue Engineering. *Biomaterials* **2004**, *25* (7), 1339–1348. https://doi.org/10.1016/j.biomaterials.2003.08.014.

(106) Choh, S.-Y.; Cross, D.; Wang, C. Facile Synthesis and Characterization of Disulfide-Cross-Linked Hyaluronic Acid Hydrogels for Protein Delivery and Cell Encapsulation. *Biomacromolecules* **2011**, *12* (4), 1126–1136. https://doi.org/10.1021/bm101451k.

(107) Nimmo, C. M.; Owen, S. C.; Shoichet, M. S. Diels-Alder Click Cross-Linked Hyaluronic Acid Hydrogels for Tissue Engineering. *Biomacromolecules* **2011**, *12* (3), 824–830. https://doi.org/10.1021/bm101446k.

(108) Kim, K. S.; Park, S. J.; Yang, J.-A.; Jeon, J.-H.; Bhang, S. H.; Kim, B.-S.; Hahn, S. K. Injectable Hyaluronic Acid-Tyramine Hydrogels for the Treatment of Rheumatoid Arthritis. *Acta Biomater* **2011**, *7* (2), 666–674. https://doi.org/10.1016/j.actbio.2010.09.030.

(109) Yang, B.; Guo, X.; Zang, H.; Liu, J. Determination of Modification Degree in BDDE-Modified Hyaluronic Acid Hydrogel by SEC/MS. *Carbohydrate Polymers* **2015**, *131*, 233–239. https://doi.org/10.1016/j.carbpol.2015.05.050.

(110) Borzacchiello, A.; Russo, L.; Malle, B. M.; Schwach-Abdellaoui, K.; Ambrosio, L. Hyaluronic Acid Based Hydrogels for Regenerative Medicine Applications. *BioMed Research International* **2015**, *2015*, 1–12. https://doi.org/10.1155/2015/871218.

(111) Tomihata, K.; Ikada, Y. Crosslinking of Hyaluronic Acid with Glutaraldehyde. *Journal of Polymer Science Part A: Polymer Chemistry* **1997**, *35* (16), 3553–3559. https://doi.org/10.1002/(SICI)1099-0518(19971130)35:16<3553::AID-POLA22>3.0.CO;2-D.

(112) Eke, G.; Mangir, N.; Hasirci, N.; MacNeil, S.; Hasirci, V. Development of a UV Crosslinked Biodegradable Hydrogel Containing Adipose Derived Stem Cells to Promote

Vascularization for Skin Wounds and Tissue Engineering. *Biomaterials* **2017**, *129*, 188–198. https://doi.org/10.1016/j.biomaterials.2017.03.021.

(113) Weng, H.; Jia, W.; Li, M.; Chen, Z. New Injectable Chitosan-Hyaluronic Acid Based Hydrogels for Hemostasis and Wound Healing. *Carbohydrate Polymers* **2022**, *294*, 119767. https://doi.org/10.1016/j.carbpol.2022.119767.

(114) Wang, S.; Chi, J.; Jiang, Z.; Hu, H.; Yang, C.; Liu, W.; Han, B. A Self-Healing and Injectable Hydrogel Based on Water-Soluble Chitosan and Hyaluronic Acid for Vitreous Substitute. *Carbohydrate Polymers* **2021**, *256*, 117519. https://doi.org/10.1016/j.carbpol.2020.117519.

(115) Maiz-Fernández, S.; Pérez-Álvarez, L.; Silván, U.; Vilas-Vilela, J. L.; Lanceros-Mendez, S. Photocrosslinkable and Self-Healable Hydrogels of Chitosan and Hyaluronic Acid. *International Journal of Biological Macromolecules* **2022**, *216*, 291–302. https://doi.org/10.1016/j.ijbiomac.2022.07.004.

(116) Zhao, Y.; Liu, X.; Peng, X.; Zheng, Y.; Cheng, Z.; Sun, S.; Ding, Q.; Liu, W.; Ding, C. A Poloxamer/Hyaluronic Acid/Chitosan-Based Thermosensitive Hydrogel That Releases Dihydromyricetin to Promote Wound Healing. *Int J Biol Macromol* **2022**, *216*, 475–486. https://doi.org/10.1016/j.ijbiomac.2022.06.210.

(117) Zhang, W.; Jin, X.; Li, H.; Zhang, R.; Wu, C. Injectable and Body Temperature Sensitive Hydrogels Based on Chitosan and Hyaluronic Acid for pH Sensitive Drug Release. *Carbohydrate Polymers* **2018**, *186*, 82–90. https://doi.org/10.1016/j.carbpol.2018.01.008.

(118) Luo, Y.; Wang, Q. Recent Development of Chitosan-Based Polyelectrolyte Complexes with Natural Polysaccharides for Drug Delivery. *International Journal of Biological Macromolecules* **2014**, *64*, 353–367. https://doi.org/10.1016/j.ijbiomac.2013.12.017.

(119) Polexe, R. C.; Delair, T. Elaboration of Stable and Antibody Functionalized Positively Charged Colloids by Polyelectrolyte Complexation between Chitosan and Hyaluronic Acid. *Molecules* **2013**, *18* (7), 8563–8578. https://doi.org/10.3390/molecules18078563.

(120) Luppi, B.; Bigucci, F.; Mercolini, L.; Musenga, A.; Sorrenti, M.; Catenacci, L.; Zecchi, V. Novel Mucoadhesive Nasal Inserts Based on Chitosan/Hyaluronate Polyelectrolyte Complexes for Peptide and Protein Delivery. *J Pharm Pharmacol* **2009**, *61* (2), 151–157. https://doi.org/10.1211/jpp/61.02.0003.

(121) Joseph, B.; Mavelil Sam, R.; Balakrishnan, P.; J. Maria, H.; Gopi, S.; Volova, T.; C. M. Fernandes, S.; Thomas, S. Extraction of Nanochitin from Marine Resources and Fabrication of Polymer Nanocomposites: Recent Advances. *Polymers* **2020**, *12* (8), 1664. https://doi.org/10.3390/polym12081664.

(122) Bai, L.; Kämäräinen, T.; Xiang, W.; Majoinen, J.; Seitsonen, J.; Grande, R.; Huan, S.; Liu, L.; Fan, Y.; Rojas, O. J. Chirality from Cryo-Electron Tomograms of Nanocrystals Obtained by Lateral Disassembly and Surface Etching of Never-Dried Chitin. *ACS Nano* **2020**, *14* (6), 6921–6930. https://doi.org/10.1021/acsnano.0c01327.

(123) Goodrich, J. D.; Winter, W. T. α-Chitin Nanocrystals Prepared from Shrimp Shells and Their Specific Surface Area Measurement. *Biomacromolecules* **2007**, *8* (1), 252–257. https://doi.org/10.1021/bm0603589.

(124) Zeng, J.-B.; He, Y.-S.; Li, S.-L.; Wang, Y.-Z. Chitin Whiskers: An Overview. *Biomacromolecules* **2012**, *13* (1), 1–11. https://doi.org/10.1021/bm201564a.

(125) Zhu, Y.; Huan, S.; Bai, L.; Ketola, A.; Shi, X.; Zhang, X.; Ketoja, J. A.; Rojas, O. J. High Internal Phase Oil-in-Water Pickering Emulsions Stabilized by Chitin Nanofibrils: 3D

Structuring and Solid Foam. *ACS Appl Mater Interfaces* **2020**, *12* (9), 11240–11251. https://doi.org/10.1021/acsami.9b23430.

(126) Fan, Y.; Saito, T.; Isogai, A. Preparation of Chitin Nanofibers from Squid Pen Beta-Chitin by Simple Mechanical Treatment under Acid Conditions. *Biomacromolecules* **2008**, *9* (7), 1919–1923. https://doi.org/10.1021/bm800178b.

(127) Bai, L.; Liu, L.; Esquivel, M.; Tardy, B. L.; Huan, S.; Niu, X.; Liu, S.; Yang, G.; Fan, Y.; Rojas, O. J. Nanochitin: Chemistry, Structure, Assembly, and Applications. *Chem. Rev.* **2022**, acs.chemrev.2c00125. https://doi.org/10.1021/acs.chemrev.2c00125.

(128) Grande, R.; Bai, L.; Wang, L.; Xiang, W.; Ikkala, O.; Carvalho, A.; Rojas, O. Nanochitins of Varying Aspect Ratio and Properties of Microfibers Produced by Interfacial Complexation with Seaweed Alginate. *ACS Sustainable Chemistry & Engineering* **2019**. https://doi.org/10.1021/acssuschemeng.9b06099.

(129) Torres-Rendon, J. G.; Schacher, F. H.; Ifuku, S.; Walther, A. Mechanical Performance of Macrofibers of Cellulose and Chitin Nanofibrils Aligned by Wet-Stretching: A Critical Comparison. *Biomacromolecules* **2014**, *15* (7), 2709–2717. https://doi.org/10.1021/bm500566m.

(130) Zhang, Y.; Jiang, J.; Liu, L.; Zheng, K.; Yu, S.; Fan, Y. Preparation, Assessment, and Comparison of α-Chitin Nano-Fiber Films with Different Surface Charges. *Nanoscale Res Lett* **2015**, *10* (1), 226. https://doi.org/10.1186/s11671-015-0926-z.

(131) Xu, J.; Liu, L.; Yu, J.; Zou, Y.; Wang, Z.; Fan, Y. DDA (Degree of Deacetylation) and pH-Dependent Antibacterial Properties of Chitin Nanofibers against Escherichia Coli. *Cellulose* **2019**, *26* (4), 2279–2290. https://doi.org/10.1007/s10570-019-02287-2.

(132) Liu, L.; Lv, H.; Jiang, J.; Zheng, K.; Ye, W.; Wang, Z.; Fan, Y. Reinforced Chitosan Beads by Chitin Nanofibers for the Immobilization of β-Glucosidase. *RSC Adv.* **2015**, *5* (113), 93331–93336. https://doi.org/10.1039/C5RA14250D.

(133) Liu, L.; Wang, R.; Yu, J.; Jiang, J.; Zheng, K.; Hu, L.; Wang, Z.; Fan, Y. Robust Self-Standing Chitin Nanofiber/Nanowhisker Hydrogels with Designed Surface Charges and Ultralow Mass Content via Gas Phase Coagulation. *Biomacromolecules* **2016**, *17* (11), 3773–3781. https://doi.org/10.1021/acs.biomac.6b01278.

(134) Abe, K.; Ifuku, S.; Kawata, M.; Yano, H. Preparation of Tough Hydrogels Based on β-Chitin Nanofibers via NaOH Treatment. *Cellulose* **2014**, *21* (1), 535–540. https://doi.org/10.1007/s10570-013-0095-0.

(135) Azuma, K.; Ifuku, S.; Osaki, T.; Okamoto, Y.; Minami, S. Preparation and Biomedical Applications of Chitin and Chitosan Nanofibers. *J Biomed Nanotechnol* **2014**, *10* (10), 2891–2920. https://doi.org/10.1166/jbn.2014.1882.

(136) Ding, F.; Deng, H.; Du, Y.; Shi, X.; Wang, Q. Emerging Chitin and Chitosan Nanofibrous Materials for Biomedical Applications. *Nanoscale* **2014**, *6* (16), 9477–9493. https://doi.org/10.1039/C4NR02814G.

(137) Ma, H.; Yu, J.; Liu, L.; Fan, Y. An Optimized Preparation of Nanofiber Hydrogels Derived from Natural Carbohydrate Polymers and Their Drug Release Capacity under Different pH Surroundings. *Carbohydrate Polymers* **2021**, *265*, 118008. https://doi.org/10.1016/j.carbpol.2021.118008.

(138) Jayakumar, R.; Prabaharan, M.; Sudheesh Kumar, P. T.; Nair, S. V.; Tamura, H. Biomaterials Based on Chitin and Chitosan in Wound Dressing Applications. *Biotechnol Adv* **2011**, *29* (3), 322–337. https://doi.org/10.1016/j.biotechadv.2011.01.005.

(139) Singh, R.; Shitiz, K.; Singh, A. Chitin and Chitosan: Biopolymers for Wound Management. *Int Wound J* **2017**, *14* (6), 1276–1289. https://doi.org/10.1111/iwj.12797.

(140) Xu, X.; Jha, A. K.; Harrington, D. A.; Farach-Carson, M. C.; Jia, X. Hyaluronic Acid-Based Hydrogels: From a Natural Polysaccharide to Complex Networks. *Soft Matter* **2012**, *8* (12), 3280. https://doi.org/10.1039/c2sm06463d.

(141) Dhivya, S.; Padma, V. V.; Santhini, E. Wound Dressings – a Review. *BioMed* **2015**, *5* (4), 22. https://doi.org/10.7603/s40681-015-0022-9.

(142) Tatarusanu, S.-M.; Lupascu, F.-G.; Profire, B.-S.; Szilagyi, A.; Gardikiotis, I.; Iacob, A.-T.; Caluian, I.; Herciu, L.; Giscă, T.-C.; Baican, M.-C.; Crivoi, F.; Profire, L. Modern Approaches in Wounds Management. *Polymers* **2023**, *15* (17), 3648. https://doi.org/10.3390/polym15173648.

(143) Han, G.; Ceilley, R. Chronic Wound Healing: A Review of Current Management and Treatments. *Adv Ther* **2017**, *34* (3), 599–610. https://doi.org/10.1007/s12325-017-0478-y.

(144) Winter, G. D. Formation of the Scab and the Rate of Epithelization of Superficial Wounds in the Skin of the Young Domestic Pig. *Nature* **1962**, *193* (4812), 293–294. https://doi.org/10.1038/193293a0.

(145) Ying, H.; Zhou, J.; Wang, M.; Su, D.; Ma, Q.; Lv, G.; Chen, J. In Situ Formed Collagen-Hyaluronic Acid Hydrogel as Biomimetic Dressing for Promoting Spontaneous Wound Healing. *Materials Science and Engineering: C* **2019**, *101*, 487–498. https://doi.org/10.1016/j.msec.2019.03.093.

(146) Zhang, S.; Hou, J.; Yuan, Q.; Xin, P.; Cheng, H.; Gu, Z.; Wu, J. Arginine Derivatives Assist Dopamine-Hyaluronic Acid Hybrid Hydrogels to Have Enhanced Antioxidant Activity for Wound Healing. *Chemical Engineering Journal* **2020**, *392*, 123775. https://doi.org/10.1016/j.cej.2019.123775.

(147) Li, Q.; Liu, K.; Jiang, T.; Ren, S.; Kang, Y.; Li, W.; Yao, H.; Yang, X.; Dai, H.; Chen, Z. Injectable and Self-Healing Chitosan-Based Hydrogel with MOF-Loaded α-Lipoic Acid Promotes Diabetic Wound Healing. *Mater Sci Eng C Mater Biol Appl* **2021**, *131*, 112519. https://doi.org/10.1016/j.msec.2021.112519.

(148) Zhou, Z.; Zhang, X.; Xu, L.; Lu, H.; Chen, Y.; Wu, C.; Hu, P. A Self-Healing Hydrogel Based on Crosslinked Hyaluronic Acid and Chitosan to Facilitate Diabetic Wound Healing. *International Journal of Biological Macromolecules* **2022**, *220*, 326–336. https://doi.org/10.1016/j.ijbiomac.2022.08.076.

(149) Liang, M.; Dong, L.; Guo, Z.; Liu, L.; Fan, Z.; Wei, C.; Mi, S.; Sun, W. Collagen–Hyaluronic Acid Composite Hydrogels with Applications for Chronic Diabetic Wound Repair. *ACS Biomater. Sci. Eng.* **2023**, *9* (9), 5376–5388. https://doi.org/10.1021/acsbiomaterials.3c00695.

(150) Lozinsky, V. I.; Galaev, I. Yu.; Plieva, F. M.; Savina, I. N.; Jungvid, H.; Mattiasson, B. Polymeric Cryogels as Promising Materials of Biotechnological Interest. *Trends in Biotechnology* **2003**, *21* (10), 445–451. https://doi.org/10.1016/j.tibtech.2003.08.002.

(151) Cai, Z.; Zhang, F.; Wei, Y.; Zhang, H. Freeze–Thaw-Induced Gelation of Hyaluronan: Physical Cryostructuration Correlated with Intermolecular Associations and Molecular Conformation. *Macromolecules* **2017**, *50* (17), 6647–6658. https://doi.org/10.1021/acs.macromol.7b01264.

(152) Cheaburu Yilmaz, C.; Pamfil, D.; Vasile, C.; Bibire, N.; Lupuşoru, R.-V.; Zamfir, C.-L.; Lupuşoru, C. Toxicity, Biocompatibility, pH-Responsiveness and Methotrexate Release

from PVA/Hyaluronic Acid Cryogels for Psoriasis Therapy. *Polymers* **2017**, *9* (12), 123. https://doi.org/10.3390/polym9040123.

(153) Roether, J.; Oelschlaeger, C.; Willenbacher, N. Hyaluronic Acid Cryogels with Non-Cytotoxic Crosslinker Genipin. *Materials Letters: X* **2019**, *4*, 100027. https://doi.org/10.1016/j.mlblux.2019.100027.

(154) Yin, F.; Lin, L.; Zhan, S. Preparation and Properties of Cellulose Nanocrystals, Gelatin, Hyaluronic Acid Composite Hydrogel as Wound Dressing. *Journal of Biomaterials Science, Polymer Edition* **2019**, *30* (3), 190–201. https://doi.org/10.1080/09205063.2018.1558933.

(155) Wang, M.; Hu, J.; Ou, Y.; He, X.; Wang, Y.; Zou, C.; Jiang, Y.; Luo, F.; Lu, D.; Li, Z.; Li, J.; Tan, H. Shape-Recoverable Hyaluronic Acid–Waterborne Polyurethane Hybrid Cryogel Accelerates Hemostasis and Wound Healing. *ACS Appl. Mater. Interfaces* **2022**, *14* (15), 17093–17108. https://doi.org/10.1021/acsami.2c01310.

(156) Wang, C.; Liang, Y.; Huang, Y.; Li, M.; Guo, B. Porous Photothermal Antibacterial Antioxidant Dual–Crosslinked Cryogel Based on Hyaluronic Acid/ Polydopamine for Non-Compressible Hemostasis and Infectious Wound Repair. *Journal of Materials Science & Technology* **2022**, *121*, 207–219. https://doi.org/10.1016/j.jmst.2021.12.054.

Chapter 2. Materials and methods

1. Introduction

[English]

This chapter presents the materials and chemicals used in the work, the preparation of new materials and characterization methods of novel HA-based materials.

First, the starting raw materials, used during the PhD, are presented including HA, nanochitin fibers (nCh), solvents and other chemicals. Then, the protocols to prepare physically crosslinked HA aerogels via the freezing-thawing method, and chemically crosslinked HA aerogels, using cystamine as a cleavable crosslinker, are described. The two processes of HA hydrogels formation, solvent exchange and supercritical drying are explained. Thanks to their excellent mechanical properties and biocompatibility, nCh fibers (emerging materials) are used to reinforce neat HA.[1] The preparation method of capsules based on nCh fibers and HA are introduced.

In a second part, we detail the methods used to characterize the HA-based materials. We evaluate the physically and chemically crosslinked aerogel properties regarding volume shrinkage during the preparation steps, the aerogels bulk density, and their specific surface area. Then, the aerogel internal morphology is analyzed by SEM. We characterize the mechanical properties of physically crosslinked HA aerogels by uniaxial compression measurements. The stability of chemically and physically crosslinked HA aerogels upon exposure in PBS medium at pH 7.4 and in air are studied. We also test the cleavage of the disulfide bonds in the chemically crosslinked HA aerogel network by immersion in PBS containing a thiol reducing agent. nCh fibers are characterized regarding their morphology, degree of deacetylation and surface charge. We also analyze the HA-nCh capsule membrane morphology by optical microscopy and the complexation between HA and nCh by FTIR spectroscopy. The membrane solubility is tested in different media. Finally, we incorporate model drug (either methylene blue or fluorescein isothiocyanate-dextran) in the capsule and the kinetics release is studied.

[Français]

Ce chapitre présente les matériaux et les produits chimiques utilisés lors du doctorat, le protocole de préparation des nouveaux matériaux à base d'acide hyaluronique et les méthodes de caractérisation de ces matériaux.

Tout d'abord, les matières premières sont présentées incluant l'acide hyaluronique, les fibres de nanochitin (nCh), les solvants et d'autres produits chimiques utilisés. Ensuite, les

protocoles de préparation des aérogels réticulés physiquement via la méthode de « congélation-décongélation » et des aérogels réticulés chimiquement, en utilisant la cystamine comme agent réticulant clivable, sont décrits. Les deux procédés menant à la formation d'hydrogels d'acide hyaluronique, suivi par un échange de solvant et un séchage supercritique sont détaillés. Grâce à leurs excellentes propriétés mécaniques et leur biocompatibilité, les fibres nCh (matériaux émergeants) sont utilisées pour renforcer l'acide hyaluronique.[1] La méthode de préparation des capsules à base des fibres nCh et d'acide hyaluronique est introduite.

Dans une seconde partie, nous détaillons les méthodes utilisées pour caractériser les matériaux à base d'acide hyaluronique. Nous évaluons ensuite les propriétés des aérogels réticulés physiquement et chimiquement en fonction du rétrécissement du volume lors des différentes étapes de préparation, leur densité et leur surface spécifique. La morphologie interne des aérogels est analysée par MEB. Nous caractérisons les propriétés mécaniques des aérogels réticulés physiquement par des essais de compression uniaxiale. La stabilité des aérogels réticulés physiquement et chimiquement sont étudiées dans un milieu PBS à pH 7.4 et dans l'air. Nous testons aussi le clivage de la liaison disulfide dans le réseau d'acide hyaluronique réticulé chimiquement lors de l'immersion dans le PBS contenant un agent réducteur thiolé. Les fibres de nanochitin (nCh) sont caractérisées selon leur morphologie, leur degré de déacétylation et leur charge en surface. Nous analysons également la morphologie de la membrane de la capsule HA-nCh par microscopie optique et la complexation entre HA et nCh par spectroscopie FTIR. La solubilité de la membrane est testée dans différents milieux. Finalement, nous avons incorporé une substance active (le bleu de méthylène ou le fluorescein isothiocyanate-dextrane) dans la capsule et suivi la cinétique de libération de ces composés.

2. Starting materials

2.1. Hyaluronic acid (HA)

Hyaluronic acid (purity 95%, M_w 1.5-2.2 × 10^6 Da, as stated by the manufacturer) was purchased from Acros Organics. It was in the form of sodium salt and originated from bacterial fermentation. Its molecular weight was determined using viscometry measurements, as detailed in Section 4.1. Viscometry.

2.2. Nanochitin fibers (nCh)

nCh were prepared at the BioProducts Institute, University of British Columbia (Vancouver, Canada) as described previously.[2] In brief, chitin extracted from crab shell was partially deacetylated by alkaline treatment using 35 wt% NaOH at 90°C for 4 h. nCh fibers were prepared from deacetylated chitin by mechanical treatment, using a high pressure homogenizer at 500 bar for 4 cycles, under acidic conditions (i.e. in 1 wt% acetic acid).

2.3. Solvents and other chemicals

Absolute ethanol (purity ≥ 99%) and acetone (≥ 99%) from Fisher Chemical were used as non-solvents for solvent exchange during HA aerogels preparation.

Hydrochloric acid, from Fisher Chemical (32%, analytical grade) and from Sigma-Aldrich (37%, ACS reagent) were used to prepare 0.05 and 1 M HCl solution.

Sodium hydroxide pellets (≥ 97%, analytical grade) from Fisher Chemical were used to prepare 0.05 and 1 M NaOH solution.

Sodium chloride (NaCl, ≥ 99%), potassium chloride (KCl, ≥ 99%) and monopotassium phosphate (KH_2PO_4, ≥ 99%) were from Fisher Chemical. Disodium phosphate (Na_2HPO_4, 98+%) was from Alfa Aesar. These 4 salts were used to prepare phosphate buffered saline (PBS) solution (1X or 0.01 M, pH 7.4).

Cystamine dihydrochloride (97+%), used as crosslinker during the preparation of chemically crosslinked HA aerogels, was from Alfa Aesar.

1-ethyl-3-(3-dimethylaminopropyl) carbodiimide hydrochloride (EDC, 98+%), from Acros Organics, was used to activate the carboxylic groups of HA with N-hydroxysuccinimide (NHS, ≥ 99%), purchased from ThermoScientific, during the preparation of chemically crosslinked HA aerogels.

1,4-dithioerythreitol (DTT, 98+%), a thiol reducing agent purchased from Alfa Aesar, was used to reduce disulfide bonds in chemically crosslinked aerogel networks.

Methylene blue (MB, ≥ 97%) hydrate and fluorescein isothiocyanate-dextran (FITC-dextran 2000 kDa, purity was not stated by the manufacturer) from Sigma Aldrich were used as model drugs in HA-nCh capsules.

Glacial acetic acid (≥ 99%) was from Fisher Scientific. Ammonium chloride (NH_4Cl, ≥ 99.5%) and urea (≥ 99%) were from Sigma Aldrich. Water was distilled.

All materials described above were used as received.

3. Methods

3.1. Preparation of physically crosslinked hyaluronic acid dry materials

3.1.1. Preparation of HA hydrogels using freezing-thawing method

HA solutions were prepared by dissolving HA powder in distilled water at 1 or 1.6 wt%, under mechanical stirring overnight at room temperature. After complete dissolution, the solution pH, initially around 7, was adjusted to 1.5, 2.5 and 7.4 by drop-wise addition of 1M HCl or 1M NaOH. Then, HA solutions (13 g) were poured in cylindrical molds of 27.5 mm in diameter and centrifuged for 40 min at 6000 rpm to eliminate bubbles.

Physical gels of HA were made via freezing-thawing (FT) cycles, as follows (Figure 2.1): HA solutions were frozen at -18°C for 1 day and then thawed at room temperature for 2 h; FT cycles were performed 1 or 3 times. The number of FT cycles was selected as a compromise between checking the influence of FT cycles on the properties of dry HA materials and limiting the experimental time and energy consumption that is associated with a higher number of FT cycles. Of notice, no significant difference in gel characteristics obtained after 3 and 4 FT cycles was reported.[3]

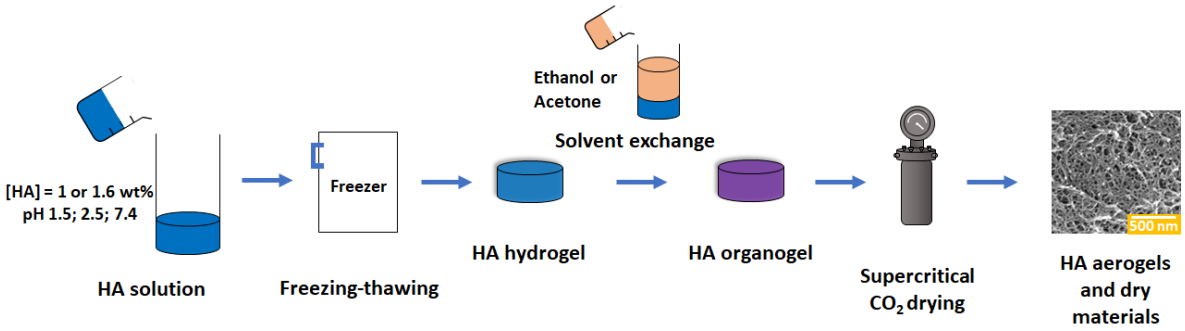

Figure 2.1. Schematic representation of the preparation of HA hydrogels via the freeze-thaw technique. Reprinted with permission from[4]. Copyright (2023) American Chemical Society.

3.1.2. Solvent exchange

To perform drying with supercritical CO_2, water must be replaced by a fluid miscible with CO_2. Ethanol or acetone was used. Ethanol and acetone are HA non-solvents and HA coagulates, forming a 3D network. The coagulated sample was washed in pure ethanol or acetone (100%), at least 6 times (twice a day), to ensure a complete replacement of water by ethanol or acetone. Volumes of non-solvent added, to ensure a complete replacement of water, were 25 mL, 26 mL, 30 mL, 30 mL, 38 mL and 7 times 100 mL. Pure non-solvent was added on HA hydrogel

because, when incremental non-solvent exchange was performed (i.e. subsequent use of water/non-solvent mixtures with vol%/vol% ratio of 90/10, 70/30, 50/50, 30/70, 10/90 and 0/100), HA was dissolving at low non-solvent concentrations in the mixture non-solvent:water. In contrast, upon the addition of pure non-solvent (i.e. 100% of acetone or ethanol), no HA was dissolved, and cylindrical samples were obtained, as expected. After complete solvent exchange, the samples obtained in ethanol and acetone, organogels, were precursors for $scCO_2$ drying (Figure 2.1).

3.1.3. Drying with supercritical CO_2

HA organogels were dried with $scCO_2$ to obtain HA dry materials, including aerogels, as described previously.[5–8] Drying was performed in the laboratory of PERSEE, MINES Paris. We gratefully acknowledge their help. Briefly, organogels were placed in a 1 L autoclave with an excess of non-solvent (acetone or ethanol). The system was pressurized under CO_2 at 50 bar and 37°C to purge progressively the non-solvent. Then, the pressure was increased to 80 bar to reach $scCO_2$ conditions; at the same time $scCO_2$ solubilizes the residual solvent inside sample pores. The system was kept at 80 bar and 37°C for 1 h with an output of 5 kg of CO_2/h to perform a dynamic washing and remove the remaining non-solvent from the precursors. Afterwards, the system was left in a static mode for 1-2 h at the same conditions and another dynamic washing step for 2 h was launched to completely remove the non-solvent. The system was depressurized at 4 bar/h at 37°C. After reaching room temperature and pressure, the autoclave was opened, the HA dry materials were collected and kept in a desiccator to protect them against moisture, as HA is highly hydrophilic, and characterization was performed quickly after $scCO_2$ drying.

3.1.4. Formulations tested

Four preparation conditions were varied to investigate their influence on the resulting HA materials: the pH of the starting HA solution (1.5, 2.5 or 7.4), the HA concentration of the starting solution (1.0 or 1.6 wt%), the number of FT cycles (1 or 3) and the fluid used during solvent exchange (ethanol or acetone). Although this leads in theory to 24 potential formulations, in view of efficiency, only 12 formulations were tested, which allows for the determination of the influence of each individual preparation parameter. An overview of the tested formulations is given in Table 3.4 – Chapter 3.

3.2. Chemically crosslinked HA aerogels

3.2.1. Preparation of HA hydrogels

Chemically crosslinked HA hydrogels were prepared via reaction between the carboxylic acid groups of HA with the amine groups of cystamine dihydrochloride, the latter acting as crosslinker. This reaction was catalyzed by two coupling agents: N-hydroxysuccinimide (NHS) and 1-ethyl-3-(3-dimethylaminopropyl) carbodiimide (EDC).

In total, 17 different hydrogel protocols were tested, inspired by what is known in literature.[9–13] The parameters that were varied include the method to remove bubbles, the conditions to induce gelation and the inclusion of an immersion step or not in a buffer solution at pH 2.5. The reaction conditions for each protocol, together with the resulting formulation properties, characterized visually and by tilting (a weak gel or a solution or a robust hydrogel, presence of bubbles or not), are presented in Annex 1 of this manuscript.

A hydrogel, which is not moving from the bottom of the plastic vial when tilted, and with practically no bubbles, was obtained with protocol n°17, which is detailed below.

3.2.2. Formulations tested

Using protocol n°17, three different HA concentrations (0.7, 1 or 1.6 wt%) and four molar ratios between the carboxyl of HA and amino groups of cystamine (3:1, 2:1, 1.3:1 and 1:1) were used. The COOH:EDC molar ratio (1:1.5) and the COOH:NHS molar ratio (1:1.5) were kept constant. Although this leads in theory to 12 potential formulations, in view of efficiency, only 6 formulations were tested. An overview of the tested formulations is given in Table 4.1 – Chapter 4.

An example of a detailed synthesis procedure of 1.6 wt% HA hydrogel, prepared with 2:1 as $COOH:NH_2$ molar ratio, 1:1.5 as COOH:EDC molar ratio and 1:1.5 as COOH:NHS molar ratio (i.e. Formulation "1.6-$COOH:NH_2$ 2:1" – in Chapter 4), is as follows. First of all, HA solution was prepared by dissolving 0.1 g of HA powder at 1.6 wt% in 5.65 mL of distilled water under mechanical stirring overnight. After complete HA dissolution, EDC and NHS were added (61.5 mg and 45.5 mg, respectively, each in 0.3 mL of water). 1.6 wt% HA was calculated taking in account water present in EDC and NHS addition. To this mixture, cystamine (14.8 mg) was added in powder form. The mixture was stirred for 5 min at 220 rpm at room temperature and centrifugated at 6000 rpm for 5 min to remove bubbles. The vial was incubated at 37°C for 24 h to for gelation (Figure 2.2). The total volume of water in the hydrogel was 6.25 mL.

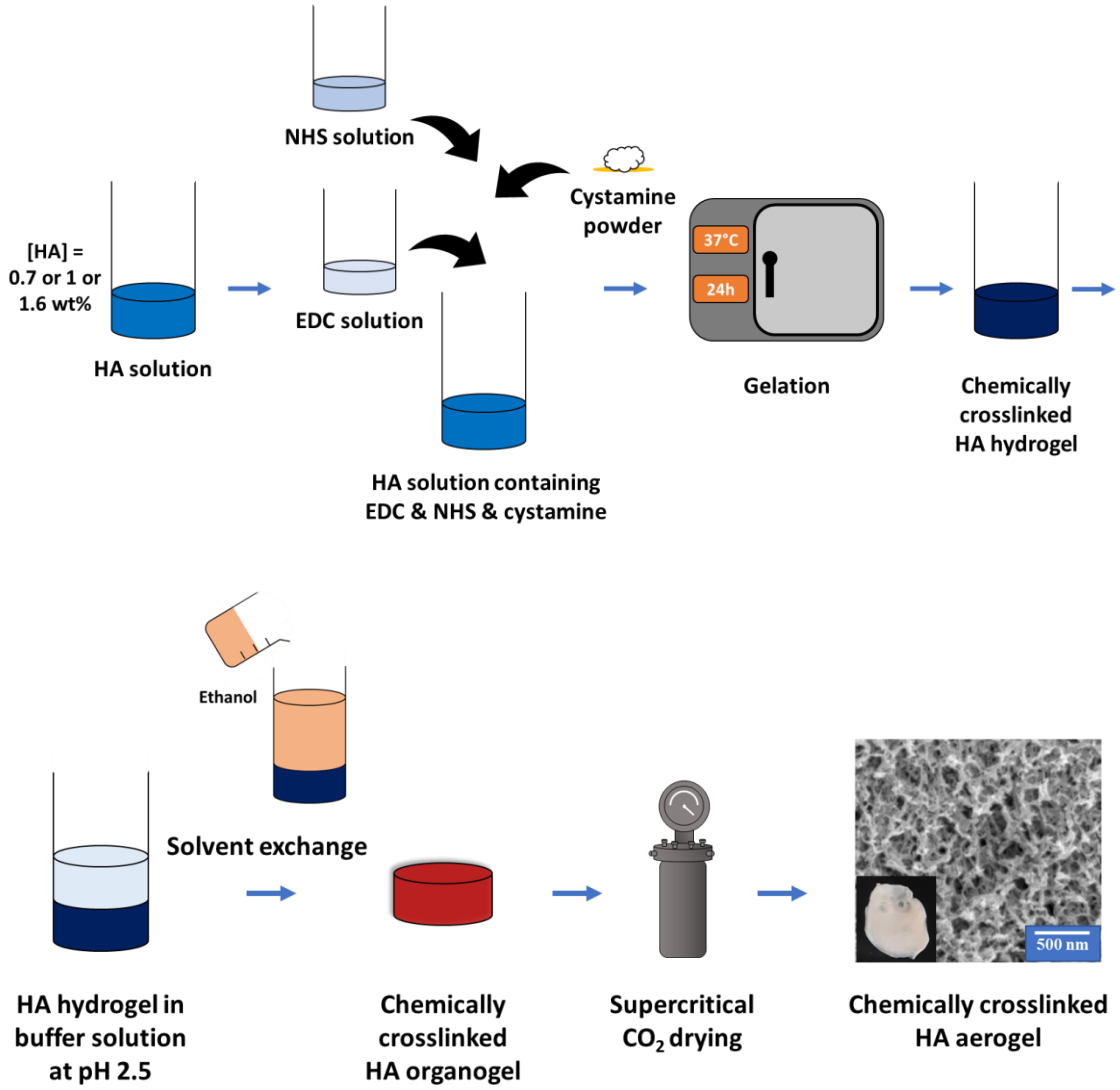

Figure 2.2. Schematic representation of the preparation of HA hydrogels using cystamine as crosslinker.

During the reaction of EDC and NHS activating the HA carboxyl group, CO_2 bubbles were generated inside the hydrogel network. We used centrifugation to try to remove bubbles. Several centrifugation times and speeds were tested (see Annex 1 of this manuscript for the experimental procedures that were attempted to obtain HA materials without bubbles). Centrifugation for 25 min at 6000 rpm and for 25 min at 9000 rpm was chosen to remove as many bubbles as possible. However, some air bubbles remained entrapped in the gel network and were impossible to remove.

The first screening of different formulations showed that when HA solution before crosslinking was at pH 1.5 or 7.4, the materials obtained after supercritical drying were either not self-standing or with low specific surface area. As it will be shown in Chapter 3, aerogels

with the highest specific surface areas were obtained when the starting HA solution was at pH 2.5.[4] Thus, after centrifugation of the chemically crosslinked hydrogels, 20 mL of a buffer solution at pH 2.5 was added on the top of the hydrogel (volume 6.25 mL) for one night (Figure 2.2). During this step, nothing happened to hydrogel (for example, no hydrogel dissolution or swelling occurred).

3.2.3. Solvent exchange

To perform drying with $scCO_2$, water present in the hydrogel was replaced by ethanol, which is miscible with CO_2. Ethanol was poured on the top of hydrogel, thereby inducing HA coagulation. After 8 h, the non-solvent was removed and replaced by a fresh one. The procedure was repeated four times to achieve a complete replacement of water with ethanol. Volumes of non-solvent used were 30 mL, 30 mL, 35 mL and 35 mL. The solubility of EDC and NHS was, previously, tested in ethanol. As EDC and NHS are soluble in ethanol, solvent exchange allowed for removal of these products from the sample. The resulting samples, organogels, were used as precursors for $scCO_2$ drying.

To summarize, before $scCO_2$ drying, we used two «washing» steps:

- Addition of a buffer solution at pH 2.5
- Solvent exchange with ethanol to get an organogel

3.2.4. Drying with $scCO_2$

HA organogels were dried with $scCO_2$ to obtain chemically crosslinked HA aerogels, as described in Section 3.1.3 – Chapter 2.

3.3. HA-nCh capsules

3.3.1. Preparation of capsules

We prepared 0.5 wt% HA solution and 0.1 wt% nCh suspension. HA-nCh capsules were formed by injection of one aqueous phase into the other with a plastic pipette (Figure 2.3). Either 0.5 wt% HA solution was injected in 0.1 wt% nCh suspension (Figure 2.3 (a)), or 0.1 wt% nCh suspension was introduced to 0.5 wt% HA solution (Figure 2.3 (b)).

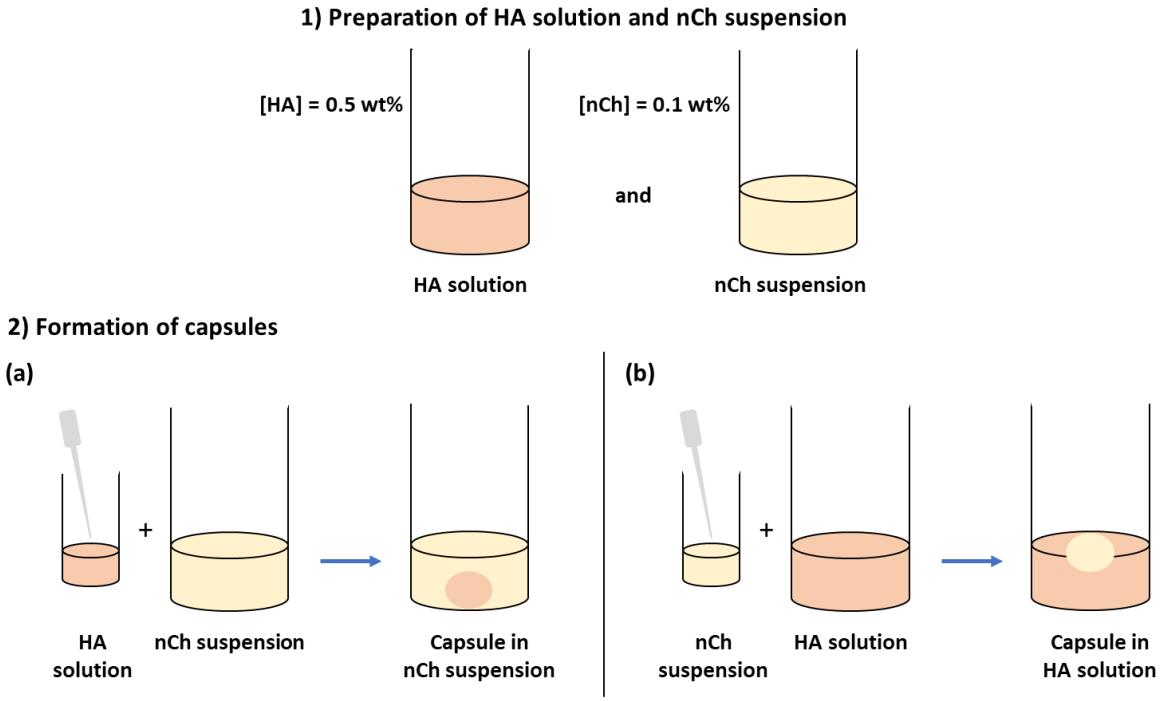

Figure 2.3. Scheme representing the preparation of HA-nCh capsules using 0.5 wt% HA solution and 0.1 wt% nCh suspension.

3.3.2. Preparation of model drug loaded HA-nCh capsules

Model drug, (i) 0.2 g/L of methylene blue (MB) or fluorescein isothiocyanate-dextran (FITC-dextran) and (ii) 2 g/L of FITC-dextran, was dissolved in 0.5 wt% HA solution. Then, 0.5 mL of HA-model drug solution was injected in 10 mL of 0.1 wt% nCh suspension to form the capsule. The model drug loaded capsule was transferred to 80 mL of PBS at pH 7.4 and the drug release was studied via spectrophotometric measurements (see Section 4.15 Model drug release from HA-nCh capsule).

4. Characterization methods

4.1. Viscometry

The intrinsic viscosity [η] of HA was determined at 25°C in 0.1 M NaCl, according to reference[14], using an Ubbelohde type capillary viscometer (LAUDA iVisc). The flow time of solvent and diluted HA solutions (from 0.01 wt% to 0.25 wt%) was recorded between two markers on the capillary. The reduced viscosity of each solution was calculated using the following equation:

$$\eta_{reduced} = \frac{(\frac{t_{solution}}{t_{solvent}} - 1)}{C} \quad (1)$$

where $t_{solution}$ and $t_{solvent}$ are flow times and C is the concentration of the HA solution (g/dL).

The HA molecular weight was then calculated according to the Mark-Houwink equation:

$$[\eta] = KM^{\alpha} \quad (2)$$

where M is the molecular weight and α and K are empirical constants. We used K = 0.0336 mL/g and α = 0.79.[14]

4.2. Rheology

Rheological experiments were performed on a Bohlin Gemini rheometer, at 25°C, using plate-plate geometry. The viscosity η of HA solutions at pH 1.5, 2.5 and 7.4 as a function of shear rate was recorded from 0.01 to 10 s^{-1}. We also performed oscillatory tests by varying shear strains from 1 to 100% at a fixed frequency ω of 10 Hz. Some frequency sweeps were performed at 1% strain.

4.3. Sample shrinkage

During the preparation of HA dry materials, we calculated volume shrinkage after solvent exchange and overall volume shrinkage with the following equations:

$$V_{shrinkage\ solvent\ exchange} = \frac{V_i - V_{org}}{V_i} \times 100 \quad (3)$$

$$V_{shrinkage\ overall} = \frac{V_i - V_f}{V_i} \times 100 \quad (4)$$

where V_i, V_{org} and V_f are the volumes of the initial HA solution, of the organogel and of the final dry material, respectively.

Volume was determined in two ways: 1) using a high-precision digital caliper, and ii) using a Geopyc 1360 Envelope Density Analyzer (Micromeritics) with DryFlow powder, a chamber of 19.1 mm diameter and applied force of 25 N.

4.4. Bulk density, porosity, and pore specific volume

The bulk density (ρ_{bulk}) of HA dry materials was determined as the ratio of mass (m, measured with a high-precision balance) to volume of the final dry sample (V_f):

$$\rho_{bulk}\ (g/cm^3) = \frac{m}{V_f} \quad (5)$$

Porosity was calculated from the bulk and the skeletal densities ($\rho_{skeletal}$):

$$\text{Porosity} = \frac{\rho_{skeletal} - \rho_{bulk}}{\rho_{skeletal}} \times 100 \quad (6)$$

where $\rho_{skeletal}$ of HA is 1.4 g/cm^3.[15]

The specific pore volume was calculated using the following equation:

$$V_{pores} = \frac{1}{\rho_{bulk}} - \frac{1}{\rho_{skeletal}} \quad (7)$$

4.5. Specific surface area

The specific surface area (S_{BET}) was evaluated by an ASAP 2020 instrument (Micromeritics), using nitrogen adsorption and the Brunauer, Emmett and Teller (BET) method. The Barrett, Joyner and Halenda approach was used to determine pore size distribution and pore volume of samples. Prior to analysis, samples were degassed under high vacuum at 70 °C for 10 h.

4.6. Scanning electron microscopy (SEM)

The morphology of HA dry materials and the HA-nCh fibers capsule membrane was analyzed using a MAIA 3 microscope (Tescan) equipped with a field emission gun at an accelerating voltage of 3 kV. Prior to analysis, HA sample was sputter-coated with a layer of 14 nm of platinum using a Q150T Quarum metallizer. Before analyzing HA-nCh membrane, it was dried at room temperature.

4.7. Absorption capacity

To investigate aerogel absorption capacity, it was immersed in phosphate-buffered saline solution, PBS (1X, pH 7.4). The sample mass was determined several times after carefully removing the excess of PBS. The normalized mass was calculated using the following equation:

$$\text{Normalized mass} = \frac{W_t}{W_i} \times 100 \qquad (8)$$

where W_i is the initial sample weight and W_t is the sample weight at time t.

A thiol reducing agent, DTT, was also dissolved in PBS to study its influence on the absorption capacity of chemically crosslinked HA aerogels.[16]

Moisture adsorption by HA aerogels was assessed at room temperature. HA is generally highly hydrophilic. At regular time intervals, the sample mass was weighed, and moisture adsorption was calculated using equation 8.

4.8. Uniaxial compression testing

The mechanical properties of physically crosslinked HA aerogels were characterized by uniaxial compression measurements on an Instron 5967 testing machine. Cylindrical aerogels, with a ratio length/diameter around 0.4, were prepared. The upper and lower surfaces of physically crosslinked HA aerogels were polished with sandpaper to be planar and parallel (Figure 2.4).

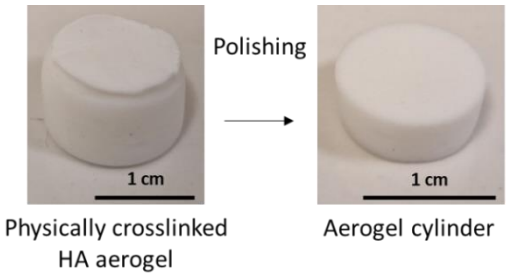

Figure 2.4. Example of a HA aerogel cylinder used for compression testing.

To monitor the local deformation of the HA aerogel cylinder during the mechanical test, random black points were added on the rounded side of the cylinder with a stamp, as demonstrated in Figure 2.5.

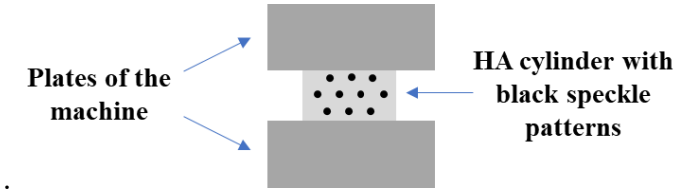

Figure 2.5. Example of a HA aerogel cylinder having black speckled dots, placed in between the two compression plates of the machine.

A pre-loading of 1 N was applied to ensure the contact between the sample and machine. Compression was performed at a displacement rate of 0.05 1/min. Four identical samples per formulation were measured.

The mechanical properties of HA aerogel were investigated using two approaches. One is based on data directly obtained from the Instron machine, and the other uses the digital image correlation (DIC) technique, employing two cameras in stereo-correlation.[17] The second approach monitors local displacements of the sample, by tracking the positions of speckled dots on a sample surface during the deformation of the sample. Images of the sample were recorded during the compression test, continuously, by two fixed cameras with in-between fixed angle. The displacement fields were built from images using VIC 3D software. On the image, a meshing in the region of interest allowed to track speckle patterns during the compression test. A virtual extensometer was placed on the region of interest to monitor the sample strain evolution along the vertical axis. Figure 2.6 depicts the position of the virtual extensometer on the HA aerogel (orange line).

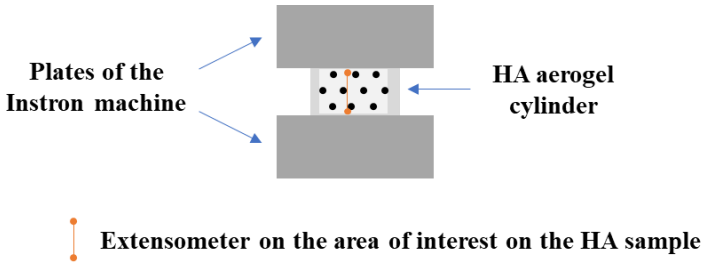

Figure 2.6. Scheme showing the virtual extensometer used by VIC3D software to determine local deformation.

Stress-strain graphs were built to characterize the mechanical properties of the HA aerogels. The nominal strain ε_N, and the nominal stress σ_N applied to the sample, during the compressive test were calculated according to the following equations:

$$\varepsilon_N = \frac{\Delta h}{h_0} = \frac{h_0 - h}{h_0} \times 100 \qquad (9)$$

$$\sigma_N = \frac{F}{S_0} \qquad (10)$$

where Δh is the difference between the initial height of the cylinder, h_0, and the height at a given applied force, h; F is the force and S_0 is the initial surface of the cylinder. Compression modulus E was calculated in the linear region.

4.9. Fourier Transform Infrared spectroscopy

FTIR spectra were acquired in attenuated total reflectance mode using a Bruker Tensor 27 spectrometer (PERSEE, MINES Paris) and an Invenio Bruker Spectrometer (BioProducts Institute, Vancouver, Canada), by accumulation of 64 scans, with a resolution of 4 cm^{-1} in the 4000-400 cm^{-1} region. We thank Xuetong SHI for her help in FTIR spectroscopy in Vancouver.

4.10. Atomic force microscopy

The morphology of nCh fibers was characterized at the BioProducts Institute of the University of British Columbia (Vancouver, Canada) using AFM in tapping mode (Jupiter XR Asylum Research AFM instrument) with a silicon cantilever tip. Prior to analysis, 0.0005 wt% nCh suspension was prepared, then sonicated for 15 min and deposited on a mica substrate. The width and length of nCh fibers were determined using Gwyddion software by averaging the dimensions of 100 fibers. We thank Yi LU for his help in AFM characterization of nCh fibers.

4.11. Conductimetric titration

The conductivity titration method was used at the BioProducts Institute of the University of British Columbia (Vancouver, Canada) to quantify acidic groups on Ch fibers and deduce the degree of deacetylation (DDA), as reported previously.[18] The technique is based on the substitution of ions by ions with different conductivity. Briefly, 0.1 g vacuum-dried sample was dispersed in 60 g of water ([nCh suspension] = 0.16 wt%). 0.05 M HCl was added to nCh suspension to fully protonate amino groups, and the whole system was titrated with 0.05 M NaOH at 100 µL/min under continuous stirring. The suspension conductivity was recorded using an Orion Star A212 Conductivity meter (ThermoScientific).

The DDA of nCh fibers is given by the following equation:

$$\text{DDA (\%)} = \frac{M_A}{(M_A - M_D) + \frac{m}{(v_2 - v_1) \times 0{,}001 \times C}} \qquad (11)$$

where M_A is the molar mass of the acetyl unit (203 g/mol), M_D is the molar mass of the deacetyl unit (161 g/mol), m is the weight of nCh dispersed (0.1 g), V_1 and V_2 are the NaOH volumes corresponding to the two inflexion points and C is the concentration of the titrant (0.05 mol/L).

We thanked Xiaoya SU for her help in conductimetric titration of nCh fibers.

4.12. Zeta potential

The surface charge of 0.1 wt% nCh dispersed in water was determined using electrophoretic mobility (Zeta Sizer, Malvern Instruments) at the BioProducts Institute of the University of British Columbia (Vancouver, Canada). The pH values of nCh suspensions were varied from 3.5 to 12. All measurements were carried out in a dip cell at 25°C.

4.13. Optical microscopy

Optical microscopy images of the HA-nCh capsule membrane were made using a LV100N POL microscope (Nikon) at the BioProducts Institute of the University of British Columbia (Vancouver, Canada).

4.14. Dissolution of the HA-nCh capsule membrane

The robustness of the HA-nCh capsule membrane against dissolution in different media was analyzed visually. 0.1 M NaCl, 1 wt% acetic acid or 0.05 M NaOH solutions are examples of media added on the membrane for 1 day.

4.15. Model drug release from HA-nCh capsule

The release of two model drugs from HA-nCh capsules was followed via periodical spectrophotometric measurements in the UV-Vis range. The absorbance properties of each model drug and the release method used are described below.

- Model drug absorbance properties
    - Methylene blue (MB)

MB is a blue dye, soluble in water, with a molecular weight of 319.85 g/mol (Figure 2.7).

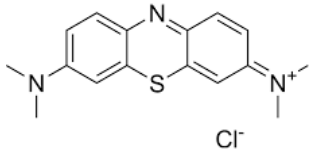

Figure 2.7. Chemical structure of MB.

In order to follow its release from the HA-nCh capsule with spectrophotometry, a calibration curve of MB in the release medium was constructed. 1X PBS at pH 7.4 was used as medium to mimic the physiological conditions.[19] Figure 2.8 presents the MB absorption properties in the UV-visible range.

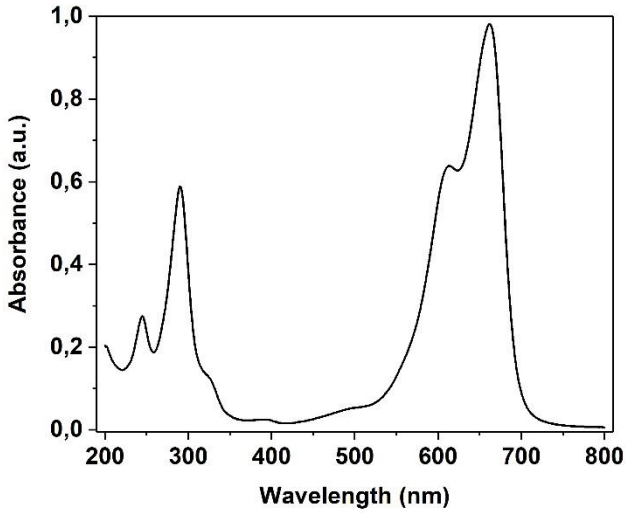

Figure 2.8. UV-Vis absorbance of 0.005 g/L MB solution.

The highest signal at 663 nm was selected to detect MB in solution, as reported in literature.[20]

Figure 2.9 presents the calibration curve of MB in 1X PBS at pH 7.4. Solutions with concentrations ranging from 0.001 g/L to 0.01 g/L were prepared.

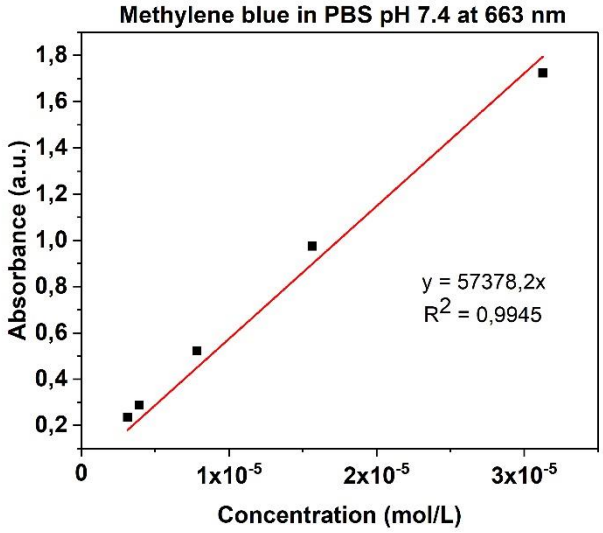

Figure 2.9. Calibration curve of MB at 663 nm.

The molar extinction coefficient ε_i of MB in solution was calculated using Beer-Lambert law:

$$A = C_i \times l \times \varepsilon_i \qquad (12)$$

where A is the measured absorbance at a given wavelength, C_i is the concentration of the absorbing species in solution and l is the path length of the light through the solution, here 1 cm.

The molar extinction coefficient of MB in PBS at pH 7.4 was found around 5.7×10^4 L/mol/cm, which is close to the value reported in literature (≈ 5×10^4 L/mol/cm).[21]

- Fluorescein isothiocyanate-dextran (FITC-dextran)

Another model drug was FITC-dextran. It is a dextran molecule functionalized with a fluorescent group, fluorescein.[22,23] This model drug is yellow, soluble in water, with a molecular weight of 2×10^6 g/mol (Figure 2.10).

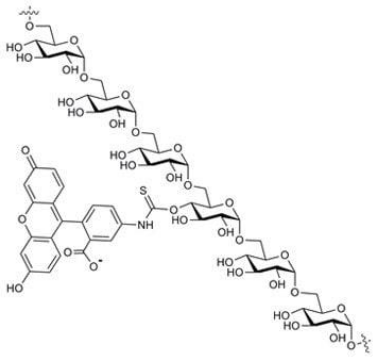

Figure 2.10. Chemical structure of FITC-dextran.

The absorbance properties of FITC-dextran were measured following the same procedure as for MB. Figure 2.11 shows a maximum absorption at 493 nm, as reported in literature.[22]

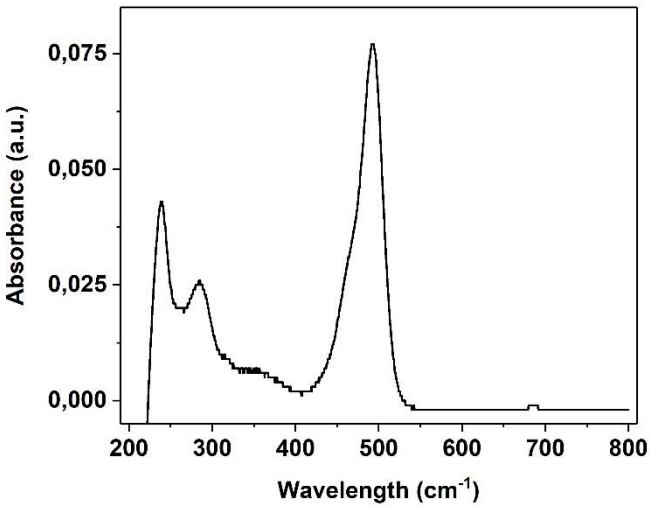

Figure 2.11. UV-Vis absorbance of 0.01 g/L FITC-dextran solution.

The absorbance of FITC-dextran at 493 mm in PBS (pH 7.4) as a function of FITC-dextran concentration is shown in Figure 2.12.

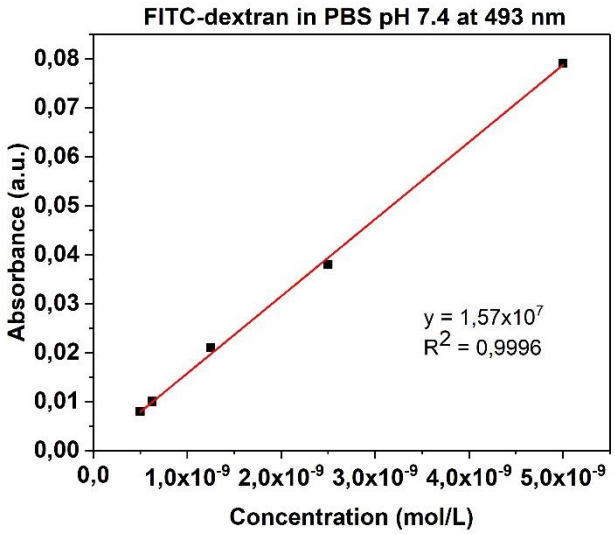

Figure 2.12. Calibration curve of FITC-dextran.

The molar extinction coefficient of FITC-dextran in PBS at pH 7.4 is around 1.5×10^7 L/mol/cm.

- Model drug release experiments

Model drug (i.e. MB or FITC-dextran) release experiments were conducted at 25°C in 80 mL medium, with stirring at 100 rpm to ensure homogenization. The model drug-loaded HA-nCh capsule (volume 0.5 mL) was immersed in 80 mL of PBS at pH 7.4. A grid was used to separate the capsule from the magnetic stirrer. Figure 2.13 presents examples of HA-nCh capsules loaded with MB and with FITC-dextran in PBS.

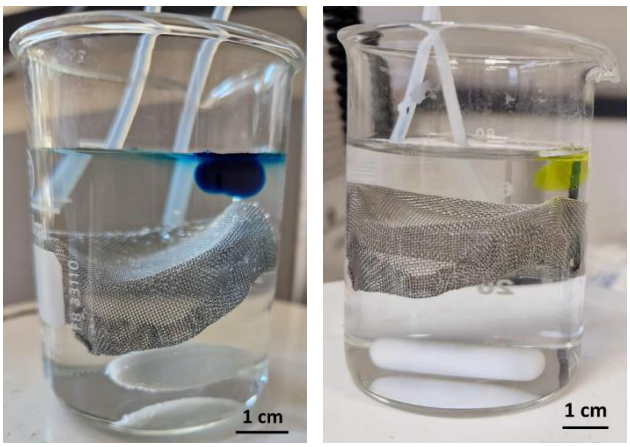

Figure 2.13. Examples of HA-nCh capsules loaded with MB (left) and with FITC-dextran (right) in PBS.

After introducing the capsule in the release bath, two plastic tubes connected to the spectrophotometer were immersed in the PBS to study drug release kinetics. During release, the beaker was protected with aluminum foil to avoid interactions with light.

Drug release kinetics was followed by periodical spectrophotometric measurements at 663 nm for MB or 493 nm for FITC-dextran, using an automated set-up, consisting of a UV-1800 UV/Visible Scanning spectrophotometer coupled to a Peristaltic Sipper Pump and a 160C Sipper Unit (all from Shimadzu, Figure 2.14).

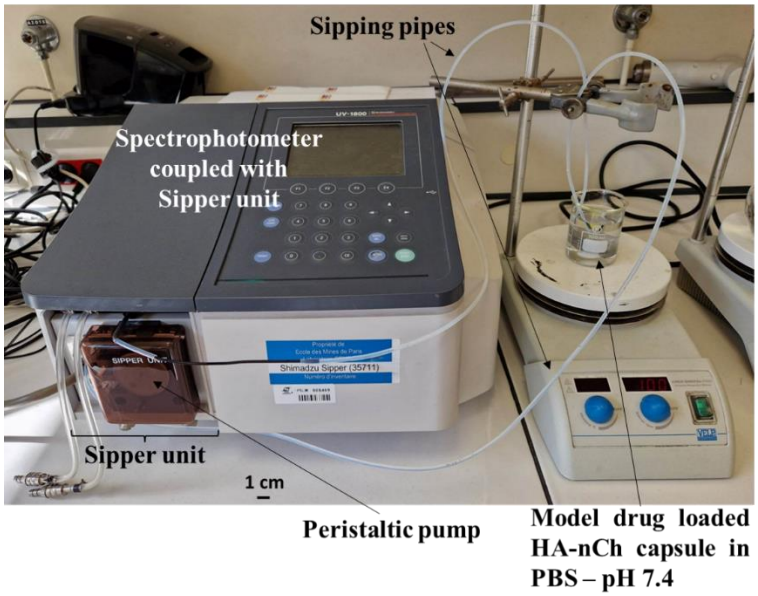

Figure 2.14. Set-up used to perform model drug release experiments.

The concentration of model drug in solution overtime was determined using the absorbance measured every 5 min by the spectrophotometer with the equation below:

$$C_{\text{experimental model drug at t}}\ (\text{g/L}) = \frac{A(t)}{\varepsilon_{\text{model drug}} \times M_{\text{model drug}}} \qquad (13)$$

with A(t) is the absorbance of the solution measured at time t, $\varepsilon_{\text{model drug}}$, the molar extinction coefficient of the model drug (L/mol/cm) and M, the molar mass of the model drug (g/mol).

The cumulative release of model drug over time was calculated using the equation below:

$$\text{Cumulative release} = \frac{C_{\text{experimental model drug at t}}}{C_{\text{theoretical model drug in the capsule}} \times V_{\text{release medium}}} \times 100 \qquad (14)$$

Where $C_{\text{experimental model drug at t}}$ is the concentration of the model drug in the medium at time t, $C_{\text{theoretical model drug in the capsule}}$ (0.2 g/L) is the initial concentration of model drug in the capsule and $V_{\text{release medium}}$ is the volume of the release medium (80 mL).

5. Conclusions

This chapter described the materials and protocols developed to prepare three novel HA-based materials, and methods used to characterize these materials.

First, physically crosslinked HA aerogels were prepared via freeze-thaw gelation of HA solution, solvent exchange and drying with supercritical CO_2. Freezing-thawing is an efficient and mild technique to induce hydrogen bonds between HA chains in solution, resulting in hydrogel formation. These intermolecular interactions form physical crosslinks. Opposite to our previous work[15], where the HA network was formed via direct non-solvent induced phase separation, an alternative method for the formation of the HA network was presented.

Chemically crosslinked HA aerogels were prepared via chemical crosslinking of HA, solvent exchange and $scCO_2$ drying. The reaction between the carboxylic acid groups of HA with the amine groups of cystamine, acting as crosslinker, forms amide links between HA chains. This creates covalent crosslinks, resulting in hydrogel formation.

Lastly, chitin nanofibers were used to make HA-nCh capsules. The model drugs MB and FITC-dextran were introduced in the HA-nCh capsules and drug release kinetics was monitored in PBS medium at pH 7.4.

The polymer of interest in this thesis, HA, the nCh fibers, as well as new materials based on them, were characterized. The effect of processing conditions on the properties and the structure of these materials was investigated using the characterization methods described in this chapter.

6. References

(1) Bai, L.; Liu, L.; Esquivel, M.; Tardy, B. L.; Huan, S.; Niu, X.; Liu, S.; Yang, G.; Fan, Y.; Rojas, O. J. Nanochitin: Chemistry, Structure, Assembly, and Applications. *Chem. Rev.* **2022**, acs.chemrev.2c00125. https://doi.org/10.1021/acs.chemrev.2c00125.

(2) Zhu, Y.; Huan, S.; Bai, L.; Ketola, A.; Shi, X.; Zhang, X.; Ketoja, J. A.; Rojas, O. J. High Internal Phase Oil-in-Water Pickering Emulsions Stabilized by Chitin Nanofibrils: 3D Structuring and Solid Foam. *ACS Appl Mater Interfaces* **2020**, *12* (9), 11240–11251. https://doi.org/10.1021/acsami.9b23430.

(3) Cai, Z.; Zhang, F.; Wei, Y.; Zhang, H. Freeze–Thaw-Induced Gelation of Hyaluronan: Physical Cryostructuration Correlated with Intermolecular Associations and Molecular Conformation. *Macromolecules* **2017**, *50* (17), 6647–6658. https://doi.org/10.1021/acs.macromol.7b01264.

(4) Legay, L.; Budtova, T.; Buwalda, S. Hyaluronic Acid Aerogels Made Via Freeze–Thaw-Induced Gelation. *Biomacromolecules* **2023**, *24* (10), 4502–4509. https://doi.org/10.1021/acs.biomac.2c01518.

(5) Chartier, C.; Buwalda, S.; Van Den Berghe, H.; Nottelet, B.; Budtova, T. Tuning the Properties of Porous Chitosan: Aerogels and Cryogels. *International Journal of Biological Macromolecules* **2022**, *202*, 215–223. https://doi.org/10.1016/j.ijbiomac.2022.01.042.

(6) Groult, S.; Budtova, T. Tuning Structure and Properties of Pectin Aerogels. *European Polymer Journal* **2018**, *108*, 250–261. https://doi.org/10.1016/j.eurpolymj.2018.08.048.

(7) Druel, L.; Bardl, R.; Vorwerg, W.; Budtova, T. Starch Aerogels: A Member of the Family of Thermal Superinsulating Materials. *Biomacromolecules* **2017**, *18* (12), 4232–4239. https://doi.org/10.1021/acs.biomac.7b01272.

(8) Gavillon, R.; Budtova, T. Aerocellulose: New Highly Porous Cellulose Prepared from Cellulose-NaOH Aqueous Solutions. *Biomacromolecules* **2008**, *9* (1), 269–277. https://doi.org/10.1021/bm700972k.

(9) Wang, L.; Dong, S.; Liu, Y.; Ma, Y.; Zhang, J.; Yang, Z.; Jiang, W.; Yuan, Y. Fabrication of Injectable, Porous Hyaluronic Acid Hydrogel Based on an In-Situ Bubble-Forming Hydrogel Entrapment Process. *Polymers* **2020**, *12* (5), 1138. https://doi.org/10.3390/polym12051138.

(10) Liu, Y.; Ren, L.; Wang, Y. Crosslinked Collagen–Gelatin–Hyaluronic Acid Biomimetic Film for Cornea Tissue Engineering Applications. *Materials Science and Engineering: C* **2013**, *33* (1), 196–201. https://doi.org/10.1016/j.msec.2012.08.030.

(11) Deng, S.; Li, X.; Yang, W.; He, K.; Ye, X. Injectable in Situ Cross-Linking Hyaluronic Acid/Carboxymethyl Cellulose Based Hydrogels for Drug Release. *Journal of Biomaterials Science, Polymer Edition* **2018**, *29* (13), 1643–1655. https://doi.org/10.1080/09205063.2018.1481005.

(12) Yegappan, R.; Selvaprithiviraj, V.; Mohandas, A.; Jayakumar, R. Nano Polydopamine Crosslinked Thiol-Functionalized Hyaluronic Acid Hydrogel for Angiogenic Drug Delivery. *Colloids and Surfaces B: Biointerfaces* **2019**, *177*, 41–49. https://doi.org/10.1016/j.colsurfb.2019.01.035.

(13) Han, S.-J.; Yoo, M.; Kim, D.-W.; Wee, J.-H. Carbon Dioxide Capture Using Calcium Hydroxide Aqueous Solution as the Absorbent. *Energy Fuels* **2011**, *25* (8), 3825–3834. https://doi.org/10.1021/ef200415p.

(14) García-Abuín, A.; Gómez-Díaz, D.; Navaza, J. M.; Regueiro, L.; Vidal-Tato, I. Viscosimetric Behaviour of Hyaluronic Acid in Different Aqueous Solutions. *Carbohydrate Polymers* **2011**, *85* (3), 500–505. https://doi.org/10.1016/j.carbpol.2011.02.028.

(15) Aguilera-Bulla, D.; Legay, L.; Buwalda, S. J.; Budtova, T. Crosslinker-Free Hyaluronic Acid Aerogels. *Biomacromolecules* **2022**, *23* (7), 2838–2845. https://doi.org/10.1021/acs.biomac.2c00207.

(16) Cleland, W. W. 1,4-Dithiothreitol. In *Encyclopedia of Reagents for Organic Synthesis (EROS)*; John Wiley & Sons, Ltd, 2001. https://doi.org/10.1002/047084289X.rd473.

(17) Chen, F.; Bouvard, J.-L.; Sawada, D.; Pradille, C.; Hummel, M.; Sixta, H.; Budtova, T. Exploring Digital Image Correlation Technique for the Analysis of the Tensile Properties of All-Cellulose Composites. *Cellulose* **2021**, *28* (7), 4165–4178. https://doi.org/10.1007/s10570-021-03807-9.

(18) Bai, L.; Kämäräinen, T.; Xiang, W.; Majoinen, J.; Seitsonen, J.; Grande, R.; Huan, S.; Liu, L.; Fan, Y.; Rojas, O. J. Chirality from Cryo-Electron Tomograms of Nanocrystals Obtained by Lateral Disassembly and Surface Etching of Never-Dried Chitin. *ACS Nano* **2020**, *14* (6), 6921–6930. https://doi.org/10.1021/acsnano.0c01327.

(19) Proksch, E. pH in Nature, Humans and Skin. *The Journal of Dermatology* **2018**, *45* (9), 1044–1052. https://doi.org/10.1111/1346-8138.14489.

(20) Khan, I.; Saeed, K.; Zekker, I.; Zhang, B.; Hendi, A. H.; Ahmad, A.; Ahmad, S.; Zada, N.; Ahmad, H.; Shah, L. A.; Shah, T.; Khan, I. Review on Methylene Blue: Its Properties, Uses, Toxicity and Photodegradation. *Water* **2022**, *14* (2), 242. https://doi.org/10.3390/w14020242.

(21) Patil, V.; Hardikar, H.; Joshi, S.; Tembe, S. Optical Detection of Total Cholesterol Based on a Dye-Displacement Method. *Spectrochimica Acta Part A: Molecular and Biomolecular Spectroscopy* **2023**, *293*, 122425. https://doi.org/10.1016/j.saa.2023.122425.

(22) de Belder, A. N.; Granath, K. Preparation and Properties of Fluorescein-Labelled Dextrans. *Carbohydrate Research* **1973**, *30* (2), 375–378. https://doi.org/10.1016/S0008-6215(00)81824-8.

(23) Andrieux, K.; Lesieur, P.; Lesieur, S.; Ollivon, M.; Grabielle-Madelmont, C. Characterization of Fluorescein Isothiocyanate-Dextrans Used in Vesicle Permeability Studies. *Anal. Chem.* **2002**, *74* (20), 5217–5226. https://doi.org/10.1021/ac020119l.

Chapter 3. Physically crosslinked HA aerogels prepared via freeze-thaw induced gelation

1. Introduction

[English]

Thanks to its interesting properties, HA can be transformed into high value-added porous materials for biomedical applications. Literature reports several HA-based hydrogels[1–4] and cryogels[5–7] promoting wound healing. However, very few publications concern HA aerogels, despite their high potential.

Only three articles report on the use of HA for the preparation of aerogels. Two describe alginate-HA aerogel microspheres as potential carriers for pulmonary drug delivery.[8,9] Microspheres were prepared from HA and alginate using an emulsion-gelation process, ionic crosslinking with Ca^{2+} ions, and drying with $scCO_2$. HA-alginate aerogels had a low density (0.035−0.063 g/cm^3), a high porosity, and good *in vitro* aerodynamic properties. Recently, our group reported on crosslinker-free neat HA aerogels, prepared using non-solvent induced phase separation, solvent exchange, and $scCO_2$ drying.[10] Various preparation conditions (HA concentration, solution pH, type of non-solvent) were tested, and only a few resulted in aerogels. These aerogels were obtained from HA solutions of low pH (either 1.5 or 2.5) and had a high specific surface area (up to 510 m^2/g) and low density (> 0.057 g/cm^3). In view of the great potential of HA aerogels, a need exists to further develop these materials and investigate, e.g., additional crosslinking methods, to tailor their properties.

Opposite to our previous work where the HA network was formed upon the addition of a non-solvent directly to the polymer solution[10], in this work, we report an alternative method, freeze−thawing, for the formation of the HA network. We prepare physically crosslinked HA dry materials, including aerogels, via freeze thaw-induced gelation of HA solutions, followed by solvent exchange and drying with $scCO_2$. Freeze−thawing is an efficient and mild technique inducing hydrogen bonds between HA chains in solution, resulting in hydrogel formation.[11,12] Side-by-side chain associations, mainly consisting of H-bonds among −COOH and $-NHCOCH_3$ groups of HA, form physical crosslinks. These interactions remain intact on thawing, acting as the junction zones of the hydrogel. Before preparing HA aerogels, we characterize the molecular weight of HA and the rheological properties of HA solutions. Then, we investigate the effects of processing conditions (HA concentration, solution pH, number of FT cycles, and type of non-solvent) on the properties and structure of the obtained HA dry materials. Finally, we examine the mechanical properties of HA aerogels upon compression, their behavior in PBS medium and upon exposure in air. Part of this chapter has already been published.[13]

[Français]

Grâce à ses propriétés intéressantes, l'acide hyaluronique peut être transformé en matériau poreux à haute valeur ajoutée pour des applications biomédicales. Les recherches bibliographiques rapportent plusieurs hydrogels[1–4] et cryogels[5–7] à base d'acide hyaluronique favorisant la guérison d'une blessure. Cependant, très peu de publications concernent les aérogels d'acide hyaluronique, malgré leur fort potentiel.

Seulement trois articles traitent de l'utilisation de l'acide hyaluronique pour la préparation d'aérogels. Deux décrivent des microsphères d'aérogels à base d'alginate et d'acide hyaluronique comme systèmes potentiels pour administration de médicaments par voie pulmonaire.[8,9] Les microsphères ont été préparées à base d'acide hyaluronique et d'alginate en utilisant un procédé d'émulsion-gélification, une réticulation ionique avec les ions Ca^{2+}, et un séchage avec le CO_2 supercritique. Les aérogels à base d'alginate et d'acide hyaluronique ont une faible densité (0.035−0.063 g/cm^3), une grande porosité, et de bonnes propriétés aérodynamiques *in vitro*. Récemment, notre groupe a développé des aérogels à base d'acide hyaluronique sans agent réticulant, en utilisant la méthode de séparation de phase induite par un non-solvant, un échange de solvant, et un séchage supercritique avec du CO_2.[10] Plusieurs conditions de préparation (concentration en acide hyaluronique, pH de la solution, type du non-solvant) ont été testées, et seulement quelques-unes ont permis de fabriquer des aérogels. Ces aérogels ont été obtenus à partir de solutions d'acide hyaluronique à bas pH (1.5 ou 2.5). Ils possèdent une grande surface spécifique (jusqu'à 510 m^2/g) et une faible densité (> 0.057 g/cm^3). En vue de l'énorme potentiel des aérogels d'acide hyaluronique, il est nécessaire d'investiguer plus largement le développement de ces matériaux et d'explorer, par exemple, d'autres méthodes de réticulation, pour adapter leurs propriétés.

Contrairement à notre travail précédent où le réseau d'acide hyaluronique était formé par l'addition directe d'un non-solvant sur la solution de polymère[10], dans ce travail, nous décrivons une méthode alternative, congélation-décongélation, afin de former le réseau d'acide hyaluronique. Nous préparons des matériaux secs à base d'acide hyaluronique réticulés physiquement, incluant des aérogels, via la gélification induite par congélation-decongélation des solutions d'acide hyaluronique, suivie par un échange de solvant et un séchage avec du CO_2 supercritique. Le processus de congélation-décongélation est une technique efficace et douce qui provoque la formation de liaisons hydrogène entre les chaînes d'acide hyaluronique en solution, et résulte en la formation d'hydrogel.[11,12] Les associations des chaînes, constituées principalement de liaisons hydrogène entre les groupes −COOH et $-NHCOCH_3$ de l'acide

hyaluronique, forment des liaisons physiques. Ces interactions restent intactes après décongélation et agissent comme points de jonction de l'hydrogel. Avant de préparer les aérogels, nous caractérisons la masse moléculaire de l'acide hyaluronique et les propriétés rhéologiques des solutions d'acide hyaluronique. Ensuite, nous étudions les effets des conditions de préparation (concentration en acide hyaluronique, pH de la solution d'acide hyaluronique, nombre de cycles de congelation-décongélation, et type du non-solvant) sur les propriétés et la structure des matériaux secs obtenus. Pour finir, nous examinons les propriétés mécaniques des aérogels d'acide hyaluronique sous compression, leur comportement dans un milieu PBS et sous exposition à l'air libre. Une partie de ce chapitre a déjà été publiée.[13]

2. Characterization of hyaluronic acid

2.1. Determination of HA molecular weight

The intrinsic viscosity [η] of HA was determined as described in Section 4.1 – Chapter 2. Flow times of HA solutions and solvent allowed to calculate the reduced viscosity at various concentrations. The dependence of reduced viscosity on HA concentration is shown in Figure 3.1. The intersection of the line with the Y axis gives the intrinsic viscosity of HA.

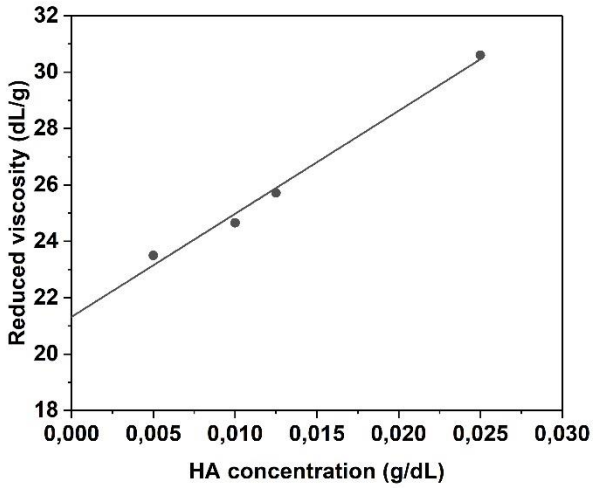

Figure 3.1. Reduced viscosity of HA solutions versus HA concentration. Experiments were performed at 25°C using 0.1M NaCl as solvent.

The HA intrinsic viscosity was found to be 21.27 dL/g and was used to calculate the molecular weight of HA using the Mark-Houwink equation[14] (See Chapter 2 – Section 4.1 Viscosimetry). The HA molecular weight was estimated to be around 1.2×10^6 g/mol, which is slightly lower than the one given by the manufacturer.

The HA molecular weight depends on the pH value of the initial HA solution. HA dry materials (described in Section 3 of this Chapter) prepared at different pH (1.5, 2.5, 7.4 and 12 - only for the last pH, a sample was taken from a previous study[10]) were dissolved in 0.1 M NaCl and the intrinsic viscosity of each solution was measured. Figure 3.2 shows the reduced viscosity versus HA concentration for the different pH values. pH 1.5 was investigated because it was used previously to prepare HA aerogels via non-solvent induced phase separation.[10] A gel-like behavior for HA solution was found at pH 2.5, due to the HA isoelectric point.[15] pH 7.4 was investigated as it is the physiological pH of some human tissues (such as bone) and fluids (such

as blood and synovial fluid).[16] The HA molecular weight in basic conditions (pH 12) was studied for completeness.

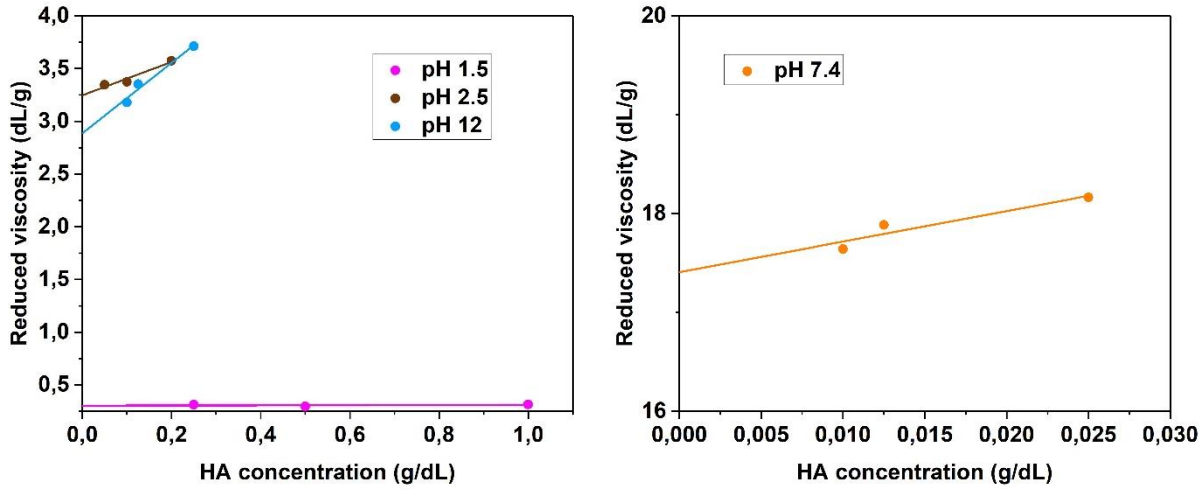

Figure 3.2. Reduced viscosity of HA solutions in 0.1M NaCl at 25°C versus HA concentration. Dry HA materials were prepared from solutions at pH 1.5, 2.5, 7.4 and dissolved in 0.1M NaCl; for more details see the text above.

When dissolved at pH 1.5, the intrinsic viscosity of HA [η] was found to be 0.30 dL/g, giving a molecular weight around 5.5×10^3 g/mol. Our finding is in line with previous research[17], reporting severe HA degradation at pH < 2. When HA was dissolved at the isoelectric point, i.e. pH 2.5, the molecular weight was found to be 1.1×10^5 g/mol. The HA molecular weight after being dissolved at pH 7.4 (physiological pH) was 0.93×10^6 g/mol, slightly below that of neat HA (i.e. 1.2×10^6 g/mol for pH 7.2 – Figure 3.1), due to some slight hydrolysis. When dissolved at pH 12, only ~8% of the molecular weight of the starting HA (95.4×10^3g/mol) was measured, likely because of backbone degradation (basic hydrolysis).[17]

2.2. Rheological properties of HA solutions

It is known that the rheological properties of HA solutions depend on the HA concentration, the pH of the solution and its ionic strength.[18,19] HA solutions have a non-Newtonian behavior.[18] They have an extremely high shear rate dependency, called pseudoplasticity (or shear-thinning), because at low shear rates, they behave as a soft gel, and by increasing shear rate, the viscosity drops.[20] For example, at low concentration (≈ 0.02%), molecules form a network, which is very viscous at very low shear rates (< 0.01 s^{-1}), and very elastic at relatively high frequencies (> 1 Hz).[20]

In this chapter, rheological measurements were performed only as a screening to help the interpretation of the properties of HA aerogels, and not to deeply investigate their rheological properties.

2.2.1. Steady state viscosity

First, to perform rheology, we removed air bubbles from HA solution with strong centrifugation. We started by studying the potential influence of centrifugation on the viscosity of HA solutions. 0.7 wt% HA solutions at pH 7.4 were centrifuged at 6000 and 9000 rpm before measurements. Figure 3.3 shows the steady state viscosity of HA solutions as a function of shear rate. The viscosity shows a Newtonian plateau at low shear rates and decreases upon increasing shear rate. The viscosity of solutions, after using different centrifugation conditions, is found to be similar. Thus, centrifugation does not impact the HA solution viscosity.

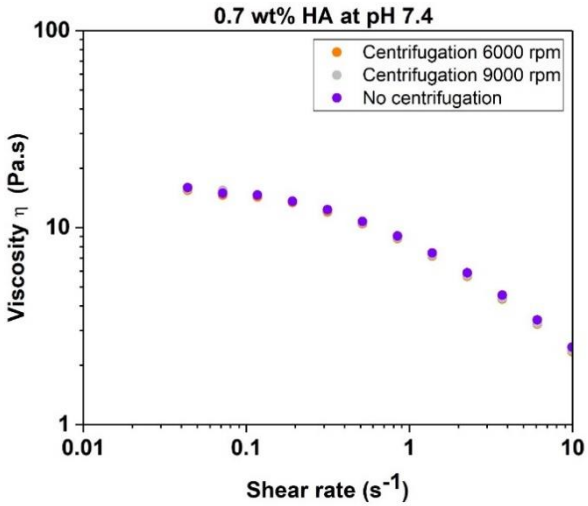

Figure 3.3. Steady state viscosity of 0.7 wt% HA solutions (pH 7.4) as a function of shear rate at 25°C.

Next, we investigated the influence of HA concentration on the viscosity of solutions at pH 7.4. Analysis was done on fresh solutions. Figure 3.4 presents the results.

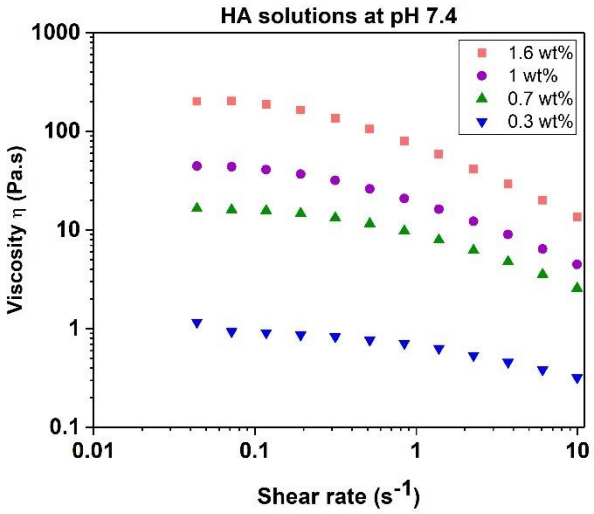

Figure 3.4. Steady state viscosity of 0.3, 0.7, 1 and 1.6, wt% HA solutions at pH 7.4 as a function of shear rate at 25°C.

Higher HA concentration led to higher solution viscosity, as expected, confirming the results found by Balazs et al.[19], and solutions are shear thinning. The same behavior was observed for solutions at pH 1.5 and 2.5 (Figure 3.5). Again, in both cases, rheological analysis was performed on fresh solutions.

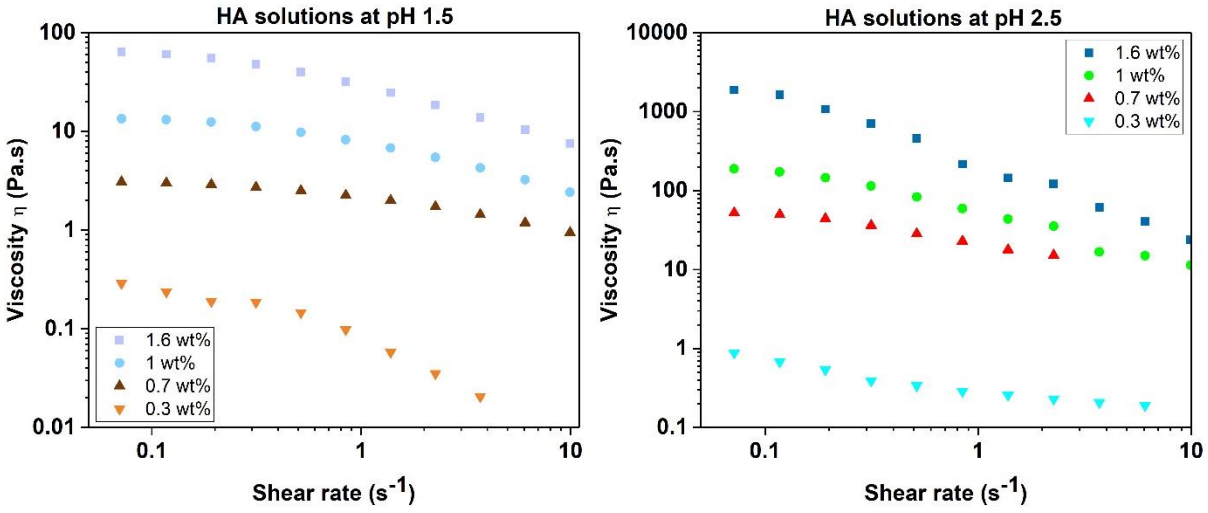

Figure 3.5. Steady state viscosity of HA solutions at pH 1.5 (left) and at pH 2.5 (right) as a function of shear rate measured at 25°C.

We analyzed the zero-shear viscosity on the Newtonian plateau (or Newtonian viscosity) of HA solutions presented above. Solutions pH 2.5 have a very high zero-shear viscosity compared to solutions at pH 7.4 and 1.5: at pH 2.5 they behave more as gels than as solution (a

deeper analysis will be shown below). At pH 2.5, at low shear rates, the substance is a gel and by increasing the shear rate, the gel is broken.

Due to their lower zero-shear viscosity, solutions at pH 7.4 and 1.5 behave more as solution. Their zero-shear viscosity was plotted as function of HA concentration (Figure 3.6).

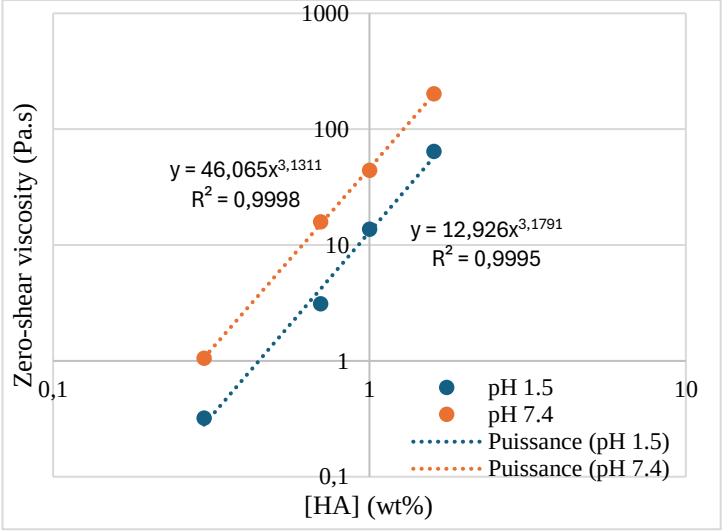

Figure 3.6. Zero-shear viscosity of solutions at pH 7.4 (left) and at pH 1.5 (right) as a function of HA concentration.

In both cases, viscosity vs concentration dependence is described by power-law with exponent around 3, which shows that the polymer is in the concentrated regime. At pH 7.4, the Newtonian viscosity is higher than at pH 1.5, because of higher HA degradation at low pH as demonstrated by intrinsic viscosity values, see Figure 3.2. This trend was already demonstrated by Maleki et al.[17]

We tested HA solution stability over time. The steady state viscosity of 0.7 wt% HA solutions at pH 2.5 was monitored over time: at t_0 (fresh solution), and at 3 days and 6 days after the 1st measurement (Figure 3.7). Between each measurement, HA solutions were stored at room temperature in a drawer. By increasing storage time, the viscosity of HA solution decreases, most probably because of polymer degradation.

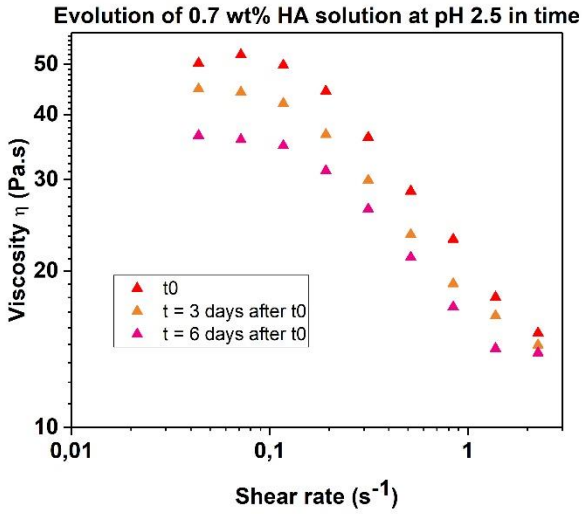

Figure 3.7. Steady state viscosity of 0.7 wt% HA solution at pH 2.5 as a function of shear rate at 25°C for different storage times.

Finally, we investigated the influence of solution pH on zero-shear viscosity over time. We followed the zero-shear viscosity of HA solutions at three different pH (1.5, 2.5 and 7.4) at t_0 (fresh solution), and at 3 days and 6 days after the 1st measurement. Table 3.1 summarizes the zero-shear viscosity for all 0.7 wt% HA solutions and the reduction in viscosity in comparison with the first measurement (t_0).

Table 3.1. Evolution of zero-shear viscosity of 0.7 wt% HA solutions at pH 1.5, 2.5 and 7.4 over time.

	[HA] = 0.7 wt%		
	pH	Zero shear viscosity (Pa.s)	Reduction in viscosity / t_0 (%)
At t_0	1.5	3.1	-
	2.5	51.2	-
	7.4	15.8	-
At t = 3 days after 1st measurement	1.5	0.55	82
	2.5	44.5	13
	7.4	15.2	4
At t = 6 days after 1st measurement	1.5	0.44	86
	2.5	36.1	29
	7.4	15	5

At pH 2.5, the Newtonian viscosity after 3 days at room temperature decreases with time by 13%, and even by 30% after 6 days. At pH 1.5, a Newtonian viscosity decrease of around 80%

was observed after 3 days and at pH 7.4, practically no viscosity reduction (around 4 %) was recorded, suggesting that HA strongly degrades at low pH. These results confirm what Maleki et al.[17] found: a stronger HA molecular weight degradation occurs at pH 1, compared to pH 7.

2.2.2. Oscillatory tests

Dynamic oscillatory tests, such as Small Amplitude Oscillatory Shear (SAOS), are used to characterize the viscoelastic behavior of materials.[21] The upper plate is rotating and oscillating. SAOS tests are dynamic oscillating analyses, describing the flow behavior of samples in the non-destructive deformation range. The non-destructive deformation range is also called the linear viscoelastic (LVE) range. To find the LVE range, first oscillatory tests are performed at variable shear strain amplitudes or shear stresses, while an angular frequency ω is fixed.

Figure 3.8 shows an example of the evolution of elastic and viscous moduli of 0.7 wt% HA solution at pH 2.5 as function of shear strain at a fixed frequency ω of 10 Hz. This Figure shows that, at low shear strains, G' and G'' exhibit a plateau value, corresponding to the linear viscoelastic (LVE) range. The limit of this region is characterized by shear strain around 0.03. At higher shear strains, G' shows a noticeable drop showing that the system is not in the LVE region anymore.

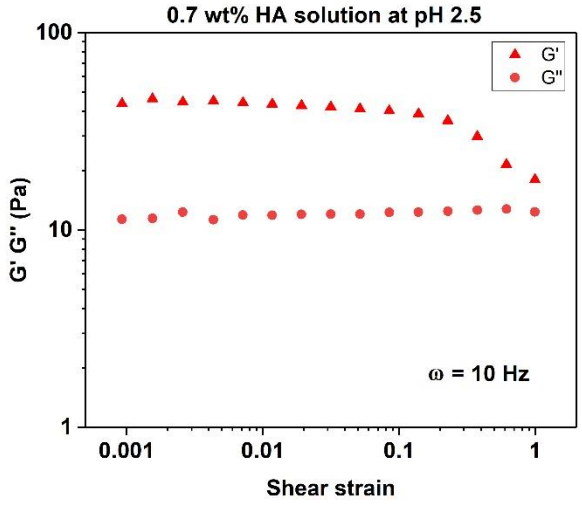

Figure 3.8. Storage G' and loss G'' modulus of 0.7 wt% HA solution at pH 2.5 and at 25°C as a function of shear strain. 1 corresponds to 100% strain.

The influence of centrifugation before rheological measurements on HA viscoelastic properties was investigated. Figure 3.9 shows storage G' and loss G'' moduli of HA solutions at pH 7.4 as a function of frequency. The viscoelastic behavior of HA solutions remains identical,

whether centrifugation occurs before rheological measurement or not, as discussed above (Figure 3.3).

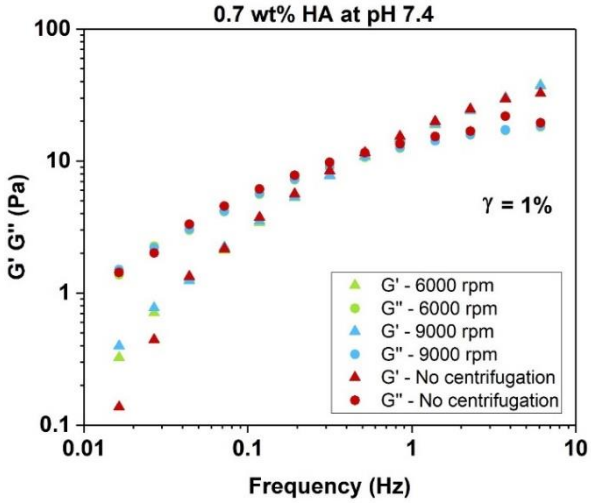

Figure 3.9. Storage G' and loss G'' moduli of HA solutions, subjected to different centrifugation conditions, as a function of frequency, recorded at 25°C.

Figure 3.10 shows an example of G' and G" frequency sweep tests performed on solutions at pH 2.5 for various HA concentrations at 1% strain. Frequencies were varied from 0.01 to 10 Hz. In the case of 1.6 wt% HA, G' is higher than G" in the entire frequency region, and G' slightly decreases at lower frequencies, while G" stays frequency independent. This solution has a viscoelastic solid behavior. For 1 wt% HA solution, G' is still higher than G". In the case of 0.7 wt% HA, at low frequencies, G" becomes slightly higher than G', demonstrating that the dissipated energy is higher than the elastically stored energy.

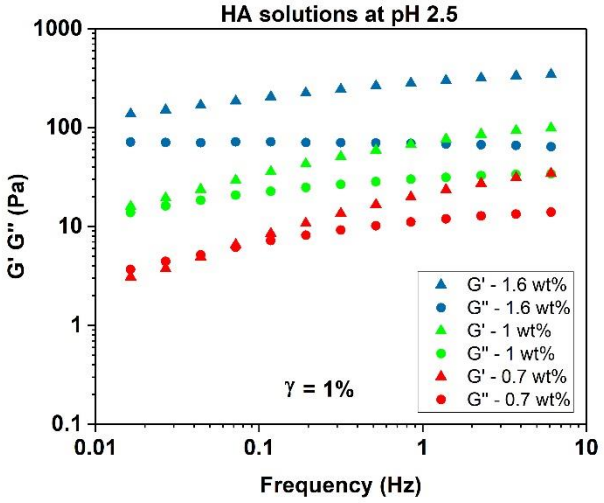

Figure 3.10. Storage G' and loss G'' moduli of HA solutions at pH 2.5 as a function of frequency for different HA concentrations recorded at 25°C.

We fitted G' and G'' with power law dependence on frequency for HA solutions. For un-entangled polymer solution, at low frequencies, the Maxwell model predicts power law exponents in $G' \sim \omega^x$ and $G'' \sim \omega^y$, where x = 2 and y = 1, respectively. Terminal slopes of G' and G'' in the low frequencies region were determined for 0.7, 1 and 1.6 wt% HA solutions at pH 1.5, 2.5 and 7.4 and are given in Tables 3.2 and 3.3.

Table 3.2. Slope of G' for 0.7, 1 and 1.6 wt% HA solutions in the low frequencies region.

HA solutions at pH 1.5		HA solutions at pH 7.4		HA solutions at pH 2.5	
[HA] (wt%)	Slope of G'	[HA] (wt%)	Slope of G'	[HA] (wt%)	Slope of G'
1.6	0.90	1.6	0.80	1.6	0.20
1	1.02	1	0.99	1	0.41
0.7	1.10	0.7	1.06	0.7	0.52

Table 3.3. Slope of G'' for 0.7, 1 and 1.6 wt% HA solutions in the low frequencies region.

HA solutions at pH 1.5		HA solutions at pH 7.4		HA solutions at pH 2.5	
[HA] (wt%)	Slope of G''	[HA] (wt%)	Slope of G''	[HA] (wt%)	Slope of G''
1.6	0.58	1.6	0.47	1.6	0
1	0.64	1	0.59	1	0.25
0.7	0.68	0.7	0.65	0.7	0.34

At no concentration and solution pH investigated, we found $G' \sim \omega^2$ and $G'' \sim \omega$. One reason may be that at 1.6 wt%, HA is in the gel state; another is that much lower frequencies are needed to apply the model for lower-concentrated HA solutions. Unfortunately, at frequencies below 0.01 Hz data scatter.

The pH of 1.6 wt% HA solutions was varied and the viscoelastic properties were measured. Figure 3.11 illustrates the results for 1.6 wt% HA solutions at 25°C and three pH values: 1.5, 2.5 and 7.4.

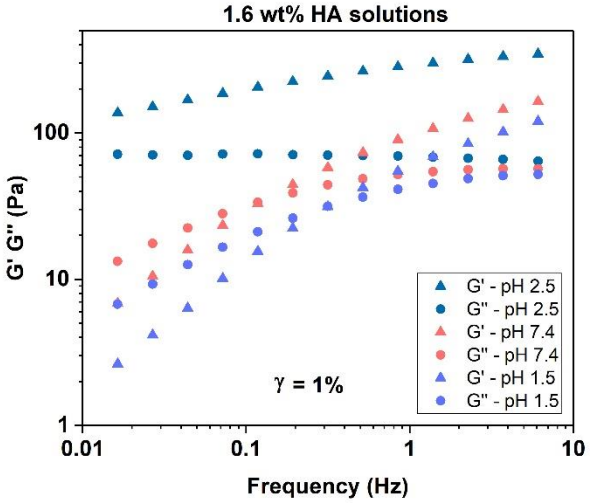

Figure 3.11. Storage (G') and loss (G'') moduli of 1.6 wt% HA solutions at pH 1.5, 2.5 and 7.4 as a function of frequency, recorded at 25 °C.

The curves at pH 1.5 and 7.4 show that at low frequencies, G'' is higher than G': these solutions are viscoelastic liquids. As also shown in Figure 3.10, the pH 2.5 solution has an entirely different behavior: G' is higher than G'' at all frequencies studied. The energy dissipated as heat is lower than the energy elastically stored. Thus, the solution at pH 2.5 appears as a viscoelastic body and not as a viscoelastic liquid. These results correlate well with those obtained by Gibbs et al., who showed that the viscoelastic behavior of HA solutions depends on the solution pH.[18]

We checked whether the Cox-Merz rule is applicable to HA solutions, postulating the equality of steady state and complex viscosities.[22] Figure 3.12 presents complex viscosity vs frequency and viscosity vs shear rate for 0.7, 1 and 1.6 wt% HA solutions at pH 1.5, 2.5 and 7.4. Figure 3.12 outlines a very good match of steady state viscosity η and complex viscosity η*, for all solutions at pH 1.5 and pH 7.4; some deviations are observed for solutions at pH 2.5 as at this pH, the solution is in the gel state. The Cox-Merz relation is well known to be applicable to polymer solutions[23,24] and is used to predict the viscosity at higher shear rates using oscillation mode.

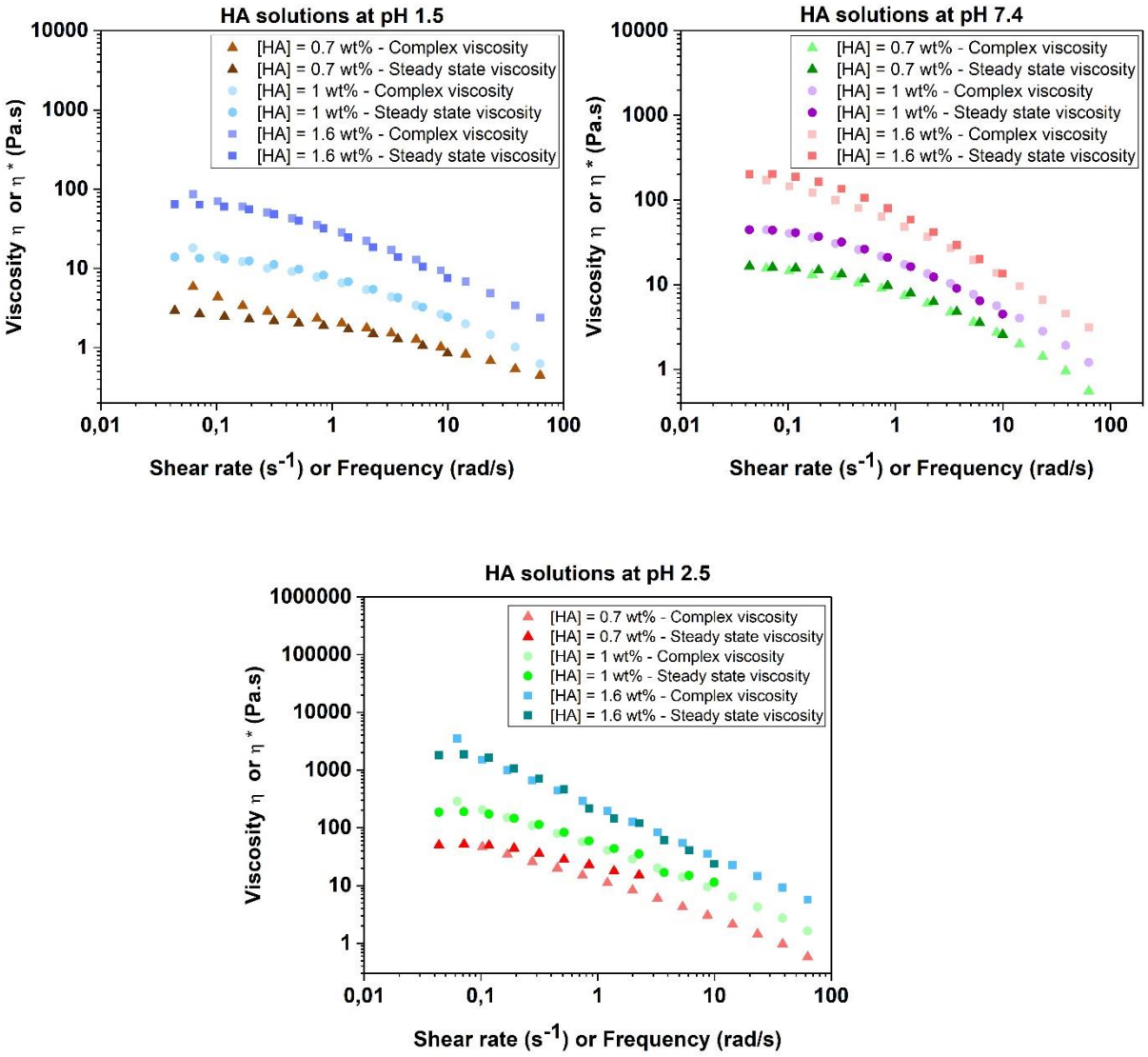

Figure 3.12. Steady state and complex viscosities of HA solutions at pH 1.5, 2.5 and 7.4 as a function of shear rate or frequency at 25°C.

Rheological measurements were also performed on HA solutions and gels after FT cycles (Figures 3.17, 3.19 and 3.20) and will be discussed within the next section.

3. Properties of physically crosslinked hyaluronic acid aerogels

3.1. Volume shrinkage, density and porosity

The preparation of HA dry materials, including aerogels, consisted of 3 steps: hydrogel formation, solvent exchange from water to acetone or ethanol and, lastly, supercritical drying with CO_2. HA hydrogel formation occurred via freeze-thawing, which is a physical cryostructuration process.[11,12] The solvent exchange step consists of replacing water in hydrogels by a liquid miscible with CO_2, such as ethanol or acetone. After the solvent exchange step, the ethanol or acetone in the pores was removed by gaseous CO_2, the latter being then evacuated under supercritical conditions. Since there is no meniscus at any interface above the critical point, the capillary pressure is no longer acting. Consequently, the network morphology of the HA organogels can theoretically be preserved. (See the process of preparation in Figure 2.1 – Chapter 2)

Table 3.4 gives an overview of the formulations studied for the preparation of HA dry materials. Two HA concentrations were tested (1 and 1.6 wt%), three pH values of the initial HA solution were used (pH = 1.5, 2.5 and 7.4), two FT cycles (# = 1 and 3) and the coagulation of HA was performed using acetone (A) or ethanol (E) as non-solvent, resulting in 12 different preparation conditions.

Table 3.4. Formulations tested to prepare HA dry materials. Sample name summarizes the formulation parameters: the first number indicates solution pH, the second number the HA concentration in solution, the third term is the number of freeze−thaw cycles, A, acetone and E, ethanol. Reprinted with permission from[13]. Copyright (2023) American Chemical Society.

Name	pH	HA concentration (wt%)	# of FT cycles	Non-solvent	Resulting material can be manipulated?
1.5-1.6-3FT-A	1.5	1.6	3	Acetone	Yes
1.5-1.6-3FT-E	1.5	1.6	3	Ethanol	Yes
2.5-1.0-1FT-A	2.5	1.0	1	Acetone	Yes
2.5-1.0-1FT-E	2.5	1.0	1	Ethanol	Yes
2.5-1.0-3FT-A	2.5	1.0	3	Acetone	Yes
2.5-1.0-3FT-E	2.5	1.0	3	Ethanol	Yes
2.5-1.6-1FT-A	2.5	1.6	1	Acetone	Yes

2.5-1.6-1FT-E	2.5	1.6	1	Ethanol	Yes
2.5-1.6-3FT-A	2.5	1.6	3	Acetone	Yes
2.5-1.6-3FT-E	2.5	1.6	3	Ethanol	Yes
7.4-1.6-3FT-A	7.4	1.6	3	Acetone	Yes
7.4-1.6-3FT-E	7.4	1.6	3	Ethanol	No

Thus, it follows that 11 out of the 12 formulations could be handled after $scCO_2$ drying and characterized. Only the 7.4-1.6-3FT-E sample was too friable for manipulation, and accordingly, this sample was not considered and analyzed further. As it will be shown below, not all dry HA materials resulted in aerogels, i.e. materials with low density (< 0.2 g/cm^3) and high specific surface area (> 100 m^2/g).[25] We will use the term "aerogel" when material properties meet these requirements, and "HA dry material" as a general term.

Let us first consider the macroscopic transformation occurring during the preparation of dry HA materials (Figures 3.13 and 3.14).

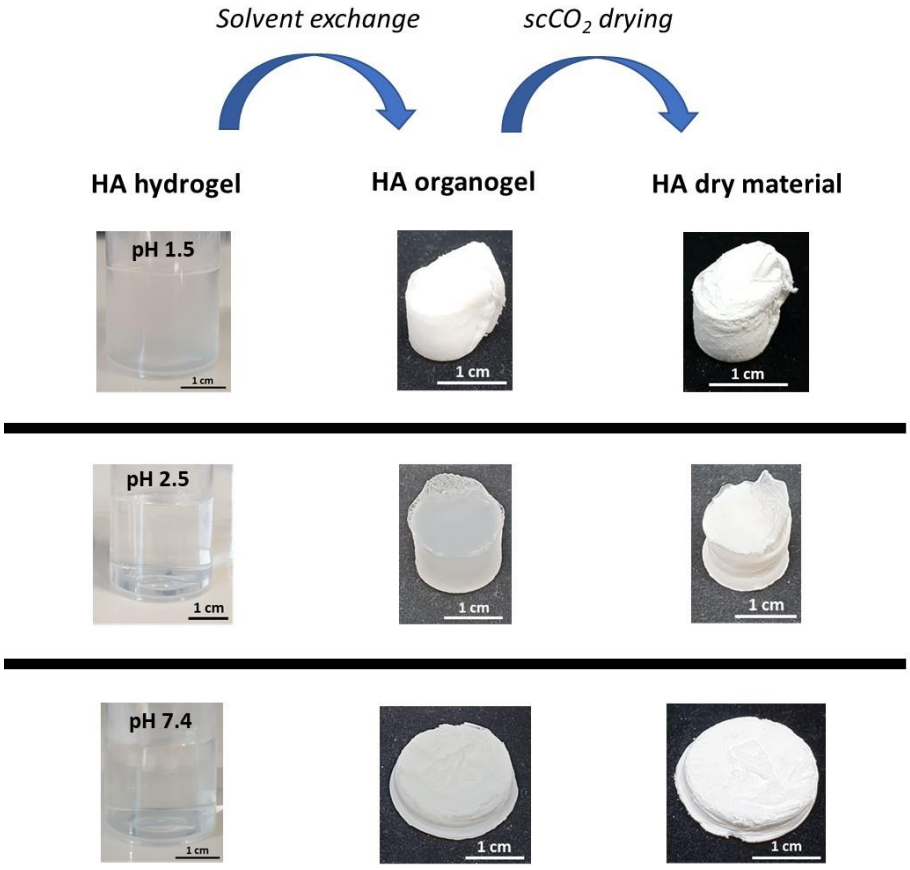

Figure 3.13. Photos of HA hydrogels, organogels, and dry materials for different pH values of the starting HA solutions. The HA concentration was 1.6 wt %, 3 FT cycles were applied, and

acetone was used as non-solvent in all cases. Reprinted with permission from[13]. Copyright (2023) American Chemical Society.

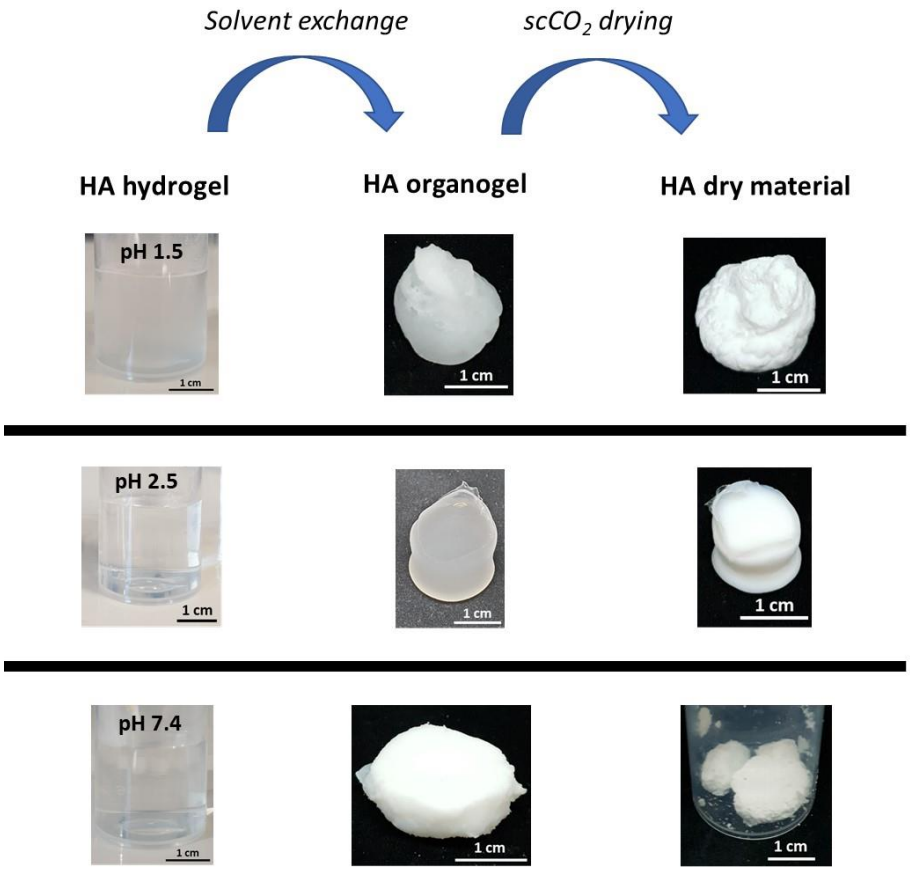

Figure 3.14. Photos of HA hydrogels, organogels, and dry materials for different pH values of the starting HA solutions. The HA concentration was 1.6 wt %, 3 FT cycles were applied, and ethanol was used as non-solvent in all cases. Reprinted with permission from[13]. Copyright (2023) American Chemical Society.

Ethanol or acetone was added to cylindrical HA hydrogels, obtained after 1 or 3 freeze−thaw cycles, to allow further drying with $scCO_2$. Ethanol and acetone are HA non-solvents, and thus hydrogels are shrinking during solvent exchange. Non-solvent induced phase transitions in synthetic polymer gels are well-known and have been extensively studied experimentally and theoretically (see, for example, refs[26–28]). Shrinkage of some polysaccharide solutions and gels during the preparation of bio-aerogels has also been reported[10,29,30] but nothing is known about the behavior of HA hydrogels when placed in a non-solvent. The changes in sample shape and volume due to solvent to non-solvent exchange and $scCO_2$ drying are illustrated in Figures 3.13 and 3.14. The volume shrinkage during solvent to non-solvent exchange and the total volume

shrinkage are presented in Figures 3.15 and 3.16. Volume shrinkage was high in all cases with values above 70% after solvent exchange and around 90% for overall shrinkage. While drying under supercritical conditions is supposed to preserve network morphology, shrinkage of HA in CO_2 occurs due to the poor affinity between both, with Hansen solubility parameters being 35.8 $MPa^{1/2}$ for HA[10] versus around 5−8 $MPa^{1/2}$ for $scCO_2$ in the conditions used.[31]

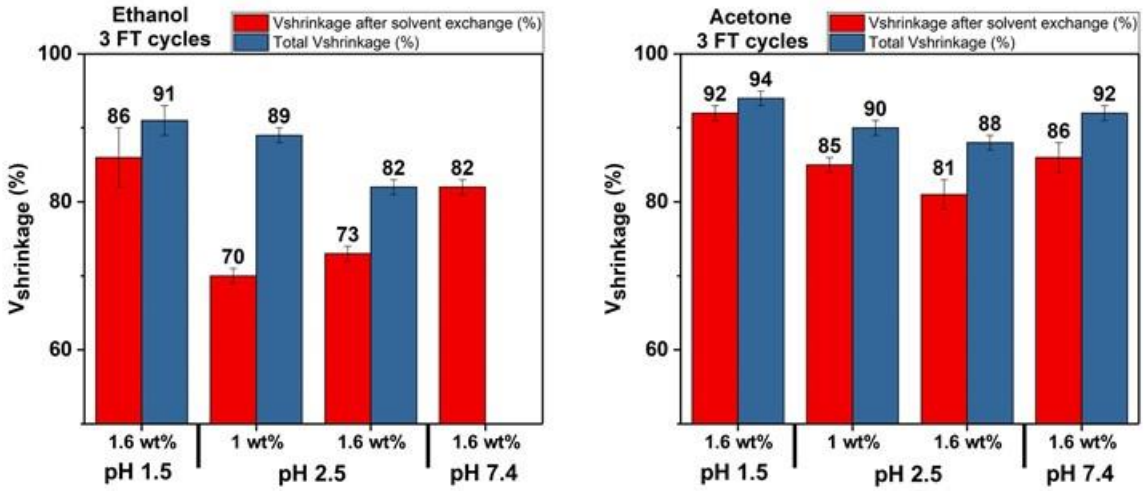

Figure 3.15. Volume shrinkage during the preparation of HA dry materials using 3 FT cycles and ethanol (left) or acetone (right) as non-solvent. Red bars correspond to the volume shrinkage during solvent exchange and blue bars to the overall volume shrinkage. Data for the 7.4−1.6−3FT-E are not available, as the sample was highly friable. Data are expressed as means ± standard deviation. Reprinted with permission from[13]. Copyright (2023) American Chemical Society.

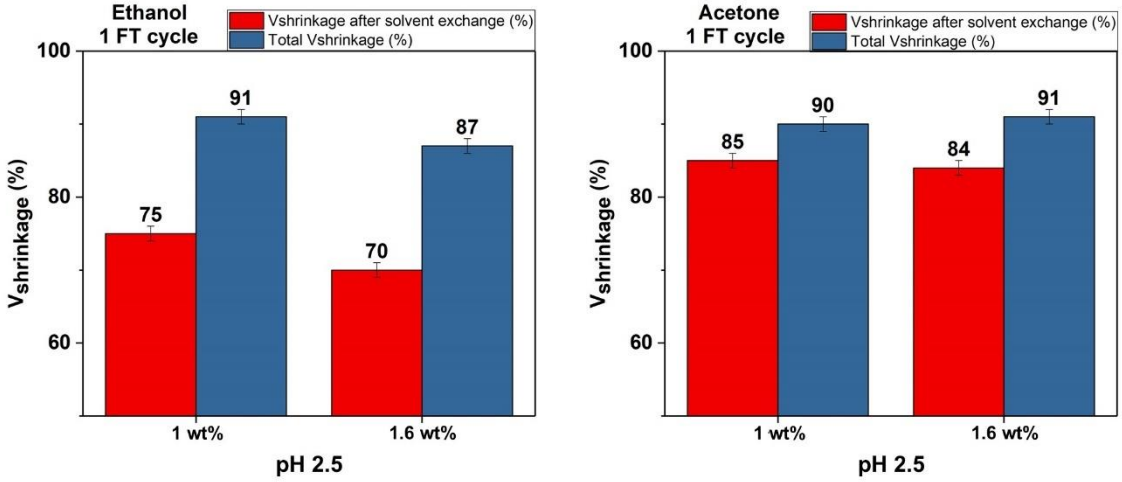

Figure 3.16. Volume shrinkage during the preparation of HA dry materials using 1 FT cycle and ethanol (left) or acetone (right) as non-solvent. Data are expressed as means ± standard deviation. Reprinted with permission from[13]. Copyright (2023) American Chemical Society.

The pH of the HA solution turned out to be the main parameter influencing organogel shape and volume shrinkage. Despite solution gelation during the FT cycle (Figure 3.17 with G' becoming higher than G" for a 1.0 wt% HA solution), at the lowest pH, 1.5, and for both HA concentrations and non-solvents used, a strong hydrogel shrinkage upon solvent exchange occurred (Figure 3.15), and organogels of rather distorted shape were obtained (Figure 3.13). As a consequence, dry materials were of the highest density among the obtained porous HA: 0.14 g/cm^3 (using ethanol) and 0.19 g/cm^3 (using acetone) for 3 FT cycles (Figure 3.18). The strong collapse of HA hydrogels made from solutions at pH 1.5 and placed in a non-solvent is most probably due to the more than 200 fold decrease of HA molecular weight (which was found to be 5500 g/mol, see Section 2.1)[10], suggesting that HA degrades at such low pH, as also reported in literature.[17] Due to HA degradation at low pH, the network is very weak, therefore not withstanding solvent exchange.

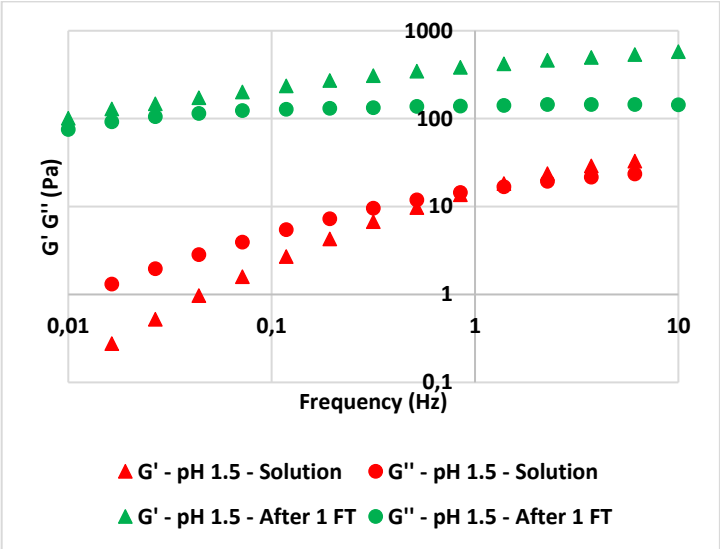

Figure 3.17. Storage (G') and loss (G'') moduli as a function of frequency for 1 wt% HA at pH 1.5 before and after 1 FT cycle. Reprinted with permission from[13]. Copyright (2023) American Chemical Society.

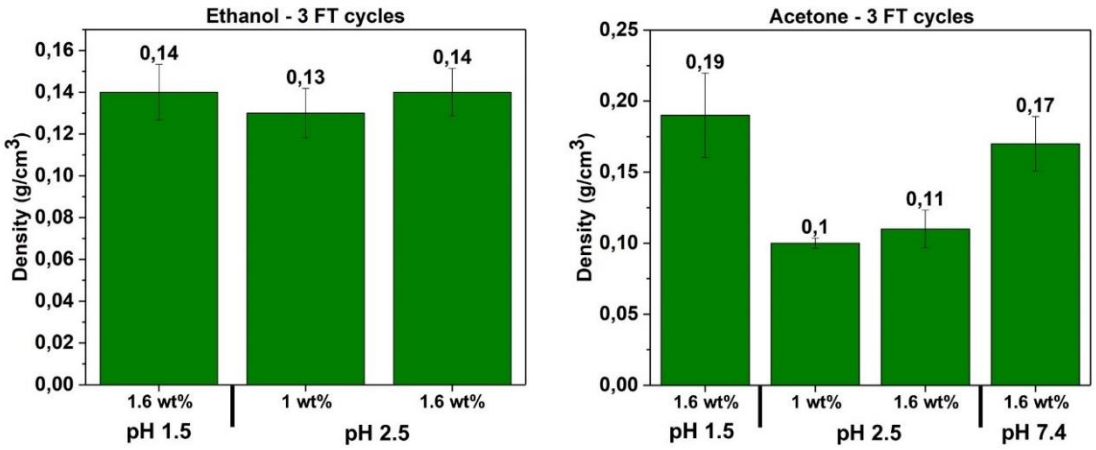

Figure 3.18. Bulk density of HA dry materials using 3 FT cycles and ethanol (left) or acetone (right) as non-solvent. Data are expressed as means ± SD. Reprinted with permission from[13]. Copyright (2023) American Chemical Society.

At the highest solution pH, 7.4, freezing did not lead to gelation (Figure 3.19). Organogels and dry materials were thin disks (Figure 3.13), which crumbled in case of ethanol as non-solvent (Figure 3.14). At pH > 2.5, most carboxylic groups of HA are ionized, so only few hydrogen bonds can be formed.[32] Moreover, Coulomb repulsion prevents hydrogen bond formation. As a result, inter- and intramolecular hydrogel bonding is limited, and the solution viscosity remains low. Hence, even after 3 FT cycles, HA samples collapsed during solvent exchange. In the absence of a strong network, the material exhibited a high shrinkage (92%) and a density of 0.17 g/cm^3 (Figure 3.15 and Figure 3.18, respectively).

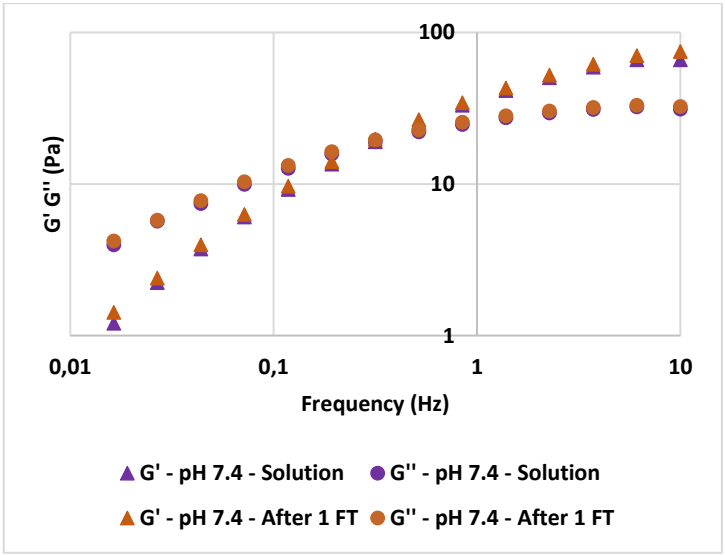

Figure 3.19. Storage (G') and loss (G'') moduli as a function of frequency for 1 wt% HA at pH 7.4 before and after 1 FT cycle. Reprinted with permission from[13]. Copyright (2023) American Chemical Society.

When solutions were at pH 2.5, solutions were gel-like, which is attributed to cooperative interchain interactions.[12,15] Freezing-thawing induced only around 10-15% increase of the elastic modulus (Figure 3.20). When acetone was used as non-solvent for both 1 and 1.6 wt% HA solutions, self-standing cylindrical organogels were obtained (Figure 3.13). A pH value of 2.5 corresponds to a critical balance of charges in the polymer resulting in a neutral net electrical charge; furthermore, the reduction of carboxylic group dissociation at low pH favors hydrogen bond formation. The abundant interactions between the HA chains lead to a strong network, resulting in the lowest volume shrinkage in comparison with other pH values (Figure 3.15) and hence the lowest density (Figure 3.18).

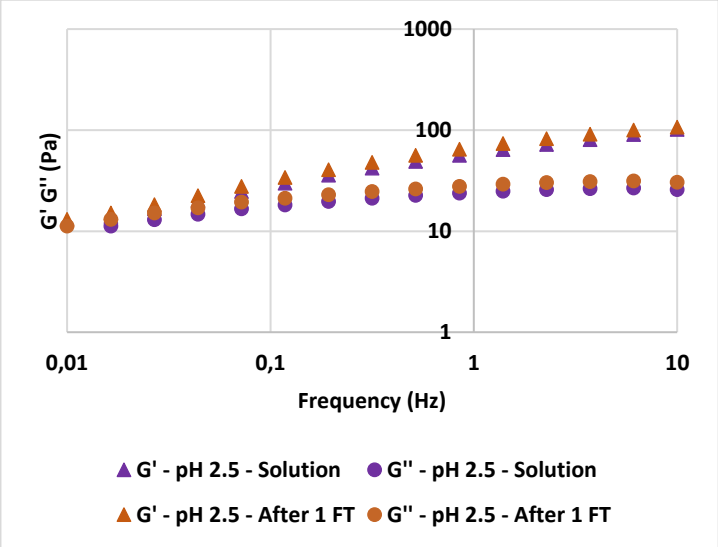

Figure 3.20. Storage (G') and loss (G'') moduli as a function of frequency for 1 wt% HA at pH 2.5 before and after 1 FT cycle. Reprinted with permission from[13]. Copyright (2023) American Chemical Society.

Higher shrinkage was observed for samples prepared with acetone as non-solvent (case of 3 FT cycles in Figure 3.15); the same trend was observed for materials made with 1 FT cycle (Figure 3.16). This can be ascribed to the lower affinity of HA to acetone, compared to ethanol, as indicated by the total solubility parameters of HA, ethanol and acetone (35.8, 26.5, and 19.9 $MPa^{1/2}$, respectively[10]), leading to a 'harsher' coagulation in acetone. No particular influence of the number of FT cycles on HA shrinkage and density was recorded (compare Figures 3.15 and 3.16, Figures 3.18 and 3.21). We suppose that the HA network remains weak, whatever HA

solution pH and number of FT cycles, with strong shrinkage prevailing over the influence of the number of FT cycles.

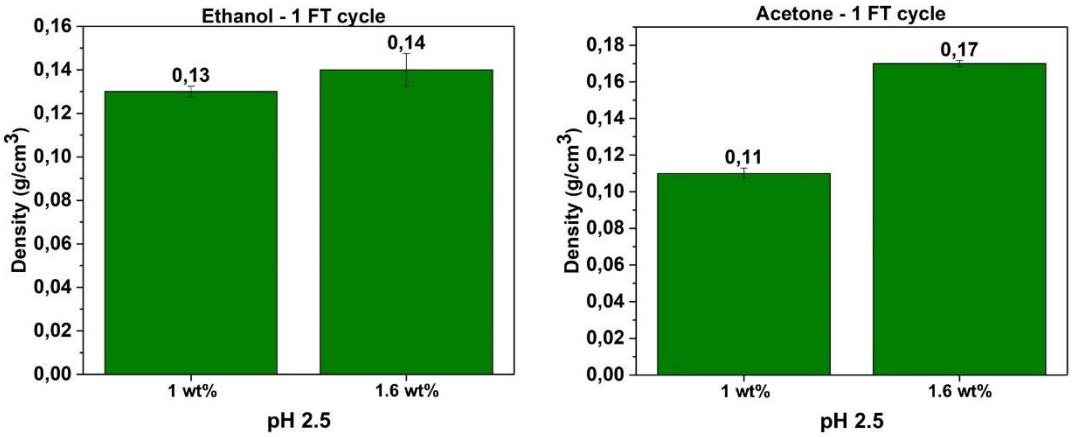

Figure 3.21. Bulk density of HA aerogels using 1 FT cycle and ethanol (left) or acetone (right) as non-solvent. Data are expressed as means ± standard deviation. Reprinted with permission from[13]. Copyright (2023) American Chemical Society.

It follows from Figures 3.15 and 3.16 that a higher HA concentration in the initial solution (1.6 vs 1.0 wt%) leads to reduced overall volume shrinkage, which can be ascribed to a more robust network. However, a higher HA concentration leads to materials with a slightly higher density (Figures 3.18 and 3.21), as reported for other biobased aerogels.[10,29,33] The results suggest that the effect of a higher polymer concentration outweighs the effect of increased resistance to non-solvent.

As expected from the low density of all dry HA materials, the porosity (Eq.6 – Chapter 2) is high, above 80% (Table 3.5). It is the lowest for samples made from solutions at pH 1.5 (85−89%) and the highest for samples made from solutions at pH 2.5 (87−92%). The specific pore volume of samples (Eq.7 – Chapter 2) follows the same trend as porosity: it is the lowest for the materials made from HA dissolved at pH 1.5, 4.5−6.3 cm^3/g, and the highest for the materials made at pH 2.5, 5.2− 8.9 cm^3/g (Table 3.5).

Table 3.5. Bulk density, porosity and pore volume of HA dry materials. Data are expressed as means ± standard deviation. Reprinted with permission from[13]. Copyright (2023) American Chemical Society.

Name	ρ_{bulk} (g/cm^3)	ε (%)	V_{pores} (cm^3/g)
1.5-1.6-3FT-A	0.19 ± 0.03	85 ± 2	4.5 ± 0.8
1.5-1.6-3FT-E	0.14 ± 0.01	89 ± 1	6.3 ± 0.7

2.5-1.0-1FT-A	0.11 ± 0.003	92 ± 1	8.5 ± 0.3
2.5-1.0-1FT-E	0.13 ± 0.002	90 ± 1	6.9 ± 0.1
2.5-1.0-3FT-A	0.10 ± 0.004	92 ± 1	8.9 ± 0.3
2.5-1.0-3FT-E	0.13 ± 0.01	90 ± 1	6.9 ± 0.7
2.5-1.6-1FT-A	0.17 ± 0.002	87 ± 1	5.2 ± 0.1
2.5-1.6-1FT-E	0.13 ± 0.003	89 ± 1	6.5 ± 0.4
2.5-1.6-3FT-A	0.11 ± 0.01	92 ± 1	8.8 ± 1.1
2.5-1.6-3FT-E	0.14 ± 0.01	89 ± 1	6.3 ± 0.5
7.4-1.6-3FT-A	0.17 ± 0.01	87 ± 1	5.1 ± 0.4
7.4-1.6-3FT-E	/	/	/

3.2. Specific surface area and morphology

Figure 3.22 presents the specific surface area of various HA dry materials. A strong influence of HA solution pH can be observed: materials that were prepared at pH 7.4 or pH 1.5 (using acetone as non-solvent) have a very low surface area (below 10 m^2/g) and therefore these materials cannot be considered as aerogels. At pH 7.4, no hydrogen bonds are formed, and the solution is of low viscosity. Upon freezing, HA is not gelling (see Figure 3.19) but concentrating around the growing ice crystals and forms pore walls. When HA is dissolved at pH 1.5, the polymer is strongly degrading[10,17] and a weak network built of low-molecular weight HA is formed. Freezing-thawing helps the formation of the network (Figure 3.17), however, upon the addition of a strong non-solvent, acetone, HA is collapsing resulting in a material with thick pore walls and pores that are replicas of ice crystals (Figure 3.23, top row); no signs of smaller pores are visible. A material with such large macropores and non-porous pore walls cannot possess high specific surface area (7 ± 1 m^2/g). When a "mild" non-solvent, ethanol, is used for HA solution at pH 1.5 after 3 FT cycles, the network structure is partly maintained (Figure 3.23, bottom row) resulting in a specific surface area of 275 ± 6 m^2/g.

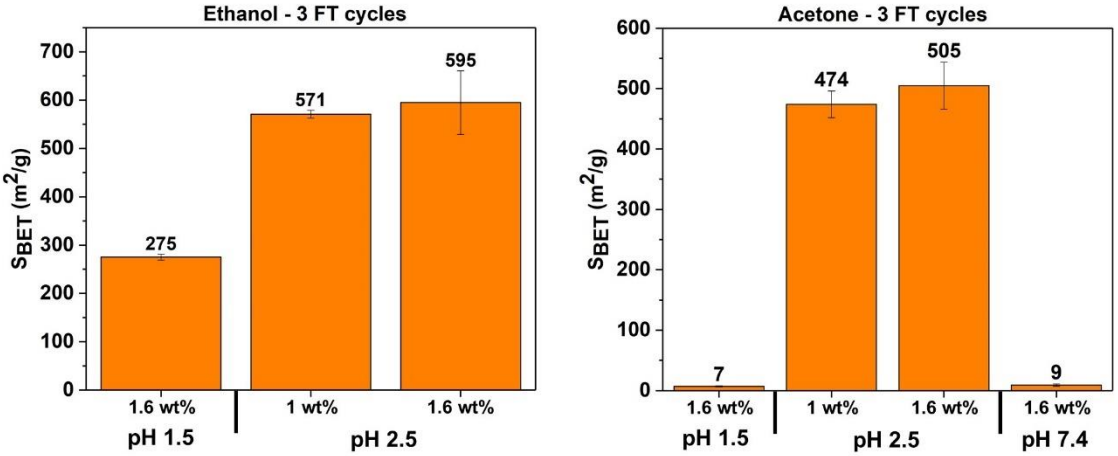

Figure 3.22. Specific surface area of HA dry materials using 3 FT cycles obtained by coagulating in ethanol (left) and in acetone (right). Data are expressed as means ± SD. Reprinted with permission from[13]. Copyright (2023) American Chemical Society.

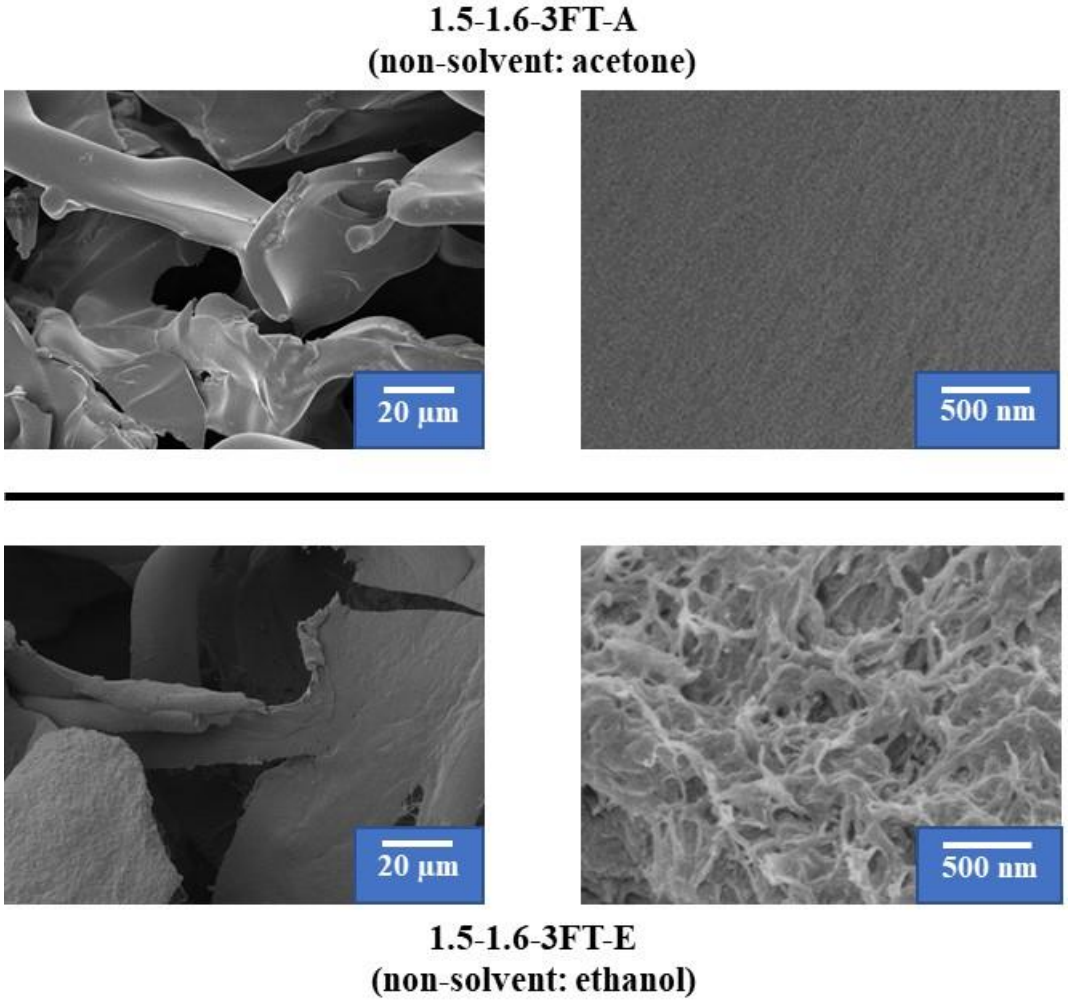

Figure 3.23. SEM images of HA dry material coagulated in acetone (top row) or in ethanol (bottom row). Both materials were prepared at pH 1.5 using 1.6 wt% as concentration and 3 FT cycles. Reprinted with permission from[13]. Copyright (2023) American Chemical Society.

Finally, aerogels, i.e., materials of low density and high S_{BET} (500 - 600 m^2/g), were obtained when HA was dissolved at pH 2.5 (Figures 3.22 and 3.24). The strong HA network formed at this pH, as evidenced by G' > G" (Figure 3.20), resists growing ice crystals and limits shrinkage upon the addition of a non-solvent; a network of fine entangled HA fibrils forming small pores is established (Figure 3.25). No larger pores are visible, suggesting that at pH 2.5, the interactions between HA chains are sufficiently strong to prevent deformation of the network and avoid the creation of large pores by growing ice crystals. In line with previous results[10], the use of ethanol as non-solvent resulted in the highest surface areas, thanks to the higher affinity of HA with ethanol in comparison with acetone (Figure 3.22, left and right). An increase in HA concentration results in a slight increase of the specific surface area (Figure 3.22). The number of FT cycles does not have a clear influence on the specific surface area (Figures 3.22 and 3.24).

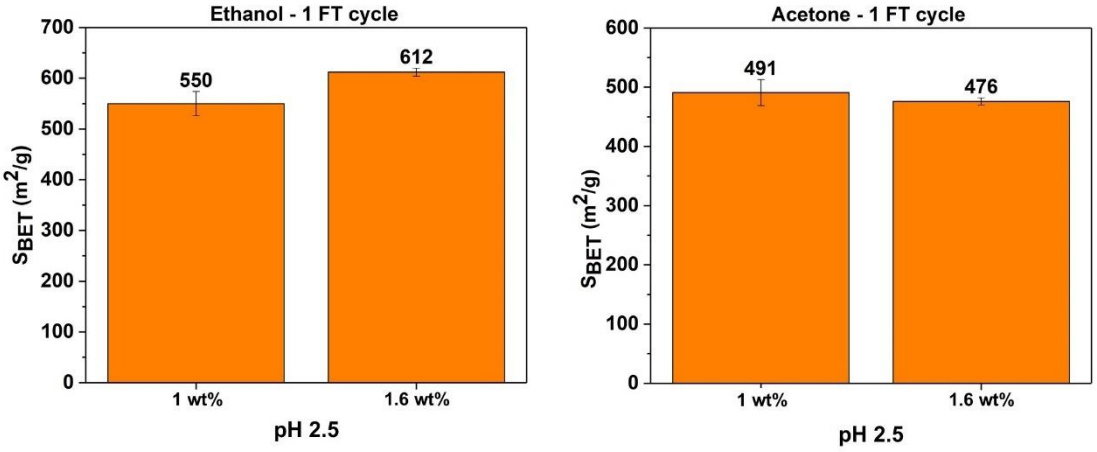

Figure 3.24. Specific surface area of HA aerogels using 1 FT cycle obtained by coagulating in ethanol (left) and in acetone (right). Data are expressed as means ± standard deviation. Reprinted with permission from[13]. Copyright (2023) American Chemical Society.

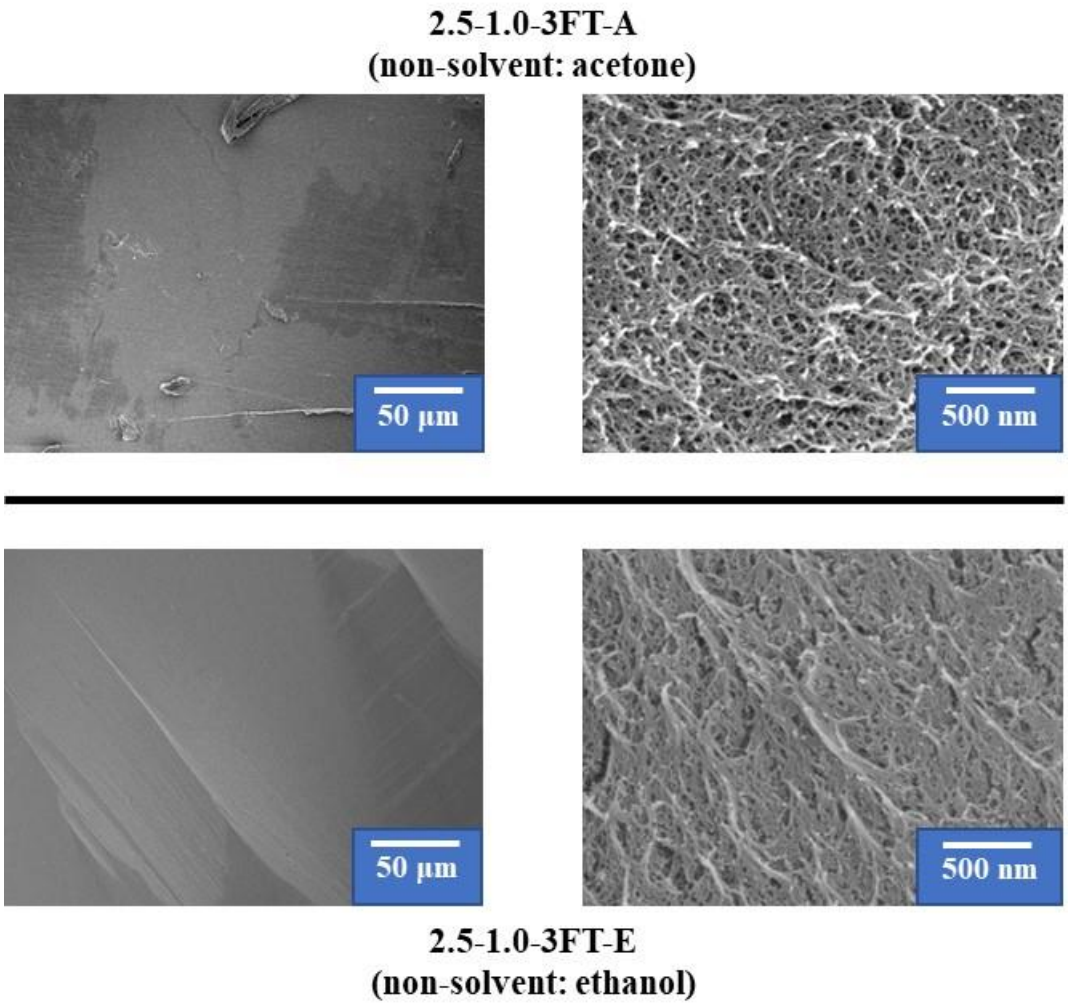

Figure 3.25. SEM images of HA dry material coagulated in acetone (top row) or in ethanol (bottom row). Both materials were prepared at pH 2.5 using 1 wt% as concentration and 3 FT cycles. Reprinted with permission from[13]. Copyright (2023) American Chemical Society.

3.3. Pore size distribution and pore volume

The pore size distribution and pore volume of the 2.5-1.6-3FT-A aerogel were characterized using the BJH method. Figure 3.26 presents an example of a nitrogen adsorption/desorption curve. The BJH method only considers the mesopores and small macropores region. For several bio-aerogels, however, the pore size distribution was shown to be much wider, and the pore volume obtained with the BJH approach considered only a small fraction of whole pores (as low as 10-20% of the pore volume).[34]

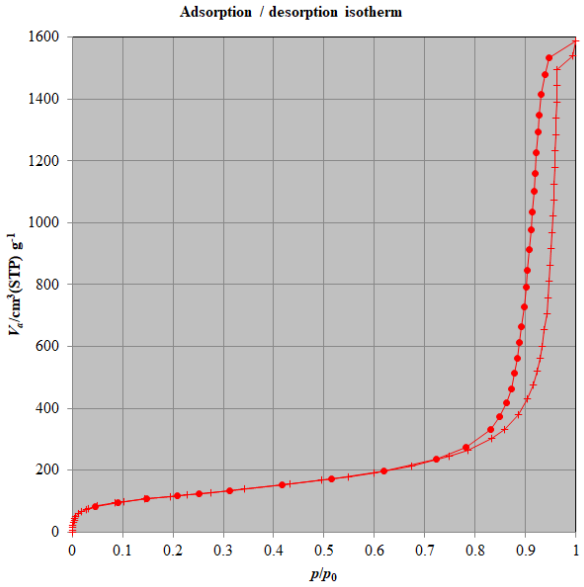

Figure 3.26. Nitrogen adsorption/desorption curve for the 2.5-1.6-3FT-A aerogel. Reprinted with permission from[13]. Copyright (2023) American Chemical Society.

From this isotherm, the BJH approach yields 65 % (2.42 cm^3/g) of the total pore volume (3.75 cm^3/g calculated from bulk and skeletal density (See Eq.7 – Chapter 2), indicating that many small (< 200 nm) pores are present in the HA aerogel. The classical formula for calculating average pore size D, using BJH method, is given by the following equation:

$$D = \frac{4 \times V_{p,BJH}}{S_{BET}} \qquad (1)$$

The average pore diameter of this aerogel calculated from the specific surface area (here, S_{BET} = 414 m^2/g) is 23 nm, which is, however, an underestimation as only part of the pore volume is considered.

3.4. Mechanical properties of HA aerogels

Uniaxial compression tests were performed to characterize the mechanical properties of HA aerogels. Two methods were used to measure sample deformation, see details in Chapter 2. The Instron machine directly measured the deformation of the sample when a force was applied to it. The local deformation of the sample was also tracked over time using digital image correlation (DIC) technique, employing two cameras in stereo correlation. In this case, images were analyzed by VIC 3D software and an extensometer was used to track the positions of speckled points on the sample during compression and to determine the sample strain evolution along the vertical axis (see details in Section 4.8 – Chapter 2). Typical nominal stress-strain curves obtained with the two methods are shown in Figure 3.27. Two types of aerogels were

prepared using an initial solution pH of 2.5, 3 FT cycles and ethanol as non-solvent: only the HA concentration was varied (1.6 and 1 wt%). For each formulation, four samples were tested. In Figure 3.27, an example of each formulation is also shown. Similar results were obtained for all the other investigated HA aerogels.

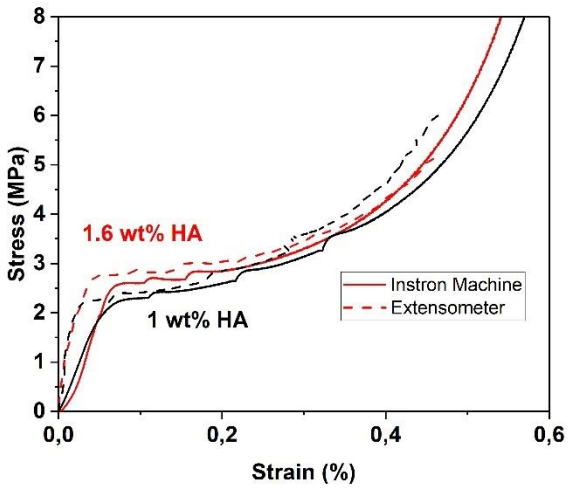

Figure 3.27. Typical stress-strain curves obtained for the 1 wt% (black) and the 1.6 wt% (red) HA aerogels by the Instron machine (continuous line) and by the extensometer (dashed line).

As already reported for mechanical properties of various bio-aerogels[35,36], the stress-strain curve contains three regions (obtained with both methods): i) a linear elastic region at low strains, from which the compressive (or Young's or elastic) modulus E can be determined – in this zone, the stress increase is proportional to the deformation; ii) a stress plateau, corresponding to progressive pores' walls elastic buckling followed by their collapse when the plastic yield is reached and iii) a densification region at high stresses, when opposing pore walls touch each other, broken fragments pack together and further deformation starts to compress the pore wall material itself. After compression, the density of HA aerogels increased by a factor 4, becoming around 1.2 – 1.3 g/cm^3. After the test, the sample diameter remained practically unchanged, which means that the Poisson ratio is zero. The linear elastic region ends when the material starts to yield and reaches its yield strength σ. The second region of the compression curve is characterized by a low slope. This "plateau" enables porous materials to absorb a large amount of energy, W (J/m^3), without experiencing a large increase in stress. The absorption energy during the plastic deformation is defined as the area under the stress-strain curve taken up to 40% strain. The third region is characterized by a steep increase in stress-strain curve corresponding to material densification.

The curves obtained with the extensometer (DIC technique, shown in Figure 3.27 with dashed lines) gives more reliable information on the deformation of the sample as it does not consider displacement induced by the stiffness of the tensile machine. The parameters deduced from stress-strain data with both approaches are compared below.

Table 3.6 shows the HA sample density before and after compression and the mechanical properties (i.e. compressive E modulus, yield stress σ, energy absorbed during plastic deformation and stress at 40% strain) of HA aerogels. Two formulations of HA aerogels were tested: 2.5-1.6-3FT-E and 2.5-1-3FT-E.

Table 3.6. Density before and after compression and mechanical properties of HA aerogels.

			Mechanical properties of HA aerogels				
Formulation Name	ρ_{bulk} before compression (g/cm^3)		Compressive modulus E (MPa)	Yield stress σ (MPa)	Absorption energy W (J/m^3)	Stress at 40% strain (MPa)	ρ_{bulk} after compression (g/cm^3)
2.5-1.6-3FT-E	0.33 ± 0.03	Extenso-meter	82 ± 10	2.74 ± 0.26	1.39 ± 0.25	4.97 ± 0.89	1.33 ± 0.02
		Instron machine	33 ± 4	2.68 ± 0.23	1.29 ± 0.16	5.13 ± 0.77	
2.5-1-3FT-E	0.30 ± 0.01	Extenso-meter	76 ± 8	1.90 ± 0.18	1.14 ± 0.24	4.87 ± 1.42	1.24 ± 0.02
		Instron machine	46 ± 7	1.98 ± 0.24	1.01 ± 0.16	3.87 ± 0.54	

The initial density of the HA aerogels is above the density reported in Section 3.1, due to water vapor adsorption by HA aerogels when kept in open air.

Concerning the mechanical properties, for both formulations, higher compressive moduli were obtained with data from the extensometer, as expected. In both cases, the compressive modulus, the yield strength, and the absorption energy increase with bulk density. For example, with a density of 0.33 g/cm^3, the 1.6 wt% HA sample had a higher compressive modulus (82 ± 10 MPa), a higher yield stress (2.74 ± 0.26 MPa) and a higher absorbed energy (1.39 ± 0.25 MPa). This behavior was also observed for organic and inorganic aerogels.[35,37–39] The compressive moduli of the obtained HA aerogels (around 80 MPa) are close to those of cellulose aerogels of similar density (prepared from zinc chloride salt hydrate melt and using acetone as non-solvent[40]).

Here, only a screening of the mechanical properties of HA aerogels was performed. As demonstrated in the previous Sections of this chapter, the aerogel properties, such as morphology

and density, depend on several preparation parameters; in addition, samples were aging. More work should be done to deduce the trends.

3.5. Absorption properties of HA aerogels

HA is a promising polymer for wound healing applications. The absorption of wound exudate by the dressing material is important to guarantee a good healing process and limit infections. An example of absorption of PBS by a physically crosslinked HA aerogel is shown for the 2.5-1.6-3FT-A aerogel. Figure 3.28 presents the normalized sample mass evolution (Eq.8 – Chapter 2) as a function of time. The sample rapidly absorbs PBS and the maximum absorption is reached after 15 minutes. Subsequently, the sample gradually dissolves.

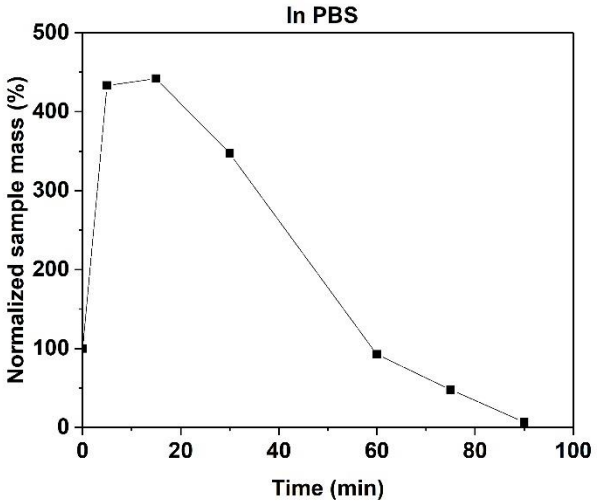

Figure 3.28. Normalized mass evolution over time of the 2.5-1.6-3FT-A aerogel upon immersion in PBS at room temperature. Data was obtained from a single experiment.

3.6. Behavior of HA aerogels upon exposure to the air

The mass, density and specific surface area of HA aerogels exposed to air were monitored over time in view of long-term storage of the materials.

We demonstrated the mass evolution of a physically crosslinked HA aerogel with the 2.5−1.6−3FT-A aerogel. The mass of the aerogel was recorded over time at room temperature (27°C) and 51 % relative humidity. Figure 3.29 presents the normalized sample mass (Eq.8 – Chapter 2) as function of time. The HA sample mass increases up to reaching a plateau after 225 min, which is likely due to adsorption of moisture from the air. This experiment was performed only one time.

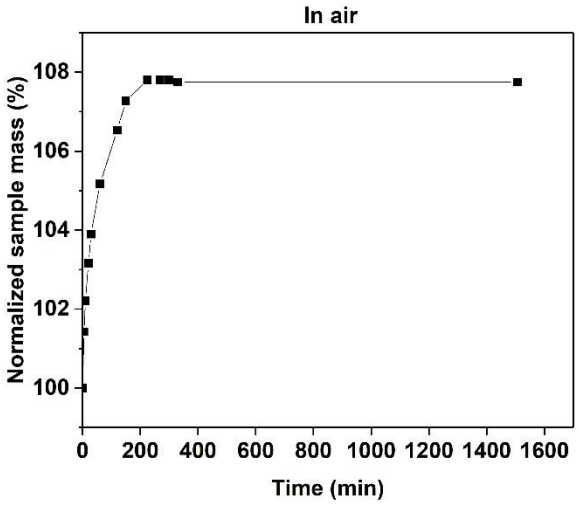

Figure 3.29. Normalized mass of the 2.5-1.6-3FT-A aerogel upon exposure to the air at 27°C and 51 % relative humidity. Data was obtained from a single experiment.

The volume of the 2.5−1.6−3FT-A aerogel was also measured over time at room temperature (27°C) and 51 % relative humidity. Figure 3.30 presents the evolution of the sample volume and density as function of time. The HA sample density significantly increases up to reaching a plateau around 0.6 g/cm^3 after about 300 min, while the HA sample volume strongly decreases up to reaching a plateau around 0.35 cm^3 after the same time. Such an increase in density is due to high sample shrinkage, which probably occurs because of water vapor condensation, polymer swelling and pores closure.

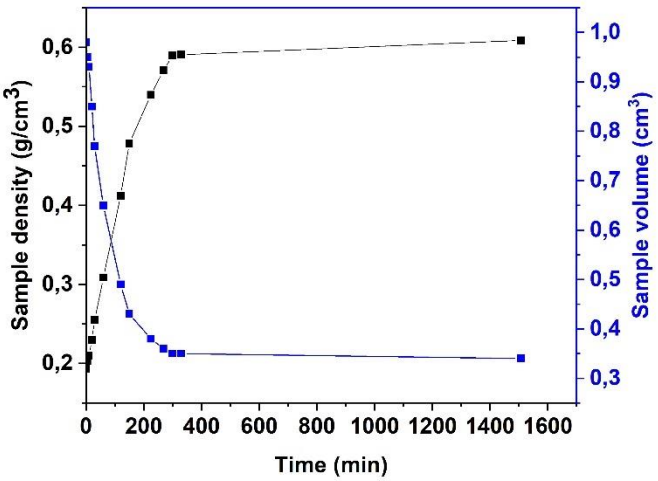

Figure 3.30. Normalized density and volume of the 2.5-1.6-3FT-A aerogel upon exposure to the air at 27°C and 51 % relative humidity.

The evolution of the specific surface area of two HA aerogels, prepared at pH 2.5 and with ethanol as non-solvent, was studied over time. Between each measurement, samples were let in a drawer at room temperature. Figure 3.31 presents the specific surface area of 2.5-1.0-1FT-E and 2.5-1.6-3FT-E aerogels over 2 months.

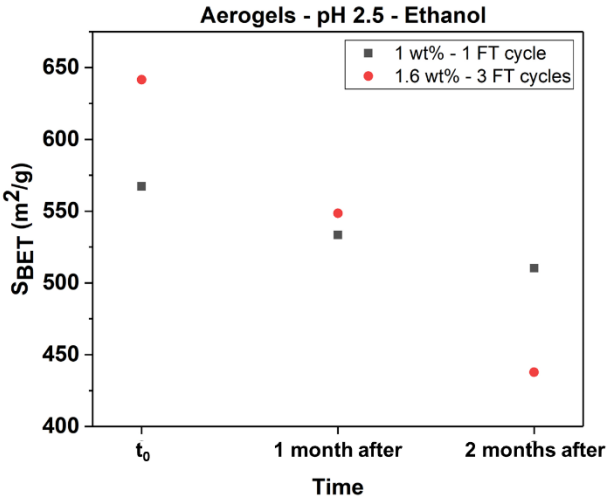

Figure 3.31. Evolution of 2.5-1.0-1FT-E and 2.5-1.6-3FT-E aerogels S_{BET} over time. Data was obtained from a single experiment for each formulation.

The specific surface area of 2.5-1.0-1FT-E and 2.5-1.6-3FT-E HA aerogels decreases over time. This trend is likely due to adsorption of moisture from the air, resulting in pore collapse. More work should be done to deduce trends. These results show the importance of storing the aerogels under an inert atmosphere to minimize pore collapse and deterioration of aerogel properties.

4. Conclusions

This chapter presented the preparation and the characterization of HA aerogels obtained via physical crosslinking. The molecular weight of HA, given by the manufacturer, was 1.2×10^6 g/mol. First, the influence of pH and time on HA molecular weight was investigated: at physiological pH (i.e. 7.4), HA degrades very slowly whereas at basic pH (pH 12) degradation occurs very rapidly via basic hydrolysis. At pH 2.5, the HA molecular weight decreases due to acid hydrolysis, and the degradation continues in solution for several days. At more acid pH (i.e. 1.5), severe HA degradation occurs, and its initial viscosity is reduced by around 80% after 6 days (see Rheological analysis for HA solutions at pH 1.5).

The rheological properties of HA solutions as a function of polymer concentration and solution pH were studied. HA solutions have a shear-thinning behavior, as expected. Higher viscosity was obtained for higher HA concentration. Changing the pH also influences the HA solutions viscoelastic properties. HA solutions at pH 2.5 behave more as gel compared to solutions at pH 7.4 and 1.5. The use of centrifugation did not impact the rheological properties of HA solution. The Cox-Merz rule was shown to be applicable for solutions at pH 1.5 and 7.4.

HA aerogels were produced using the FT gelation technique, solvent exchange, and drying with $scCO_2$. The FT method allows for the formation of physically crosslinked hydrogels, through hydrogen bonds, that serve as precursors for HA aerogels. Despite that all self-standing materials were of low density (below 0.2 g/cm^3), only some formulations resulted in aerogels, i.e., materials with high specific surface area. The highest surface areas, 500−600 m^2/g, were obtained for HA aerogels made from solutions at pH 2.5 (HA isoelectric point). The internal morphology of aerogels is a network of fine entangled fibrils. At other pH values, 1.5 or 7.4, the materials were either not self-standing or with negligible specific surface area due to large pores and thick non-porous walls (in case of pH 7.4 with both coagulants, and in case of pH 1.5 with acetone as coagulant), or with lower surface area as compared to pH 2.5, around 275 m^2/g (3 FT cycles, pH 1.5, ethanol as coagulant). The reasons are that at pH 7.4, HA is deprotonated and does not form a network, whereas, at pH 1.5, HA is strongly degraded forming a weak network, which collapses in a “harsh” non-solvent (acetone), but partly resists when coagulated in ethanol.

The mechanical properties of HA aerogels were characterized upon compression. The deformation of HA aerogel was followed using 2 techniques: Instron machine and DIC method. The DIC technique gave more reliable information on the deformation of the sample as it does not consider the stiffness of the tensile machine which influences displacement. The compressive

modulus of HA aerogels was around 80 MPa for samples with a density of around 0.3 g/cm^3. Higher compressive modulus, higher yield stress and higher absorbed energy were obtained for HA aerogels prepared with 1.6 wt% HA. After compression tests, densification of HA aerogels occurred, due to pores collapse. The values of compressive moduli of HA aerogels were found to be close to the ones of some cellulose aerogels of similar density. The obtained results present a preliminary screening of the mechanical properties of HA aerogels; more experiments and better sample preservation against aging are needed to deduce trends.

Physically crosslinked HA aerogels are very sensitive to humidity. They dissolved rapidly in PBS medium (≈ 90 minutes). Upon exposure to the air, the mass of HA aerogels increased by 8%, the volume decreased by 65% and the density increased by 215% after 6h in air. The specific surface area of aerogels also decreases upon 2-month storage (by 32% for 1.6 wt% HA, pH 2.5 and 3 FT cycles and by 10% for 1 wt% HA, pH 2.5 and 1 FT cycle). Storing HA aerogels under an inert atmosphere is essential to minimize pore collapse and deterioration of their properties.

The results confirm that HA is an appealing polymer for the preparation of aerogels provided appropriate conditions are used. These novel HA aerogels have interesting, tunable properties that make them promising biomaterials, for example, for wound dressing applications.

5. References

(1) Graça, M. F. P.; Miguel, S. P.; Cabral, C. S. D.; Correia, I. J. Hyaluronic Acid—Based Wound Dressings: A Review. *Carbohydrate Polymers* **2020**, *241*, 116364. https://doi.org/10.1016/j.carbpol.2020.116364.

(2) Ying, H.; Zhou, J.; Wang, M.; Su, D.; Ma, Q.; Lv, G.; Chen, J. In Situ Formed Collagen-Hyaluronic Acid Hydrogel as Biomimetic Dressing for Promoting Spontaneous Wound Healing. *Materials Science and Engineering: C* **2019**, *101*, 487–498. https://doi.org/10.1016/j.msec.2019.03.093.

(3) Zhou, Z.; Zhang, X.; Xu, L.; Lu, H.; Chen, Y.; Wu, C.; Hu, P. A Self-Healing Hydrogel Based on Crosslinked Hyaluronic Acid and Chitosan to Facilitate Diabetic Wound Healing. *International Journal of Biological Macromolecules* **2022**, *220*, 326–336. https://doi.org/10.1016/j.ijbiomac.2022.08.076.

(4) Liang, M.; Dong, L.; Guo, Z.; Liu, L.; Fan, Z.; Wei, C.; Mi, S.; Sun, W. Collagen–Hyaluronic Acid Composite Hydrogels with Applications for Chronic Diabetic Wound Repair. *ACS Biomater. Sci. Eng.* **2023**, *9* (9), 5376–5388. https://doi.org/10.1021/acsbiomaterials.3c00695.

(5) Roether, J.; Oelschlaeger, C.; Willenbacher, N. Hyaluronic Acid Cryogels with Non-Cytotoxic Crosslinker Genipin. *Materials Letters: X* **2019**, *4*, 100027. https://doi.org/10.1016/j.mlblux.2019.100027.

(6) Wang, M.; Hu, J.; Ou, Y.; He, X.; Wang, Y.; Zou, C.; Jiang, Y.; Luo, F.; Lu, D.; Li, Z.; Li, J.; Tan, H. Shape-Recoverable Hyaluronic Acid–Waterborne Polyurethane Hybrid Cryogel Accelerates Hemostasis and Wound Healing. *ACS Appl. Mater. Interfaces* **2022**, *14* (15), 17093–17108. https://doi.org/10.1021/acsami.2c01310.

(7) Wang, C.; Liang, Y.; Huang, Y.; Li, M.; Guo, B. Porous Photothermal Antibacterial Antioxidant Dual–Crosslinked Cryogel Based on Hyaluronic Acid/ Polydopamine for Non-Compressible Hemostasis and Infectious Wound Repair. *Journal of Materials Science & Technology* **2022**, *121*, 207–219. https://doi.org/10.1016/j.jmst.2021.12.054.

(8) Athamneh, T.; Amin, A.; Benke, E.; Ambrus, R.; Leopold, C. S.; Gurikov, P.; Smirnova, I. Alginate and Hybrid Alginate-Hyaluronic Acid Aerogel Microspheres as Potential Carrier for Pulmonary Drug Delivery. *The Journal of Supercritical Fluids* **2019**, *150*, 49–55. https://doi.org/10.1016/j.supflu.2019.04.013.

(9) Athamneh, T.; Amin, A.; Benke, E.; Ambrus, R.; Gurikov, P.; Smirnova, I.; Leopold, C. S. Pulmonary Drug Delivery with Aerogels: Engineering of Alginate and Alginate–Hyaluronic Acid Microspheres. *Pharmaceutical Development and Technology* **2021**, *26* (5), 509–521. https://doi.org/10.1080/10837450.2021.1888979.

(10) Aguilera-Bulla, D.; Legay, L.; Buwalda, S. J.; Budtova, T. Crosslinker-Free Hyaluronic Acid Aerogels. *Biomacromolecules* **2022**, *23* (7), 2838–2845. https://doi.org/10.1021/acs.biomac.2c00207.

(11) Cai, Z.; Tang, Y.; Wei, Y.; Wang, P.; Zhang, H. Physically Cross-Linked Hyaluronan-Based Ultrasoft Cryogel Prepared by Freeze-Thaw Technique as a Barrier for Prevention of Postoperative Adhesions. *Biomacromolecules* **2021**, *22* (12), 4967–4979. https://doi.org/10.1021/acs.biomac.1c00878.

(12) Cai, Z.; Zhang, F.; Wei, Y.; Zhang, H. Freeze–Thaw-Induced Gelation of Hyaluronan: Physical Cryostructuration Correlated with Intermolecular Associations and Molecular

Conformation. *Macromolecules* **2017**, *50* (17), 6647–6658. https://doi.org/10.1021/acs.macromol.7b01264.

(13) Legay, L.; Budtova, T.; Buwalda, S. Hyaluronic Acid Aerogels Made Via Freeze–Thaw-Induced Gelation. *Biomacromolecules* **2023**, *24* (10), 4502–4509. https://doi.org/10.1021/acs.biomac.2c01518.

(14) García-Abuín, A.; Gómez-Díaz, D.; Navaza, J. M.; Regueiro, L.; Vidal-Tato, I. Viscosimetric Behaviour of Hyaluronic Acid in Different Aqueous Solutions. *Carbohydrate Polymers* **2011**, *85* (3), 500–505. https://doi.org/10.1016/j.carbpol.2011.02.028.

(15) Gatej, I.; Popa, M.; Rinaudo, M. Role of the pH on Hyaluronan Behavior in Aqueous Solution. *Biomacromolecules* **2005**, *6* (1), 61–67. https://doi.org/10.1021/bm040050m.

(16) Gaohua, L.; Miao, X.; Dou, L. Crosstalk of Physiological pH and Chemical pKa under the Umbrella of Physiologically Based Pharmacokinetic Modeling of Drug Absorption, Distribution, Metabolism, Excretion, and Toxicity. *Expert Opinion on Drug Metabolism & Toxicology* **2021**, *17*. https://doi.org/10.1080/17425255.2021.1951223.

(17) Maleki, A.; Kjøniksen, A.-L.; Nyström, B. Effect of pH on the Behavior of Hyaluronic Acid in Dilute and Semidilute Aqueous Solutions. *Macromol. Symp.* **2008**, *274* (1), 131–140. https://doi.org/10.1002/masy.200851418.

(18) Gibbs, D. A.; Merrill, E. W.; Smith, K. A.; Balazs, E. A. Rheology of Hyaluronic Acid. *Biopolymers* **1968**, *6* (6), 777–791. https://doi.org/10.1002/bip.1968.360060603.

(19) Balazs, E. A. Chapter 20 - Viscoelastic Properties of Hyaluronan and Its Therapeutic Use In *Chemistry and Biology of Hyaluronan*; Garg, H. G., Hales, C. A., Eds.; Elsevier Science Ltd: Oxford, **2004**; pp 415–455. https://doi.org/10.1016/B978-008044382-9/50051-0.

(20) Evered, D.; Whelan, J. *The Biology of Hyaluronan*; John Wiley & Sons, **2008**.

(21) Mezger, T. G. *The Rheology Handbook: 4th Edition*; Vincentz Network, **2014**.

(22) Cox, W. P.; Merz, E. H. Correlation of Dynamic and Steady Flow Viscosities. *Journal of Polymer Science* **1958**, *28* (118), 619–622. https://doi.org/10.1002/pol.1958.1202811812.

(23) Rudaz, C.; Budtova, T. Rheological and Hydrodynamic Properties of Cellulose Acetate/Ionic Liquid Solutions. *Carbohydrate Polymers* **2013**, *92* (2), 1966–1971. https://doi.org/10.1016/j.carbpol.2012.11.066.

(24) Negrier, M.; El Ahmar, E.; Sescousse, R.; Sauceau, M.; Bouet, G.; Eglin, D.; Budtova, T. Upcycling Cellulose Waste Textile into Aerogel Beads via Prilling Technique. *Cellulose* **2023**. https://doi.org/10.1007/s10570-023-05659-x.

(25) *Aerogels Handbook*; Aegerter, M. A., Leventis, N., Koebel, M. M., Eds.; Springer New York: New York, NY, **2011**. https://doi.org/10.1007/978-1-4419-7589-8.

(26) Tanaka, T. Collapse of Gels and the Critical Endpoint. *Phys. Rev. Lett.* **1978**, *40* (12), 820–823. https://doi.org/10.1103/PhysRevLett.40.820.

(27) Osada, Y.; Ping Gong, J.; Tanaka, Y. Polymer Gels. *Journal of Macromolecular Science, Part C* **2004**, *44* (1), 87–112. https://doi.org/10.1081/MC-120027935.

(28) Ilavsky, M. Phase Transition in Swollen Gels. 2. Effect of Charge Concentration on the Collapse and Mechanical Behavior of Polyacrylamide Networks. *Macromolecules* **1982**, *15* (3), 782–788. https://doi.org/10.1021/ma00231a019.

(29) Groult, S.; Budtova, T. Tuning Structure and Properties of Pectin Aerogels. *European Polymer Journal* **2018**, *108*, 250–261. https://doi.org/10.1016/j.eurpolymj.2018.08.048.

(30) Budtova, T. Cellulose II Aerogels: A Review. *Cellulose* **2019**, *26* (1), 81–121. https://doi.org/10.1007/s10570-018-2189-1.

(31) Zhang, M.; Dou, M.; Wang, M.; Yu, Y. Study on the Solubility Parameter of Supercritical Carbon Dioxide System by Molecular Dynamics Simulation. *Journal of Molecular Liquids* **2017**, *248*, 322–329. https://doi.org/10.1016/j.molliq.2017.10.056.

(32) Giubertoni, G.; Burla, F.; Martinez-Torres, C.; Dutta, B.; Pletikapic, G.; Pelan, E.; Rezus, Y. L. A.; Koenderink, G. H.; Bakker, H. J. Molecular Origin of the Elastic State of Aqueous Hyaluronic Acid. *J. Phys. Chem. B* **2019**, *123* (14), 3043–3049. https://doi.org/10.1021/acs.jpcb.9b00982.

(33) Druel, L.; Bardl, R.; Vorwerg, W.; Budtova, T. Starch Aerogels: A Member of the Family of Thermal Superinsulating Materials. *Biomacromolecules* **2017**, *18* (12), 4232–4239. https://doi.org/10.1021/acs.biomac.7b01272.

(34) Groult, S.; Budtova, T. Thermal Conductivity/Structure Correlations in Thermal Super-Insulating Pectin Aerogels. *Carbohydr Polym* **2018**, *196*, 73–81. https://doi.org/10.1016/j.carbpol.2018.05.026.

(35) Buchtová, N.; Pradille, C.; Bouvard, J.-L.; Budtova, T. Mechanical Properties of Cellulose Aerogels and Cryogels. *Soft Matter* **2019**, *15* (39), 7901–7908. https://doi.org/10.1039/C9SM01028A.

(36) Rudaz, C.; Courson, R.; Bonnet, L.; Calas-Etienne, S.; Sallée, H.; Budtova, T. Aeropectin: Fully Biomass-Based Mechanically Strong and Thermal Superinsulating Aerogel. *Biomacromolecules* **2014**, *15* (6), 2188–2195. https://doi.org/10.1021/bm500345u.

(37) Scherer, G. W.; Smith, D. M.; Qiu, X.; Anderson, J. M. Compression of Aerogels. *Journal of Non-Crystalline Solids* **1995**, *186*, 316–320. https://doi.org/10.1016/0022-3093(95)00074-7.

(38) Woignier, T.; Reynes, J.; Hafidi Alaoui, A.; Beurroies, I.; Phalippou, J. Different Kinds of Structure in Aerogels: Relationships with the Mechanical properties. *Journal of Non-Crystalline Solids* **1998**, *241* (1), 45–52. https://doi.org/10.1016/S0022-3093(98)00747-9.

(39) Sescousse, R.; Gavillon, R.; Budtova, T. Aerocellulose from Cellulose–Ionic Liquid Solutions: Preparation, Properties and Comparison with Cellulose–NaOH and Cellulose–NMMO Routes. *Carbohydrate Polymers* **2011**, *83* (4), 1766–1774. https://doi.org/10.1016/j.carbpol.2010.10.043.

(40) Schestakow, M.; Karadagli, I.; Ratke, L. Cellulose Aerogels Prepared from an Aqueous Zinc Chloride Salt Hydrate Melt. *Carbohydr Polym* **2016**, *137*, 642–649. https://doi.org/10.1016/j.carbpol.2015.10.097.

Chapter 4. Chemically crosslinked HA aerogels

1. Introduction

[English]

The biodegradability, biocompatibility and bioactivity of HA make this polymer attractive for biomedical applications.[1] Previously, we developed HA aerogels via non-solvent induced phase separation and via physical crosslinking.[2,3] Unfortunately, those HA aerogels show brittle behavior and dissolve rapidly in water.[3] We propose to overcome these issues by covalently crosslinking the HA, which should potentially result in increased strength and flexibility.

In order to control the dissolution rate and to improve the mechanical properties of a HA network, different strategies including chemical crosslinking have been used.[4] For example, HA hydrogels for regenerative medicine were reinforced using divinylsulfone.[5] Tomihata et al.[6] used glutaraldehyde as crosslinker under acidic conditions. Crosslinking of methacrylated HA can be performed upon exposure to UV light.[7] In addition, Kim et al.[8] employed butanediol diglycildyl ether for the crosslinking of HA. These reactions involve the hydroxyl groups of HA, but crosslinking can be also performed on the HA carboxylic group.[9] The esterification or amidation reaction usually is carried out with the help of carbodiimides such as *N,N′*-dicyclohexylcarbodiimide (DCC) or the water-soluble 1-ethyl-3-(3-dimethylaminopropyl) carbodiimide (EDC).

The use of a stimulus-responsive crosslinker for HA network formation such as cystamine potentially offers the advantage of on-demand degradation of the crosslinks. In the case of cystamine, which contains a disulfide linkage, the application of a reducing agent may result in cleavage of the S-S bond and dissolution of the network. So far, the reaction of HA with cystamine as crosslinker and EDC and NHS as catalysts has been mainly used for the production of hydrogels.[10] One article is found mentioning cystamine-crosslinked HA hydrogels, whose morphology is examined using drying with supercritical CO_2.[11] SEM pictures show that HA aerogels have a nanoporous structure, which is more evident for samples with higher crosslinking degrees. However, no other information about dry material properties is given.

In the present work, we prepare chemically crosslinked HA aerogels via chemical crosslinking of HA, solvent exchange and $scCO_2$ drying. The reaction between the carboxylic acid groups of HA with the amine groups of cystamine, acting as crosslinker, forms amide links between HA chains. This creates covalent crosslinks, resulting in hydrogel formation. In comparison with our previous work, in which the HA network was formed upon physical

interactions such as hydrogen bonds[3], here we report an alternative method, covalent crosslinking, for the formation of the HA network. Chemically crosslinked HA aerogels using cystamine have never been reported, which offers the scientific challenge to understand the processing−structure−properties relationships. The effects of processing conditions (e.g. HA concentration and COOH:NH_2 molar ratio) on the properties and structure of HA aerogels are investigated. Finally, we study the cleavability of the crosslinker upon application of a reducing agent.

[Français]

La biodegradabilité, la biocompatibilité et la bioactivité de l'acide hyaluronique rendent ce polymère attractif pour des applications biomédicales.[1] Précédemment, nous avons développé des aérogels d'acide hyaluronique par la méthode de séparation de phase induite par un non-solvant et par la réticulation physique.[2,3] Malheureusement, ces aérogels d'acide hyaluronique sont fragiles et se dissolvent rapidement dans l'eau.[3] Nous proposons de surmonter ces problèmes en réticulant de manière covalente l'acide hyaluronique, qui doit potentiellement être plus résistant et flexible.

L'étude de la littérature montre qu'afin de pouvoir contrôler la vitesse de dissolution et pour renforcer les propriétés mécaniques du réseau d'acide hyaluronique, différentes stratégies, incluant la réticulation chimique, ont été utilisées.[4] Par exemple, des hydrogels d'acide hyaluronique pour la médecine régénérative ont été renforcés en utilisant la divinylsulfone.[5] Tomihata et al.[6] ont utilisé la glutaraldéhyde comme agent réticulant sous conditions acides. La réticulation de l'acide hyaluronique méthacrylé a été réalisée sous exposition à la lumière UV.[7] De plus, Kim et al.[8] ont employé l'éther diglycidique de 1,4-butanediol pour réticuler l'acide hyaluronique. Ces réactions impliquent les groupes hydroxyl de l'acide hyaluronique, mais la réticulation peut également être réalisée sur le groupe carboxyle de l'acide hyaluronique.[9] L'estérification et la réaction d'amidation sont généralement réalisées en présence de carbodiimides comme le *N,N'*-dicyclohexylcarbodiimide (DCC) ou le 1-ethyl-3-(3-dimethylaminopropyl) carbodiimide (EDC) hydrosoluble.

L'utilisation d'un agent réticulant (comme la cystamine), capable de répondre à un stimulus, pour la formation d'un réseau d'acide hyaluronique offre potentiellement l'avantage d'une dégradation sur-demande des liaisons. Dans le cas de la cystamine, qui contient une liaison disulfide, l'application d'un agent réducteur pourrait donner lieu au clivage du lien S-S et de la dissolution du réseau. Jusqu'à présent, la réaction de l'acide hyaluronique avec la cystamine

comme agent réticulant et EDC et NHS comme catalyseurs, a principalement été utilisée pour la production d'hydrogels.[10] Un article sur des hydrogels d'acide hyaluronique réticulés avec la cystamine, puis séchés avec le CO_2 supercritique étudie leur morphologie.[11] Les images SEM montrent que les aérogels d'acide hyaluronique ont une structure nanoporeuse, qui est plus évidente pour les échantillons ayant des degrés de réticulation plus élevés. Cependant, aucune autre information sur les propriétés des matériaux secs n'est mentionnée.

Dans ce présent travail, nous préparons des aérogels réticulés chimiquement via la réticulation chimique de l'acide hyaluronique, un échange de solvant et un séchage supercritique avec le CO_2. La réaction entre le groupe acide carboxylique de l'acide hyaluronique avec les groupes amine de la cystamine (agent réticulant) forme des liaisons amide entre les chaînes d'acide hyaluronique. Cela crée des liaisons covalentes, formant un hydrogel. Par rapport à notre travail précédent, dans lequel le réseau d'acide hyaluronique a été formé par des interactions physiques (i.e. liaisons hydrogène[3]), ici, nous décrivons une méthode alternative, la réticulation covalente, pour la formation du réseau d'acide hyaluronique. Des aérogels d'acide hyaluronique réticulés chimiquement utilisant la cystamine n'ont encore jamais été étudiés, ce qui offre le challenge scientifique de comprendre la relation de fabrication−structure−propriétés. Les effets des conditions de préparation (i.e. concentration en acide hyaluronique et ratio molaire $COOH:NH_2$) sur les propriétés et la structure des aérogels d'acide hyaluronique sont explorés. Enfin, nous étudions le clivage de l'agent réticulant après application d'un agent réducteur.

2. Chemically crosslinked HA aerogels

2.1. Preparation and characterization of chemically crosslinked HA hydrogels and organogels

Chemically crosslinked HA hydrogels were formed via reaction between the carboxylic acid groups of HA with the amine groups of cystamine dihydrochloride, acting as crosslinker.[12,13] The reaction was catalyzed using two coupling agents: 1-ethyl-3-(3-dimethylaminopropyl) carbodiimide (EDC) and N-hydroxysuccinimide (NHS). Figure 4.1 shows the mechanism of reaction of HA with cystamine in the presence of EDC and NHS.

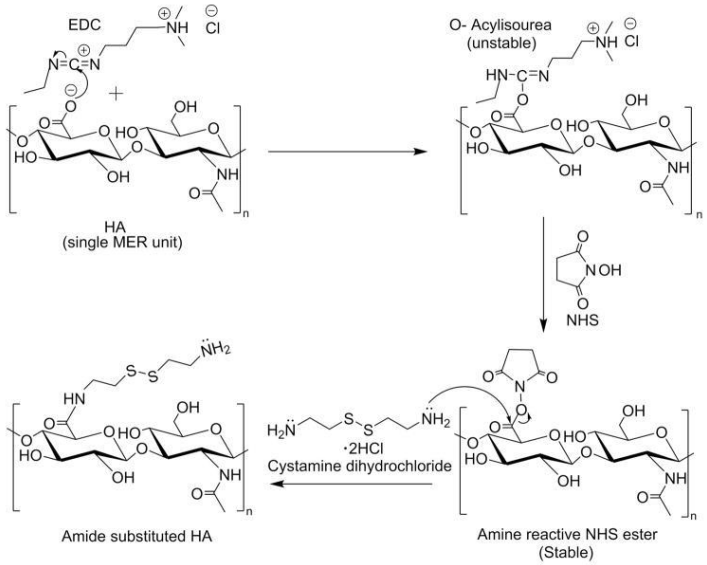

Figure 4.1. Crosslinking of HA using cystamine as crosslinker and EDC and NHS as coupling agents. Reprinted with permission from[13]. Copyright (2014) Wiley.

The reaction starts with the attack of the negatively charged carboxylate group of HA on the electron deficient carbon of EDC, leading to the formation of an intermediate.[13] Because of its high instability, the O-acylisourea is replaced by NHS, which activates the carboxyl group towards nucleophilic reaction. Lastly, the carbon atom of the HA carboxylate group reacts with one primary amine of cystamine, forming an amide-functionalized HA molecule. This reaction, performed at 37°C and in aqueous solution, was used to covalently link HA chains and form hydrogels.

Three HA concentrations were tested (0.7, 1 or 1.6 wt%) and four molar ratios between the carboxyl groups of HA and amino groups of cystamine were used (3:1, 2:1, 1.3:1 and 1:1) (Table 4.1). The COOH:EDC molar ratio (1:1.5) and the COOH:NHS molar ratio (1:1.5) were

kept constant in most cases, and the solvent exchange was carried out using ethanol as non-solvent. Although this leads in theory to 12 potential formulations, in view of efficiency, only 6 formulations were tested, which allows for the determination of the influence of the preparation parameters. Table 4.1 provides an overview of the prepared HA formulations. For two formulations, by mistake, 1:1 and 1:1.24 were used as COOH:EDC and COOH:NHS molar ratios (Table 4.1). In the following, the samples will be named X-COOH:NH_2 A:B, where X is the HA concentration in solution, A is the molar number of COOH groups of HA ; B is the molar number of NH_2 groups of cystamine. More details on synthesis procedures are provided in Chapter 2 – Section 3.2.2 Formulations tested.

Table 4.1. Formulations tested to prepare chemically crosslinked HA aerogels.

Formulation name	HA concentration (wt%)	COOH:NH_2 molar ratio	COOH:EDC molar ratio	COOH:NHS molar ratio
1.6-COOH:NH_2 2:1	1.6	2:1	1:1.5	1:1.5
1.6-COOH:NH_2 1:1	1.6	1:1	1:1.5	1:1.5
1.0-COOH:NH_2 3:1	1.0	3:1	1:1	1:1
1.0-COOH:NH_2 1.3:1	1.0	1.3:1	1:2.4	1:2.4
1.0-COOH:NH_2 1:1	1.0	1:1	1:1.5	1:1.5
0.7-COOH:NH_2 2:1	0.7	2:1	1:1.5	1:1.5

Before gelation, HA solutions were centrifuged for 5 min to remove bubbles. After centrifugation, none of the HA solutions contained any bubbles.

Then, gelation for 1 day at 37°C was performed and HA hydrogels were obtained. The reaction of COOH groups of HA with NH_2 groups of cystamine led to the formation of new bubbles (probably caused by released CO_2). To try to remove bubbles, each plastic vial containing the hydrogel was centrifuged at 6000 min for 25 min and at 9000 rpm for 25 min. However, in most cases, some bubbles in the hydrogel were impossible to remove. We decided to continue the fabrication of HA aerogel using the hydrogel with bubbles (see Annex 1 of the manuscript – Protocol n°17).

In Chapter 3, we reported that physically crosslinked HA aerogels were obtained when the starting HA solution was at pH 2.5 (HA isoelectric point).[3] Thus, a buffer solution at pH 2.5 was added on the top of chemically crosslinked HA hydrogels. Nothing remarkable was noticed (for example, no hydrogel dissolution occurred).

To perform $scCO_2$ drying, water in the hydrogel needs to be replaced by a fluid miscible with supercritical CO_2. In this study, ethanol was selected as it offers the advantage of being a good solvent for both EDC and NHS, which must be removed from the HA materials in view of their toxicity. The catalysts can be potentially removed from HA hydrogels with ethanol during solvent exchange, which is required for $scCO_2$ drying. We tried to remove the catalysts using washing with water, but this method was not practical as it was difficult to distinguish the gel phase and water phase.

To confirm that EDC and NHS are washed out during solvent exchange, FTIR was used to compare the spectra of neat EDC and NHS with that of crosslinked HA after solvent exchange. Figure 4.2 shows the FTIR spectra of EDC and NHS.

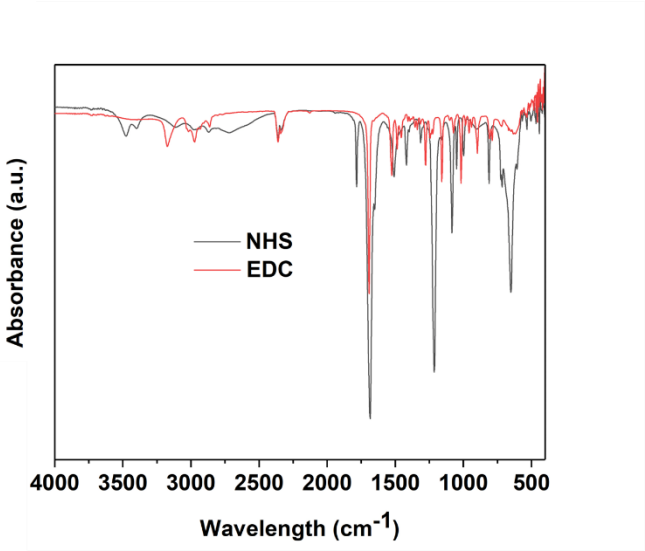

Figure 4.2. FTIR spectra of NHS and EDC.

In case of NHS, the peak around 3400 cm^{-1} is attributed to the OH stretching vibration.[14,15] The intense peak at 1700 cm^{-1} represents the C=O band of the amide. The peaks at 1313 cm^{-1} and 1213 cm^{-1} are assigned to N-OH and C-N-C stretching vibrations, respectively. Three bands characterize the FTIR spectrum of EDC. A small peak, corresponding to the N=C=N stretching of carbodiimide, is found at 2150 cm^{-1}.[16] Near 3176 cm^{-1} corresponds to the NH stretching.[17] The C=N vibration is represented at 1690 cm^{-1}.

In each FTIR spectra, peaks at 2340 and 2360 cm^{-1} correspond to CO_2 absorption from the air.[18]

Figure 4.3 presents the FTIR spectra of the crosslinked HA networks after solvent exchange together with the spectra of EDC and NHS. No peaks resulting from EDC & NHS were found in the spectra of the HA networks, confirming that EDC and NHS were removed after solvent exchange with ethanol.

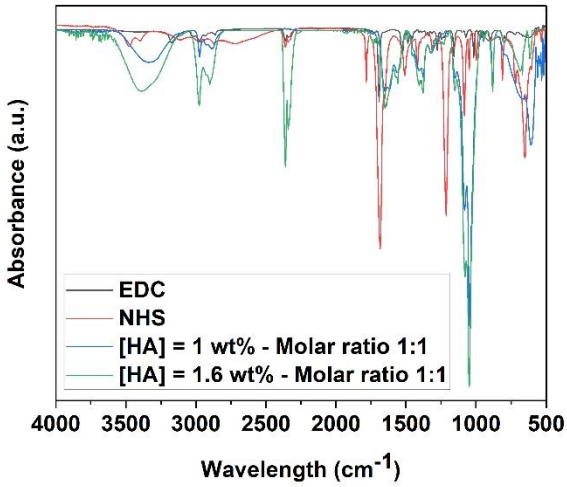

Figure 4.3. FTIR spectra of EDC, NHS and HA organogels.

Figure 4.4 shows pictures of HA organogels prepared using 0.7 wt% or 1.6 wt% as HA concentration and 2:1 as COOH:NH_2 molar ratio.

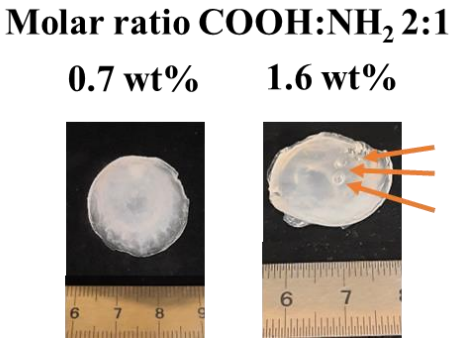

Figure 4.4. Examples of chemically crosslinked HA organogels at 0.7 and 1.6 wt% HA concentration and 2:1 as COOH:NH_2 molar ratio.

After gelation, all HA hydrogels (0.7 and 1.6 wt%) contained bubbles, due to the reaction of HA with cystamine. Before performing solvent exchange, we used centrifugation (i.e. 6000 min for 25 min and at 9000 rpm for 25 min. to try to remove bubbles - see Annex 1 at the end of the manuscript for the experimental procedures that were attempted to obtain HA materials without bubbles). For 0.7 wt% sample, it was possible to remove bubbles, however for samples with higher HA concentration (1.6 wt%), it was impossible to remove them, even with centrifugation, likely because of the higher viscosity of the HA hydrogel. Solvent exchange was therefore necessarily done on some samples with bubbles. An example of an organogel (1.6 wt% HA) that still contains bubbles that formed during gelation (indicated by orange arrows) is presented in Figure 4.4.

The crosslinking of selected HA organogels (obtained after complete solvent exchange; before analysis, ethanol around the sample was absorbed with a tissue) was characterized by FTIR spectroscopy. Figure 4.5 presents FTIR spectra of crosslinked HA organogels, neat HA and cystamine.

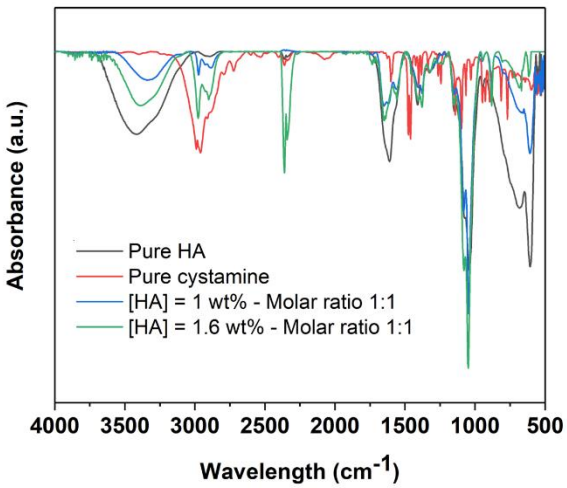

Figure 4.5. FTIR spectra of HA, cystamine and HA organogels.

The HA-cystamine networks (blue and green lines) are characterized by four main peaks. The first one is the OH stretching, characteristic of HA, around 3400 cm^{-1}. At 1650 cm^{-1} and 1560 cm^{-1}, the C=O stretching and the N-H stretching bands of amide appear, formed by the reaction of the carboxyl group of HA with the amino group of cystamine.[19] Around 2900 cm^{-1}, the peak intensity increased, due to additional CH_2 groups coming from the presence of cystamine. These results suggest that HA and cystamine successfully reacted to form a chemically crosslinked network.

Two main peaks characterize all FTIR spectra. The typical glycosidic bond of polysaccharide was found around 1000-1100 cm^{-1}.[20] The two peaks near 2340 and 2360 cm^{-1} (most pronounced for the organogel containing 1.6 wt% HA) correspond to CO_2 absorption.[18]

HA organogels were subsequently dried with $scCO_2$ to obtain HA aerogels. Figure 4.6 shows pictures of the resulting chemically crosslinked HA aerogels. Both samples have the same shape as their organogel analogs (Figure 4.4). Materials became dry and white. The 1.6 wt% HA sample still contain bubbles (indicated by orange arrows).

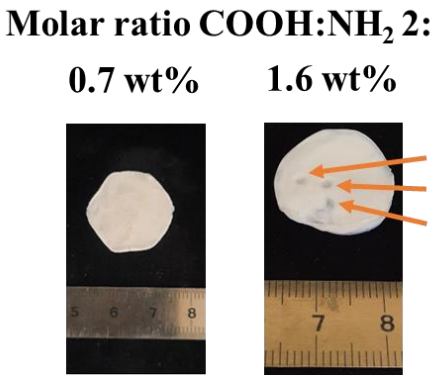

Figure 4.6. Examples of chemically crosslinked HA aerogels at 0.7 and 1.6 wt% HA concentration and 2:1 as COOH:NH_2 molar ratio.

2.2. Properties of chemically crosslinked HA aerogels

2.2.1. Volume shrinkage

As reported in literature, the solvent to non-solvent exchange and $scCO_2$ drying lead to volume shrinkage of a sample.[2,3,21] Volume shrinkage during solvent exchange and overall volume shrinkage (Eq. 3 and Eq. 4 – Chapter 2) were evaluated as function of HA concentration and the COOH:NH_2 molar ratio (Figure 4.7).

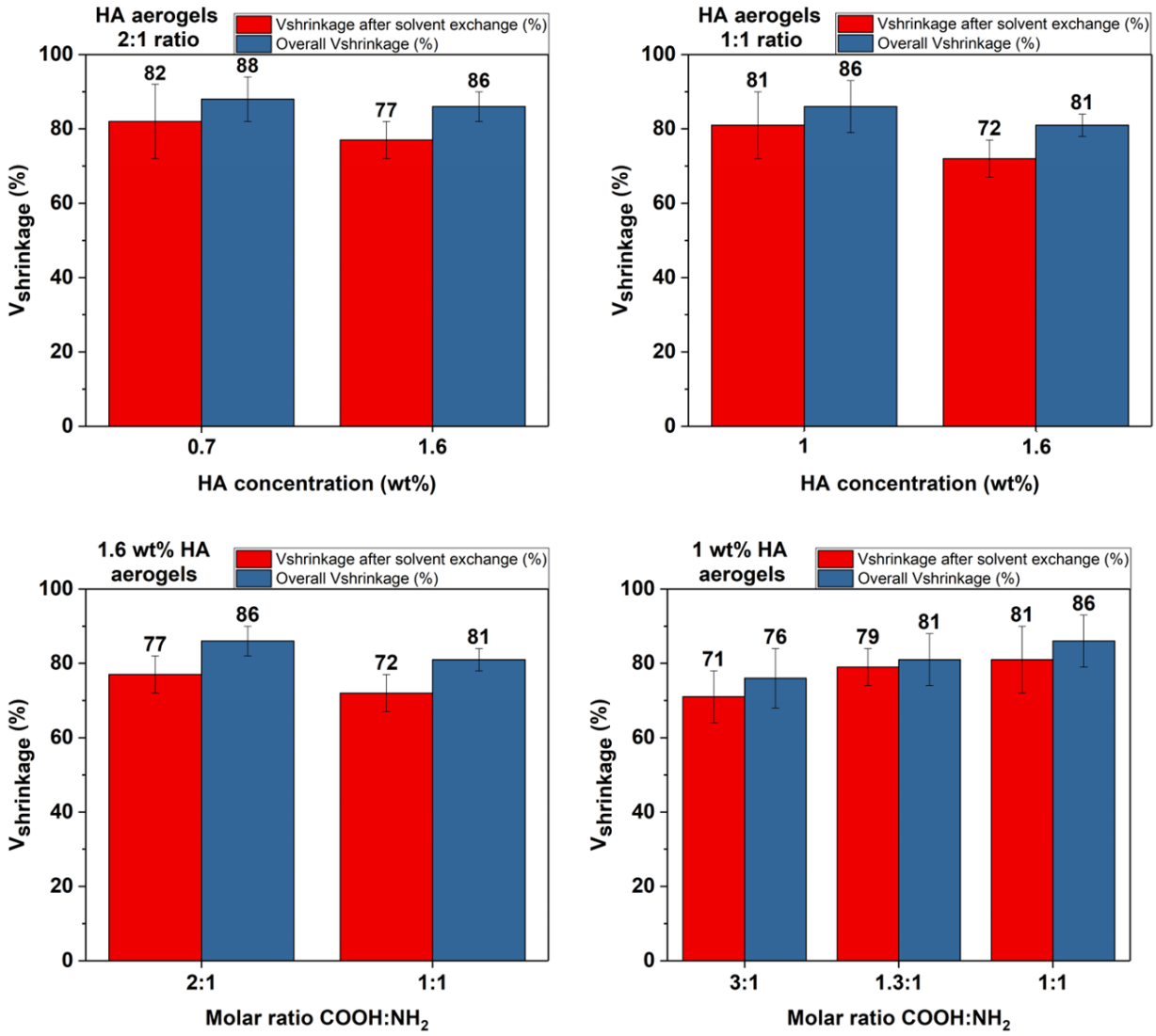

Figure 4.7. Volume shrinkage during the preparation of chemically crosslinked HA aerogels. Data are expressed as means ± standard deviation.

The volume shrinkage was high in all cases with values above 71% after solvent exchange and above 76% for overall shrinkage. A slightly lower overall volume shrinkage was obtained when a higher HA concentration was used (Figure 4.7, top row), which may be ascribed to a stronger network with increased resistance to shrinkage. No clear influence of the COOH:NH_2 molar ratio can be deduced within the experimental errors (Figure 4.7, bottom row). Shrinkage mostly occurred during solvent exchange, as with physically crosslinked HA aerogels (Chapter 3).

2.2.2. Density and porosity

The bulk density of chemically crosslinked HA aerogels was studied as a function of HA concentration (Figure 4.8).

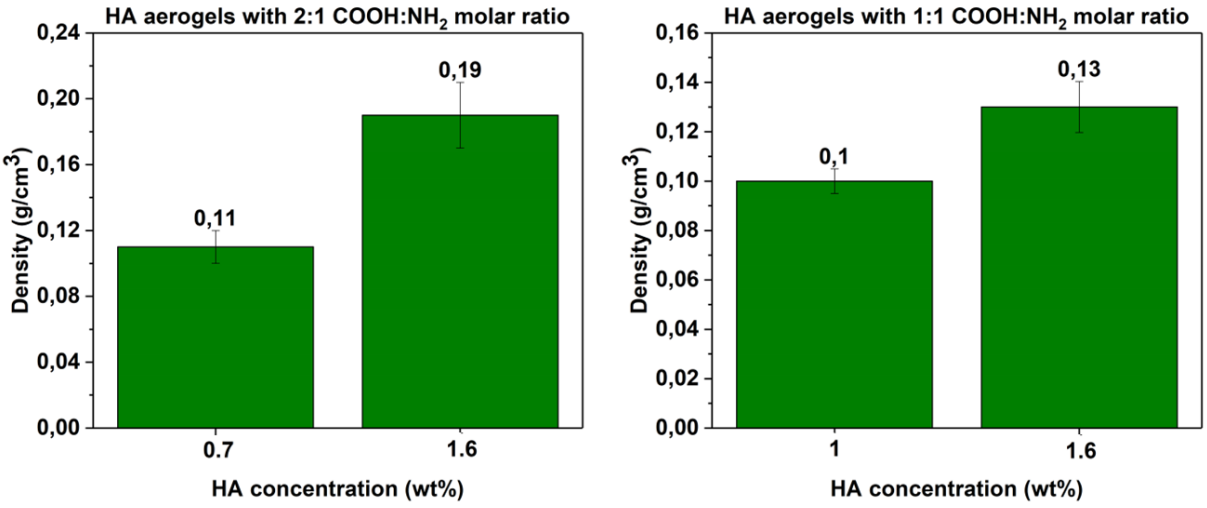

Figure 4.8. Bulk density of chemically crosslinked HA aerogels prepared with 2:1 and 1:1 $COOH:NH_2$ molar ratio. Data are expressed as means ± standard deviation.

We observe an important effect of the HA concentration on the bulk density. The density increases with polymer concentration, regardless of the $COOH:NH_2$ molar ratio. It follows from Figure 4.7 that a higher HA concentration in the initial solution leads to reduced overall volume shrinkage, which can be ascribed to a more robust network. However, a higher HA concentration leads to materials with a higher density (Figure 4.8), which has also been reported for other biobased aerogels.[2,3,21,22] Thus, the effect of the higher polymer mass in the sample is more important in determining the density than the effect of increased resistance to shrinkage.

Figure 4.9 presents the bulk density of 1 and 1.6 wt% HA aerogels as function of the $COOH:NH_2$ molar ratio.

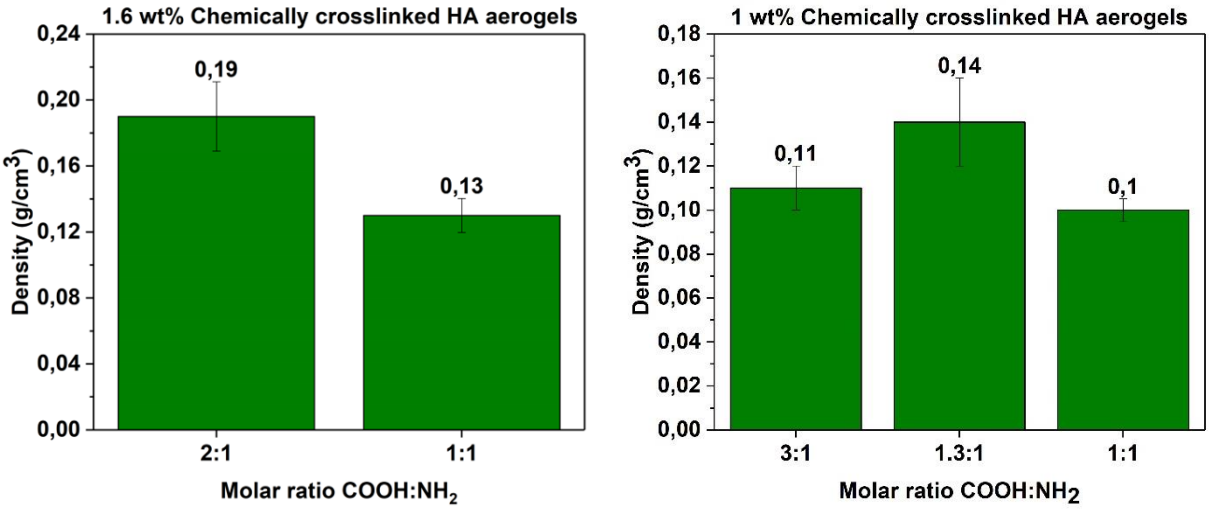

Figure 4.9. Bulk density of 1 and 1.6 wt% chemically crosslinked HA aerogels.

For 1.6 wt% HA aerogels, a 2:1 COOH:NH_2 molar ratio results in a higher density in comparison with an equimolar COOH:NH_2 ratio, which is in accordance with the higher shrinkage value for the 2:1 molar ratio (Figure 4.7).

For 1.0 wt% HA aerogels, no clear influence of the crosslinking molar ratio on the density is observed within the experimental errors. It is difficult to deduce trends, which may be caused by the presence of bubbles.

Table 4.2 summarizes the HA aerogels porosity and pore volumes (Eq. 6 and Eq. 7 – Chapter 2).

Table 4.2. Porosity and pore volume of chemically crosslinked HA aerogels.

Formulation	Density (g/cm^3)	Porosity (%)	Pore volume (cm^3/g)
1.6-COOH:NH_2 2:1	0.19 ± 0.02	86 ± 1	4.5 ± 0.6
1.6-COOH:NH_2 1:1	0.13 ± 0.01	91 ± 1	7.1 ± 0.6
1-COOH:NH_2 3:1	0.11 ± 0.01	92 ± 1	8.4 ± 0.4
1-COOH:NH_2 1.3:1	0.14 ± 0.02	90 ± 1	6.7 ± 1.0
1-COOH:NH_2 1:1	0.10 ± 0.01	93 ± 1	9.3 ± 0.5
0.7-COOH:NH_2 2:1	0.11 ± 0.01	92 ± 1	8.5 ± 1.0

Pore volume follows the same trend as porosity: it is the lowest for the 1.6-COOH:NH_2 2:1 sample, 4.5 ± 0.6 cm^3/g, and the highest for the 1-COOH:NH_2 1:1 material, 9.3 ± 0.5 cm^3/g. Porosity and pore volume were lower for the 1.6 wt% HA sample prepared with 2:1 COOH:NH_2 molar ratio in comparison with the 1.6 wt% HA sample prepared at equimolar ratio, in accordance with its higher density. No clear influence of molar ratio on porosity or pore volume can be deduced for the 1.0 wt% HA samples. The porosity and pore volume of the 0.7 wt% HA sample are in the range of the values observed for the 1.0 wt% HA samples.

2.2.3 Specific surface area and morphology

Figure 4.10 shows the specific surface area of HA aerogels as a function of concentration. Regardless of the COOH:NH_2 molar ratio, higher specific surface areas were observed for samples prepared with 1.6 wt% HA. An increase in HA concentration results in the formation of a network with a higher density (Figure 4.8), lower porosity and lower pore volume (Table 4.2).

The 1.6 wt% HA samples may contain a higher number of small pores in the network, resulting in higher S_{BET} values, in comparison with less concentrated samples.

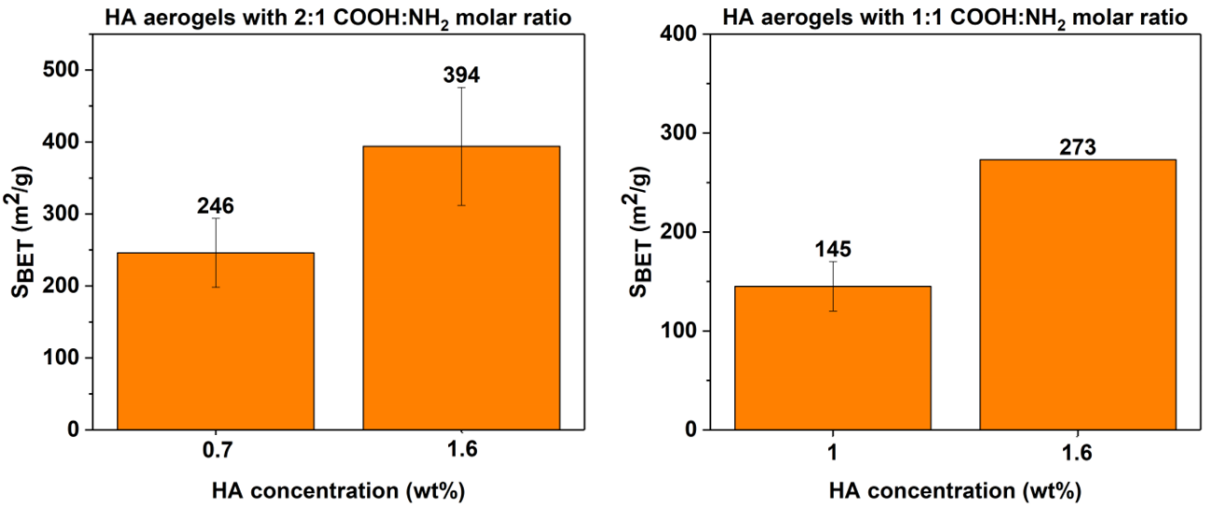

Figure 4.10. Specific surface area of chemically crosslinked HA aerogels prepared with 2:1 and 1:1 COOH:NH_2 molar ratio. Data are expressed as means ± SD. For the 1.6-COOH:NH_2 1:1 sample, only one S_{BET} value was obtained.

The specific surface area of 1.6 and 1 wt% HA aerogels is presented as a function of the COOH:NH_2 molar ratio in Figure 4.11. In both cases, lower specific surface areas were observed for samples prepared with a 1:1 molar ratio between reactive groups. We suppose that these aerogels have larger pores, but to deduce trends, more data are needed. Moreover, the analyzed HA aerogels contain bubbles. Thus, the measured specific surface area values do not necessarily reflect the «real» material S_{BET}.

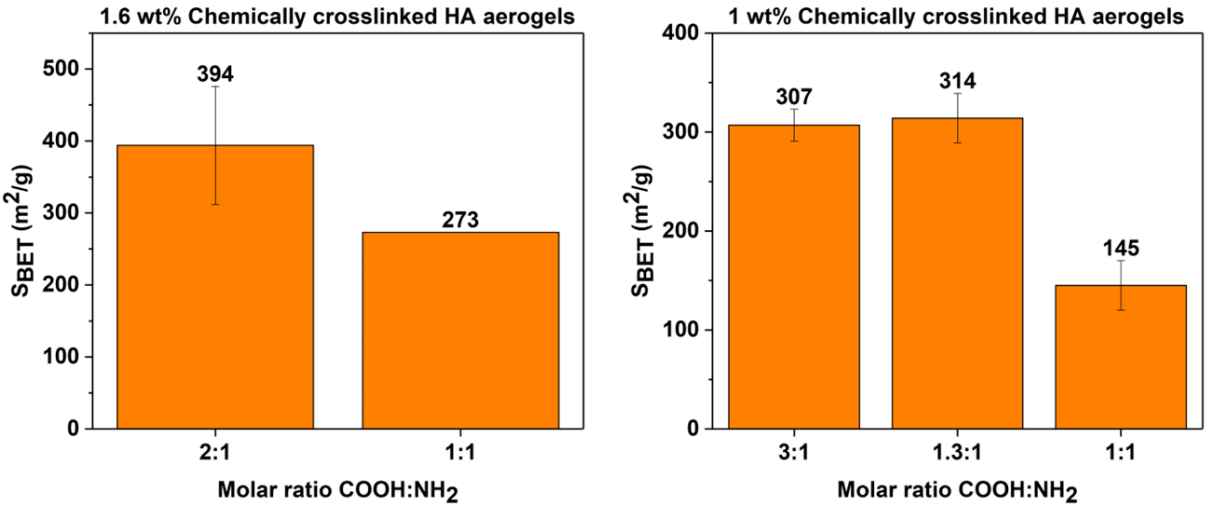

Figure 4.11. Specific surface area of 1 and 1.6 wt% HA chemically crosslinked aerogels.

We used SEM to characterize the aerogel morphology. SEM images at different magnification present aerogels made from solutions of 0.7 and 1.6 wt% HA, both prepared with 2:1 COOH:NH_2 molar ratio and ethanol as non-solvent (Figure 4.12).

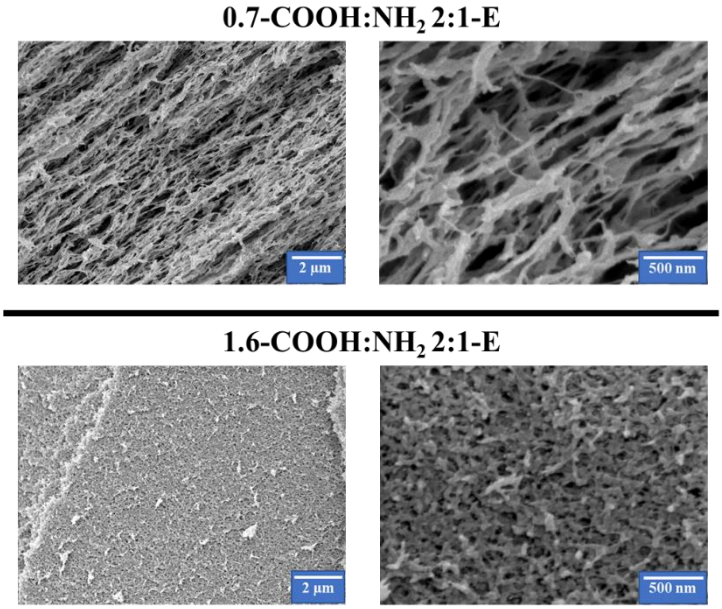

Figure 4.12. SEM images of 0.7 and 1.6 wt% chemically crosslinked HA aerogels prepared with a COOH:NH_2 2:1 molar ratio.

For both aerogels, a network of fine entangled HA fibrils is observed. An increase in HA concentration results in a HA network with smaller pores, which is in line with the higher S_{BET} value (Figure 4.10).

We also analyzed the aerogel morphology as a function of the COOH:NH_2 molar ratio. Figure 4.13 shows the cross-section of aerogels prepared from 1 wt% HA with two different COOH:NH_2 molar ratios.

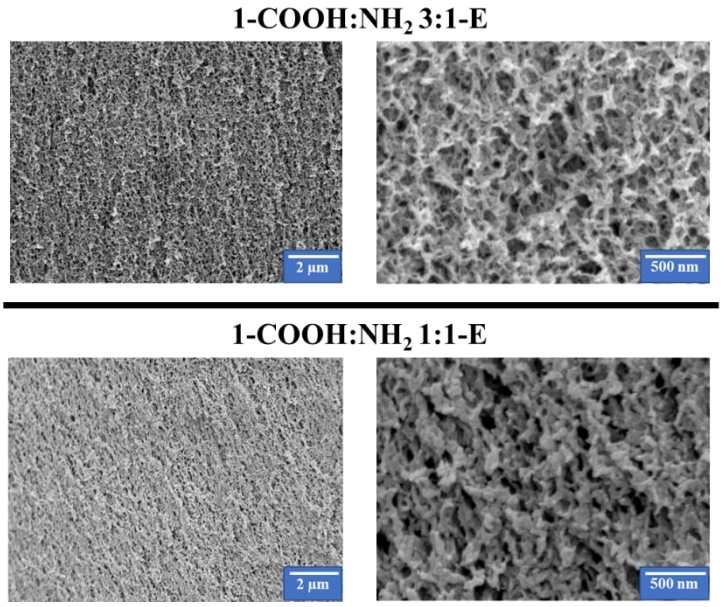

Figure 4.13. SEM images of 1 wt% chemically crosslinked HA aerogels prepared with a $COOH:NH_2$ 3:1 and 1:1 molar ratios.

The 1 wt% HA aerogels present a network of entangled HA fibrils. More SEM data are needed to confirm the morphology of the networks and deduce trends.

2.2.4. Overview of properties of chemically and physically crosslinked HA aerogels

Table 4.3 summarizes the properties of 1.6 wt% chemically crosslinked aerogels prepared with 2:1 and 1:1 COOH molar ratios and 1.6 wt% physically crosslinked aerogels, prepared with the non-solvent induced phase separation (NIPS) method[2].

Table 4.3. Properties of 1.6 wt% physically and chemically crosslinked HA aerogels.

	Physically crosslinked HA aerogels	**Chemically crosslinked HA aerogels**	
[HA] (wt%)	1.6		
Solution pH	2.5		
Preparation method	Non-solvent phase induced phase separation[15]	Chemical crosslinking – Method described in Chapter 2	
Gel or solution?	Solution	Gel - after gelation at 37°C	
Non-solvent used	Ethanol		
$scCO_2$ drying applied to get aerogels			
Aerogels properties			
Molar ratio $COOH:NH_2$	1:0 (physically crosslinked)	1:1	2:1
$V_{shrinkage}$ after solvent exchange (%)	60 ± 4	72 ± 5	75 ± 4

Overall $V_{shrinkage}$ (%)	82 ± 2	81 ± 3	84 ± 2
Bulk density (g/cm^3)	0.15	0.13 ± 0.01	0.19 ± 0.02
Porosity (%)	88	91 ± 1	86 ± 1
V_{pores} (cm^3/g)	5.9	7.1 ± 0.6	4.5 ± 0.6
S_{BET} (m^2/g)	394 ± 82	273	404 ± 66

The properties of the physically crosslinked HA aerogel are of the same order of magnitude as those of chemically crosslinked HA aerogels, except for the specific surface area of the sample, with a 1:1 molar ratio between reactive groups. However, we have only one S_{BET} value for the 1:1 sample. Moreover, the chemically crosslinked samples contain bubbles. More experiments are needed to be able to establish trends.

2.2.5. Behavior of HA aerogels upon exposure to the air

HA is a highly hydrophilic polymer. To investigate the potential uptake of moisture from the air, the mass of chemically crosslinked HA aerogels was monitored over 1 day. We studied the influence of HA concentration on the mass of aerogels upon exposure to the air. Figure 4.14 shows the normalized mass (Eq.8 – Chapter 2) of HA aerogels, prepared with a 2:1 COOH:NH_2 molar ratio, over time at 25°C and 45 % relative humidity. Each experiment was performed one time.

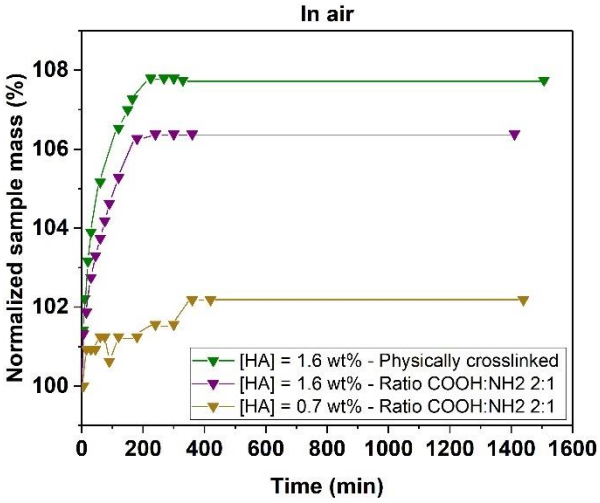

Figure 4.14. Normalized mass of HA aerogels upon exposure to the air of 0.7 and 1.6 wt% chemically crosslinked HA aerogels prepared at 2:1 COOH:NH_2 molar ratios as well as of a 1.6 wt% physically crosslinked HA aerogel (prepared via freezing-thawing).

The mass of all HA samples increases up to reaching a plateau after a certain time, which is likely due to absorption of moisture from the air. For chemically crosslinked HA aerogels, increased moisture adsorption is obtained for the sample prepared with a higher HA concentration (1.6 wt%), probably due to a higher S_{BET} (Figure 4.10) and thus a larger number of hydrophilic groups (e.g. -OH) accessible for water vapors.

We also compared the moisture adsorption of chemically crosslinked HA aerogels with that of a physically crosslinked HA aerogel (see Chapter 3).[3] The physically crosslinked HA aerogel absorb more moisture than the chemically crosslinked HA aerogels, in accordance with its higher specific surface area ($S_{BET} \approx 600$ m^2).

2.2.6. Behavior of HA aerogels in PBS

The absorption of wound exudate by a dressing is important to guarantee a good healing process and limit infections. We studied the influence of the COOH:NH_2 molar ratio and the HA concentration on the PBS absorption of chemically crosslinked HA aerogels over time. Figure 4.15 presents the normalized mass (Eq.8 – Chapter 2) of chemically crosslinked HA aerogels, prepared with different molar ratios, as function of time. Each experiment was performed one time.

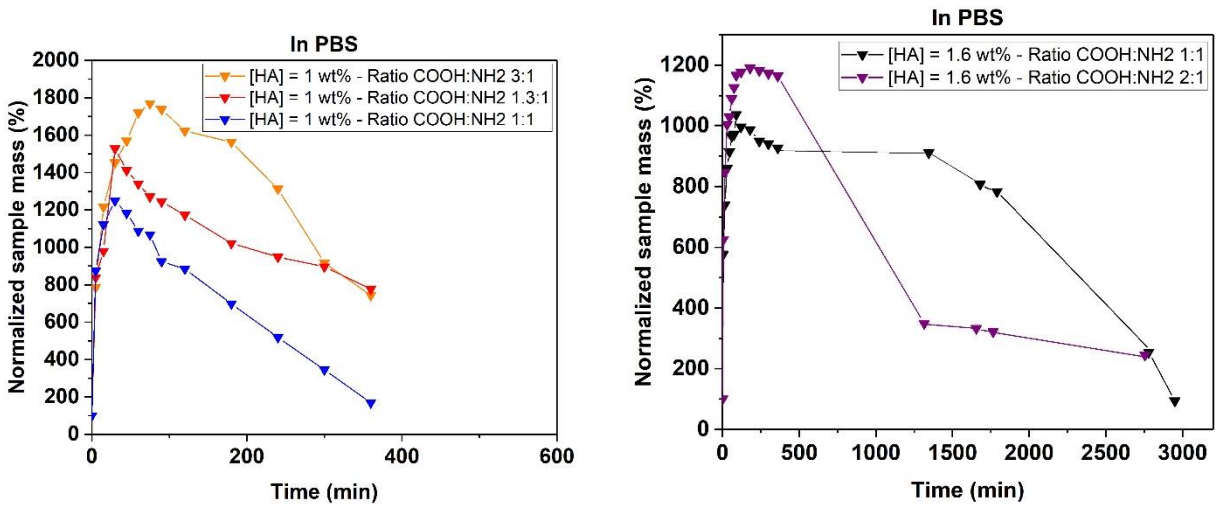

Figure 4.15. Normalized sample mass over time after immersion in PBS of 1 wt% HA (left) and 1.6 wt% HA (right) chemically crosslinked aerogels, prepared with different COOH:NH_2 molar ratios.

For both HA concentrations, the mass of aerogels increases up to reaching a maximum and the samples subsequently dissolve.

Lower swelling degrees were observed for samples prepared with an equimolar COOH:NH_2 ratio (1:1). Possibly, the higher amount of cystamine, containing 2 hydrophobic -CH_2-CH_2- moieties, reduces swelling in aqueous media. No clear influence of the COOH:NH_2 molar ratio on dissolution time can be deduced. The dissolution is slower for more concentrated samples (1.6 wt% HA), which may be due to a denser network.

We also compared the PBS absorption of a 1.6 wt% chemically crosslinked HA aerogel with that of a 1.6 wt% physically crosslinked HA aerogel, prepared previously with the freeze-thaw technique.[3] Figure 4.16 presents the normalized mass of samples as a function of time. Each experiment was performed one time.

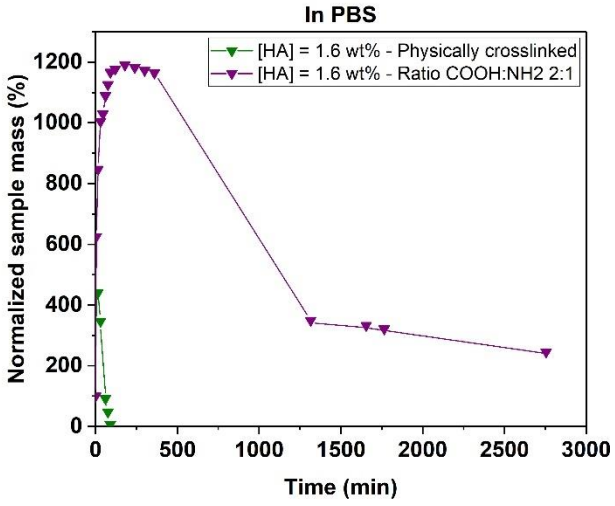

Figure 4.16. Normalized sample mass over time after immersion in PBS of a 1.6 wt% HA chemically crosslinked aerogel prepared with a 2:1 COOH:NH_2 molar ratio and of a 1.6 wt% HA physically crosslinked aerogel, prepared via freezing-thawing.

A lower maximum swelling (442 %) and a shorter dissolution time (within 90 min) are observed for the physically crosslinked HA aerogel. The results show that chemical crosslinking with cystamine leads to the formation of HA aerogels, which are more resistant to dissolution. Possibly, the physical crosslinks (hydrogen bonds) of the HA aerogel break rapidly in PBS. However, in case of chemical crosslinking, HA aerogels dissolved. Burdick et al.[23] reported that chemically crosslinked hydrogels based on thiolated HA undergo degradation over time in solution and that the rate of degradation depends on several parameters such as the molecular weight of the starting HA, the concentration of the thiolated HA and the crosslinking density.

2.2.7. Behavior of HA aerogels under reducing conditions

The stimulus-responsiveness of the HA aerogels was assessed by immersing them in PBS at pH 7.4 supplemented with 1,4-dithioerythritol (DTT), a thiol reducing agent that can theoretically cleave the disulfide (S-S) linkage in the chemically crosslinked network of the HA aerogels. Figure 4.17 presents the chemical formula of DTT.

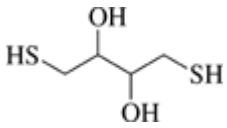

Figure 4.17. Chemical structure of DTT.

This reducing agent, highly soluble in water, has two pKa values: 9.2 and 10.1. DTT was selected because it was previously shown that DTT specifically reduces the disulfide links of the network without any undesired side-reaction.[24] Figure 4.18 presents the mechanism of disulfide reduction by DTT.

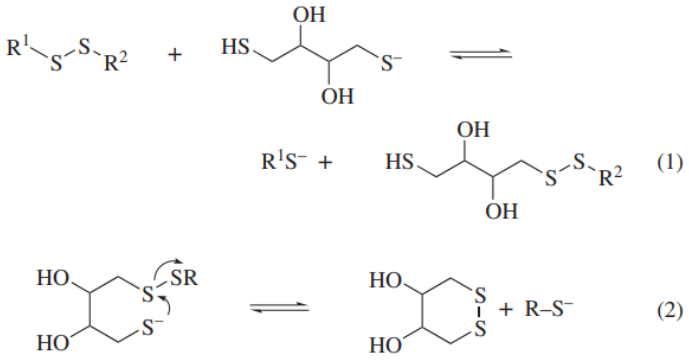

Figure 4.18. Mechanism of disulfide reduction by DTT. Reprinted with permission from[25]. Copyright (2001) Wiley.

The reduction of the disulfide bond is a reversible process, involving two sequential thiol–disulfide exchange reactions.[24,25] During the first step, one of the thiol groups deprotonates and performs a nucleophilic attack on one of the two sulfurs of the S-S bond, forming a mixed disulfide intermediate. During the second step, the mixed disulfide bond is broken by the second thiol of DTT, generating a new disulfide bond and a new structure.

The potential cleavage of the disulfide bond was monitored for 1 day in PBS at pH 7.4 containing 5mM of DTT. Figure 4.19 presents the normalized mass of a 1 wt% chemically crosslinked HA aerogel, prepared with a 1:1 COOH:NH_2 molar ratio. Each experiment was performed one time.

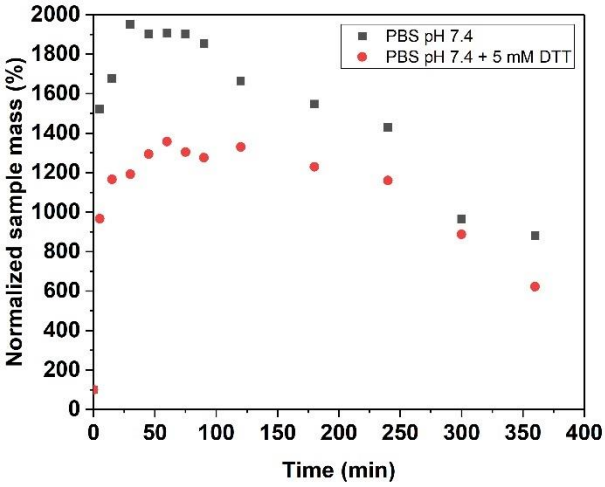

Figure 4.19. Normalized sample mass over time of chemically crosslinked HA aerogels upon immersion in PBS and PBS + DTT.

Both curves present an increase in normalized sample mass up to a maximum (around 30 min for the sample in PBS and around 60 min for the sample in PBS containing DTT) and then a decrease. When DTT is used, a limited swelling is observed, but the maximum is reached at a different time and the aerogel dissolution is very slow, similar to the experiment in the absence of DTT, in contrast with expectations. In literature, it was found that at pH 7, DTT is a slow reducing agent.[25]

It could be interesting to perform additional experiments using an increased amount of DTT or an alternative, more powerful reducing agent, to be able to deduce trends.

3. Conclusions

This chapter presented a screening work on the preparation of chemically crosslinked HA aerogels. Chemically crosslinked HA hydrogels were prepared via reaction between the carboxylic acid groups of HA with the amine groups of cystamine dihydrochloride, acting as crosslinker. Covalently crosslinked hydrogels were obtained, then solvent exchange was performed and finally, drying with supercritical CO_2. The influence of processing parameters (HA concentration and molar ratio between COOH and NH_2) was investigated.

All conditions allowed to obtain HA aerogels, i.e. materials with low density (< 0.2 g/cm^3), high porosity (> 86 %) and high specific surface area (> 150 m^2/g). A higher HA concentration resulted in reduced volume shrinkage, a higher density and a higher specific surface area. For 1.6 wt% HA aerogels, the use of a 2:1 COOH:NH_2 molar ratio instead of a 1:1 ratio resulted in a higher density. SEM demonstrated that the aerogels contain meso- and small macropores. The absorption of PBS by aerogels depends on HA concentration and COOH:NH_2 ratio. An equimolar COOH:NH_2 ratio 1:1 led to a lower maximum swelling and a higher HA concentration resulted in a longer dissolution time. Despite being covalently crosslinked, the HA aerogels slowly dissolved. The presence of DTT did not significantly change the dissolution rate of the samples, which may be due to the low amount of reactive thiolate groups under the current experimental conditions. The chemically crosslinked aerogels are more resistant to dissolution than physically crosslinked HA aerogels prepared with the freezing-thawing method.

As this work presented the first results on chemically crosslinked HA aerogels, more experimental work should be performed to optimize material properties and deduce trends.

4. References

(1) Xu, X.; Jha, A. K.; Harrington, D. A.; Farach-Carson, M. C.; Jia, X. Hyaluronic Acid-Based Hydrogels: From a Natural Polysaccharide to Complex Networks. *Soft Matter* **2012**, *8* (12), 3280. https://doi.org/10.1039/c2sm06463d.

(2) Aguilera-Bulla, D.; Legay, L.; Buwalda, S. J.; Budtova, T. Crosslinker-Free Hyaluronic Acid Aerogels. *Biomacromolecules* **2022**, *23* (7), 2838–2845. https://doi.org/10.1021/acs.biomac.2c00207.

(3) Legay, L.; Budtova, T.; Buwalda, S. Hyaluronic Acid Aerogels Made Via Freeze–Thaw-Induced Gelation. *Biomacromolecules* **2023**, *24* (10), 4502–4509. https://doi.org/10.1021/acs.biomac.2c01518.

(4) Collins, M. N.; Birkinshaw, C. Hyaluronic Acid Based Scaffolds for Tissue Engineering—A Review. *Carbohydrate Polymers* **2013**, *92* (2), 1262–1279. https://doi.org/10.1016/j.carbpol.2012.10.028.

(5) Borzacchiello, A.; Russo, L.; Malle, B. M.; Schwach-Abdellaoui, K.; Ambrosio, L. Hyaluronic Acid Based Hydrogels for Regenerative Medicine Applications. *BioMed Research International* **2015**, *2015*, 1–12. https://doi.org/10.1155/2015/871218.

(6) Tomihata, K.; Ikada, Y. Crosslinking of Hyaluronic Acid with Glutaraldehyde. *Journal of Polymer Science Part A: Polymer Chemistry* **1997**, *35* (16), 3553–3559. https://doi.org/10.1002/(SICI)1099-0518(19971130)35:16<3553::AID-POLA22>3.0.CO;2-D.

(7) Eke, G.; Mangir, N.; Hasirci, N.; MacNeil, S.; Hasirci, V. Development of a UV Crosslinked Biodegradable Hydrogel Containing Adipose Derived Stem Cells to Promote Vascularization for Skin Wounds and Tissue Engineering. *Biomaterials* **2017**, *129*, 188–198. https://doi.org/10.1016/j.biomaterials.2017.03.021.

(8) Yang, B.; Guo, X.; Zang, H.; Liu, J. Determination of Modification Degree in BDDE-Modified Hyaluronic Acid Hydrogel by SEC/MS. *Carbohydrate Polymers* **2015**, *131*, 233–239. https://doi.org/10.1016/j.carbpol.2015.05.050.

(9) Khunmanee, S.; Jeong, Y.; Park, H. Crosslinking Method of Hyaluronic-Based Hydrogel for Biomedical Applications. *J Tissue Eng* **2017**, *8*, 204173141772646. https://doi.org/10.1177/2041731417726464.

(10) Pérez, L. A.; Hernández, R.; Alonso, J. M.; Pérez-González, R.; Sáez-Martínez, V. Hyaluronic Acid Hydrogels Crosslinked in Physiological Conditions: Synthesis and Biomedical Applications. *Biomedicines* **2021**, *9* (9), 1113. https://doi.org/10.3390/biomedicines9091113.

(11) Pérez, L. A.; Hernández, R.; Alonso, J. M.; Pérez-González, R.; Sáez-Martínez, V. Granular Disulfide-Crosslinked Hyaluronic Hydrogels: A Systematic Study of Reaction Conditions on Thiol Substitution and Injectability Parameters. *Polymers* **2023**, *15* (4), 966. https://doi.org/10.3390/polym15040966.

(12) Wang, L.; Dong, S.; Liu, Y.; Ma, Y.; Zhang, J.; Yang, Z.; Jiang, W.; Yuan, Y. Fabrication of Injectable, Porous Hyaluronic Acid Hydrogel Based on an In-Situ Bubble-Forming Hydrogel Entrapment Process. *Polymers* **2020**, *12* (5), 1138. https://doi.org/10.3390/polym12051138.

(13) Santhanam, S.; Liang, J.; Baid, R.; Ravi, N. Investigating Thiol-Modification on Hyaluronan via Carbodiimide Chemistry Using Response Surface Methodology. *Journal*

of Biomedical Materials Research Part A **2015**, *103* (7), 2300–2308. https://doi.org/10.1002/jbm.a.35366.

(14) Stan, C. S.; Albu, C.; Coroaba, A.; Popa, M.; Sutiman, D. One Step Synthesis of Fluorescent Carbon Dots through Pyrolysis of N-Hydroxysuccinimide. *J. Mater. Chem. C* **2015**, *3* (4), 789–795. https://doi.org/10.1039/C4TC02382J.

(15) Zhuang, C.; Tao, F.; Cui, Y. Properties of Gelatin Films Cross–Linked by N-Hydroxysuccinimide–Activated Furandicarboxylic Acid (NHS-FDCA). *Polym. Bull.* **2016**, *73* (6), 1565–1580. https://doi.org/10.1007/s00289-015-1563-5.

(16) Pottorf, R. S.; Szeto, P. 1-Ethyl-3-(3′-Dimethylaminopropyl)Carbodiimide Hydrochloride. In *Encyclopedia of Reagents for Organic Synthesis (EROS)*; John Wiley & Sons, Ltd, **2001**. https://doi.org/10.1002/047084289X.re062.

(17) *IR Spectrum Table*. https://www.sigmaaldrich.com/CA/en/technical-documents/technical-article/analytical-chemistry/photometry-and-reflectometry/ir-spectrum-table?fbclid=IwAR3p0Yv-j6sfRt2ZwYzIAgclMRvDK4oTbS7Y49znzE3vjcNmwnq0Jeazl0w (accessed 2023-12-07).

(18) Schott, J. A.; Do-Thanh, C.-L.; Shan, W.; Puskar, N. G.; Dai, S.; Mahurin, S. M. FTIR Investigation of the Interfacial Properties and Mechanisms of CO2 Sorption in Porous Ionic Liquids. *Green Chemical Engineering* **2021**, *2* (4), 392–401. https://doi.org/10.1016/j.gce.2021.09.003.

(19) Laffleur, F.; Hörmann, N.; Gust, R.; Ganner, A. Synthesis, Characterization and Evaluation of Hyaluronic Acid-Based Polymers for Nasal Delivery. *International Journal of Pharmaceutics* **2023**, *631*, 122496. https://doi.org/10.1016/j.ijpharm.2022.122496.

(20) Gilli, R.; Kacuráková, M.; Mathlouthi, M.; Navarini, L.; Paoletti, S. FTIR Studies of Sodium Hyaluronate and Its Oligomers in the Amorphous Solid Phase and in Aqueous Solution. *Carbohydrate Research* **1994**, *263* (2), 315–326. https://doi.org/10.1016/0008-6215(94)00147-2.

(21) Groult, S.; Budtova, T. Tuning Structure and Properties of Pectin Aerogels. *European Polymer Journal* **2018**, *108*, 250–261. https://doi.org/10.1016/j.eurpolymj.2018.08.048.

(22) Druel, L.; Bardl, R.; Vorwerg, W.; Budtova, T. Starch Aerogels: A Member of the Family of Thermal Superinsulating Materials. *Biomacromolecules* **2017**, *18* (12), 4232–4239. https://doi.org/10.1021/acs.biomac.7b01272.

(23) Burdick, J. A.; Prestwich, G. D. Hyaluronic Acid Hydrogels for Biomedical Applications. *Adv. Mater.* **2011**, *23* (12), H41–H56. https://doi.org/10.1002/adma.201003963.

(24) Singh, R.; Whitesides, G. M. Thiol—Disulfide Interchange. In *PATAI'S Chemistry of Functional Groups*; Patai, S., Rappoport, Z., Eds.; Wiley, **1993**; pp 633–658. https://doi.org/10.1002/9780470034408.ch13.

(25) Cleland, W. W. 1,4-Dithiothreitol. In *Encyclopedia of Reagents for Organic Synthesis (EROS)*; John Wiley & Sons, Ltd, **2001**. https://doi.org/10.1002/047084289X.rd473.

Chapter 5. Development of hyaluronic acid and nanochitin capsules for drug delivery applications

1. Introduction

[English]

Thanks to its excellent biocompatibility, biodegradability and hydrophilicity, HA is already used in several biomedical applications.[1] For example, HA hydrogels have been used to protect eye tissues, in viscosupplementation (HA injection in arthritic joints to improve mobility and relieve pain) and as dermal filler. However, physically crosslinked HA hydrogels generally have poor mechanical properties and degrade rapidly in water. The HA network can be reinforced using another polymer, forming a composite or an interpenetrated network.

Recently, nanochitins (nanofibers and nanocrystals) have attracted interest, due to their excellent mechanical properties and biocompatibility. However, these biobased materials were used very rarely in combination with HA, most probably because they are new materials. Till now, we found only two articles on the combination of HA with nanochitins. HA-chitin nanowhiskers biofilms for tissue engineering were developed by Abdelrahman et al.[2] Higher chitin nanocrystals content improved the mechanical properties of HA films. Another composite, for drug release applications, was made by dissolving HA and nCh fibers in acidic medium and freeze-drying.[3] No hydrogels based on HA with nanochitin were found in literature. Whereas literature on HA-nCh fibers composites is thus very limited, several publications report on HA-chitosan polyelectrolytes complexes, as detailed in Chapter 1.[4–6]

In our case, we were willing to reinforce HA aerogels with nCh fibers. However, it turned out that upon mixing HA solutions and nCh suspensions, strong polyelectrolyte complexation occurred leading to the formation of HA-nCh membrane. This raised several questions, leading our research: what are the interactions between HA and nCh? what are the film properties? Can the new material be useful for biomedical applications? These studies were carried out in collaboration with the BioProducts Institute of the University of British Columbia in Canada.

In this chapter, we interest in the fabrication of capsules made via mixing a drop of HA solution with nCh fibers suspension (and vice versa). Such capsules based on HA and nCh fibers have never been reported. This present work aims:

- to characterize the nCh fibers properties
- to evaluate the conditions leading to the formation of HA-nCh films and capsules
- to characterize the films and capsules and investigate their application as drug delivery systems

In this chapter, we will use the terminology “chitin nanofibers” to designate nCh fibers as described in ref [7].

[Français]

Nous avons vu que les hydrogels d’acide hyaluronique réticulés physiquement ont généralement de mauvaises propriétés mécaniques et se dégradent rapidement dans l’eau. Toutefois, ils peuvent être renforcés en utilisant un autre polymère, afin de former un composite ou un réseau interpénétré.

Récemment, les nanochitins (les nanofibres et nanocrystaux) ont suscité de l’intérêt en raison de leurs excellentes propriétés mécaniques et leur biocompatibilité. Cependant, ces matériaux biosourcés ont très rarement été utilisés en association avec l’acide hyaluronique, très probablement car il s’agit de nouveaux matériaux. Jusqu’à maintenant, nous avons seulement trouvé deux articles sur la combinaison de l’acide hyaluronique avec les nanochitins. Des biofilms à base de HA-chitin nanowhiskers pour l’ingénierie tissulaire ont été développés par Abdelrahman et al.[2] L’utilisation d’une concentration plus élevée en cristaux de nanochitin a permis d’améliorer les propriétés mécaniques des films d’acide hyaluronique. Un autre composite, pour des applications de libération de substances actives, a été fabriqué en dissolvant l’acide hyaluronique et les fibres nCh fibers en milieu acide et en congélant-séchant.[3] Aucun hydrogel à base d’acide hyaluronique avec les nanochitins n’a été trouvé dans la littérature. Bien que la bibliographie sur les composites HA-fibres nCh soit très limitée, plusieurs publications font état de complexes polyélectrolytiques à base d’acide hyaluronique et de chitosan, comme précisé dans le Chapitre 1.[4–6]

Dans notre cas, nous voulions renforcer les aérogels d’acide hyaluronique avec des fibres nCh. Cependant, il s’est avéré qu’en mélangeant les solutions d’acide hyaluronique et les suspensions de nCh, une forte complexation polyélectrolytique est apparue, formant une membrane HA-nCh. Cela a soulevé plusieurs questions qui ont guidé nos recherches : quelles sont les types d’interactions entre l’acide hyaluronique et les fibres nCh? Quelles sont les propriétés du film formé? Le nouveau matériau peut-il être utilisé pour des applications biomédicales? Ces études ont été réalisées en collaboration avec le BioProducts Institute de l’Université de Colombie Britannique au Canada.

Dans ce chapitre, nous nous intéressons à la fabrication de capsules obtenues en mélangeant une goutte de solution d’acide hyaluronique avec une suspension de fibres nCh (ou

inversement). Ces capsules à base d'acide hyaluronique et de fibres nCh n'ont encore jamais été rapportées. Ce présent travail a donc pour objectif :

- de caractériser les propriétés des fibres nCh
- d'évaluer les conditions menant à la formation des films HA-nCh et des capsules
- de caractériser les films et les capsules et examiner leur application comme systèmes de libération de substances actives

Nous utiliserons la terminologie "chitin nanofibers" pour désigner les fibres de nCh ainsi que décrit dans la réf [7].

2. Characterization of chitin nanofibers

2.1. Morphology

The diameter and the length of nCh fibers were determined using AFM. Topographical images revealed the fiber morphology (Figure 5.1).

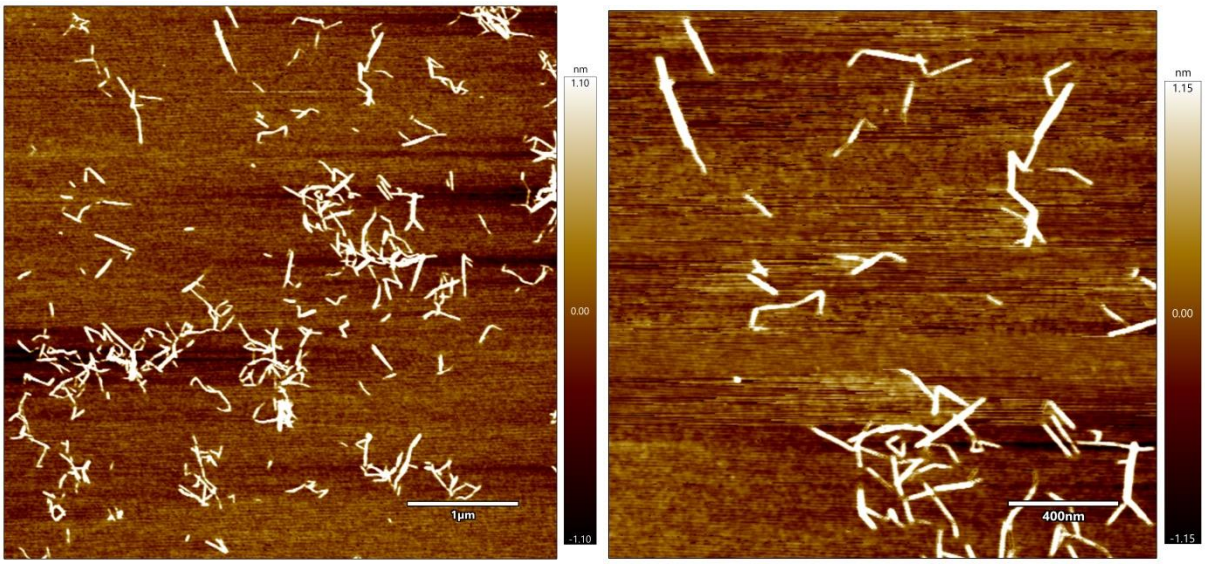

Figure 5.1. AFM images of nCh fibers. Scale bar of 1 µm (left) and scale bar of 400 nm (right).

AFM images of nCh fibers indicate well-dispersed long fibers. nCh fibers were in the range of 130-300 nm in length and of 7-11 nm in width. Thus, the corresponding aspect ratio (length/width) was in the range of 19 – 27. The aspect ratio depends on the chitin source. For example, chitin nanofibers with aspect ratios of more than 500 were obtained from squid pen.[8] The width and length of those nanofibers were 3-4 nm and a few microns, respectively.

2.2. Degree of deacetylation

The amount of positively charged amino groups in nCh fibers was determined by conductimetric titration. Figure 5.2 presents the titration curve of an aqueous suspension of nCh fibers.

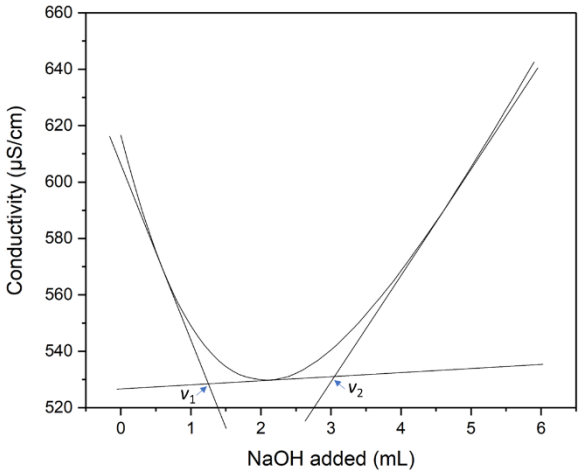

Figure 5.2. Conductimetric titration of 0.16 wt% nCh fiber suspension with NaOH.

The first rapidly descending part of the curve corresponds to the neutralization of the free H^+ ions in the system. The second part is due to the neutralization of the protonated amino groups of nCh, it corresponds to the minimum of the titration curve. The final slope shows an increase in conductivity, due to an excess of OH^- ions. The volume of base needed to neutralize the amino groups was given by the difference between the two inflexion points v_1 and v_2 (Figure 5.2).
The degree of deacetylation (DDA) of our nCh fibers was around 18% (Eq 11 – Chapter 2). This value is in accordance with literature. A DDA of 16% was obtained by Xu et al.[9] for chitin nanofibers having a length from hundreds of nm to a few µm and a width of 5–15 nm.

2.3. Zeta potential

The surface charge of 0.1 wt% nCh fiber suspensions was measured. Figure 5.3 presents the zeta potential of the suspension as a function of pH.

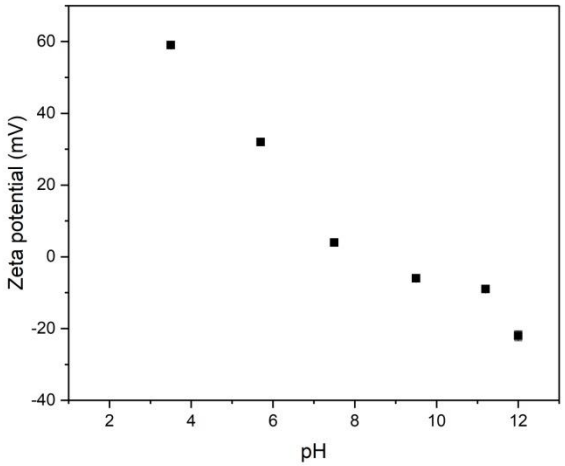

Figure 5.3. Zeta potential of nCh fiber suspensions between pH 3 and pH 12.

nCh fiber suspensions exhibit a high cationic charge, around 60 mV at pH 3, and the value decreases with increasing pH, as reported in literature.[10] We also observe a zero net charge around pH 7-7.2, close to the pKa of the amino groups of chitin (pH ≈ 6.3).

3. Formation and characterization of HA-chitin nanofibers capsules

3.1. Formation of HA-nCh capsules

The preparation of HA-nCh fiber capsules is described in Chapter 2 – Section 3.3.1. Two types of HA-nCh capsules were formed, as shown in Figure 5.4: 1) when HA solution is added to nCh suspension, or 2) when nCh suspension is added to HA solution. In the last case, the capsule floats, due to its lower density in comparison with the medium. For example, the density of 0.7 wt% nCh suspension was around 0.9734 g/cm^3, while that of 0.7 wt% HA solution was 0.9908 g/cm^3.

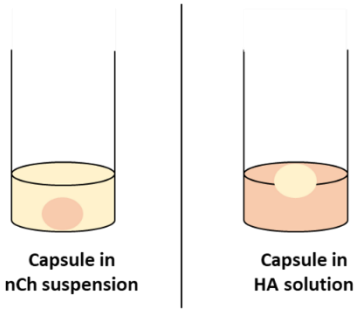

Figure 5.4. Scheme illustrating the two types of HA-nCh capsules formed.

Figure 5.5 shows an example of a HA-nCh capsule. A drop of 0.5 wt% HA solution was injected into 0.1 wt% nCh suspension.

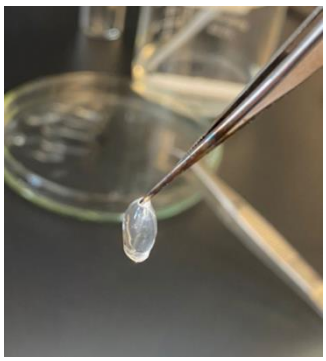

Figure 5.5. Example of HA-nCh capsule.

The capsule is composed of a film, which encapsulates a liquid inside, and is sufficiently robust to be manipulated with tweezers.

3.2. Membrane morphology

The capsule membrane was analyzed by optical microscopy. Figure 5.6 presents three optical microscopy images of the membrane.

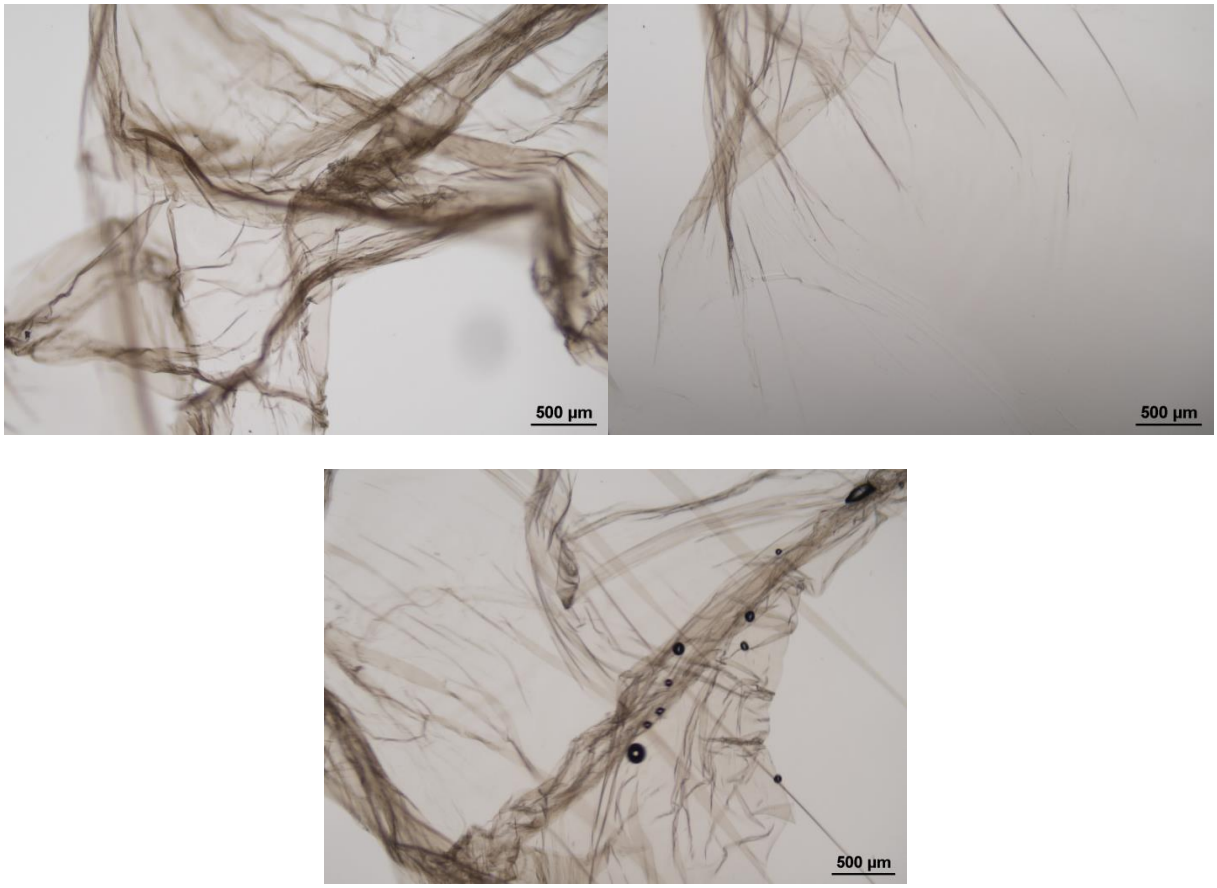

Figure 5.6. Optical microscopy images of the HA-nCh capsule membrane.

The thickness of the capsule membrane could not be deduced from the images. A method to determine the membrane thickness must be found. For example, confocal laser scanning microscopy or computed tomography could potentially be used to establish a 3D image and determine the thickness.

3.3. Membrane porosity

To see if the membrane was porous, we used SEM. SEM images are shown in Figure 5.7.

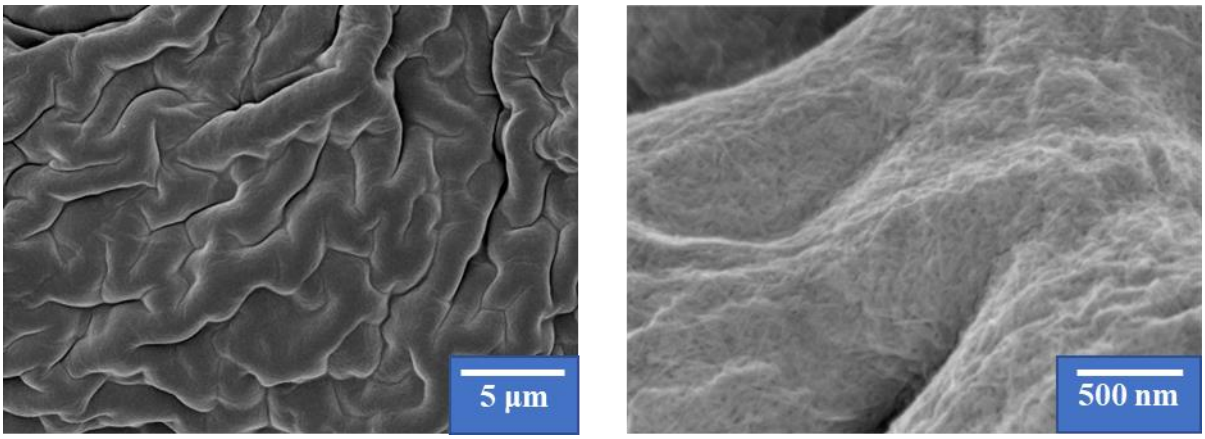

Figure 5.7. Examples of SEM image of the HA-nCh capsule membrane with 5 µm scale bar (left) and at 500 nm scale bar (right).

The left SEM image (5 µm scale) shows a wavy surface of the membrane. A higher magnification (500 nm scale) reveals that the membrane is composed of a network with small pores. The pore size could not be determined using SEM; potentially cryo-TEM could be employed for this purpose.

3.4. Analysis of capsule – membrane and liquid phase – composition

An important question is the composition of the membrane and of the liquid phase inside the capsule formed after mixing HA solution and nCh suspension.

First, the starting compounds, HA and nCh fibers, were analyzed, in powder form, by FTIR spectroscopy (Figure 5.8).

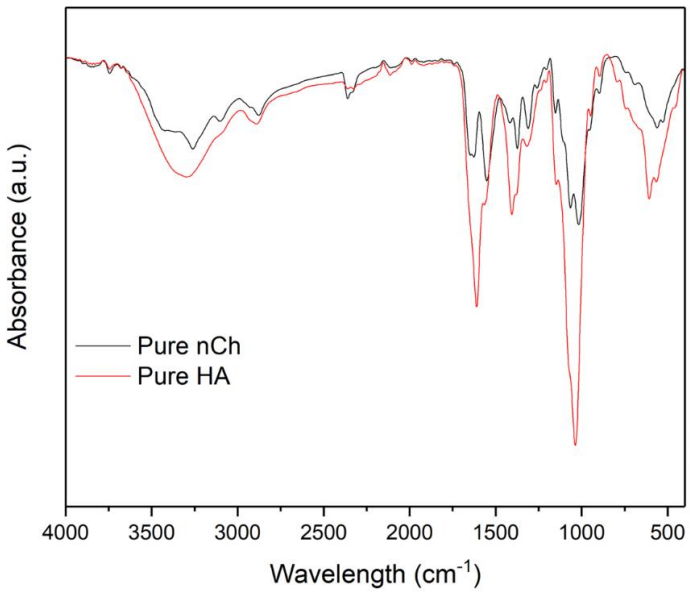

Figure 5.8. FTIR spectra of HA and nCh.

One major peak of HA is around 3400 cm^{-1}; it was attributed to OH stretching.[11] The NH stretching band is near 3100 cm^{-1}, appearing as a shoulder. At 2900 cm^{-1}, the low intensity peak corresponds to the CH_2 stretching vibration. The C=O band of the HA carboxylate group was found at 1612 cm^{-1}. At 1566 cm^{-1} and 1650 cm^{-1} were amide II (N-H stretching vibration) and amide I (C=O stretching vibration) bands of HA, respectively. The FTIR spectrum of HA obtained is similar to the one found by Gilli et al.[11] Concerning the FTIR spectrum of nCh fibers, the peak at 1550 cm^{-1} was attributed to the amino II band of α-chitin, and the peaks at 1655 cm^{-1} and 1630 cm^{-1} were assigned to the amino I band of α-chitin.[12]

Two main peaks characterize both FTIR spectra. The typical glycosidic bond of polysaccharides was found around 1000-1100 cm^{-1}. The two small peaks near 2340 and 2360 cm^{-1} correspond to CO_2 absorption.[13]

Next, we characterized the liquid phase inside the capsule formed after introducing nCh suspension in HA solution. The FTIR spectrum of the liquid inside this capsule is presented in Figure 5.9.

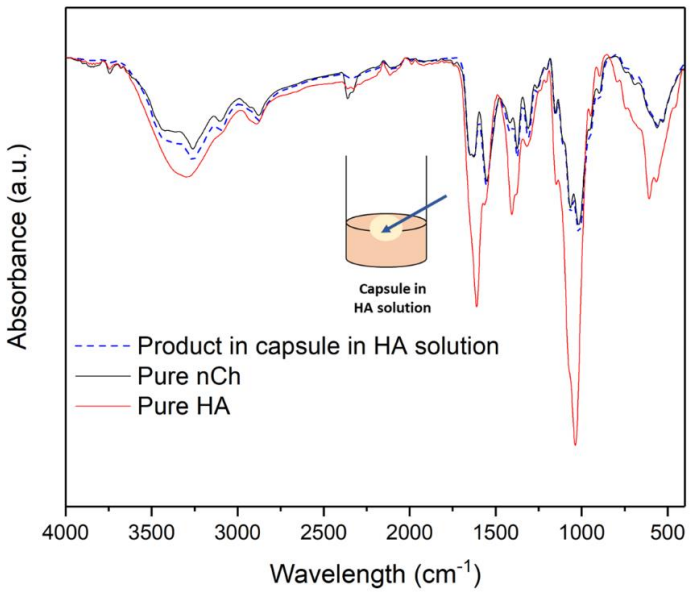

Figure 5.9. FTIR spectrum of substance inside the capsule; continuous phase: HA solution.

The blue arrow shows the characterized product. The FTIR spectrum of the liquid, the dotted blue line, was compared with FTIR spectra of HA and nCh powders (red and black lines, respectively). The spectrum of the liquid in the capsule is similar to the spectrum of neat nCh. For example, in both spectra, the amide I band of α-chitin was found around 1550 cm^{-1} and the two amide II peaks at 1655 and 1624 cm^{-1}.[12] This shows that the substance inside the capsule formed when placing a droplet of nCh suspension in HA solution is nCh suspension.

Then, we inserted a droplet of HA solution in nCh suspension, forming another type of capsule. The liquid inside this capsule was also characterized by FTIR spectroscopy (Figure 5.10).

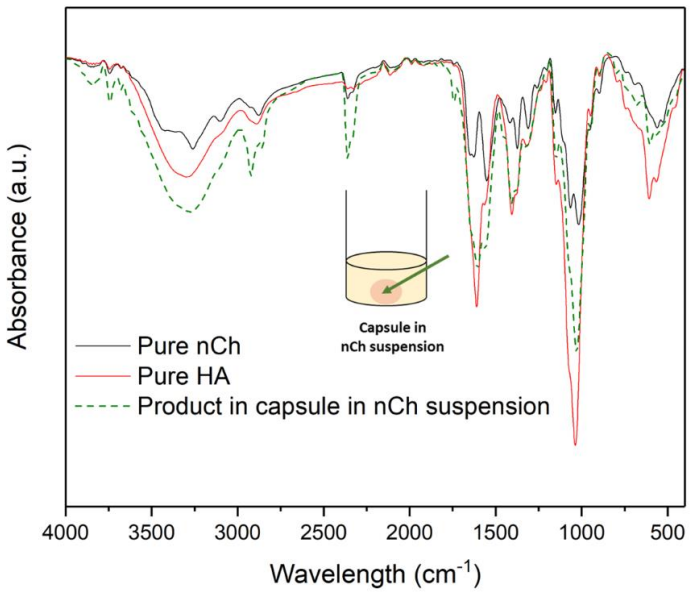

Figure 5.10. FTIR spectrum of the substance inside the capsule; continuous phase: nCh suspension.

The green arrow shows the analyzed product. The FTIR spectrum of the substance inside the capsule, the dotted green line, was compared with FTIR spectra of neat HA and nCh powders (red and black lines, respectively). The spectrum of the liquid in the capsule is identical to the spectrum of neat HA. Indeed, the wide band of the OH stretching was found around 3400 cm^{-1}.[11] At 1560 cm^{-1} and 1650 cm^{-1} are the amide II and amide I bands of HA, respectively. Thus, the substance inside the capsule formed by placing a droplet of HA solution in nCh suspension is HA solution.

The analysis of the liquid phase inside both types of capsules (Figure 5.9 and 5.10) shows that as soon as the film is formed due to the contact of the droplet with the continuous phase, the capsule only contains the substance of the droplet, not mixed with the continuous phase.

Finally, we characterized the capsule membrane with FTIR spectroscopy (Figure 5.11). This capsule was prepared by depositing a droplet of HA solution in nCh suspension.

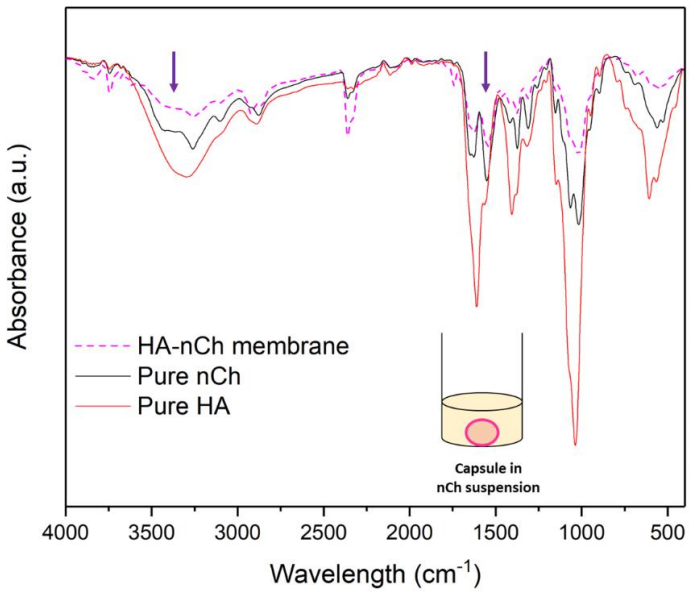

Figure 5.11. FTIR spectrum of the HA-nCh capsule membrane.

The FTIR spectrum of capsule membrane is in pink. The dotted line was compared with FTIR spectra of pure HA and nCh. The HA-nCh membrane formation resulted in a reduced intensity for the OH and NH vibration peaks (around 3100-3400 cm^{-1}, left arrow).[2] At 1550 cm^{-1} (right arrow) the peak intensity of free amino groups was weakened because of strong ionic interactions between the amino and the carboxylic groups of nCh and HA, respectively.

We characterized the membrane of another capsule, prepared in HA solution, with FTIR spectroscopy. A droplet of 0.5 mL of nCh suspension was added inside 10 mL of HA solution, leading to the formation of a capsule. Figure 5.12 compares the FTIR spectrum of this capsule membrane with the spectrum of the capsule prepared by depositing a droplet of 0.5 mL of HA solution in 0.5 mL of nCh suspension.

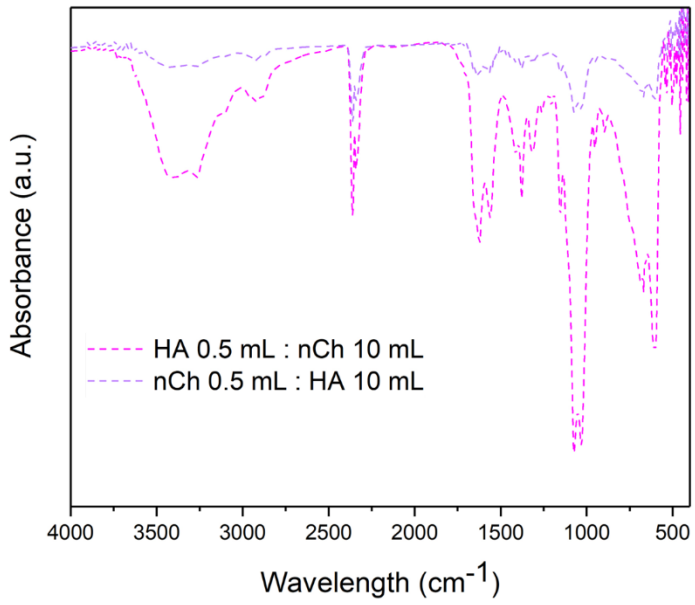

Figure 5.12. FTIR spectrum of different HA-nCh capsule membranes.

Even though the peak intensities are different, the membranes of the capsules prepared via both methods present the same FTIR spectrum.

With FTIR spectroscopy, we tried to quantify how many groups of HA interacted with amino groups of nCh fibers to form the capsule membrane. The experiment was performed one time. More experiments are needed to confirm the proportion of HA and nCh fibers participating to the complexation.

In view of the similar data obtained by FTIR related to the interactions of HA and nCh fibers[2], our FTIR study suggests that nCh fibers complexed with HA to form a membrane.

3.5. Membrane robustness

To explore the properties of the capsule membrane, we tested its solubility in several media. Table 5.1 summarizes the results obtained.

Table 5.1. Media used to test membrane dissolution.

Salts	Acids	Base	Other aqueous media
• 0.1 M and 5M NaCl solution • 1M NH_4Cl solution	• 1% acetic acid solution • 0.01 M PBS at pH 2	• 0.05 M NaOH solution	• Distilled water • Electrically neutral solution (HA solution at pH 2.5 and nCh

		• 20 wt% NaOH/4 wt% urea	dispersion at 0-zeta potential) • 4 wt% urea
➔ No membrane dissolution			

Remarkably, the HA-nCh membrane was not dissolved in all media presented in Table 4.1, even when using a strong base such as 20 wt% NaOH. Thus, the HA-nCh fibers complexation forms a strong membrane.

3.6. Influence of salt concentration on complex formation between HA and nCh fibers

To see whether the interactions between HA and nCh could be influenced by the presence of a salt, we decided to add NaCl to 0.1 wt% nCh suspension and 0.5 wt% HA solution. Then, 2 mL of 0.1 wt% nCh suspension and 2 mL of 0.5 wt% HA solution, both containing 5M NaCl, were mixed.

In the glass beaker, we observed a clear solution, without any traces of membrane formation. Thus, the presence of NaCl prevents the complexation between HA and nCh fibers, leading to the membrane formation. We also tried this experiment with a lower salt concentration (0.1 M NaCl), but in this case the mixing of HA solution and nCh dispersion led to the formation of a membrane. Hence, 0.1 M NaCl was not enough to prevent complexation.

As the membrane was not formed in the presence of a high concentration of NaCl, we took the mixture and added some droplets to distilled water, while the mixture was stirred. Figure 5.13 presents what happened in solution.

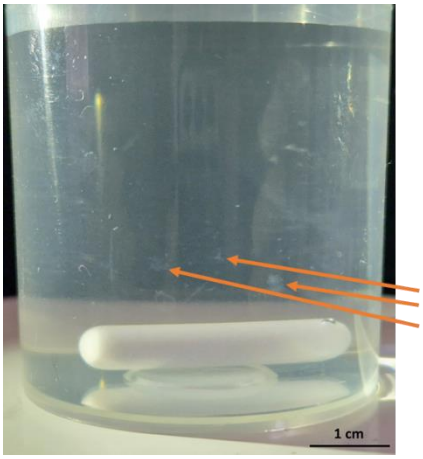

Figure 5.13. Example of droplets formed.

Following addition to water, the salt is diluted and we can see a few opaque droplets inside. The most visible are indicated by the orange arrows. These droplets result from the complexation of HA with nCh fibers forming capsules. Some of these droplets were extracted from water and deposited on the bottom of a beaker (Figure 5.14). These droplets are very promising, due to the simple and cost-effective method of fabrication. A further interesting experience that could be done is to control the morphology of droplets.

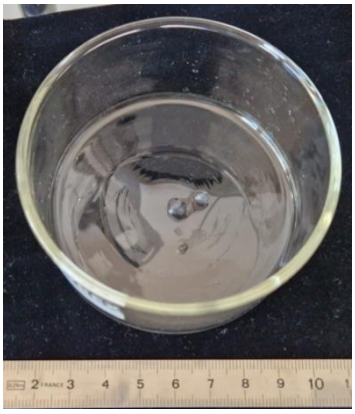

Figure 5.14. Example of droplets formed.

3.7. Model drug release from the capsule

We tested the prepared capsules as drug delivery devices. Methylene blue (MB) was selected as a model compound, whose concentration is easy to follow with a spectrophotometer. Figure 5.15 depicts the preparation of a MB-loaded capsule.

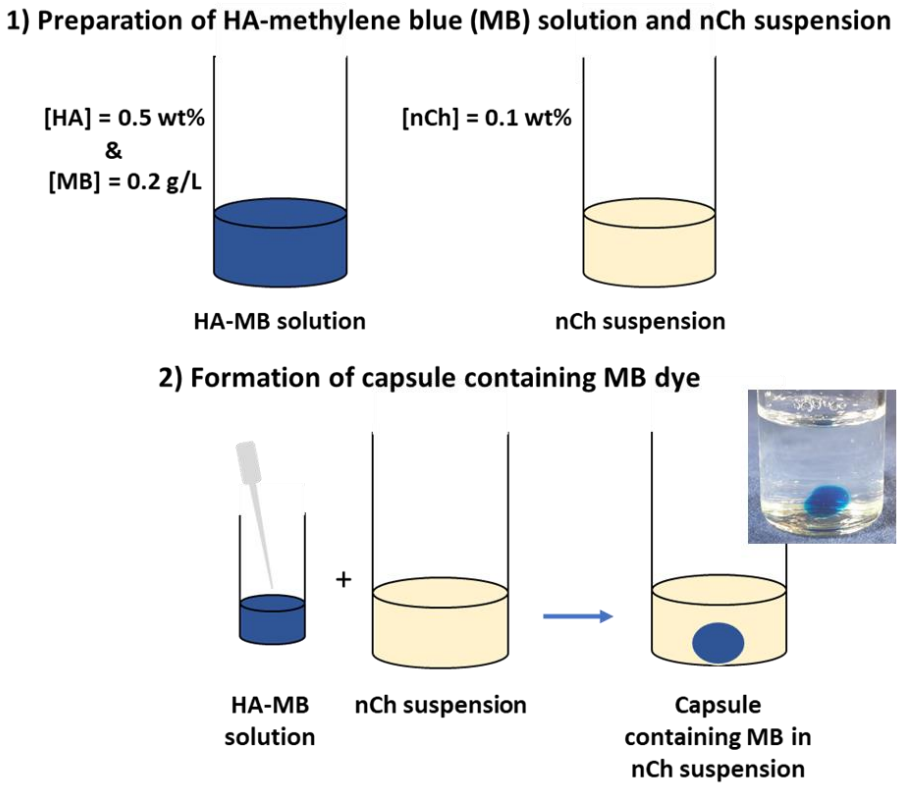

Figure 5.15. Scheme illustrating the preparation of a capsule loaded with MB.

First, MB was dissolved at 0.2 g/L in 0.5 wt% HA solution. A droplet of HA-MB solution was injected in nCh fiber suspension using a pipette, and a blue capsule was formed. Because of its higher density in comparison with the nCh fiber suspension, the capsule was found at the bottom of the vial, similar to the case when a HA droplet was added to nCh suspension (Section 3.1 Formation of HA-nCh capsules of this Chapter). Figure 5.16 shows an example of the capsule and the gradual release of MB in 0.1 wt% nCh suspension. After 1 day, MB was completely released, the surrounding nCh fiber suspension had turned blue, and the "empty" capsule remained at the bottom of the vial. This suggests that MB diffused through the porous membrane of the capsule.

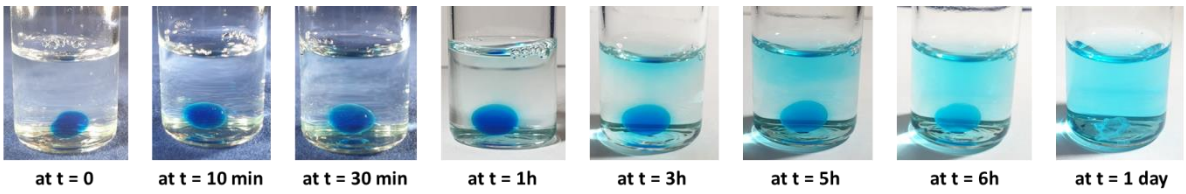

Figure 5.16. Release of MB in 0.1 wt% nCh suspension.

The properties of the nCh fiber suspension, in which the capsule forms, were optimized by testing different nCh fiber concentrations. 0.1 wt% nCh suspension was found suitable because it was

not too viscous, which allowed facile transfer of the MB-loaded capsule to PBS medium in order to quantify the MB release under physiological conditions. Due to its lower density, the capsule floats in the PBS medium (Figure 5.17). A progressive release of MB can be seen.

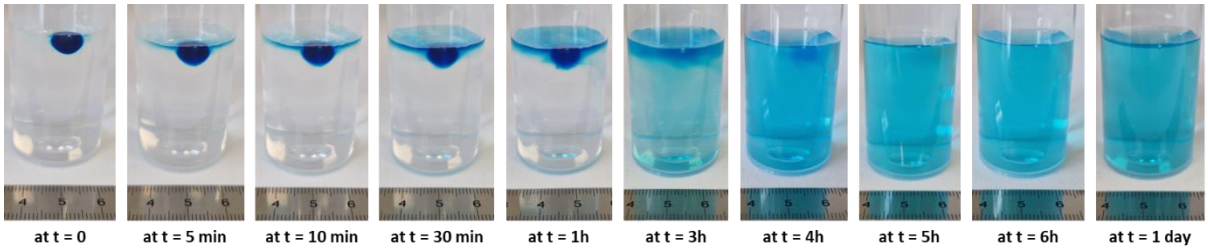

Figure 5.17. Release of MB in PBS as a function of time.

We followed the MB release from 2 types of capsules, which differ in the HA concentration used during the preparation (0.5 or 0.7 wt%). UV-Vis spectrophotometric measurements were performed to measure the absorbance of the medium at 663 nm every 5 minutes (Figure 5.18).

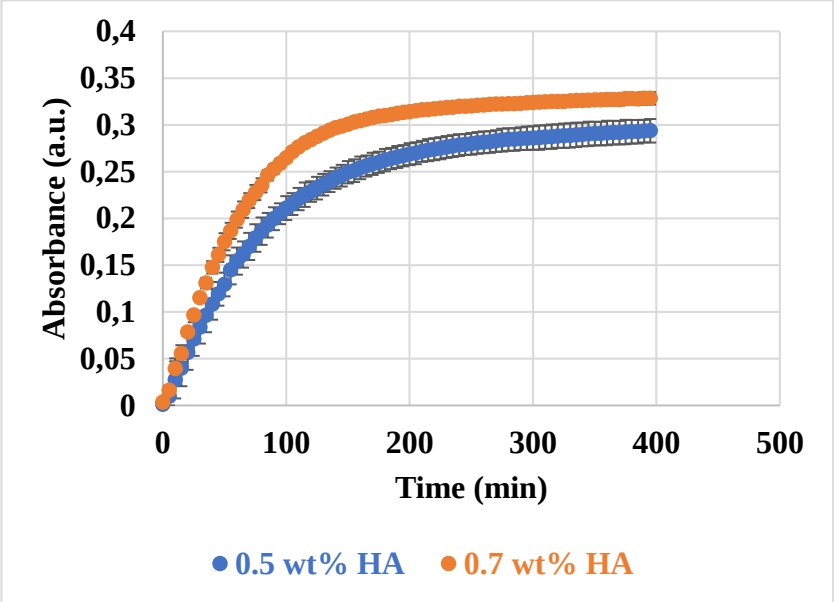

Figure 5.18. Absorbance of MB in PBS release medium over time for two HA concentrations. If not visible, the error bars are smaller than the size of the symbols. Data are expressed as means ± SD and correspond to measurements in triplicate.

In both cases, the absorbance of the solution increases over time, however, it was not possible to obtain the complete release as the process was too long.

In order to have the complete release curves and the influence of the HA concentration on the release kinetics, we need to repeat these experiments with both capsules, made with 0.5 and 0.7 wt% HA.

To test the influence of the releasing substance molecular weight on release kinetics, or, said in another way, to test capsule membrane "permeability", fluorescein isothiocyanate-dextran (FITC-dextran) with a molecular weight of 2×10^6 g/mol was used. Capsule preparation was the same as for the case of MB: FITC-dextran was dissolved in HA solution, a droplet of this solution was placed in nCh suspension, the formed capsule was extracted and placed in PBS to follow drug release, see example in Figure 5.19 As in the case of the capsule containing MB, the capsule containing FITC-dextran was floating. Figure 5.19 illustrates the FITC-dextran release in PBS.

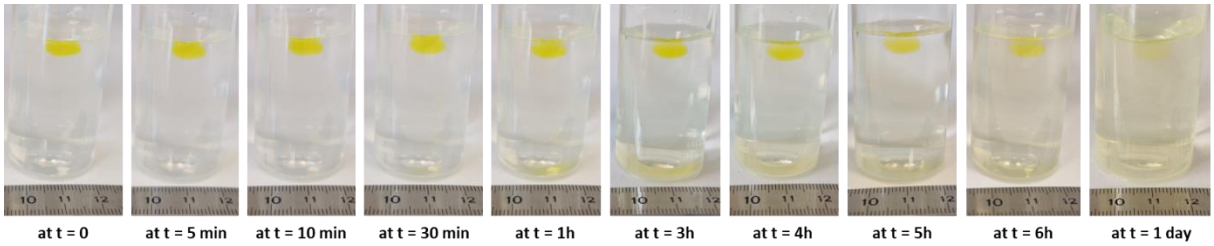

Figure 5.19. Example of FITC-dextran release into PBS from the capsule as a function of time.

The absorbance of the medium at 493 nm was measured using a UV-Vis spectrophotometer. Figure 5.20 presents the comparison of release kinetics for two FITC-dextran concentrations in the capsule, 0.2 g/L and 2 g/L.

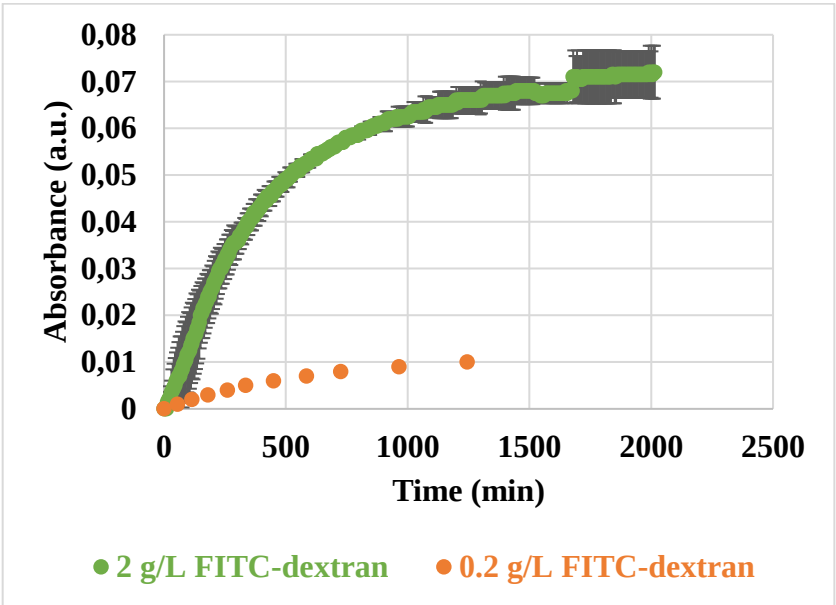

Figure 5.20. Absorbance as a function of time for capsules containing 2 g/L and 0.2 g/L of FITC-dextran. For the model drug concentration of 2 g/L, data are expressed as means ± SD and correspond to measurements in duplicate. For the model drug concentration of 0.2 g/L, a single release experiment was performed.

As said previously with MB, we need to repeat these experiments to deduce the cumulative release for each release kinetics.

4. Conclusions

In this chapter, new materials, HA-nanochitin fiber complexes were prepared, characterized, and tested for drug release.

The nCh fibers characterized are long (130-300 nm) and thin (7-11 nm), with an aspect ratio in the range of 19 – 27. nCh fibers have a degree of deacetylation of 18%. The surface charge of nCh fibers suspensions decreases by increasing pH.

After characterizing the nCh fibers, we mixed HA solution with nCh fiber suspension. New capsules were formed, due to the complexation between HA and nCh fibers. One of the ways to make these capsules is injection of one aqueous phase into another. An alternative method is to mix two phases in the presence of a salt, which suppresses complexation, and then "remove" the salt by dilution and mixing leading to a "water-in-water emulsion" composed of micro-capsules. Strong electrostatic interactions occurring between HA and nCh were confirmed by FTIR spectroscopy. HA-nCh capsules consisted of liquid, whose composition depended on the preparation method, and of a robust membrane, impossible to dissolve in various acids and bases tested. The morphology of the capsule membrane was probed by SEM.

The release kinetics from HA/nCh capsules of low- and high-molecular weight substances, methylene blue and FITC-dextran as model drugs, was investigated. The influence of model drug molecular weight on release kinetics was evaluated.

These new capsules are promising biomaterials, with potential in drug delivery applications, as aside from hyaluronic acid and nanochitin fibers, they do not contain any other component, and both are known to be biocompatible.

5. References

(1) Balazs, E. A. Chapter 20 - Viscoelastic Properties of Hyaluronan and Its Therapeutic Use In *Chemistry and Biology of Hyaluronan*; Garg, H. G., Hales, C. A., Eds.; Elsevier Science Ltd: Oxford, **2004**; pp 415–455. https://doi.org/10.1016/B978-008044382-9/50051-0.

(2) Abdelrahman, R. M.; Abdel-Mohsen, A. M.; Zboncak, M.; Frankova, J.; Lepcio, P.; Kobera, L.; Steinhart, M.; Pavlinak, D.; Spotaz, Z.; Sklenářévá, R.; Brus, J.; Jancar, J. Hyaluronan Biofilms Reinforced with Partially Deacetylated Chitin Nanowhiskers: Extraction, Fabrication, in-Vitro and Antibacterial Properties of Advanced Nanocomposites. *Carbohydrate Polymers* **2020**, *235*, 115951. https://doi.org/10.1016/j.carbpol.2020.115951.

(3) Anraku, M.; Tabuchi, R.; Ifuku, S.; Ishiguro, T.; Iohara, D.; Hirayama, F. Surface-Deacetylated Chitin Nano-Fiber/Hyaluronic Acid Composites as Potential Antioxidative Compounds for Use in Extended-Release Matrix Tablets. *International Journal of Molecular Sciences* **2015**, *16* (10), 24707–24717. https://doi.org/10.3390/ijms161024707.

(4) Luo, Y.; Wang, Q. Recent Development of Chitosan-Based Polyelectrolyte Complexes with Natural Polysaccharides for Drug Delivery. *International Journal of Biological Macromolecules* **2014**, *64*, 353–367. https://doi.org/10.1016/j.ijbiomac.2013.12.017.

(5) Polexe, R. C.; Delair, T. Elaboration of Stable and Antibody Functionalized Positively Charged Colloids by Polyelectrolyte Complexation between Chitosan and Hyaluronic Acid. *Molecules* **2013**, *18* (7), 8563–8578. https://doi.org/10.3390/molecules18078563.

(6) Luppi, B.; Bigucci, F.; Mercolini, L.; Musenga, A.; Sorrenti, M.; Catenacci, L.; Zecchi, V. Novel Mucoadhesive Nasal Inserts Based on Chitosan/Hyaluronate Polyelectrolyte Complexes for Peptide and Protein Delivery. *J Pharm Pharmacol* **2009**, *61* (2), 151–157. https://doi.org/10.1211/jpp/61.02.0003.

(7) Bai, L.; Liu, L.; Esquivel, M.; Tardy, B. L.; Huan, S.; Niu, X.; Liu, S.; Yang, G.; Fan, Y.; Rojas, O. J. Nanochitin: Chemistry, Structure, Assembly, and Applications. *Chem. Rev.* **2022**, acs.chemrev.2c00125. https://doi.org/10.1021/acs.chemrev.2c00125.

(8) Wang, Z.; Wang, R.; Xu, P.; Yu, J.; Liu, L.; Fan, Y. Physical Nanochitin/Microemulsion Composite Hydrogels for Hydrophobic Nile Red Release under in Vitro Physiological Conditions. *Cellulose* **2019**, *26* (2), 1221–1230. https://doi.org/10.1007/s10570-018-2119-2.

(9) Xu, J.; Liu, L.; Yu, J.; Zou, Y.; Wang, Z.; Fan, Y. DDA (Degree of Deacetylation) and pH-Dependent Antibacterial Properties of Chitin Nanofibers against Escherichia Coli. *Cellulose* **2019**, *26* (4), 2279–2290. https://doi.org/10.1007/s10570-019-02287-2.

(10) Fan, Y.; Saito, T.; Isogai, A. Preparation of Chitin Nanofibers from Squid Pen Beta-Chitin by Simple Mechanical Treatment under Acid Conditions. *Biomacromolecules* **2008**, *9* (7), 1919–1923. https://doi.org/10.1021/bm800178b.

(11) Gilli, R.; Kacuráková, M.; Mathlouthi, M.; Navarini, L.; Paoletti, S. FTIR Studies of Sodium Hyaluronate and Its Oligomers in the Amorphous Solid Phase and in Aqueous Solution. *Carbohydrate Research* **1994**, *263* (2), 315–326. https://doi.org/10.1016/0008-6215(94)00147-2.

(12) Joseph, B.; Mavelil Sam, R.; Balakrishnan, P.; J. Maria, H.; Gopi, S.; Volova, T.; C. M. Fernandes, S.; Thomas, S. Extraction of Nanochitin from Marine Resources and

Fabrication of Polymer Nanocomposites: Recent Advances. *Polymers* **2020**, *12* (8), 1664. https://doi.org/10.3390/polym12081664.

(13) Schott, J. A.; Do-Thanh, C.-L.; Shan, W.; Puskar, N. G.; Dai, S.; Mahurin, S. M. FTIR Investigation of the Interfacial Properties and Mechanisms of CO2 Sorption in Porous Ionic Liquids. *Green Chemical Engineering* **2021**, *2* (4), 392–401. https://doi.org/10.1016/j.gce.2021.09.003.

General conclusions and perspectives

Conclusions

This PhD thesis presents the work done for developing hyaluronic acid-based aerogels and capsules for potential biomedical applications.

The first Chapter is devoted to an overview of the state-of-the-art on aerogels with a focus on bio-aerogels, hyaluronic acid (HA) properties and its current applications.

After giving the definition of aerogels (materials with low density < 0.2 g/cm^3, high porosity > 90% and high specific surface area > 100 m^2/g), the state-of-the-art on silica aerogels (first generation) and on organic synthetic aerogels was examined, and the new trends in aerogels based on polysaccharides, bio-aerogels, were explored. Thanks to their biocompatibility, non-toxicity and biodegradability, and their intrinsic properties (low density, high porosity and high specific area), bio-aerogels have many applications in life science, in engineering (such as catalysis, energy storage, supercapacitors, batteries) but also in thermal insulation.

The thesis being focused on the HA polymer, this polysaccharide and its properties (particularly those interesting for biomedical applications) were presented. HA is a natural macromolecule used in wound healing materials and regenerative medicine. HA is highly hydrophilic and can be chemically modified through its hydroxyl and carboxyl groups to adjust polymer properties to the targeted application. HA-based porous materials, such as hydrogels and cryogels, which are already used for wound dressing applications, were also presented.

Finally, the state-of-the-art regarding HA based aerogels was explored. Thanks to the combination of aerogel characteristics, HA properties, and requirements for wound dressings (promotion of wound healing: absorption of excess exudate, protection against bacterial infection, O_2/CO_2 exchanges, release of therapeutic agents), HA-based aerogels appear to be good candidates for developing efficient wound dressings. Currently, very few work has been published on this subject. Only two articles report on HA/alginate aerogels for biomedical applications, and only one article describes the preparation of neat HA aerogels *via* non-solvent induced phase separation. Consequently, the advancement in the preparation of HA aerogels and the better understanding of processing-structure-properties relationships remain interesting scientific challenges that are addressed in this PhD project.

The first two chapters related to the results obtained in this work are devoted to HA aerogels. The following protocols were used to obtain:

- Physically crosslinked HA aerogels (prepared using freeze-thaw gelation of HA solution, solvent exchange and drying with supercritical CO_2). Freezing-thawing is an efficient and mild technique to induce hydrogen bonds between HA chains in solution, resulting in hydrogel formation. These intermolecular interactions form physical crosslinks. Opposite to our previous work[1], where the HA network was formed via direct non-solvent induced phase separation, an alternative method for the formation of the HA network was presented.
- Chemically crosslinked HA aerogels (obtained via chemical crosslinking of HA, solvent exchange and $scCO_2$ drying). The reaction between the carboxylic acid groups of HA with the amine groups of cystamine, acting as crosslinker, forms amide links between HA chains, resulting in the formation of a HA network.

The first steps were to explore the fabrication conditions of physically crosslinked HA aerogels by investigating different parameters involved such as HA concentration, initial solution pH, number of FT cycles and non-solvent. This work demonstrated the conditions where aerogels are formed. More specifically, at pH 2.5 (HA isoelectric point) using ethanol or acetone and at pH 1.5 using ethanol, we produced HA-based aerogels with a density below 0.2 g/cm^3 and a specific surface area around 500−600 m^2/g. A manuscript describing these results was published in the journal *Biomacromolecules* in 2023.

This study also demonstrated that physically crosslinked HA aerogels are very sensitive to humidity, which degrades their structure. For example, the mass of HA aerogels increases by 8%, the volume decreases by 65% and the density increases by 215% after 6 h of exposure to air, and the specific surface area of HA aerogels decreases after 2-month storage at room temperature (by 32% for aerogels prepared using 1.6 wt% HA, pH 2.5 and 3 FT cycles and by 10% for aerogels prepared using 1 wt% HA, pH 2.5 and 1 FT cycle). HA aerogels should thus be stored in an inert atmosphere.

Next, the conditions to prepare chemically crosslinked HA aerogels were investigated. Chapter 4 presented an explorative study on the preparation of chemically crosslinked HA aerogels using covalent crosslinking for the formation of HA hydrogels, followed by solvent exchange and $scCO_2$ drying. One of the problems was the formation of CO_2 bubbles during the chemical reaction between the carboxylic acid groups of HA with the amine groups of cystamine,

with no way to avoid them. One hydrogel protocol was chosen to minimize bubbles. Briefly, an example of a formulation protocol consists of: preparation of the 1.6 wt% HA solution, addition of EDC and NHS (catalysts) and cystamine (crosslinker) with 2:1 as $COOH:NH_2$ molar ratio, 1:1.5 as COOH:EDC molar ratio and 1:1.5 as COOH:NHS molar ratio, centrifugation at 6000 rpm for 5 min to remove bubbles, gelation at 37°C for 24 h, centrifugation at 6000 rpm for 25 min and subsequently at 9000 rpm for 25 min to remove bubbles. Then, to get aerogels, solvent exchange and $scCO_2$ drying were performed. Aerogels with varying HA concentration or $COOH:NH_2$ molar ratio were prepared. The influence of these processing parameters on the aerogels properties was investigated. We succeeded to obtain HA aerogels for all conditions tested, i.e. materials with low density (< 0.2 g/cm^3), high porosity (> 86 %) and high specific surface area (> 150 m^2/g). A higher HA concentration resulted in reduced overall volume shrinkage (86% for aerogels prepared using 1.6 wt% HA at 2:1 molar ratio and 81% for aerogels prepared using 1.6 wt% HA at 1:1 molar ratio), a higher density (0.19 ± 0.02 g/cm^3 for aerogels prepared using 1.6 wt% HA at 2:1 molar ratio and 0.13 ± 0.01 g/cm^3 for aerogels prepared using 1.6 wt% HA at 1:1 molar ratio) and a higher specific surface area (394 ± 82 m^2/g for aerogels prepared using 1.6 wt% HA at 2:1 molar ratio and 273 m^2/g for aerogels prepared using 1.6 wt% HA at 1:1 molar ratio). Aerogel behavior in PBS medium was studied in the view of biomedical applications. Dissolution time depends on HA concentration and $COOH:NH_2$ molar ratio. Chemically crosslinked aerogels are more resistant to dissolution than physically crosslinked HA aerogels prepared with the freezing-thawing method. It was anticipated that the presence of the reduction-sensitive disulfide bridge in the cystamine crosslinks would allow for accelerated degradation of the network in the presence of the reducing agent DTT in the PBS medium, but no clear experimental evidence was found for this stimulus-responsiveness.

The final chapter describes the formation of capsules based on HA and nCh fibers. This work was performed in the frame of a French-Canadian collaboration. Initially, we were willing to reinforce neat HA aerogels with nCh fibers, due to their excellent mechanical properties and biocompatibility, but upon mixing HA solutions and nCh suspensions, strong polyelectrolyte complexation occurred leading to the formation of a HA-nCh “membrane”. The electrostatic interactions occurring between HA and nCh were confirmed by FTIR spectroscopy. Opposite to “neat” HA aerogels, these membranes were not soluble in all media tested, ranging from rather strong acids to strong bases. When dropping HA solution in nCh suspension (or vice versa), HA-nCh capsules were formed. HA-nCh capsules consisted of a liquid, of which the composition

depends on the preparation method. As the membrane was porous, the feasibility of the capsule for drug delivery was investigated, and hence a model drug was introduced inside. The release kinetics of two model drugs, methylene blue and FITC-dextran, was investigated. A slower release was observed for FITC-dextran, due to its higher molecular weight. These new capsules are promising biomaterials, with potential in drug delivery applications.

Perspectives

This work focused on the development of novel HA-based materials (aerogels and capsules) that could be interesting for biomedical applications. Hereafter, some perspectives are suggested as this research could be continued:

- **Improvement of the chemically crosslinked HA aerogel properties**

As a first perspective, the work on chemically crosslinked HA aerogels could be deepened. We have shown that the chemically crosslinked HA aerogels, prepared using cystamine as crosslinker, have higher stability in PBS medium than in comparison with physically crosslinked HA aerogels. The obtained properties of HA aerogels are compliant with wound dressing applications. However, the presence of bubbles, due to the reaction of HA with cystamine during gelation, may impact some results. Thus, we need to find a way to remove bubbles during the preparation. HA gelation under reduced pressure can be tested to avoid bubbles. A comparison of the material properties with and without bubbles should be performed to detect potential impacts of bubbles. Also, an alternative synthesis crosslinking scheme, avoiding the formation of CO_2, could be investigated.

HA network reticulation could be improved by testing formulations with a higher amount of cystamine (i.e. 1:4 or 1:8 $COOH:NH_2$ molar ratios). A more crosslinked network could be obtained, leading to a material with potentially higher density and higher specific surface area.

Further work regarding the cleavage of the S-S bonds in the chemically crosslinked HA network with DTT, a thiol reducing agent, should be performed. We have demonstrated that DTT reduces the swelling of chemically crosslinked HA aerogels in PBS at pH 7.4 and slows down their dissolution rate, contrary to expectations. This could be explained by an insufficient amount of DTT relative to S-S bonds in the HA network. It could be interesting to perform other tests using an increased amount of DTT. Also, alternative reducing agents could be explored.

To go deeper in the analysis of chemically crosslinked HA aerogels, we could characterize the degree of crosslinking by NMR or by determining the amount of remaining COOH groups in the hydrogel via e.g. titration.

- **Better understanding of the mechanical properties of physically and chemically crosslinked HA aerogels**

To be efficient as wound dressing, HA aerogels should be strong. In this work, we started to test the mechanical properties of HA aerogels; we used a few aged samples, which were potentially impacted by vapor absorption. No clear trend was deduced. Thus, to advance the understanding of the mechanical properties of HA aerogels, more experimental data should be cumulated. New HA aerogel formulations could be prepared and characterized via compression tests directly after $scCO_2$ drying. This could lead to increased knowledge about the influence of preparation parameters (HA concentration, pH, number of FT cycles, non-solvent) on the HA aerogel mechanical properties. Once the optimization is performed for physically crosslinked HA aerogels, the mechanical properties of chemically crosslinked HA aerogels could be tested using the same approach.

- **To test the drug release kinetics from HA aerogels**

In order to test the feasibility of HA aerogels for drug release, it could be interesting to load a model drug during the preparation of the chemically crosslinked HA aerogel and follow its release kinetics in PBS medium at pH 7.4 to mimic physiological conditions. FITC-dextran could be such a model drug. FITC-dextran is insoluble in both acetone and ethanol non-solvents; it would probably not be removed during solvent exchange. The preparation of FITC-dextran loaded chemically crosslinked aerogels could be as follows: addition of the model drug with EDC, NHS (catalysts) and cystamine (crosslinker) in HA solution, gelation at 37°C to form the covalently crosslinked HA hydrogel, followed by solvent exchange and $scCO_2$ drying. The resulting HA aerogels could be then placed in a permeable stainless-steel basket in PBS and the release kinetics could be followed using periodical UV-Vis spectrophotometric measurements. Several aerogel formulations could be prepared varying the preparation parameters (HA concentration, COOH:NH_2 molar ratio) in order to study the influence of these parameters on the release kinetics. This protocol could also be applied to physically crosslinked HA aerogels. Following these model drug experiments, FITC-dextran could be replaced by a therapeutic agent promoting wound healing such as curcumin or gentamicin.

- **To perform biomedical tests**

Once the chemically crosslinked HA aerogel formulation is optimized, biomedical tests could be performed to check whether aerogels can be used as wound dressings. In vitro studies could be performed such as cytotoxicity and antibacterial tests. The performance of HA aerogels in wound closure and in bio-adhesion could also be tested.

- **To test 3D printing of HA aerogels**

HA aerogels with shapes adapted to the wound could be prepared using 3D printing in a support bath. This approach uses a 3D printer that deposits material not on a flat surface ('classical' method), but in a support bath, thereby preventing the disadvantages of printing-in-air such as collapse and needle clogging.[2] Once the ink is deposited, it should retain the deposited shape because it is constrained by the surrounding support bath. HA inks have never been printed using this technique. Thus, before any printing, a study towards the optimization of the solution rheological properties for making stable HA gels should be performed. In literature, one article has been found on the stabilization of HA bioinks with dual crosslinking (mixing of admantane-methacrylated HA and β-cyclodextrin-methacrylated HA followed by photocrosslinking with UV light).[3] More recently, a review summarized methods such as photocrosslinking with UV-Vis light to stabilize HA bioinks.[4] Once the stabilization method is established, HA hydrogels can be 3D printed with the desired shape in the bath. Then, solvent exchange with ethanol or acetone and supercritical drying to obtain HA aerogels with the desired shape should be performed.

- **To extend the study to composite HA based aerogels**

A composite aerogel with HA and another polymer, insoluble in water, such as cellulose, starch or chitosan, could be made to reinforce the neat HA network, on the basis of Ref[5]. The mixture of these two compounds may form an interpenetrated network, exhibiting different characteristics from the individual components and offering synergistic properties.

- **To continue the work on HA-nCh fibers based capsules**

As described in Chapter 5, new HA-nCh materials, qualified as capsules, were developed. Capsules were isolated and drug release through the membrane was tested. This material could be interesting for biomedical applications, and further investigations of the characteristics of this material are needed. For example, analysis in FTIR spectroscopy can be continued to estimate the weight fraction of HA and nCh fibers participating in the membrane formation. Also, the

FITC-dextran release kinetics from capsules could be studied in-depth to deduce trends because in this work only an explorative study was performed.

References

(1) Aguilera-Bulla, D.; Legay, L.; Buwalda, S. J.; Budtova, T. Crosslinker-Free Hyaluronic Acid Aerogels. *Biomacromolecules* **2022**, *23* (7), 2838–2845. https://doi.org/10.1021/acs.biomac.2c00207.

(2) McCormack, A.; Highley, C. B.; Leslie, N. R.; Melchels, F. P. W. 3D Printing in Suspension Baths: Keeping the Promises of Bioprinting Afloat. *Trends in Biotechnology* **2020**, *38* (6), 584–593. https://doi.org/10.1016/j.tibtech.2019.12.020.

(3) Ouyang, L.; Highley, C. B.; Rodell, C. B.; Sun, W.; Burdick, J. A. 3D Printing of Shear-Thinning Hyaluronic Acid Hydrogels with Secondary Cross-Linking. *ACS Biomater. Sci. Eng.* **2016**, *2* (10), 1743–1751. https://doi.org/10.1021/acsbiomaterials.6b00158.

(4) Jo Jang, E.; Patel, R.; Sankpal, N. V.; Bouchard, L.-S.; Patel, M. Alginate, Hyaluronic Acid, and Chitosan-Based 3D Printing Hydrogel for Cartilage Tissue Regeneration. *European Polymer Journal* **2024**, *202*, 112651. https://doi.org/10.1016/j.eurpolymj.2023.112651.

(5) Groult, S.; Buwalda, S.; Budtova, T. Tuning Bio-Aerogel Properties for Controlling Drug Delivery. Part 2: Cellulose-Pectin Composite Aerogels. *Biomaterials Advances* **2022**, *135*, 212732. https://doi.org/10.1016/j.bioadv.2022.212732.

Annexes

Annex 1. Protocols tested for chemical HA hydrogel formulation. In order to prepare chemically crosslinked HA aerogels, we needed to prepare a chemically crosslinked HA hydrogel as a precursor. We tested several parameters to obtain a strong hydrogel with no bubbles inside. The parameters varied between each formulation are in orange.

N° Protocol	Protocol	Observations	Literature
1	1) Preparation of the HA solution ([HA] = 1.6 wt%, distilled water) 2) Cystamine addition in powder form 3) EDC & NHS addition in powder form 4) Mixture stirred at 220 rpm 5) Gelation in the oven at 37°C for 30 min 6) Centrifugation to remove bubbles at 2000 rpm for 20 min	• After stirring ➔ Bubbles • After gelation at 37°C ➔ Bubbles still present • After centrifugation ➔ Impossible to remove bubbles ➔ Strong hydrogel	1
2	1) Preparation of the HA solution ([HA] = 1.6 wt%, distilled water) 2) Cystamine addition in powder form 3) EDC & NHS addition in powder form 4) Mixture stirred at 220 rpm 5) Centrifugation to remove bubbles at 6000 rpm for 15 min 6) Gelation at 37°C for 30 min 7) Centrifugation to remove bubbles at 6000 and 9000 rpm	• After centrifugation at 6000 rpm for 15 min ➔ No bubbles • After centrifugation at 6000 and 9000 rpm ➔ Appearance of bubbles, impossible to remove them ➔ Strong hydrogel	/
3	1) Preparation of the HA solution ([HA] = 1.6 wt%, distilled water) 2) Cystamine addition in powder form 3) EDC & NHS addition in solution form 4) Mixture stirred at 220 rpm	• EDC & NHS addition ➔ Easier mixing when added in solution form • After crosslinking at RT ➔ After waiting for 1 h, no flowing => completely crosslinked?	/

	5) Crosslinking at RT 6) Centrifugation to remove bubbles at 9000 rpm for 1 h	• After centrifugation at 9000 rpm ➔ Some parts remained on spatula => Weak gel or solution ➔ Impossible to remove bubbles	
4	1) Preparation of the HA solution ([HA] = 1.6 wt%, distilled water) 2) Cystamine addition in powder form 3) EDC & NHS addition in solution form 4) Mixture stirred at 220 rpm 5) Crosslinking at RT 6) Vacuum to remove bubbles	• After vacuum process ➔ Swelling of the solution ➔ Appearance of many bubbles ➔ No removal of bubbles	/
5	1) Preparation of the HA solution ([HA] = 1.6 wt%, degassed water obtained using nitrogen gas) 2) Cystamine addition in powder form 3) EDC & NHS addition in solution form 4) Mixture stirred at 220 rpm 5) Crosslinking at RT 6) Centrifugation to remove bubbles at 8000 rpm for 30 min and at 9000 rpm for 40 min and at 6000 rpm for 30 min	• After stirring in degassed water ➔ Bubbles • After centrifugation process ➔ Some parts remained on spatula => Weak gel or solution ➔ Impossible to remove bubbles	/
6	1) Preparation of the HA solution ([HA] = 1.6 wt%, distilled water) 2) Storage in the fridge for 1 night 3) Warm up of the centrifuge to 37°C 4) Cystamine addition in powder form 5) EDC & NHS addition in solution form	• After 1 night in the fridge ➔ No bubbles • After centrifugation at 37°C at 6000 rpm ➔ Preparation flowing => Weak gel or solution ➔ Bubbles • After centrifugation at 9000 rpm	/

	6) Centrifugation – Reaction at 37°C a) at 6000 rpm for 20 min b) at 9000 rpm for 10 min	➔ Preparation flowing => Weak gel or solution ➔ Few bubbles	
7 (1st protocol optimized)	1) Preparation of the HA solution ([HA] = 1.6 wt%, distilled water) 2) Cystamine addition in powder form 3) EDC & NHS addition in solution form 4) Mixture stirred for 5 min at 220 rpm 5) Centrifugation to remove bubbles at 6000 rpm for 15 min 6) Gelation at 37°C for 1h 7) Centrifugation to remove bubbles at 6000 rpm for 25 min and at 9000 rpm for 25 min	➔ After stirring ➔ Bubbles ➔ EDC & NHS addition ➔ Easier mixing when added in liquid form ➔ After centrifugation at 6000 rpm for 15 min ➔ No bubbles ➔ After gelation ➔ Increase of crosslinking time ➔ Still bubbles ➔ After centrifugation at 6000 and 9000 rpm ➔ Still some bubbles ➔ Strong hydrogel	/
8	1) Preparation of the HA solution ([HA] = 1.6 wt%, distilled water) 2) Cystamine addition 3) EDC & NHS addition 4) Mixture stirred at 4°C for 4h 5) Centrifugation done directly after for 30 min at 6000 rpm	• After stirring at 4°C ➔ System flowing => Weak gel or solution ➔ Practically no bubbles	2
9	1) Preparation of the HA solution ([HA] = 1.6 wt%, distilled water) 2) Cystamine addition 3) EDC & NHS addition 4) Mixture stirred at RT at 220 rpm for 4h 5) Centrifugation to remove bubbles at 6000 rpm for 5 min	• After stirring at RT ➔ Bubbles ➔ Strong hydrogel	/

10	1) Preparation of the HA solution ([HA] = 1.6 wt%, distilled water) 2) Addition of EDC & NHS 3) Stirring for 2h at RT for 220 rpm 4) Cystamine addition 5) Mixture stirred for 24h at RT at 220 rpm Storage of the sample during the weekend at RT 6) Centrifugation to remove bubbles for 10 min at 6000 rpm 7) Gelation at 37°C for 1 day	• After stirring 2h at RT • Few bubbles • After stirring 24h at RT • Some bubbles • After centrifugation ➔ Preparation flowing => Weak gel or solution ➔ No bubbles • After gelation ➔ System flowing	3
11	1) Preparation of the HA solution ([HA] = 1.6 wt%, distilled water) 2) Cystamine addition 3) EDC & NHS addition 4) Mixture stirred for 30 min at RT at 210 rpm 5) Gelation at 4°C for 24h 6) Centrifugation to remove bubbles at 6000 rpm for 20 min and at 9000 rpm for 10 min	• After stirring ➔ Bubbles • After gelation at 4°C ➔ Few bubbles • After centrifugation ➔ System flowing => Weak gel or solution ➔ Impossible to remove bubbles	/
12	1) Preparation of the HA solution ([HA] = 1.6 wt%, distilled water) 2) EDC & NHS addition 3) Solution pH change to 5 4) Mixture stirred for 30 min at RT at 220 rpm 5) Cystamine addition 6) Reaction carried out at RT overnight	• After pH change and stirring ➔ A lot of small bubbles • After reaction at RT overnight ➔ Some bubbles ➔ Weak gel or solution	4
13	1) Preparation of the HA solution ([HA] = 1.6 wt%, distilled water) 2) Preparation of 0.1 wt% $Ca(OH)_2$ solution 3) EDC & NHS addition 4) Cystamine addition	• After stirring ➔ Presence of bubbles • After gelation ➔ Bubbles • After centrifugation ➔ Still bubbles present => No	5

	5) Addition of 2 mL of $Ca(OH)_2$ solution 6) Stirring for 30 min at RT at 220 rpm 7) Centrifugation to remove bubbles for 10 min at 6000 rpm 8) Gelation at 37°C for 20h to see if bubbles appear 9) Centrifugation done for 44 min at 6000 rpm and for 10 min at 9000 rpm	impact of $Ca(OH)_2$ solution ➔ System flowing => Weak gel or solution	
14	1) Preparation of the HA solution ([HA] = 1.6 wt%, distilled water) 2) Preparation of 0.1 wt% $Ca(OH)_2$ solution at pH 2 3) EDC & NHS addition 4) Cystamine addition 5) Addition of 3 drops of acidic $Ca(OH)_2$ solution 6) Stirring for 5 min at RT at 220 rpm 7) Centrifugation to remove bubbles for 5 min at 6000 rpm 8) Gelation at 37°C for 1 day	• After stirring ➔ Bubbles • After gelation ➔ Still bubbles present => No impact of acidic $Ca(OH)_2$ solution	/
15	1) Preparation of the HA solution ([HA] = 1.6 wt%, distilled water) 2) Preparation of 0.1 wt% $Ca(OH)_2$ solution at pH 12 3) EDC & NHS addition 4) Cystamine addition 5) Addition of 3 drops of basic $Ca(OH)_2$ solution 6) Stirring for 5 min at RT at 220 rpm 7) Centrifugation to remove bubbles for 5 min at 6000 rpm 8) Gelation at 37°C for 1 day	• After stirring ➔ Bubbles observed • After gelation ➔ Still bubbles present => No impact of basic $Ca(OH)_2$ solution	/

16	1) Preparation of the HA solution ([HA] = 1.6 wt%, distilled water) 2) EDC & NHS addition 3) Cystamine addition 4) Stirring for 5 min at RT at 220 rpm 5) Centrifugation to remove bubbles at 6000 rpm for 5 min 6) Gelation at 37°C for 1 day 7) Centrifugation at 6000 rpm for 25 min and for 25 min at 9000 rpm 8) Preparation of buffer solution at pH 2.5 9) Introduction of the preparation in a solution buffer at pH 2.5 for 1 night 10) 3 washings (3x10 mL) with water to remove EDC&NHS – Waiting for 10 min between each washing 11) Solvent exchange with ethanol	• After gelation & immersion in buffer solution at pH 2.5 ➔ Strong hydrogel ➔ Bubbles ➔ Loss of matter ○ During transfer from vial to beaker ○ During beaker to vial	/
17 (Final optimized protocol and further used to prepare aerogels)	1) Preparation of the HA solution ([HA] = 1.6 wt%, distilled water) 2) EDC & NHS addition 3) Cystamine addition 4) Stirring at RT at 220 rpm for 5 min 5) Centrifugation to remove bubbles at 6000 rpm for 5 min 6) Gelation at 37°C for 1 day 7) Centrifugation at 6000 rpm for 25 min and at 9000 rpm for 25 min 8) Preparation of buffer solution at pH 2.5 9) Addition of 20 mL of the buffer solution at pH 2.5 on the hydrogel 10) Solvent exchange with ethanol	• After immersion of the buffer solution at pH 2.5 in the vial ➔ Strong hydrogel ➔ Bubbles ➔ No matter lost because all steps performed in the same plastic vial • EDC & NHS removal ➔ Remove of washings with water as compared to formulation n°16 ➔ Washed out with buffer at pH 2.5 and during solvent exchange with ethanol	/

The protocol n°17 was chosen for the preparation of chemically crosslinked hydrogels because we obtained a strong hydrogel (according to the vial tilting test). Bubbles could not be removed, despite the variation of several parameters. Moreover, we found a way to efficiently remove EDC and NHS. Thus, we decided to continue with this protocol to prepare chemically crosslinked aerogels.

References

(1) Wang, L.; Dong, S.; Liu, Y.; Ma, Y.; Zhang, J.; Yang, Z.; Jiang, W.; Yuan, Y. Fabrication of Injectable, Porous Hyaluronic Acid Hydrogel Based on an In-Situ Bubble-Forming Hydrogel Entrapment Process. *Polymers* **2020**, *12* (5), 1138. https://doi.org/10.3390/polym12051138.

(2) Liu, Y.; Ren, L.; Wang, Y. Crosslinked Collagen–Gelatin–Hyaluronic Acid Biomimetic Film for Cornea Tissue Engineering Applications. *Materials Science and Engineering: C* **2013**, *33* (1), 196–201. https://doi.org/10.1016/j.msec.2012.08.030.

(3) Deng, S.; Li, X.; Yang, W.; He, K.; Ye, X. Injectable in Situ Cross-Linking Hyaluronic Acid/Carboxymethyl Cellulose Based Hydrogels for Drug Release. *Journal of Biomaterials Science, Polymer Edition* **2018**, *29* (13), 1643–1655. https://doi.org/10.1080/09205063.2018.1481005.

(4) Yegappan, R.; Selvaprithiviraj, V.; Mohandas, A.; Jayakumar, R. Nano Polydopamine Crosslinked Thiol-Functionalized Hyaluronic Acid Hydrogel for Angiogenic Drug Delivery. *Colloids and Surfaces B: Biointerfaces* **2019**, *177*, 41–49. https://doi.org/10.1016/j.colsurfb.2019.01.035.

(5) Han, S.-J.; Yoo, M.; Kim, D.-W.; Wee, J.-H. Carbon Dioxide Capture Using Calcium Hydroxide Aqueous Solution as the Absorbent. *Energy Fuels* **2011**, *25* (8), 3825–3834. https://doi.org/10.1021/ef200415p.

RÉSUMÉ

Le projet consiste à développer de nouveaux matériaux à base d'acide hyaluronique pour des applications biomédicales. Ce polysaccharide biocompatible et hydrophile a été utilisé pour préparer des aérogels, réseaux de polymères solides, très poreux et très légers. Plusieurs méthodes de réticulation (physique et chimique) ont été explorées et les relations fabrication-structure-propriétés ont été étudiées. Les pansements sont un domaine d'application potentiel pour ces nouveaux matériaux, en raison des propriétés uniques des aérogels qui leur permettent potentiellement d'absorber une grande quantité d'exsudat de la blessure, de faciliter les échanges gazeux (O_2 et CO_2), de couvrir la blessure et d'être utilisés en tant que matrice pour des agents bioactifs. En plus du développement des aérogels, le mélange d'une solution d'acide hyaluronique avec une suspension de nanofibres de chitin a permis de fabriquer des capsules solides via des interactions entre les charges opposées des biopolymères. Les cinétiques de libération de plusieurs composés à partir de la capsule ont été étudiées et cela a permis de démontrer leur potentiel pour des applications de libération de molécules actives.

MOTS CLÉS

Acide hyaluronique, Aérogels, Capsules, Pansements, Applications biomédicales

ABSTRACT

The project targets the development of new materials based on hyaluronic acid for biomedical applications. This biocompatible and hydrophilic polysaccharide was used for the preparation of aerogels, which are dry, highly porous and ultra-light polymer networks. Several physical and chemical crosslinking methods were explored and processing-structure-properties relations were developed. Wound dressings are a potential application area for these novel materials, as the unique properties of aerogels potentially allow them to absorb a large amount of wound exudate, to facilitate O_2 and CO_2 exchange, to cover the wound and to act as a depot for active agents. In addition to the work on aerogels, it was found that mixing a solution of HA and a suspension of chitin nanofibers led to the formation of robust capsules via interactions between the oppositely charged biopolymers. The release kinetics of different model compounds from the capsules were investigated, which demonstrated their potential for drug delivery applications.

KEYWORDS

Hyaluronic acid, Aerogels, Capsules, Wound dressings, Biomedical applications